PASSIVE AND SEMI-ACTIVE TUNED MASS DAMPER BUILDING SYSTEMS

A thesis
submitted in fulfilment of
the requirements for the Degree of
Doctor of Philosophy
of
Civil and Natural Resources Engineering
in the
University of Canterbury
by
Min Ho Chey

University of Canterbury,
Christchurch, New Zealand
2007

ABSTRACT

This thesis explores next generation passive and semi-active tuned mass damper (PTMD and SATMD) building systems for reducing the seismic response of tall structures and mitigating damage. The proposed structural configuration separates the upper storey(s) of a structure to act as the 'tuned' mass, either passively or semi-actively. In the view point of traditional TMD system theory, this alternative approach avoids adding excessive redundant mass that is rarely used.

In particular, it is proposed to replace the passive spring damper system with a semi-active resetable device based system (SATMD). This semi-active approach uses feedback control to alter or manipulate the reaction forces, effectively re-tuning the system depending on the structural response. In this trade-off parametric study, the efficacy of spreading stiffness between resetable devices and rubber bearings is illustrated. Spectral analysis of simplified 2-DOF model explores the efficacy of these modified structural control systems and the general validity of the optimal derived parameters is demonstrated. The end result of the spectral analysis is an optimally-based initial design approach that fits into accepted design methods.

Realistic suites of earthquake ground motion records, representing seismic excitations of specific return period probability, are utilised, with lognormal statistical analysis used to represent the response distribution. This probabilistic approach avoids bias toward any particular type of ground motion or frequency content. Statistical analysis of the performance over these suites thus better indicates the true overall efficacy of the PTMD and SATMD building systems considered.

Several cases of the segregated multi-storey TMD building structures utilising passive devices (PTMD) and semi-active resetable devices (SATMD) are described and analysed. The SATMD building systems show significant promise for applications of structural control, particularly for cases where extra storeys might be added during retrofit, redevelopment or upgrade. The SATMD approach offers advantages over PTMD building systems in the consistent response reductions seen over a broad range

of structural natural frequencies. Using an array of performance metrics the overall structural performance is examined without the typically narrow focus found in other studies. Performance comparisons are based on statistically calculated storey/structural hysteretic energy and storey/structural damage demands, as well as conventional structural response performance indices.

Overall, this research presents a methodology for designing SATMD building systems, highlighting the adaptable structural configuration and the performance obtained. Thus, there is good potential for SATMD building systems, especially in retrofit where lack of space constrains some future urban development to expand upward. Finally, the approach presented offers an insight into how rethinking typical solutions with new technology can offer dramatic improvements that might not otherwise be expected or obtainable.

ACKNOWLEDGEMENT

I am very grateful to my supervisors who worked with the author very closely during the PhD process in University of Canterbury. These include Prof. Athol J. Carr, Prof. J. Geoffrey Chase, and Prof. John B. Mander. I remember that when we had a first meeting for my research, Prof. Mander called our team as a 'Good Team'. During last several years at the civil and mechanical engineering building, I had helpful discussions with these learned professors on the many aspects of seismic response mitigation and related design methods.

Acknowledgement is owed to my room mates, David, Vinod and Koichi; semi-active group members, Roberto, Kerry and Geoff; and other postgraduate students, Jung-Ki, Brian, Brandon and Kam for their friendship, encouragement and many helpful suggestions during the preparation of the thesis.

In addition, I want to express my appreciation for the brothers and sisters in Christchurch Full Gospel Church. Over the past 12 years of my church life in Christchurch, my pastors and many church members have prayed for my ministries and postgraduate studies.

A heartfelt thanks is due to my parents, my brother, Seiho, and his family who shared with me New Zealand immigration life. To my wonderful vivacious wife, June, and my priceless children, Hannah and John… Thank you for your patience and understanding. This thesis could never have come close to completion if it were not for your involvement and encouragement.

Finally, no acknowledgments can be complete without mention of Jesus Christ, the unseen helper who never failed to amaze me with the way in which he turned up information, books, articles, and the right people at just the right time. I wrote with a strong awareness and confidence that he was overseeing the whole project.

CONTENTS

LIST OF FIGURES

LIST OF TABLES

1 Introduction

1.1 Background and Motivation

It is well accepted that earthquakes will continue to occur, and cause significant social structural and economic damage if we are not prepared. Assessing earthquake risk and improving engineering strategies to mitigate damage are thus the only viable options to create more resilient cities and communities. Geologists, seismologists and engineers are continuing their efforts to improve zoning maps, create reliable databases of earthquake processes and their effects, increase understanding of site characteristics, and develop earthquake resistant designs. As for the engineer, the ultimate goal is to design damage free, cost effective structures that will behave in a predictable and acceptable manner to maximise life safety and minimise damage.

Today, we understand to a great deal about *how* our built environment will respond to a wide range of earthquake motions. The challenges are therefore to develop new techniques and to improve on the existing practices so that the performance of these structures is *predictable* and *acceptable*. In this case, *acceptable* means minimal or no damage for credible design events with no loss of life safety.

As a multi-disciplinary field of engineering, the design of earthquake resistant structures is at a threshold from which many exciting developments are possible in the coming years. New techniques and new materials that are not traditionally used in civil engineering structures offer significant promise in reducing the seismic risk. Notable improvements have also been made in the nonlinear dynamic understanding of earthquakes and the response of structures. These improvements include improving the structural configuration (Arnold 1984; Arnold and Reitherman 1982; Challa and Hall 1994; Lagorio 1990; Sabouni 1995; Shustov 1999), more optimally determining the size and shape of various elements (Gu et al. 2000; Ohkubo and Asai 1992; Sfakianakis and Fardis 1991; Wang et al. 2002), the increased understanding of construction materials and improved methods of fabrication (Aref and Jung 2006; Moncarz et al. 2001; Pieplow 2006; Saadatmanesh 1997). These ‘modern’ design techniques were developed primarily during the last five decades, mostly in developed

countries with active seismic regions, such as the United States, Japan and New Zealand.

Clearly, the problem of loads and structures interacting in such a complex, hard-to-predict fashion requires a multi-disciplinary approach. Hence, modern earthquake resistant design involves specialists from a variety of other disciplines including geoscientists, seismologists, structural engineers, geotechnical engineers, mechanical engineers and material scientists, as well as others. As a result, many new devices, techniques and strategies have been proposed to reduce seismic demand and/or enhance the strength, ductility or energy dissipation capacity of a given structure.

In view of the discussion on the nature of the earthquake resistant design problem, it is not very difficult to identify some likely future growth areas. In addition to identifying those areas, the factors that could define the success of earthquake resistant design concepts, approaches and techniques in the future should also be considered. Particularly, in the light of ever changing and rising regulatory standards for seismic protection.

Hence, in the coming years, the field of earthquake resistant design of structures is likely to witness the following significant developments:

- Performance-based design processes will increasingly take centre stage, making conventional prescriptive (minimum standard) codes obsolete (Moehle 1992; Priestley 2000)
- The acceptable risk criterion for design purposes will be defined in terms of performance objectives and hazard levels, creating a more site and structure specific standard (Kircher 1997; Mehrain and Krawinkler 1997; Shapiro et al. 1997)
- Multiple annual probability maps for response spectral accelerations and peak ground accelerations, along with more realistic predictions of the effects of site soils, topography, near-source rupture mechanisms and spatial variation, should provide better characterization of design earthquakes and expected ground motions (Bolt 1997; Frankel et al. 1996)

- Analytical tools for reliable prediction of structural response, essential tools in performance-based design processes, will continue to improve and include new devices and materials (Mackie and Stojadinovic 2006; Min Liu 2005)
- The area of soil–structure interaction, perhaps the least understood aspect in the field of earthquake engineering, is poised to witness the emergence of new numerical techniques to model nonlinear soils and structures in a manner that was not possible until now, due to the significant computational effort required (Chen et al. 2000a; Chen et al. 2000b; Choi et al. 2004; Takewaki 2007; Takewaki and Fujimoto 2004; Wu 1997; Wu and Chen 2002; Wu and Smith 1993; Wu and Smith 1995)
- The development of new structural systems and devices will continue for base-isolation, and passive, active and semi-active control systems. These will progress, in part, with the increasing proliferation of non-traditional civil engineering materials and systems (Chase et al. 2006; Housner et al. 1997; Hunt 2002; Mulligan et al. 2005a; Mulligan et al. 2006; Rodgers et al. 2007a; Soong and Spencer 2000)
- A complete probabilistic analysis and design approach that rationally accounts for uncertainties present in the structural system will gradually replace deterministic approaches, especially in the characterization of the loading environment (Annaka and Yashiro 2000; Refice and Capolongo 2002; Robinson et al. 2006)

This thesis is based on the second to last topic and the now well understood concept that the performance of seismic-isolated structures is enhanced by the use of passive energy dissipation devices. A control system consisting of a combination of the seismic isolation system and control devices, such as passive, active or semi-active control elements is often referred to as a hybrid control system (Akira Nishitani 2001; Nagashima et al. 2001; Ricciardelli et al. 2003; Skinner et al. 1993; Watakabe et al. 2001; Yang and Agrawal 2002). Among different combinations that are possible for a hybrid approach, semi-active control systems are attractive for use with base isolation systems because of their mechanical simplicity, low power requirements, and large controllable force capacity (Chase et al. 2007; Feng 1993; Feng and Shinozuka 1992; Yang and Agrawal 2002). However, the range of applicable structures for this type of

base isolation is still narrow due to technical difficulties in the isolation layer. Thus, a modified system concept needs to be defined to broaden the applicability and efficacy of these approaches to cover a wider range of structures. Especially, tall and flexible buildings those are not well suited to any form of base isolation.

The basic idea behind the proposed research is to develop a combination of semi-active resetable devices and modified structural isolation systems, and merge them into existing tuned mass damper system concepts. More specifically, to expand effective application of isolation techniques, it is proposed to focus on certain storeys of the structure as the main target for isolation. The isolation layer is thus located between separated storeys of the structure. This approach creates a large, yet fully functional tuned mass. Conceptually, it combines emerging semi-active technologies with traditional tuned mass and base isolation concepts to broaden and merge the applicability of all of these approaches to provide improved, more robust performance.

1.2 Objectives and Scope

The primary objective of this research is to evaluate the efficacy of the semi-active tuned mass damper building (SATMD) system concept. Performance will be assessed by statistically enumerating seismic response improvements compared to a traditional optimised Passive TMD (PTMD) system for multi-storey structures for a series of input ground motions. Structurally, this research focuses on the seismic response of moment resisting frames, and its scope looks at four main areas:

1) The understanding of the control ability and special features of resetable devices
2) The application of resetable devices to semi-active structural control systems
3) The overall concept of modified tuned mass damper system utilizing large partial mass of structure as a tuned mass, including design issues
4) The statistical performance-based seismic response comparison of No TMD (uncontrolled), PTMD, and SATMD building systems to provide results suitable for use in creating modern and emerging design guidelines

To investigate the fundamental ability of resetable devices in this role, spectral analysis methods have been used on standard 2-DOF TMD design models. The structures selected for MDOF time history analysis using these results are 12-storey, moment resisting linear and nonlinear frames. All analysis process have been developed using three suites of probabilistically scaled earthquakes representing a wide range of seismic excitation characteristics from the maximum likely event to the maximum possible event.

1.3 Preface

Chapter 2 introduces various structural control methodologies with the focus on a semi-active control and tuned mass damper (TMD) systems. The control properties and some aspects of TMD parameters are outlined. In addition, several modified seismic isolation systems that allow greater flexibility in structural control and applications are presented

Chapter 3 presents a structural configuration of TMD building systems. In addition, the details of the design and dynamic properties of resetable device are described in this chapter. Chapter 4 gives statistical methodology with earthquake suites that are used in the simulations to assess the TMD building systems. Chapter 5 describes the spectral analysis procedure of simplified 2-DOF TMD building systems that investigates the efficacy of TMD building systems, highlighting the benefits of SATMD systems. This chapter also provides the design, modelling and validation of TMD building systems which are utilised in MDOF applications.

Chapter 6 introduces a prototype 12-storey framed reinforced concrete structure for investigating the response properties of realistic multi-storey structures with the concept of TMD building systems. This chapter also describes modelling techniques and related computational methods. Analytical qualitative results for the prototype multi-storey TMD building systems (10+2 and 8+4 storeys) are presented in Chapter 7, while those for the retrofit or structural upgrade applications of being added new stories on a structure (12+2 and 12+4 storeys) are presented in Chapter 8. These chapters describe realistic novel structural configuration where upper several storeys

of the structure are utilised as the damping mechanism. In addition, these chapters present a selection of results for the structures investigated using several statistically calculated response indices, enabling effective comparisons of the different cases of TMD building systems.

In Chapter 9, a multi-storey nonlinear MDOF TMD building system is developed to predict the actual seismic responses of controlled buildings for possible earthquake excitations. The development of nonlinear building systems with the inclusion of structural nonlinear effects is outlined, followed by an explanation of how this is used as part of a time history analysis. In particular, energy and damage-based response indices are developed to demonstrate the accurate and valid controlled performances of the TMD building systems.

A brief summary of previous discussion and the primary conclusions of this research are presented in Chapter 10, along with suggestions for future developments leading from this research.

2 Structural Control

2.1 Introduction

The control of structural vibrations produced by earthquake or wind loads can be done by various fundamental means. These conceptual approaches include modifying rigidities, masses, damping, or shape, and by providing passive or active counter forces. To date, some methods of structural control have been used successfully and newly proposed methods offer the possibility of extending applications and improving efficiency (Housner et al. 1997).

In recent years, considerable attention has been paid to research and development of structural control devices. Furthermore, serious efforts have been undertaken in the last two decades to develop the structural control concept into a workable technology. It is now established that structural control is an important part of designing important new structures, such as hospitals, and, in some cases, for retrofitting existing structures for earthquake and wind. However, to date most existing and planned strategies are passive tuned mass or isolation approaches.

Over the years, many control algorithms and devices have been investigated, each with its own merits depending on the particular application and desired effect. Clearly, the ability to make direct comparisons between systems employing these algorithms and devices is necessary to focus future efforts and to set effective goals and specifications. One approach to achieving this goal is to consider consensus approved, high-fidelity, analytical benchmark models (He and Agrawal 2007; Loh and Chang 2006; May and Beck 1998; Samali and Al-Dawod 2003; Samali et al. 2003; Xu et al. 2006) that allow researchers in structural control to test their algorithms and devices and to directly compare results.

The structural model in early research was considered to remain perfectly elastic. However, large magnitude earthquakes cause inelastic behaviour in nonlinear responses. Therefore, the pursuit of nonlinear analysis for the seismically excited building has been advocated (Barroso 1999; Hunt 2002), as both the structural

damage and large motion hysteretic structural damping processes are inherently nonlinear. Therefore, nonlinear evaluation models can portray the salient structural dynamics for which appropriate evaluation criteria and control constraints can be presented for design problems (Barroso et al. 2003; Hunt 2002; Ohtori et al. 2004; Rodgers et al. 2007b).

The focus of many previous structural control design investigations has been the reduction of transient interstorey drifts, which have historically been used as an indicator of structural damage. However, other evaluation criteria need to be considered to include building responses, building damage and energy dissipation, control devices, and control strategy requirements for multi-purpose based seismic design (Barroso et al. 2003; Hunt 2002; Ohtori et al. 2004; Rodgers et al. 2007b). These metrics would include hysteretic energy, permanent and RMS mean drifts, peak and RMS mean acceleration, energy absorbed by control devices, and potentially others. All of these metrics represent a form of potential damage and thus repair cost to the building on occupants and contents. In addition, the use of a wide variety of realistic ground motion excitation that are representative of broad ranges of potential inputs and the suitable methods of statistical assessment are another important factor, but rarely considered, for the accurate outcome of structural control (Barroso et al. 2003; Chase et al. 2003; Chase et al. 2004b; Chase et al. 2005b; Hunt 2002; Rodgers et al. 2007b).

2.2 Passive, Active and Hybrid Control

A passive control system does not require an external power source. Passive control devices impart forces that are developed in response to the motion of the structure. The energy in a passively controlled structural system, including the passive devices, cannot be increased by the passive control devices guaranteeing stability. Passive supplemental damping strategies, including base isolation systems (Andriono and Carr 1990; Andriono and Carr 1991a; Andriono and Carr 1991b; Charng 1998; Johnson et al. 1998; Skinner et al. 1993; Xu et al. 2006; Yoshioka et al. 2002), viscoelastic dampers (Park 2001; Tzou and Wan 1989), and tuned mass dampers

(Abdel-Rohman 1984; Ghosh and Basu 2006; Murudil and Mane 2004), are well understood and widely accepted by the structural engineering community. However, these passive device methods rely on exact tuning, are unable to adapt to structural change and varying usage patterns, and are not necessarily optimal for all potential loading conditions.

In comparison with passive control, active control of structural response is essentially characterized by the following two features: (a) a certain amount of external power or energy is required; and (b) a decision-making process based on real-time-measured data is involved. In this regard, active control includes a wide range of technologies. In an active control system, an external source powers control actuator(s) that apply forces to the structure in a prescribed manner. These forces can be used to both add and dissipate energy in the structure to achieve a desired, optimised response.

From the control-engineering point of view, active control systems consist of four inter-connected components or elements. These components are: the plant (i.e. building), the sensors, the control computer or controller, and the actuators. Each of these elements works as a subsystem and are mutually integrated such that the output from one component is the input to other components in a closed feedback control loop (Franklin et al. 1994). Full-scale implementation of active control systems have been accomplished in several research structures (Akira Nishitani 2001; Nagashima 2001; Samali et al. 2003), mainly in Japan. However, cost effectiveness and potential reliability considerations have limited any wide spread or non-research acceptance to date in comparison to passive solutions.

Hybrid control strategies have been investigated by many researchers to exploit their potential to increase the overall reliability and efficiency of the actively controlled structure. The common usage of the term “hybrid control” implies the combined use of active and passive control systems. For example, a structure equipped with distributed viscoelastic damping supplemented with an active mass damper (Inman 2001; Yang et al. 2004), or a base isolated structure with actuators to actively enhance performance (Barbat et al. 1995; Huang et al. 2003; Jalihal et al. 1994; Scruggs et al. 2006). Because multiple control devices are operating, hybrid control systems can alleviate some of the restrictions and limitations that exist when each system is acting

alone. Thus, higher levels of performance may be achievable. In addition, the hybrid control system is considered more reliable than a fully active system, as the passive elements are always effective regardless of the status of the active elements.

2.3 Semi-Active Control

Semi-active (SA) control systems are a distinctly and emerging class of active control systems. In this case, the external energy requirements are orders of magnitude smaller than typical active control systems. Typically, semi-active control devices do not add mechanical energy to the structural system (including the structure and the control actuators), therefore bounded-input bounded-output stability is guaranteed (Bobrow et al. 2000; Hunt 2002). Semi-active control devices are also often viewed as controllable passive devices. More specifically, their resistive or dissipative force produced via control of internal mechanisms based on external sensor feedback. Hence, they can combine the best elements of active and passive systems, or, in contrast, mitigate their less desirable features.

Because of their low power requirements and large controllable force capacity, semi-active systems provide an attractive alternative to active and hybrid control systems. Semi-active control strategies are particularly promising in addressing many of the challenges to wider application of control to civil engineering structures, by offering the reliability of passive devices, while maintaining the versatility and adaptability of fully active systems. Studies have shown that appropriately implemented semi-active damping systems perform significantly better than passive systems and have the potential to achieve, or even surpass, the performance of fully active systems (Dyke et al. 1996a; Dyke et al. 1996b). Examples of semi-active devices include variable-orifice fluid dampers (Jung et al. 2004; Wongprasert and Symans 2005), controllable friction devices (Akbay and Aktan 1990; Akbay and Aktan 1991), variable-stiffness devices (Nagarajaiah and Varadarajan 2001; Zhou et al. 2002), tuned liquid dampers (Fujino et al. 1992; Wu et al. 2005), and controllable fluid dampers (Gordaninejad et al. 2002; Symans and Constantinou 1997).

2.3.1 SA Stiffness Control Methods

Yang and Agrawal (2002) presented the safety performances of various types of hybrid control systems, which consist of a base isolation system and SA dampers for protecting nonlinear buildings against near-field earthquakes. Djajakesukma et al. (2002) reported SA stiffness damper systems with various control laws, such as resetting control, switching control, Linear Quadratic Regulator (LQR) and modified LQR systems and compared results to uncontrolled and passive control cases. Similarly, Chase et al. (2003; 2004a) proposes a series of SA control laws based on optimal control design, and presented results as cumulative hazard distribution based on responses to suites of ground motions.

2.3.2 SA Control with Resetable Devices

Resetable devices are essentially fluid springs that are able to alleviate pressure to dissipate energy by resetting their effective rest length (Bobrow 1997; Bobrow et al. 2000; Jabbari and Bobrow 2002). They also focused on the basic analytical techniques needed to characterise structural systems that use a resetable SA device for vibration suppression. Barroso et al. (Barroso et al. 2003; Chase et al. 2003; Chase et al. 2004b) and Hunt (2002) presented extensive investigation of the ability of SA control methods utilizing resetable devices to mitigate structural response in the presence of hysteretic, geometric and yielding nonlinearities under various intensity level seismic hazard suites to define control efficiency and seismic hazard statistics. Yang et al. (2000) suggested that a general resetting control law based on the Lyapunov theory for a resetting SA damper and compared this with a switching control method through extensive numerical simulations. Finally Rodgers et al. (2007b) presented a spectral analysis and performance-based design guidelines for suing resetable SA devices.

2.4 Tuned Mass Damper Systems

2.4.1 The Principle of TMD systems

TMD systems are a practical well accepted strategy in the area of structural control for flexible structures, and particularly for tall buildings. It consists of added mass with properly tuned spring and damping elements, providing a frequency-dependent hysteresis that increases damping in the primary structure. The mechanism of suppressing structural vibrations by attaching a TMD to the structure is to transfer the vibration energy of the structure to the TMD and to dissipate the energy in the damper of the TMD. In other words, the frequency of the damper is tuned to a particular structural frequency so that when that frequency is excited, the TMD will resonate out of phase with the structural motion.

It is not always necessary to dissipate a large amount of energy. Instead, the TMD can reduce the amount of energy that goes into the system by changing the phase of the vibration. The addition of a TMD, in fact, transforms the lightly damped first mode of the uncontrolled structure into two coupled and highly damped modes of the 2-DOF modal system.

Compared to control devices that are connected to structural elements or joints, the TMD involves a relatively large mass and displacements. The method used to support the mass and provide precise frequency control is an important issue in the design of a TMD. Thus, the ultimate performance of the TMD system is limited by the size of the additional mass, where is typically 0.25~1.0% of the building's weight in the fundamental mode.

In some cases, spacing restrictions will not permit traditional TMD configurations. This limitation has led to the installation of alternative configurations, including multi-stage pendulums, inverted pendulums, and systems with mechanically-guided slide tables, hydrostatic bearings, and laminated rubber bearings. Coil springs or variable stiffness pneumatic springs typically provide the stiffness for the tuning of most types of TMDs.

A number of TMDs have been installed in tall buildings, bridges, towers, and smoke stacks for response control against primarily wind-induced loads (Kwok and Samali 1995). In terms of TMD configuration there is also a large variety. The first structure in which a TMD was installed appears to be the Centrepoint Tower in Sydney Australia (Kwok and Macdonald 1990). There are some buildings in the United States equipped with TMDs or tuned liquid dampers (TLDs), the Citicorp Center in New York City (McNamara 1977) and the John Hancock Tower in Boston (Khan 1983) and TransAmerica Tower in Sanfransisco (Balendra et al. 1998). In Japan, the first TMD was installed in the Chiba Port Tower (Kawabata et al. 1990; Obtake et al. 1992), followed by installations in the Funade Bridge Tower, Osaka (Ueda et al. 1993), and in steel stacks in Kimitsu City (Soong and Dargush 1997), among others. Table 2-1 shows a number of applications of the TMD system as a passive damping device.

Table 2-1 Worldwide applications of Tuned Mass Dampers (Kwok and Samali 1995)

Name and type of structure	City/Country	Type and number of dampers	Date of installation	Natural frequencies/ Effective damper mass
CN TowerTV antenna (553m)	Toronto, Canada	Tuned mass damper	1973	-
John Hancock Building (244m)	Boston, USA	Tuned mass dampers	1977	0. 14 Hz / 2 x 300t
City Corp Center (high-rise building) (278m)	New York, USA	Tuned mass damper	1978	0. 16Hz / 370t
Sydney Tower (305 m)	Sydney, Australia	Tuned mass damper (pendulum type)	1980/1	0. 10, 0. 50 Hz / 20 t
Al Khobar chimneys (120 m)	Saudi Arabia	Tuned mass damper	1982	0. 44 Hz / 7t
Ruwais Utilities chimney	Abu Dhabi	Tuned mass damper	1982	0. 49 Hz / 10t
Deutsche Bundespost cooling tower (278 m)	Nornberg, Germany	Tuned mass damper	1982	0. 67 Hz / 1. 5t
Yanbu Cement Plant chimney (81 m)	Saudi Arabia	Tuned mass damper	1984	0. 49 Hz / 10t
Hydro-Quebec wind generator	Canada	Tuned mass damper	1985	0. 7-1. 2 Hz / 18t
Chiba Port Tower (125m)	Chiba, Japan	2 Tuned mass dampers	1986	0. 43-0. 44 Hz / 10, 15t
Pylon, Aratsu Bridge (cable-stayed)	Japan	Tuned mass damper	1987	-
Pylon, Yokohama Bay Bridge (cable-stayed)	Yokohama, Japan	Tuned mass damper	1988	-
Bin Quasim Thermal Power Station (70 m)	Pakistan	Tuned mass damper	1988	0. 99 Hz / 4. 5 t
Tiwest Rutile Plant chimney (43 m)	Australia	Tuned mass damper	1989	0. 92 Hz / 0. 5t
Fukuoka Tower (151 m)	Fukuoka, Japan	2 Tuned mass dampers	1989	0. 31-0. 33 Hz / 25, 30 t
Higashiyama Sky Tower (134 m)	Nagoya, Japan	Tuned mass damper	1989	0. 49-0. 55 Hz / 20t
Pylon, Bannaguru Bridge (cable-stayed)	Japan	Tuned mass damper	1990	-
Crystal Tower (157 m)	Osaka, Japan	2 Tuned mass dampers	1990	0. 24-0. 28 Hz/180, 360 t
Huis Ten Bosch Domtoren	Nagasaki, Japan	Tuned mass damper	1990	0. 65-0. 67 Hz / 7. 8t
Hibikiryokuchi Sky Tower (135 m)	Kitakyushu, Japan	Tuned mass damper	1991	-
HKW chimney (120m)	Frankfurt, Germany	Tuned mass damper	1992	0. 86 Hz / 10t
BASF chimney (100 m)	Antwerp, Belgium	Tuned mass damper	1992	0. 34 Hz / 8. 5 t
Siemens power station (70 m)	Killingholme, UK	Tuned mass damper	1992	0. 88 Hz / 7t
Rokko island P & G (117 m)	Kobe, Japan	Tuned mass damper (pendulum type)	1993	0. 33-0. 62 Hz / 270 t
Chifley Tower (209 m)	Sydney, Australia	Tuned mass damper (pendulum type)	1993	400 t
Al Taweeiah chimney (70m)	Abu Dhabi	Tuned mass damper	1993	1. 4Hz / 1. 35 t
Akita Tower (112 m)	Akita, Japan	Tuned mass damper	1994	0. 41 Hz

2.4.2 Passive, Active and Hybrid TMD Systems

One of the limitations to the TMD design is the sensitivity related to the narrow bandwidth of the frequency tuned control it provides and the resulting potential fluctuation in tuning the TMD frequency to the controlled frequency of a structure. If the frequency of the disturbing force shifts even slightly, then the effect of the TMD is diminished. In some cases, poor tuning can even amplify the vibration, rather than suppress it. Mis-tuning or off-optimum damping can thus significantly reduce the effectiveness of the TMD, which means that the TMD is not entirely reliable or robust despite its passive nature.

In addition, a TMD is more effective when the ground motion has significant spectral content at the TMD fundamental mode frequency. Further away from this frequency, a TMD may have much less effect rendering it less effective for same ground motions. Therefore, it is difficult to draw general conclusions characterising the seismic effectiveness of a TMD system, especially when the structure includes inelastic behaviour (Chey 2000).

The passive TMD (PTMD) is undoubtedly a simple, inexpensive and somewhat reliable means to suppress the undesired vibrations. However, its performance is limited because of the fixed damper parameters. In an attempt to increase the performance of the TMD without incurring the problems noted above, active TMD (ATMD) systems have been proposed. Chang and Soong (1980) introduced an active force to act between the structure and the TMD system. Abdel-Rohman (1984) proposed a process for designing an effective ATMD system to control a tall building subjected to stationary random wind forces by using the pole-assignment control design method. The results suggested that the design of an optimal ATMD required at least a parametric study to select the ATMD parameters. Furthermore, common feedback control methods using displacement, velocity, full state, and acceleration feedback for the ATMD have been studied by many researchers (Chang and Yang 1995; Li et al. 2003; Nagashima 2001; Yan et al. 1999). However, while these systems avoid many issues of PTMD systems, fully active systems require significant power sources and entail significant complexity.

2.4.3 Semi-Active TMD System

It has been reported that ATMDs can provide better suppression of structural vibrations than PTMDs. However, ATMDs have the disadvantages of added complexity, high operational and maintenance costs, and high power requirements. Hence, they are considered less reliable than passive systems, limiting implementation of to special certain cases.

Recognising both performance benefits, as well as the limitations of active systems, a new class of semi-active tuned mass dampers (SATMDs) has been introduced using controllable variable damping or stiffness devices. Since only a small amount of active energy is required to modulate the damping of such devices, the need for the large energy supply required by the ATMD is eliminated. In addition, its adoptive response to structural response sensor feedback provides the wide bandwidth of control, unlike narrowly tuned PTMDs. Hence, it provides an extremely promising alternative to PTMDs and ATMDs.

Hrovat et al. (1983) used semi-active TMDs with variable damping components for the control of wind-induced vibrations in tall buildings. Abe (1996) studied a variation of semi-active TMDs with pulse generators for the seismic protection of civil structures. Setareh (2001) studied the application of semi-active 'ground hook' dampers, which have been used for vehicle body vibration control, as an element of TMD systems. He also adopted semi-active dampers for the reduction of floor vibrations due to human movements (Setareh 2002). Pinkaew and Fujino (2001) presented a SATMD with variable damping under harmonic excitation and it showed that the semi-active optimal control becomes a clipped optimal control law.

Meanwhile, an empirical algorithm for the optimization of the properties of SATMDs based on the measured response of the main structure has been presented by Ricciardelli et al. (2000). Their numerical example showed that the optimization of the TMD damping did not bring a reduction of the main structure response, but rather to a reduction of the displacement of the added mass. This result can be explained by the low sensitivity of the response of the main system to the TMD damping. Shen

(2001) developed a semi-active control scheme using a functional switch which is able to finely adjust stiffness and damping for the TMD system. Aldemir (2003) studied the optimal performance of a magnetorheological (MR) damper, as is used in a tuned mass damper to reduce peak responses of a single-degree-of-freedom structure subjected to a broad class of seismic inputs. It was numerically shown that the optimal performance of the MR damper is always better than the equivalent passive-tuned mass damper for all the investigated cases, and that the MR damper has a great potential in suppressing structural vibrations over a wide range of seismic inputs. The effectiveness of a semi-active variable stiffness tuned mass damper (SAIS-TMD) in response control of 76-storey tall buildings was studied and its performance was evaluated analytically (Varadarajan and Nagarajaiah 2004). The SAIS-TMD system had the distinct advantage of continuously retuning its frequency due to real time control, hence, the system was robust to changes in building stiffness and damping.

Finally, Mulligan et al. (2006; 2007) investigated spectral analyses and design of SATMD systems for suites of probabilistically scaled events. Their results indicated that resetable devices allowed for simpler tuning design that was very robust to variation in structural parameters. They also showed that resetable SATMD systems were more robust to variations in ground motion input than equivalent PTMD systems.

2.4.4 The optimisation of TMD parameters

While, the basic principles of TMDs on reducing structural response have been well established, optimal TMD configurations are a quite a different problem. In the design of any control device for the suppression of undesirable vibrations, the aim would be to provide optimal damper parameters to maximize its effectiveness. The chief design response oriented parameters of the TMD are its tuning ratio (the ratio of the damper frequency to the natural frequency of the structure) and damping ratio. The other important design parameter is the mass ratio (the ratio of the damper mass to the mass of the structure). This latter parameter is generally fixed at 0.5~1.0% from practical considerations and its optimization is not of general interest.

Considerable research has been devoted to the study of TMD performance, to enable proper selection of absorber parameters. In the classical work by Den Hartog (1956), simple expressions for the optimum tuning ratio and damping ratio of a mass damper were derived. These expressions were based on minimising the displacement response of an undamped primary system subjected to sinusoidal excitation.

To obtain the analytical solution for the optimal values of the parameters that minimise the dynamic response of the building measured, Crandall and Mark (1963) obtained the mean square response of the stationary process when the spectral density is known. When the input spectrum is assumed to be ideally white, a constant input for all frequencies, the mean square of the response was determined. Using their process, Chey (2000) derived simple expressions for the optimal values of the frequency ratio and damping ratio of TMD in terms of displacement and acceleration. For practical application to a real system, practical parameters for the TMD, such as the optimal TMD damping stiffness, and optimal damping coefficient were also derived.

For the case of damped primary structure, it is difficult to obtain closed-form solutions for the optimum damper parameters. Ioi and Ikeda (1978) presented empirical formulae for optimum stiffness and damping of a TMD, based on the minimization of the acceleration response of a lightly damped structure. Randall et al. (1981) used numerical optimization procedures for evaluating the optimum TMD parameters, while considering damping in the structure. In the procedure proposed by Thompson (1981) for a damped structure with TMD, the tuning ratio has been optimized numerically and then using the optimum value of the tuning ratio the optimum damping in the TMD is obtained analytically. Warburton (1982) carried out a detailed numerical study for a lightly damped structure with TMD, subjected to both harmonic and random excitations. The optimal damper parameters of tuning ratio and damping ratio for various values of mass ratio and structural damping ratio are presented in the form of design tables. Fujino and Abe (1993) employed a perturbation technique to derive formulas for optimal TMD parameters, which may be used with good accuracy for mass ratios less than 0.02 and for very low values of structural damping less than 5~10%.

Thus, for the realistic general case with damping in the primary system, the optimal TMD parameters have to be evaluated either numerically or from empirical expressions. When damping is added to the primary system, the existence of 'fixed-point' frequencies is lost. These fixed point frequencies are frequencies at which the transmissibility of vibration is independent of the damping in the attached control device making closed form design straight-forward (Den Hartog 1956).

However, it is possible that even for moderately damped structures the existence of two 'fixed-point' frequencies may still be assumed to be valid in an approximate sense. Based on the theory developed by Den Hartog (1956) in obtaining the optimal criteria of a mass damper attached to an undamped mass subjected to harmonic excitation, an alternative closed-form solution for the optimum tuning ratio of the TMD for damped structures has therefore been derived (Ghosh and Basu 2006). Ghosh and Basu presented a closed-form expression for the optimum tuning ratio of a TMD attached to a damped primary structure modelled as an SDOF system. It is based on the 'fixed-point' theory, which is approximately valid for low-to-moderate structural damping. The higher mass ratio case exhibited closer intersection of the transfer function curves to form the 'fixed-points' than lower mass ratio cases in this work. The proposed expression for the optimal tuning ratio was therefore a function of the mass ratio and the structural damping, and has been evaluated for different values of these parameters. The values of the optimum tuning ratios from the proposed expression have been found to be in close agreement with those obtained numerically validating the overall approach.

Using numerical searching techniques the optimum parameters of a TMD system for damped main systems has been investigated by several researchers (Bakre and Jangid 2006; Chey 2000; Jangid 1999; Tsai and Lin 1994). The optimum parameters have been obtained in these studies for various combinations of minimising different response parameters and/or excitation. A curve-fitting technique can then be used to determine explicit expressions for the optimum parameters of the TMD system.

Hoang and Warnitchai (2005) presented a new method to design multiple TMDs for minimising excessive vibration of linear structures. The methods used a numerical optimiser following a gradient-based non-linear programming algorithm to search for

optimal TMD parameters. The target response is formulated as a quadratic performance index which can be efficiently computed by solving a Lyapunov equation.

Meanwhile, optimisation of the absorber weight, with constraints on the combined weight of the main system and attached absorber, has been also done. Reasons behind these analyses include project specifications that limit the choice of fabrication materials, one-piece manufacturing, practical design, economic manufacturing, minimising main system vibration, and other ergonomic reasons (Jimmy 1990). Once a main structure is approximated into a one mode beam structure and a random excitation into a Gaussian white noise excitation, the optimal mass ratios can then be determined to minimise the effective main system's response, and create overall TMD design.

2.4.5 Influence of ground motion and nonlinear system

One of the central issues of TMD effectiveness is the matter of optimum TMD parameters. However, another objective of parametric studies of TMD performance is to examine how the optimum TMD for earthquake excitation is affected by the parameters that characterize the motion. This examination is particularly important considering that optimum solutions are developed from approximated systems and inputs that may not fully reflect realistic seismic excitation or structural conditions.

An examination of the effect of ground motion characteristics on the effectiveness of TMD was made using a nonstationary random vibration formulation (Bernal 1996). His results indicate that optimum TMD damping is insensitive to the bandwidth and depends on the duration to period ratio only for relatively low values of this quotient, where the optimum decreases with decreasing duration. The results suggest that TMD units may be able to provide notable reductions in spectral ordinates for periods near the dominant motion period when the excitation is narrow band and of long duration, which is not always the case in seismic events.

Soto-Broto and Ruiz (1999) analyzed the effectiveness of TMD on buildings subjected to moderate and high intensity motions. The results show that the effectiveness of TMD is higher for systems with small non-linearity produced by small and moderate earthquakes, than for systems with the highly non-linear behaviour associated with high intensity motions. They recommended using more than one TMD on the roof of the structures to cover a wider range of periods of vibration and account for such nonlinearities, but of the cost of significant added mass.

Murudil and Mane (2004) investigated the effectiveness of TMDs n controlling the seismic response of structures and the influence of various ground motions. Their research showed that the effectiveness of a TMD for a given structure depends on the frequency content, bandwidth and duration of strong motion. However, the seismic effectiveness of the TMD is not affected by the intensity of ground motion. Specifically, TMDs are more effective for long duration earthquake and when the structural frequency is close to the central frequency of ground motion. A TMD is also reasonably effective for broad banded motions across the spectrum of structural frequencies. However, a TMD is also effective for narrow banded motions, if the structure and ground motion frequencies are close to each other, but much less so if they are not close. Effectiveness and optimum TMD parameters are not affected by increasing peak ground acceleration values, keeping all other parameters constant. All of these results validate or match other results in this area.

The effectiveness of TMD in vibration control of buildings was investigated under moderate ground shaking caused by long-distance earthquakes with frequency contents resembling the 1985 Mexico City (SCT) or the 1995 Bangkok ground motion. More specifically, the accumulated hysteretic energy dissipation affected by TMD was examined (Lukkunaprasit and Wanitkorkul 2001). Unlike in an elastic system, the commonly used peak displacement ratio could not give a good indication of TMD effectiveness for an elasto-plastic building, since significant reduction in the dissipated energy may result in an elastic-plastic building with a TMD, even though only a small reduction in the displacement response is effected by the presence of the TMD. Thus, they recommended that the hysteretic energy absorption ratio should be supplemented as another performance index because it reflects the amount of dissipated energy in the yielding elements in both the controlled and uncontrolled

buildings. Hence, the extent of damage induced is separated from energy absorbed by the TMD or the TMDs effect.

Finally, Ruiz and Esteva (1995) evaluated and discussed the loss of effectiveness of TMDs on nonlinear systems. They concluded that the reductions on the structural response obtained by adding a TMD to nonlinear systems built on the compressive-clay zone of Mexico City, become small as the nonlinearity increases. This fact led to the conclusion that the use of TMDs is therefore limited to structures designed to develop a weak or a moderate nonlinear behaviour and in areas that don't have very soft soil sites on excessive soil structure interaction effects.

2.5 Seismic Isolation

Seismic isolation consists essentially of the installation of mechanisms that decouple the structures and their contents from potentially damaging earthquake-induced ground motions. This decoupling is achieved by increasing the flexibility of intervening or connecting layer, along with providing appropriate damping to the elements of this isolation layer. Careful studies have been made of structures for which seismic isolation may find widespread application (Kelly 1990; Skinner et al. 1993).

In seismic isolation, the fundamental aim is to substantially reduce the transmission of the earthquake forces and energy into the structure. This objective is achieved by mounting or linking the structure on an isolation system with significant horizontal flexibility so that during an earthquake, when the ground moves strongly under the structure, only moderate motions are transmitted to the structure itself. As isolator flexibility increases, movements of the structure relative to the ground may become a problem under other vibration loads applied above the level of the isolator. In addition, isolator flexibility is limited to prevent extensive relative motion of the structure to the ground to protect lifelines and services.

2.5.1 Base Isolation Systems and Designs

Successful base isolation design requires adequate understanding of the influence of each parameter in the isolation system and the superstructure on the overall seismic performance of the isolated building. The primary function of an isolation device is to support the superstructure, while providing a high degree of horizontal flexibility, resulting in a long fundamental period for the isolated building as a rigid mass on the isolator. Isolation devices used to meet these requirements include laminated elastometric rubber bearings (Tyler 1991), lead-rubber bearings (Cousins et al. 1992; Dowrick et al. 1992; Robinson and Greenbank 1975), yielding steel devices (Kelly et al. 1972; Skinner et al. 1975; Tyler and Skinner 1977), friction devices (PTFE sliding bearings) (Tyler and Skinner 1977) and lead extrusion devices (Cousins and Porritt 1993; Parulekar et al. 2004).

Skinner et al. (1993) indicated that a base isolator with significant hysteretic force-displacement characteristics can provide the desired properties of isolator. In particular, they have significant flexibility, high damping and force limitation under horizontal earthquake loads, as well as together with high stiffness under smaller horizontal loads to limit wind-induced motions. Kelly (1990) gave a brief introduction to the response mechanisms of base isolated buildings through a two degrees of freedom linear system for simplified design. This approach assumes that the isolation provided is enough to ensure the resulting (limited) structural response is in an elastic regime.

The effectiveness of any isolation system to mitigate the seismic response is obtained through its ability to shift the fundamental frequency of the system out of the range of frequencies where the earthquake is strongest. Similarly, Skinner et al. (1993) demonstrated that the most important feature of seismic isolation is its increasing of the natural period of the structure to achieve this task. Because the period is increased beyond that of the earthquake, resonance and strong excitation are avoided, the input motion is primarily in a lower magnitude frequency range and thus smaller, and the overall seismic acceleration response is thus reduced.

Simplified methods of design for base isolated structures have been proposed by Turkington et al. (Turkington et al. 1989a; Turkington et al. 1989b), Antriono and Carr (Andriono and Carr 1991a; Andriono and Carr 1991b; Skinner et al. 1993) and Mayes et al. (1992), among others. In particular, Andriono and Carr indicated that base isolated structures have the ability to significantly reduce the ductility demands in the superstructure compared with those of unisolated structures. This reduction makes possible the simplification of structural detailing and other seismic design considerations required by more conventional structures and design approaches. Therefore, a wider choice of architectural forms and structural materials is available to the designer with base isolated systems.

While these performance-based code provisions and simplified design procedures give high-level guidance regarding acceptable and unacceptable levels of performance, there is a mounting body of evidence that base isolation may not always provide adequate protection (Yoshioka et al. 2002). One concern is the possibility of localized buckling of the isolator devices and/or collapse of the structure caused by excessive lateral displacement of isolator elements with details on the appropriate analysis procedures being described by Naeim and Kelly (1999). A second area of concern, raised by Johnson et al. (1998) and Spencer and Nagarajaiah (2003), points to the inability of base isolation to protect structures against near-source, high-velocity, long-period pulse earthquakes. In similar studies, Hall et al. (1995) and Heaton et al. (1995) express concerns about excessively large base drifts caused by strong, near-fault ground motions.

Using isolators at the base of building is a still leading approach in the seismic design of structures. However, this technique is not applicable in a variety of buildings due to technical difficulties in the isolator technology or in tall structures where overturning is a concern. The high cost of some isolator devices and their implementation in structures are other concerns in designing such systems. Further expansion in application of isolation methods requires more affordable techniques applicable to a wider range of structures and excitations.

2.5.2 Upper Storey Isolation Systems

The seismic isolation concept using TMD design principles has been extended to convert a structural system, especially a high-rise structural system, into a TMD system by specially designing the upper storey(s). TMDs of all possible types have the added advantage of being effective and feasible for taller structures where base isolation is not possible. To overcome the typical limitations of a small TMD mass ratio, it has been suggested that using a portion of the building itself as a mass damper may be more effective. In particular, one idea is to use the building's top storey as a tuned mass.

The concept of an 'expendable top storey' (Jagadish et al. 1979), or the 'energy absorbing storey' (Miyama 1992), is an effective alternative where the top storey acts as a vibration absorber for the lower storeys. Villaverde et al. (2002) studied a 13-storey building to assess the viability and effectiveness of a 'roof isolation' system aimed at reducing the response of buildings to earthquakes. Hence, the proposal to build a vibration absorber with a building's roof or upper storeys has the potential to become an attractive way to reduce structural and nonstructural earthquake damage in low- and medium-rise buildings as well as a mean of avoiding excessive added mass for a typical TMD design.

2.5.3 Mass Isolation Systems

The concept of vibration isolation is also extended to tall buildings using a technique that targets the mass of the structure as the main goal for the isolation purposes (Ziyaeifar 2002; Ziyaeifar and Noguchi 1998). The isolator layer in this approach is placed between the horizontal component of the mass and the lateral stiffness of the structure. By using this technique the main part of the mass of the system can be shifted to the low force and energy zone of the earthquake spectrum. This approach also increases the damping ratio of the structure to a level not achievable by other techniques. One of the proposals is to convert a mega-structural system to a mega-

sub-control system that exhibits structural efficiency by allowing a high rigidity of the system while keeping a minimum amount of structural materials (Feng and Mita 1995). Its additional advantage is its planning flexibility for substructures consisting of only several floors of the mega-structure. However, to date this approach has remained confined to simulation and research studies.

Similarly, Mar and Tipping (2000) presented their new high-performance seismic technology. This approach utilises stiffness control and passive damping to achieve high performance aseismic structural response. The system consists of a building's floors and columns (the gravity frame), which are connected to the lateral load resisting elements (the reaction frames) via a unique assembly of springs and passive dampers located at each floor. In this specific case, the gravity frame is laterally isolated from the base through slide bearings, as illustrated in Figure 2-1. Again, this concept is currently only examined in research studies.

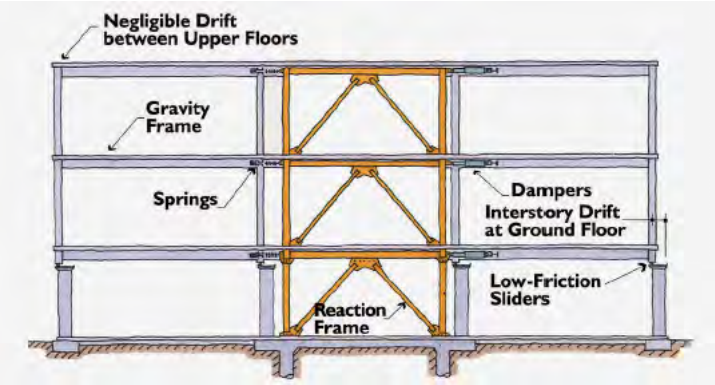

Figure 2-1 Gravity frame and reaction frame (Mar and Tipping 2000)

2.5.4 Mid-storey Isolation Systems

Some researchers (Charng 1998; Pan et al. 1995; Pan and Cui 1998) sought to evaluate the effect of using segmental structures, where isolation devices are placed at various heights in the structures and at the base to reduce displacements. Each segment may comprise a few stories and is interconnected by additional vibration isolation systems. Charng (1998) suggested three possible design methods to link two segments to prevent the occurrence of rocking modes and transmit gravity loads between the two segments as shown schematically in Figure 2-2.

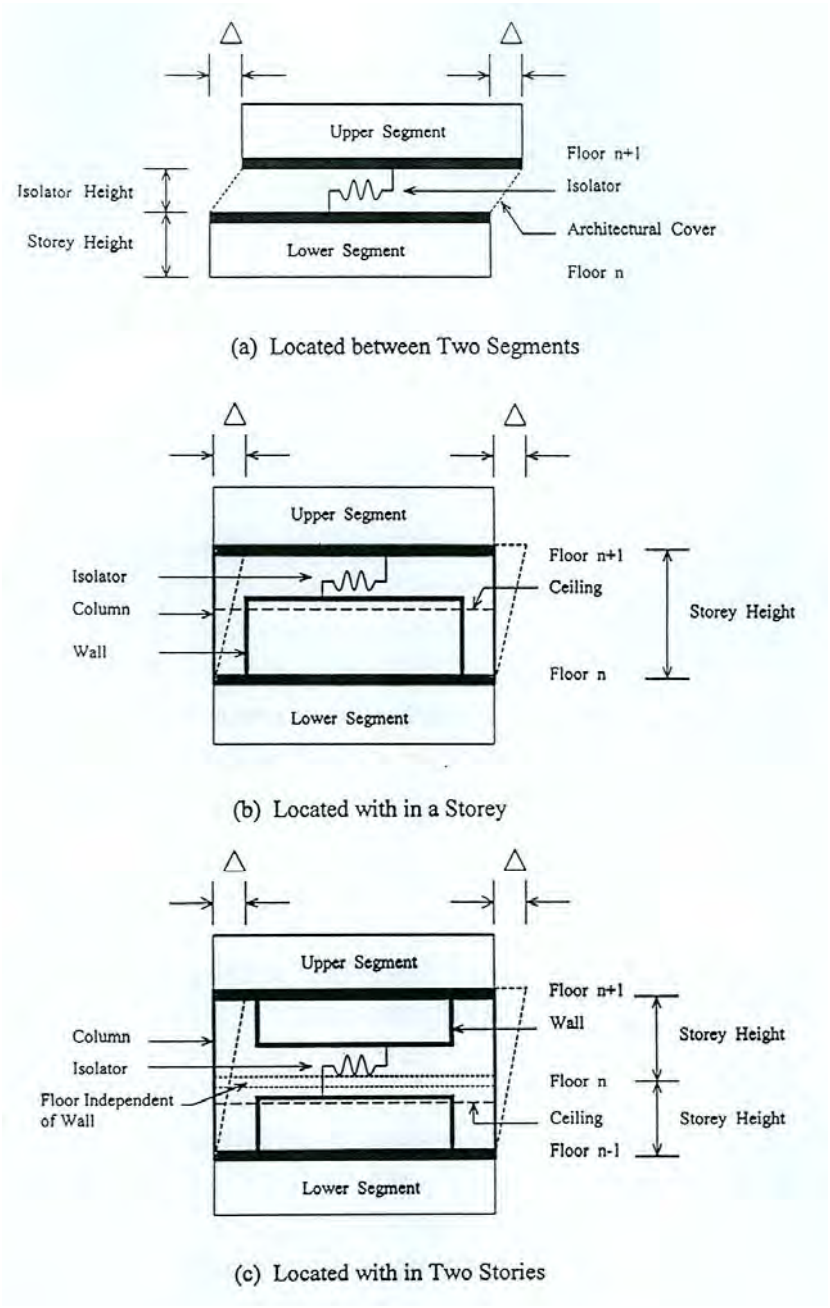

Figure 2-2 Different isolation installation options for segmental structures (Charng 1998)

Murakami et al. (2000) described the design of a multifunctional 14-storey building accommodating apartments, office rooms and shops, where a seismic isolation system is installed on the middle storey. In their paper, they obtain a result that the best building plan can be adopted by connecting different structural systems suited for each function with the mid-storey isolation structural system. Thus, seismic force to the building may be reduced by concentrating seismic energy dissipation in the isolation storey.

Sueoka et al. (2004) examined a 25-storey building with a mid-storey isolation interface between the 11^{th} floor and the 12^{th} floor. The building comprises office space at the upper floors and a hotel space at lower floors. To solve the large displacement problem at the isolation interface they introduced the different planning between the upper and lower sections by providing larger elevator shaft space in lower sections. Figure 2-3 shows the building design schematics. They also found that the response of the structure is affected by high frequency modes according to the vibration features of the upper and lower structures.

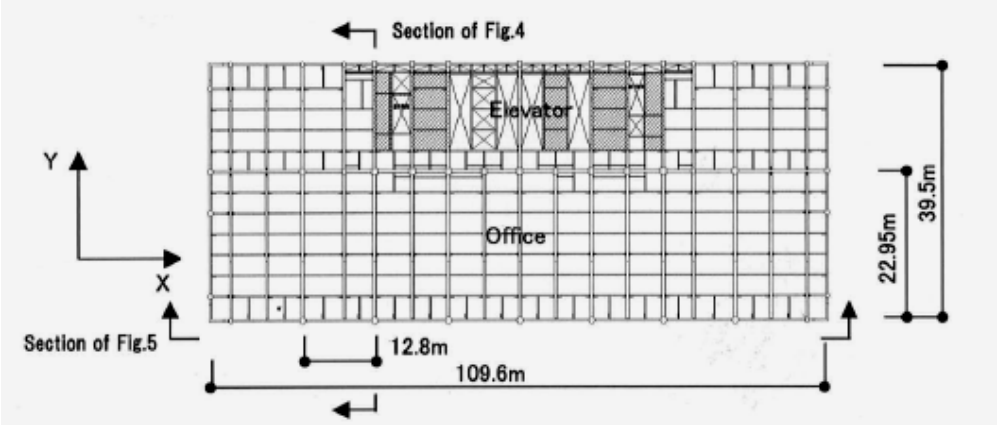

(a) Framing plan (Office)

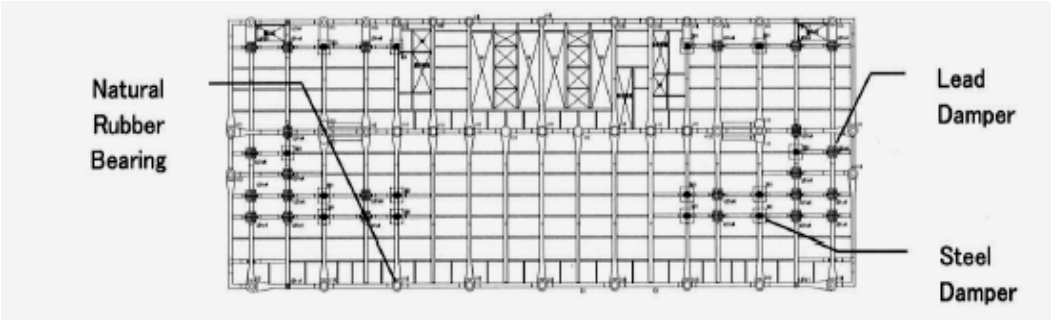

(b) Framing plan (seismic isolation interface)

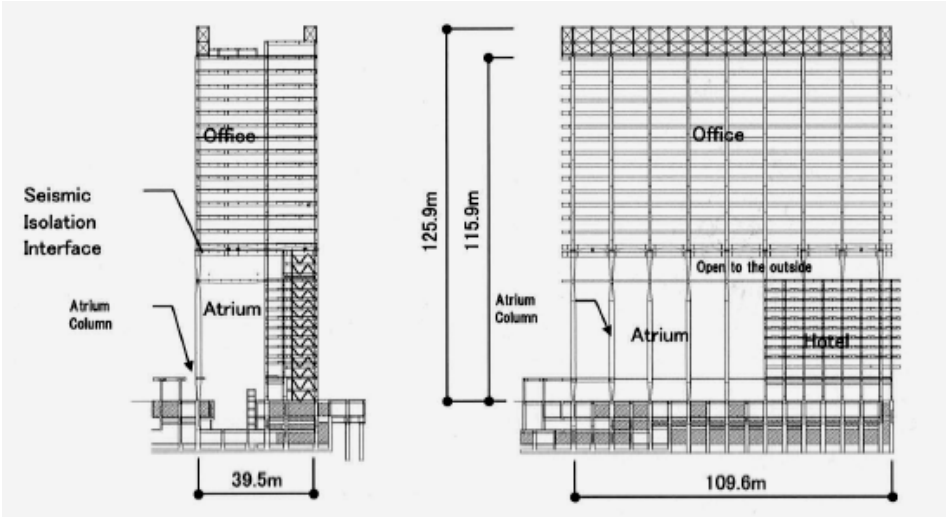

(a) Framing elevation (Y-frame) **(b) System of elevator (X-frame)**

Figure 2-3 Shiodome Sumitomo building with mid-storey isolation (Sueoka et al. 2004)

Another retrofitting application using mid-storey isolation, a 16-storey personnel-training centre of Taisei Corporation, is presented Kawamura et al. (2000). Mid-storey isolation was located at the 8th floor, as the building is partially underground from the 7th floor down. In the paper, the non-jack method was adopted to support the 6,500tf upper structure during cutting and reforming of the 22 columns. All piping, elevator shafts, staircases and walls were arranged to allow a maximum of 40cm of relative motion at the isolation layer.

Meanwhile, Zhou et al. (2004) introduced several examples of seismic isolation buildings in China using base isolation, basement isolation and storey isolation. One of these examples is the 2-storey RC frame platform with plane size 1,500m wide and 2,000m long that covers the city railway communication hub area. About 50 houses (9-storey RC frame) were built on the top floor of the platform using a storey isolation system.

Recently, semi-active coupled building control has been proposed. Zhu, et al. (2001) optimised the passive-coupling elements between two parallel structures under different circumstances. Emphasis was placed on the derivation of simple, effective algorithms for semi-active control that guarantees the power absorption from the primary structure at every time step.

Overall, isolation has been extensively studied and many concepts examined. Passive approaches predominate, but semi-active methods or combinations are emerging. Isolation as also been used at every like level. However, most concepts have remained in the province of research studies.

2.6 Summary

This chapter provides a fundamental basis and literature review to formulate present the concept of structural control as a means of mitigating or reducing earthquake damage potential. It is intended to provide the background to bridge the gap between conventional structural design and the emerging field of structural control that

actively manages structural response as it occurs. The text also contains some systematic approaches and strategy issues for structural control, highlighting the benefits of semi-active control strategies and the distinguishing features of resetable devices.

Tuned mass damper systems acting as resonance absorbers are also presented, along with a brief description of optimum TMD parameters, some TMD installed examples and the influence of ground motion on TMD systems. In these cases, added masses are placed in the uppermost storey and coupled to the building structure through springs and dampers.

Other topics covered include base isolation systems and several modified isolation systems as various approaches to earthquake resistant design. The good of these systems is to reduce the seismic demand rather than increasing the earthquake resistance capacity of the structure. Proper application of these technologies leads to better performing structures that will remain essentially elastic during large earthquakes.

Hence this chapter provides the fundamental background for active and semi-active structure. It then provides added depth on the three maim elements utilised in this thesis: 1) semi-active resetable devices; 2) tuned mass damper systems; 3) base isolation systems. These three elements are merged here to create the SATMD concepts developed and analysed in-depth in the subsequent chapters.

3 TMD Building Systems

3.1 Structural Configuration

The proposed TMD building system concept can be defined as an extension of the conventional TMD system, but using a large mass ratio. Due to the large mass ratio, the upper portion may experience large displacement. To avoid excessive lateral motion or stroke of the tuned mass, the upper portion can be interconnected by the combined isolation system of rubber bearings and a viscous damper (for the PTMD passive version) or a resetable device (for the resetable SATMD proposed here). When the building frame is implemented with the proposed TMD (PTMD or SATMD) system, the upper portion is supported by rubber bearings attached on the top of the main frame's columns. The system is shown schematically in Figure 3-1.

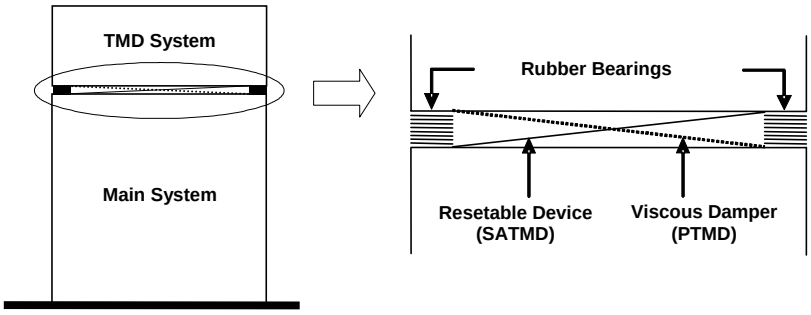

Figure 3-1 Schematic of model concept and resetable device

The overall mechanism of suppressing structural vibration induced by an earthquake is to transfer the vibration energy of the structure to the isolated upper storey. The transferred energy is dissipated at the isolation interface so that seismic force of the entire superstructure can be reduced. Thus, the overall effectiveness depends on the amount of energy transferred or the size of the tuned mass, and the ability of the isolating elements (viscous damper or resetable device) to dissipate that energy via the relative motions at the interface. Additional tradeoffs with respect to ease of tuning/design and ability to manage non-linearity and/or degradation, may also be a factor, as discussed in Chapter 2.

3.2 Spring and Damping Members

To model the effects of the TMD stiffness coefficient, the spring member which is incorporated to the program *Ruaumoko* was used. In *Ruaumoko*, this member may be used to model special effects in the structure or to represent members acting out of the plane of the frame but representing forces that act in the plane of the frame. Figure 3-2 shows the model structure of the spring member. An optimal passive TMD stiffness, $k_{2_{opt}}$ which was obtained from a parametric study, can be applied to the value of the spring stiffness option in the transverse direction. This stiffness represents optimal tuning for a PTMD. The spring member utilises a linear elastic hysteresis rule.

The TMD damping component is modelled using the damping or dash-pot member in *Ruaumoko*, and is defined as shown in Figure 3-3. This model represents the action of a local viscous energy dissipator that may exist in the structure and contribute to the damping matrix of the structure. An optimal TMD damping coefficient, $c_{2_{opt}}$, based on PTMD design can be used as the transverse damping coefficient. The linear elastic model was used as the hysteresis rule in this case, as well. The spring member and the damping member can be placed at the ends of a frame member that contains a mass providing the required mass ratio. The TMD structure is located at the top floor and has a role as a passive device to conrol the response of the framed structure. Through the response of the nodes corresponding to the TMD, the designer can examine the movement of the TMD itself such as the TMD stroke and acceleration.

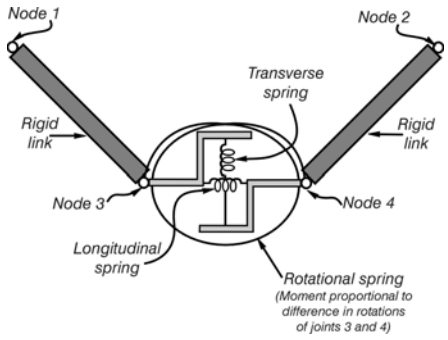

Figure 3-2 Spring member

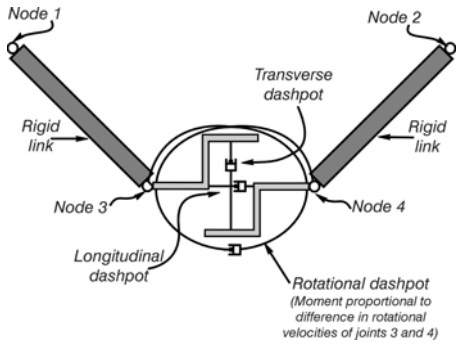

Figure 3-3 Damping member

3.3 Semi-Active Resetable Device

3.3.1 Introduction

Semi-active devices are particularly suitable in situations where the device may not be required to be active for extended periods of time, but may be suddenly required to produce large forces (Bobrow et al. 2000). The potential of semi-active devices and control methods to mitigate damage during seismic events is well documented (Barroso et al. 2003; Jansen and Dyke 2000; Yoshida and Dyke 2004). Ideally, semi-active devices should be reliable and simple.

Resetable devices fit these criteria as they can be constructed with relative ease and utilise well understood fluids, such as air. These attributes contrast with more complicated semi-active devices, such as electro-rheological and magneto-rheological devices (Dyke and Spencer 1996; Spencer et al. 1997). Instead of altering the damping of the system, resetable devices nonlinearly alter the stiffness with the stored energy of a compressed working fluid being released as the compressed fluid is allowed to revert to its initial pressure. This action releases stored energy, acting as a dissipater, and also effectively resets the device's spring rest length.

3.3.2 Device Dynamics

Resetable devices act as hydraulic or pneumatic spring elements, resisting displacement in either direction. However, they possess the ability to release the stored spring energy at any time, creating the semi-active aspect of these devices. Therefore, instead of altering the damping of the system directly, resettable devices non-linearly alter the stiffness with the stored energy being released, rather than returned to the structure, as the compressed fluid is allowed to revert to its initial pressure.

Schematically, the equilibrium position or rest length can be reset to obtain maximum energy dissipation from the structural system (Bobrow et al. 2000). Energy is stored

in the device by compressing the working fluid, such as air, as the piston is displaced from its centre position. When the piston reaches its maximum displaced position in a given cycle, the stored energy is also at a maximum and the device changes direction of motion. Thus, the reset criteria are determined to be the point of zero velocity at displacement peaks. At this point, the stored energy is released by discharging the working fluid to the non-working side of the device, thus resetting the equilibrium position of the device. Figure 3-4 shows the conventional resettable device configuration, with a valve connecting the two sides, as defined in (Bobrow et al. 2000). Note that this original design assumes that the stored energy and fluid can switch chambers relatively instantly, compared to the structural motion input to the device, or the significant supplemental damping and device performance will be lost.

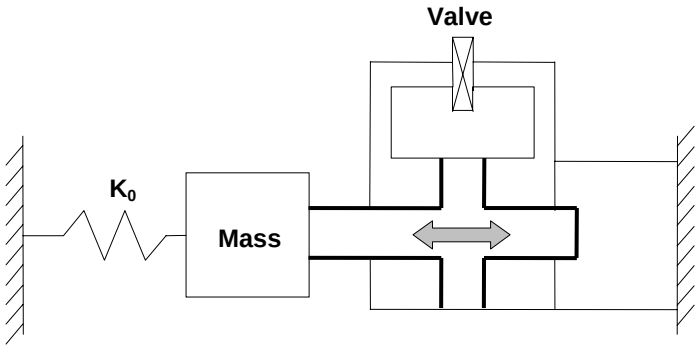

Figure 3-4 Schematic of a single-valve, resettable actuator attached to a single-degree-of-freedom system.

The prior largest capacity of experimental resettable device delivered approximately 100N and therefore offered the capability of releasing all the stored energy effectively instantaneously relative to the structural periods being considered (Jabbari and Bobrow 2002). For larger devices, the rate of energy dissipation may be more important, as the flow rates required for large systems to release large amounts of stored energy will potentially be very high, and the resulting time to release all stored energy may well be significant in comparison to the structural response and dynamics. Failure to release all stored energy would significantly reduce the effectiveness of the device and the supplemental damping it adds to the structure. Therefore, more detailed models are required (Mulligan et al. 2007; Mulligan 2007) to create effective

designs and to determine the true effectiveness of these devices at more realistic and practical sizes.

Developing equations to represent the force–displacement relationships for each chamber enables the design space to be parameterised. More specifically, each chamber volume can be related to the device's piston displacement, which in turn leads to a change in pressure and therefore the resistive force of the device. Resetting the device by opening the valve on the compressed portion releases the stored energy as the pressure equalises with, in the case of air as the working fluid, the atmosphere. Therefore, assuming air is an ideal gas, it obeys the law:

$$pV^r = c \tag{3-1}$$

where r is the ratio of specific heats, c is a constant, and p and V are, respectively, the pressure and volume in one chamber of the device (Bobrow et al. 2000). If the piston is centred in the device and the initial pressure p_0 in both chambers with initial volumes V_0, the resisting force is defined as a function of displacement, x:

$$F(x) = (p_2 - p_1)Ac = [(V_0 + Ax)^{-r} - (V_0 - Ax)^{-r}]Ac \tag{3-2}$$

where A is the piston area. Equation (3-2) can be linearised and an approximate force defined:

$$F(x) = -\frac{2A^2 r p_0}{V_0} x \tag{3-3}$$

Hence, the effective stiffness of the resettable device, k_1, is readily defined:

$$k_1 = -\frac{2A^2 r p_0}{V_0} \tag{3-4}$$

3.3.3 Resetable Device with Independent Chambers

3.3.3.1 Introduction

Unlike previous simple resetable devices, the resetable device suggested in this research eliminates the need to rapidly dissipate energy from one side of the device to the other by using a two-chambered design that utilises each piston side independently. This approach treats each side of the piston as an independent chamber with its own valve and control, as shown in Figure 3-5, rather than coupling them with a connecting valve. This approach allows a wider variety of control laws to be imposed, as each valve can be operated independently. Thus, independent control of the pressure on each side of the piston is enabled, allowing a greater diversity of device behaviours (Chase et al. 2006; Rodgers et al. 2007b).

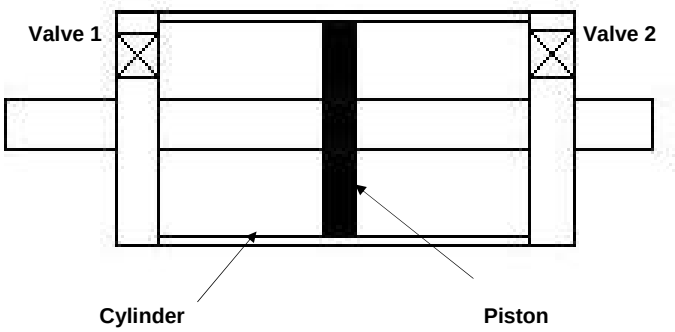

Figure 3-5 Schematic of independent chamber design. Each valve vents to atmosphere for a pneumatic or air-based device, or to a separate set of plumbing for a hydraulic fluid-based device.

For this research, air is assumed as the working fluid for simplicity and to make use of the surrounding atmosphere as the fluid reservoir. It has been successfully demonstrated up to 100kN level devices (Chase et al. 2006; Mulligan et al. 2007; Mulligan 2007). In combination with independent valves, it allows more time for the device pressures to equalise, as resetting the valve does not require all the compressed air to flow to the opposite chamber, as it would for the design in Figure 3-4. Hence, while the opposing chamber is under compression, the previously reset chamber can release pressure over a longer time period by having its valve open. This approach would not be feasible with the single-valve design in Figure 3-4, as it would eliminate the ability of the opposing chamber to store energy if the valve were still open. Thus,

for the practically sized devices considered in this research, this design has the advantage of allowing significant amounts of energy to be stored and dissipated.

Similar equations can be used to model, independently, the pressure–volume status of each chamber of the device in Figure 3-5. Equation (3-4) can then be used to design a device to produce a set resisting force at a given displacement, or a set added stiffness. Since Equation (3-4) includes the device geometry in *A* (area) and *V* (volume), it can be used to parameterise the design space to determine the appropriate device architecture (Mulligan et al. 2005a). Semi-active damping via this type resettable devices also offers unique the opportunity to sculpt or re-shape the resulting structural hysteresis loop to meet design needs, as enabled by the ability to control the device valve and reset times actively (Chase et al. 2006; Mulligan et al. 2005a; Rodgers et al. 2006; Rodgers et al. 2007b).

3.3.3.2 Device Design

Resetable devices with independent chambers were developed in Department of Mechanical Engineering, University of Canterbury, by Professor J. Geoffrey Chase and his research team (Chase et al. 2005a; Chase et al. 2006; Mulligan et al. 2005a; Mulligan et al. 2005b; Rodgers et al. 2006). The devices are for a one fifth scale, four story steel moment resisting test frame with basic dimensions of 2.1×1.2×2.1 m and a total seismic weight of 35.3 kN, as described by Kao (1998), and is widely used in the University of Canterbury Structures Laboratory. The structure is expected to have a fundamental natural period within 0.4s to 0.46s and its structural damping is approximately 5% of critical. Given that the total actuator authority might have a reasonable value of approximately 15% of the total building weight (Hunt 2002), and assuming two actuators in the structure, a stiffness of 250kN/m was required. This stiffness results in a force of 2.5kN developed at 10 mm displacement of the piston from its centre position, which represents a large story drift for this structure when subjected to a large-magnitude ground motion (Kao 1998).

Trade-off curves for a pneumatic-based resettable actuator with air as the working fluid show the relationships between the fundamental design parameters. The primary parameters are the diameter, individual chamber length, and maximum piston displacement. The trade-offs between these variables are shown in Figure 3-6 for different stiffness values. These parameters control the stiffness of the device using Equations (3-2) to (3-4). The practical design space (boxed) is determined by combining these curves with practical, cost, safety and ease of handling constraints. These added constraints include ensuring that the length of each chamber is greater than the maximum likely displacement of the piston (30mm), limiting the internal pressure to 2.5 atmospheres, and keeping the weight of the device under 20kg and the cylinder diameter at approximately 0.2m or less. The final design parameters selected are marked with an "×" and are in the upper left corner of the design space shown in Figure 3-6.

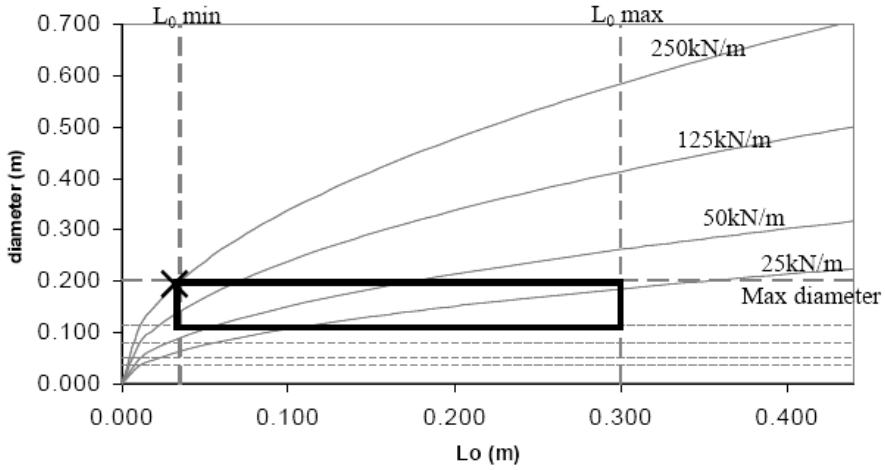

Figure 3-6 Trade off curve between the diameter and initial chamber length of the device for different stiffness values assuming a maximum piston displacement of 20mm. Each line represents a different stiffness value (Chase et al. 2006; Mulligan et al. 2005a).

An exploded view of the device is shown in Figure 3-7. The piston located inside the cylinder has four seals, each located in a groove, to ensure minimal air movement between the two chambers, as such movement would reduce the effective stiffness and energy dissipated by the device. The end caps are press fitted into the cylinder and held in place by four rods. An O-ring located between the end caps and the cylinder further ensures no leakage of air. Air is prohibited from escaping where the piston rod passes through the end caps by two seals located in the end caps. The

assembled prototype in an MTS test rig for hybrid testing is shown in Figure 3-8 (Mulligan et al. 2006) and an elevation view is shown in Figure 3-9. The final critical device dimensions selected are an internal diameter of 0.2m with a max stroke in either direction of 34.5mm from device centre.

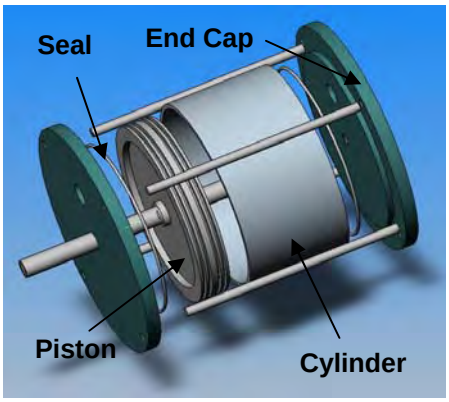

Figure 3-7 Exploded view of components of the prototype resetable device (Chase et al. 2006; Mulligan et al. 2005a)

Figure 3-8 Prototype device in MTS test rig (Chase et al. 2006; Mulligan et al. 2005a)

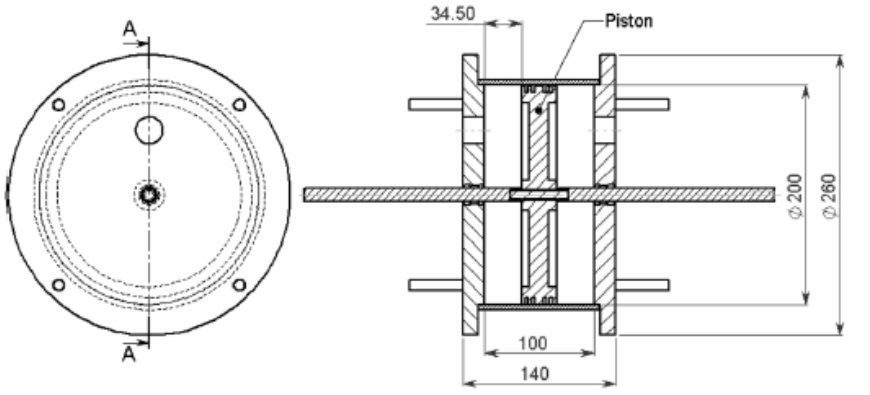

Figure 3-9 Elevation view and basic dimensions of the resetable device (Chase et al. 2006; Mulligan et al. 2005a).

3.3.3.3 Modelling

To represent the effects of the resetable device properly, a 'Semi-Active Resetable Actuator Member' has been developed for the inelastic dynamic analysis program, *Ruaumoko* (Carr 2004). Figure 3-10 shows the two different hysteretic behaviours of the SA resetable device based on experimental results (Chase et al. 2006). Figures 3-10(a) and 3-11(a) represent the hysteretic behaviour of simple resetable device where all stored energy is released at the peak of each sine-wave cycle and all other motion is resisted (Bobrow et al. 2000). This form is denoted a "1-4 device" as it provides damping in all quadrants (Chase et al. 2006; Rodgers et al. 2007b). The hysteretic behaviour shows that the force is proportional to the displacement until a saturation force is attained, Fy+ or Fy-, which might be near the yield forces for the member. At these values the resisting force is capped by gradually opening the valve, and the system appears to show a perfectly plastic response. On any reversal of displacement the force is automatically reset to zero, the origin is moved to the existing displacement, and the system will then behave as an elastic member until either saturation is reached or the displacement again changes sign.

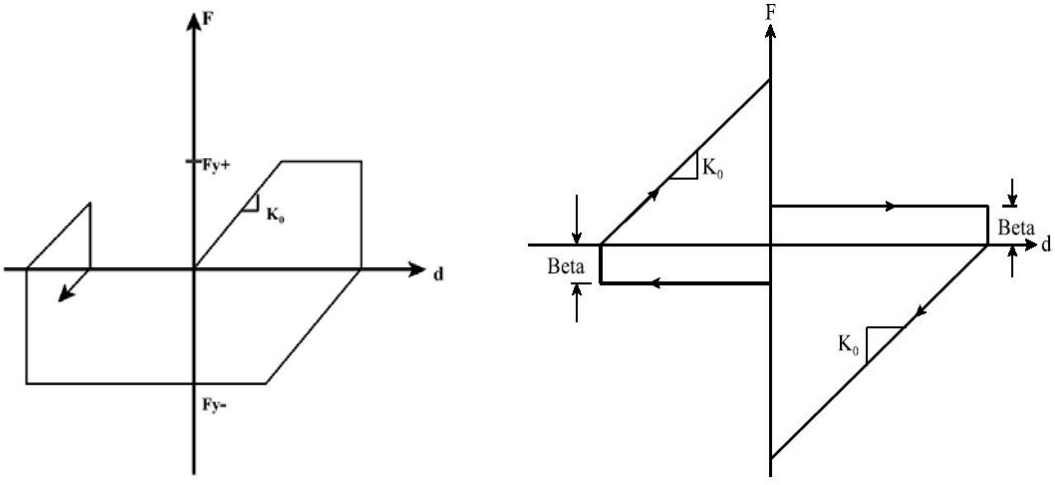

(a) 1-4 resetable device **(b) 2-4 resetable device**

Figure 3-10 Resetable device hysteresis (Carr 2004)

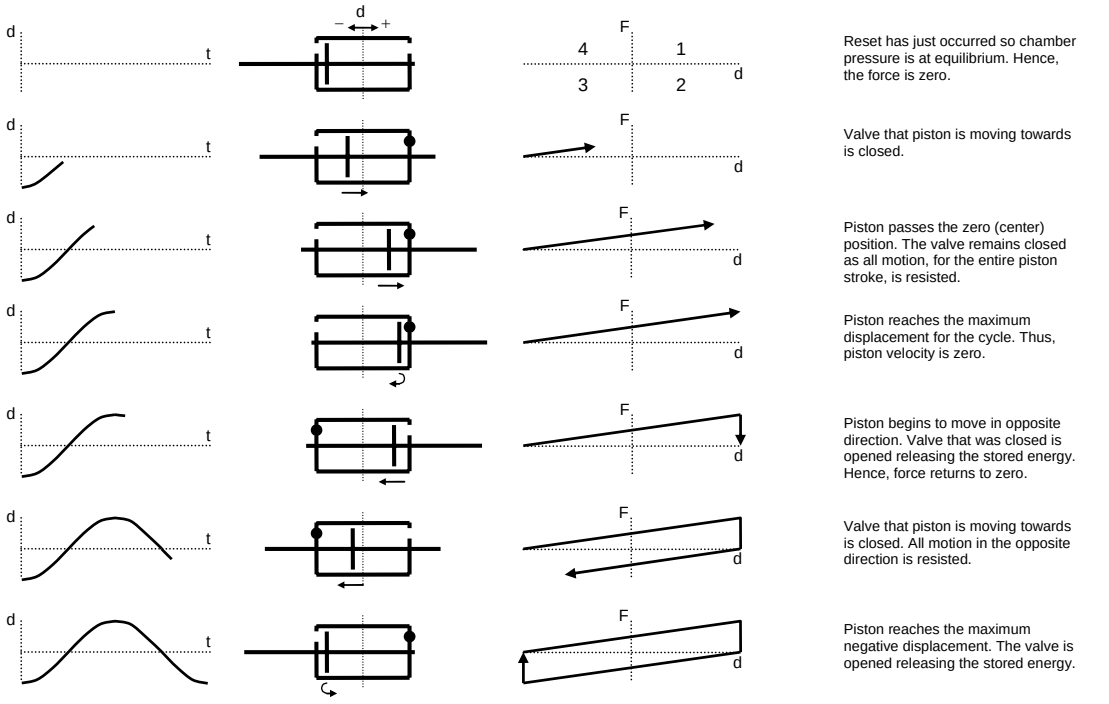

(a) 1-4 control law

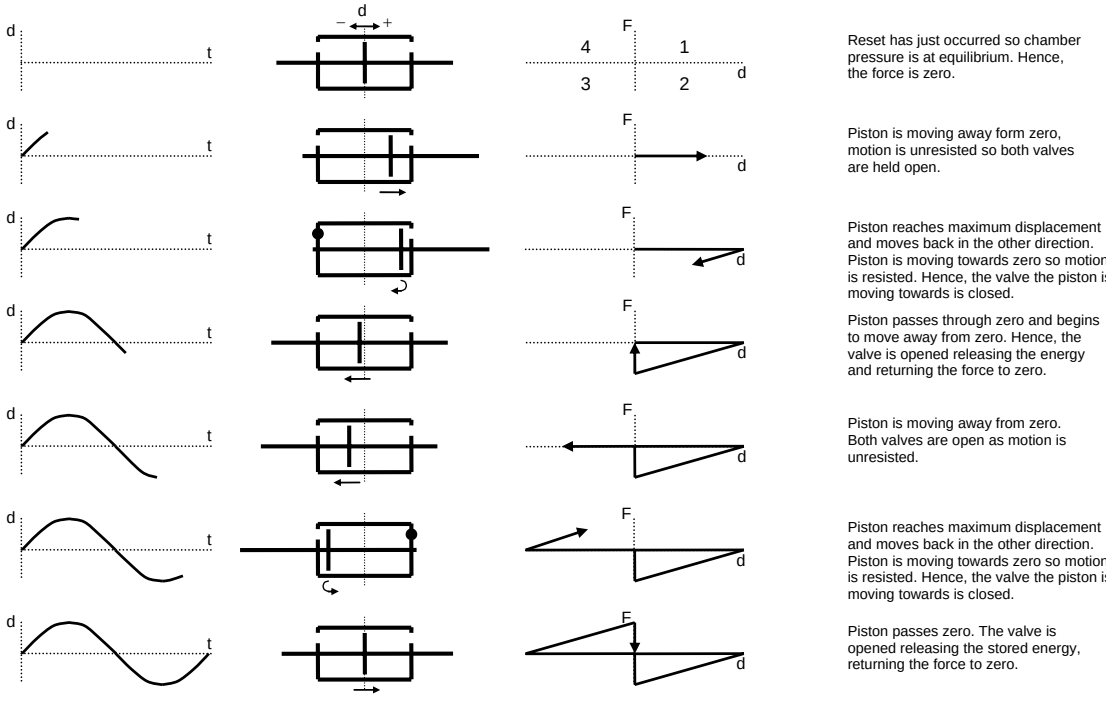

(b) 2-4 control low

Figure 3-11 Schematic showing one cycle of devices (Mulligan 2007)

If the control law is changed such that only motion *towards* the zero position (from peak values) is resisted, the force-deflection curves that result are shown in Figures 3-10(b) and 3-11(b). In this case, the device provides damping forces only in quadrants 2 and 4; a "2-4 device". The notation of 'Beta' indicates the friction force due to forcing air out and open valve. Experimentally, this error is attributed to energy release times that are not instantaneous, as well as friction between the seals and the cylinder wall.

3.4 Summary

To avoid adding more mass for effective TMD system, an alternative approach is proposed and modeled to segregate the top section of a structure to act as the 'tuned' mass. The isolated top section behaves as a primarily rigid block on top of a flexible structure. For retrofit or structural upgrade applications, additional storeys being added to the structure could be utilized in this way to achieve the same effect.

For a given structural configuration, the connections between the segregated section and main structure can be either passive for a PTMD system or resetable for a SATMD system. In each case, the segregated section for the PTMD and SATMD systems is assumed to be vertically supported on rubber bearings with a stiffness defined for the given PTMD and SATMD design.

This chapter has also introduced semi-active resetable devices with air as the working fluid and has detailed the dynamics of the resetable devices used in this research. Additionally, it has introduced a novel device design with independent chambers that disassociates the chamber pressures resulting in control low applications not possible for the original proposed design. These devices are readily scaled to higher forces, as needed, using hydraulic working fluids or similar (Mulligan 2007). Overall, this chapter introduces the basic structural concepts and elements in specific detail.

4 Earthquake Suites and Statistical Methodology

4.1 Earthquake Suites

The use of suites of accurate seismic time histories is a key feature of this research, with little prior research focusing on the importance of examining a wide range of excitation characteristics. Statistical methods are used to evaluate structural response over the suites, presenting results in a form suitable for performance-based design methods. As the characteristics of seismic excitation are entirely random and unlike other types of vibrational excitation, the use of multiple time history records over a range of seismic levels is also essential for effective controller evaluation, particularly where results from PTMDs have been found to be sensitive to the ground motion used.

Sommerville et al. (1997) developed three suites of 20 earthquake acceleration records to represent the seismic hazard at the SAC Phase II Los Angeles site. The high, medium, and low suites are grouped according to a probability of exceedance of 2%, 10%, and 50% in 50 years, respectively. The low and medium level suites are comprised solely of recorded ground motions pairs, while the high level suites contain five recorded and five artificially generated motion pairs. The time histories for the low suite are from earthquakes at a distance range of 5 to 100km, while those for the medium and high sets, with the exception of the 1992 Landers earthquake which was recorded at a distance of 40km, are near-field recordings. Near field recordings have rapid spikes in acceleration and hence, will effectively test the benefits of the SATMD concepts for effective acceleration and jerk control. Each of the ground motion pairs represents the same earthquake measured in orthogonal directions, each of which is at 45 degrees to the fault strike with respect to north, at which the fault plane intersects a horizontal plane.

The earthquakes contained within the three suites (odd half) are shown in Table 4-1. It should be noted that although in some cases multiple pairs of earthquake pairs have the same name, these are in fact different time histories, from different recordings of the same earthquake. The error between the suites of ground motions and the USGS hazard maps was minimised over the selected period range as the damped natural

frequencies of the SAC3 and SAC9 structural models fall within this band. The earthquake motion accelerations are shown in APPENDIX B.

To accurately represent the seismic hazard at the Los Angeles site, each earthquake was scaled. Thus, their response spectra, for a given probability of exceedance, were comparable with the spectrum from the United States Geological Survey (USGS) probabilistic seismic hazard maps for the Los Angeles area, in the period range of 0.3 to 4.0 seconds for stiff local soil conditions. Due to the scaling method used to ensure each suite of earthquakes falls within the prescribed probability of exceedance, the entire suite must be used for probability groupings to hold. In particular, although the median spectral acceleration for the entire suite at a given period will closely match the desired USGS value, the value for an individual scaled earthquake may not. Due to the computational time involved for simulations of the SAC9 structure it was not possible to efficiently run the full 20 earthquakes per set due to computational intensity. Instead, only the odd-half sets were used. Although this approach may introduce some potential error in the exceedance probabilities, using the first earthquake in each pair is expected to still give a fair indication of the building response for the prescribed excitation level.

Spectral acceleration diagrams allow the relative intensity of earthquakes to be assessed, and are developed by determining the response of a 1-DOF system over a spectrum of different periods. Intensity comparisons can then made using the fundamental frequency of the structure of interest. Figures 4-1 and 4-2 show the spectral acceleration and displacement plots for the odd half suites of earthquakes used. To reduce any potential skewing of the results from those of the full sets, comparisons will only be made between suites that contain the same earthquakes.

Table 4-1 Names of earthquakes scaled within suites

Probability of Exceedance (Suite)	Record	Earthquake Magnitude	Distance (km)	Scale Factor	Duration (sec)	PGA (cm/sec^2)
50% in 50 years (Low)	Coyote Lake, 1979	5. 7	8. 8	2. 28	26. 86	578. 34
	Imperial Valley, 1979	6. 5	1. 2	0. 4	39. 08	140. 67
	Kern, 1952	7. 7	107	2. 92	78. 60	141. 49
	Landers, 1992	7. 3	64	2. 63	79. 98	331. 22
	Morgan Hill, 1984	6. 2	15	2. 35	59. 98	312. 41
	Parkfield, 1966, Cholame 5W	6. 1	3. 7	1. 81	43. 92	765. 65
	Parkfield, 1966, Cholame 8W	6. 1	8	2. 92	26. 14	680. 01
	North Palm Springs, 1986	6	9. 6	2. 75	59. 98	507. 58
	San Fernando, 1971	6. 5	1	1. 3	79. 46	248. 14
	Whittier, 1987	6	17	3. 62	39. 98	753. 70
10% in 50 years (Medium)	Imperial Valley, 1940, El Centro	6. 9	10	2. 01	39. 38	452. 03
	Imperial Valley, 1979, Array #05	6. 5	4. 1	1. 01	39. 38	386. 04
	Imperial Valley, 1979, Array #06	6. 5	1. 2	0. 84	39. 08	295. 69
	Landers, 1992, Barstow	7. 3	36	3. 2	79. 98	412. 98
	Landers, 1992, Yermo	7. 3	25	2. 17	79. 98	509. 70
	Loma Prieta, 1989, Gilroy	7	12	1. 79	39. 98	652. 49
	Northridge, 1994, Newhall	6. 7	6. 7	1. 03	59. 98	664. 93
	Northridge, 1994, Rinaldi RS	6. 7	7. 5	0. 79	14. 95	523. 30
	Northridge, 1994, Sylmar	6. 7	6. 4	0. 99	59. 98	558. 43
	North Palm Springs, 1986	6	6. 7	2. 97	59. 98	999. 43
2% in 50 years (High)	Kobe, 1995	6. 9	3. 4	1. 15	59. 98	1258. 00
	Loma Prieta, 1989	7	3. 5	0. 82	24. 99	409. 95
	Northridge, 1994	6. 7	7. 5	1. 29	14. 95	851. 62
	Northridge, 1994	6. 7	6. 4	1. 61	59. 98	908. 70
	Tabas, 1974	7. 4	1. 2	1. 08	49. 98	793. 45
	Elysian Park (simulated)	7. 1	17. 5	1. 43	29. 99	1271. 20
	Elysian Park (simulated)	7. 1	10. 7	0. 97	29. 99	767. 26
	Elysian Park (simulated)	7. 1	11. 2	1. 1	29. 99	973. 16
	Palos Verdes (simulated)	7. 1	1. 5	0. 9	59. 98	697. 84
	Palos Verdes (simulated)	7. 1	1. 5	0. 88	59. 98	490. 58

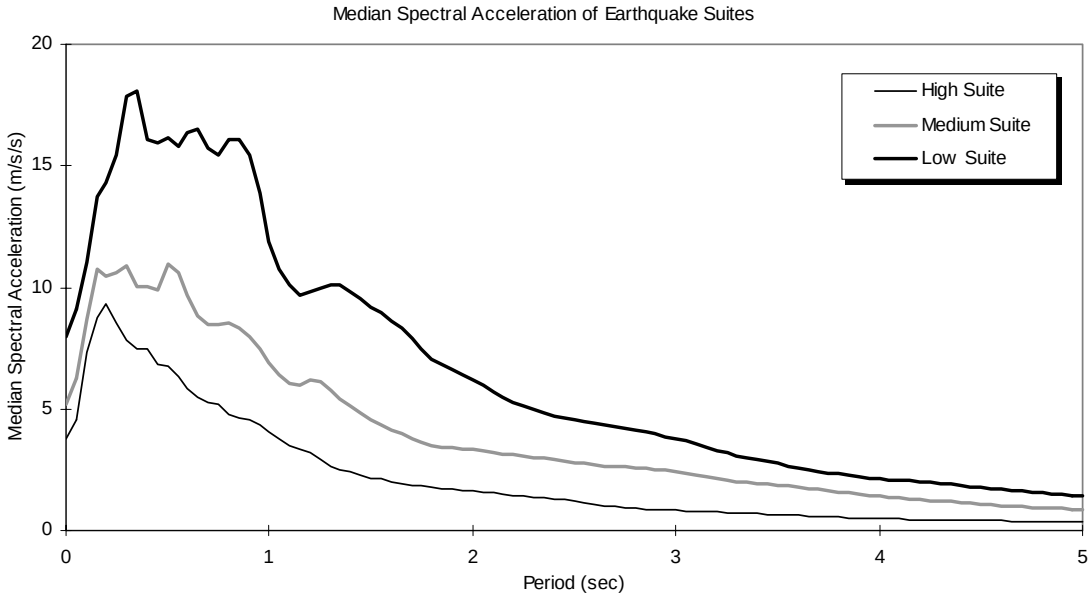

Figure 4-1 Spectral acceleration plots for odd half earthquake suite (5% critical damping)

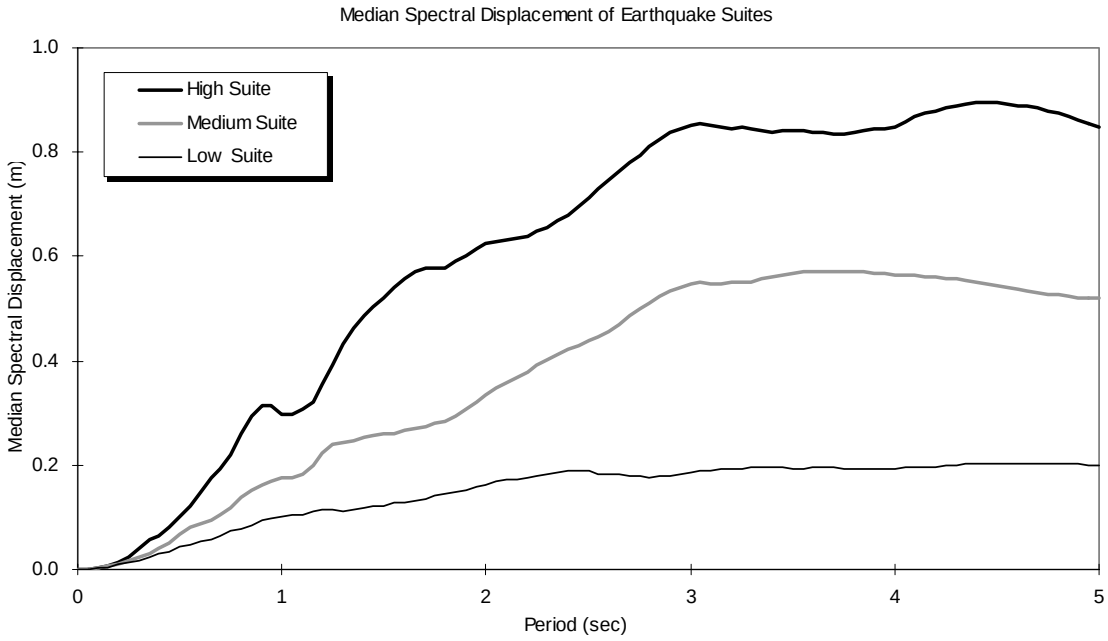

Figure 4-2 Spectral displacement plots for odd half earthquake suite (5% critical damping)

4.2 Statistical Methodology

Most often, the prime objective of the engineer is to satisfy the design requirements with the least possible cost and maximum function. However, there are numerous uncertainties associated with the determination of both demand and capacity, and the design requirements can often be satisfied only in a probabilistic manner. In other words, the odds of failure of the structure can be reduced to an acceptable minimum with the desired level of confidence, but its total safety cannot be guaranteed. Thus, it appears that having a consistent account of all uncertainties is the only rational way for proper decision-making.

Probabilistically scaled suites ensure that appropriate hazard curves can be generated from groups of results. As a result, the median likely outcome and its variability or variation can be readily defined. This overall approach leads to the generation of hazard curves and emerging probabilistic performance-based design methods. Similarly, probability theory and statistics provide an adequate mathematical framework to account for uncertainties on the *capacity side* of the design equation. Issues like the variation in material properties, construction uncertainty, dimensional errors and errors in modelling, analysis and design can thus be accounted for.

Statistical assessment of structural response is an important step in performance-based seismic design. Most prior research into active or semi-actively controlled structures employed either sinusoidal, random, single, or selected earthquake excitations to illustrate the benefits of control (Bobrow et al. 2000; Cho et al. 2005; Jansen and Dyke 2000; Narasimhan and Nagarajaiah 2005; Yang et al. 2000; Yoshida and Dyke 2004). As the characteristics of seismic excitation are entirely random and vary significantly, unlike other types of vibrational excitation, the use of a number of multiple time history records over a range of seismic levels is essential for effective controller evaluation. This approach has been used extensively to develop design guidelines and complete performance assessment of control (Barroso et al. 2003; Chase et al. 2003; Chase et al. 2004a; Hunt 2002; Mulligan et al. 2006; Rodgers et al. 2006; Rodgers et al. 2007b).

The performance measures of interest in this thesis are therefore evaluated statistically from the individual structural responses from the seismic records within each earthquake suite. Therefore, the choice of statistical tools must ensure the simulation results are accurately represented. To combine the response results across the earthquakes in a suite, log-normal statistics are used (Hunt 2002; Limpert et al. 2001), since it is widely accepted that the statistical variation of many material properties and seismic response variables is well represented by this distribution provided one is not primarily concerned with the extreme tails of the distribution (Kennedy et al. 1980). More specifically, the central limit theorem states that a distribution of a random variable consisting of products and quotients of several random variables tends to be lognormal even if the individual distributions are not lognormal.

For the statistical assessments, the response measures are each defined with respect to a single seismic event. To combine these results across the earthquakes in a suite, the following log-normal based statistical tools are employed. To combine the response values of a ground motion suite, a log-normal based median of the response quantities of a suite with *n* earthquakes is defined as

$$\hat{x} = \exp\left(\frac{1}{n}\sum_{i=1}^{n}\ln x_i\right) \tag{4-1}$$

with the corresponding log-normal based coefficient of variation defined as

$$\hat{\sigma} = \exp\left(\sqrt{\frac{1}{n-1}\sum_{i=1}^{n}\left(\ln x_i - \ln \hat{x}\right)^2}\right) \tag{4-2}$$

To present a summary of the distribution change between the controlled (PTMD and STMD) and uncontrolled (No TMD) data sets, while providing accurate statistical measures that are not highly affected by changes in any single variable, the 16th percentile ($\hat{x}/\hat{\sigma}$), 50th percentile ($\hat{x}$), and 84th percentile ($\hat{x}\times\hat{\sigma}$) are presented. It should be noted that the structural hysteretic energy does not follow a lognormal distribution, unlike peak drift and peak acceleration (Breneman 2000). To define a statistical measure of the energy dissipation response values, the standard "counted" mean and 84th percentile are presented.

4.3 Summary

This chapter has described earthquake suites used in the assessment simulations of controlled structures and an explanation of the statistical tools used. Of the three SAC Project locations, Los Angeles has the highest seismic risk and is seen as a primary candidate for implement of control systems. The development of the three earthquakes was presented, with a brief description of 2%, 10%, and 50% in 50 years according the USGS Los Angeles probabilistic seismic hazard maps. As three suites of earthquake were used, the statistical tools utilised are important to ensure the true trends of the data are represented. Using lognormal distribution, structural responses are presented, using the 16^{th}, 50^{th}, and 84^{th} percentile levels.

5 Simplified 2-DOF TMD Building System Model

5.1 Introduction and Model Elements

To represent the effects of the TMD rubber bearing stiffness, the spring member in *Ruaumoko* (Carr 2004) is used. An optimal TMD stiffness, k_{2opt}, is then applied to the sum of the stiffness of the SA device and rubber bearings (SATMD) or to the whole stiffness of the rubber bearings (PTMD) in the transverse direction. Thus, the optimal stiffness of the semi-active system is assumed to be the same as for the passive TMD case (Chey et al. 2007). Note that this approach may neglect or underuse certain qualities of the SA devices (Mulligan et al. 2005a; Mulligan et al. 2005c), but provides a clearer initial comparison for this research. The added damping to the structure for the PTMD case is modelled using the damping or dashpot member in *Ruaumoko*. Finally, Figure 5-1 shows the hysteresis loops for the idealised resetable device elements used.

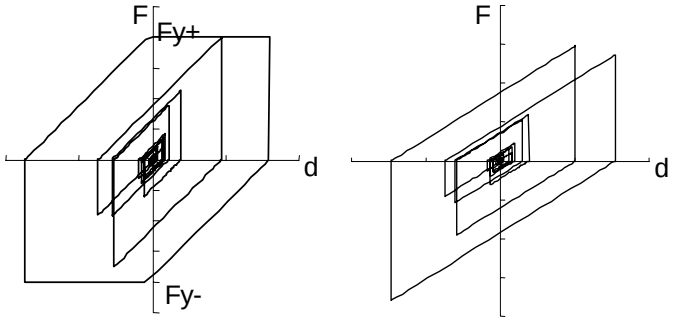

(a) With saturation **(b) Without saturation**

Figure 5-1 Hysteresis behaviour of resetable device

5.2 Modelling

5.2.1 Motion Characteristics and Equations

Being characterized by its mass, tuning and damping ratios, the PTMD system consists of a TMD system which is connected by a spring and a viscous damper, as shown in Figure 5-2(a). Figures 5-2(b) and 5-2(c) represent SATMD building systems, including passive and resetable springs at the instants of rest and reset respectively. As the relative displacement between the main system and the SATMD increases, both springs (passive and resetable spring) stretch and work together against the relative motion of the SATMD. When the relative displacement reaches its maximum position, the velocity is zero and the resetable semi-active device resets, releasing the energy stored (Williams 1994). Thus, the equilibrium position or unstretched length of the resetable spring is time variant. The linear spring elements, if any, in the SATMD system return all stored energy to the structure. In contrast, the viscous damper-based PTMD system spring acts for all motion.

For the TMD (PTMD and SATMD) building systems, 2-DOF systems can be defined for design by a pair of coupled second-order ordinary differential equations. For the PTMD and SATMD building systems, the equations of motion of the systems subjected to the earthquake load $\ddot{x}_g$ can be defined respectively:

$$\begin{aligned} m_1\ddot{x}_1 &= -k_1(x_1 - x_g) - c_1(\dot{x}_1 - \dot{x}_g) + k_{2(RB)}(x_2 - x_1) + c_2(\dot{x}_2 - \dot{x}_1) \\ m_2\ddot{x}_2 &= -k_{2(RB)}(x_2 - x_1) - c_2(\dot{x}_2 - \dot{x}_1) \end{aligned} \tag{5-1}$$

$$\begin{aligned} m_1\ddot{x}_1 &= -k_1(x_1 - x_g) - c_1(\dot{x}_1 - \dot{x}_g) + k_{2(RB)}(x_2 - x_1) + k_{2(res)}(x_2 - x_s) \\ m_2\ddot{x}_2 &= -k_{2(RB)}(x_2 - x_1) - k_{2(res)}(x_2 - x_s) \end{aligned} \tag{5-2}$$

where

m_1 = mass of main system;

m_2 = mass of TMD;

k_1 = stiffness of main system;

$k_{2(RB)}$ = stiffness of rubber bearings;

$k_{2(res)}$ = stiffness of resetable device;

c_1 = damping coefficient of main system;

c_2 = damping coefficient of TMD;

x_1 = displacement of main system;

x_2 = displacement of TMD;

x_g = displacement of ground

x_s = equilibrium position (unstretched length) of the resetable spring.

Note that a resetable device non-linearly alters the stiffness as a function of its motion, creating a non-linear dynamic system with (implicit) feedback control, in contrast to the linear PTMD system model.

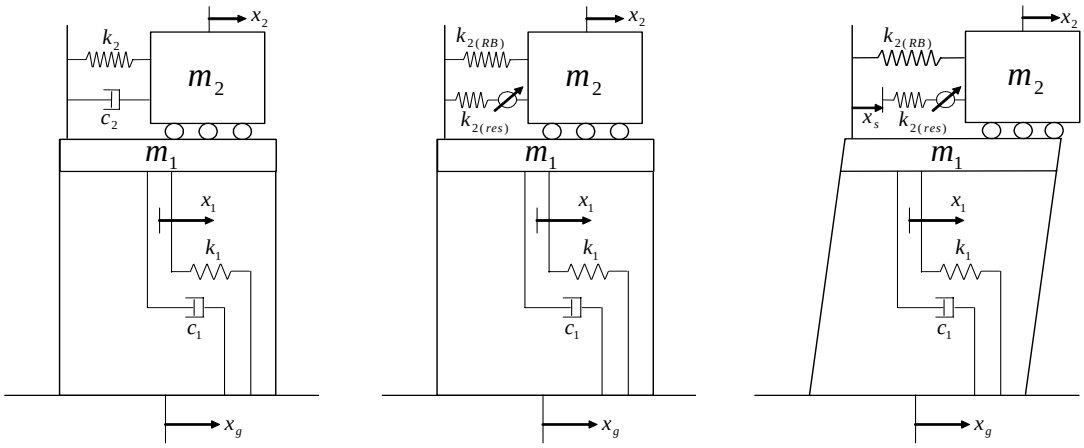

(a) PTMD at rest **(b) SATMD at rest** **(c) SATMD at peak relative displacement reset**

Figure 5-2 TMD building system models for 2-DOF design analyses

5.2.2 Parametric Optimisation for Large TMD

Performance of TMD systems is usually assessed by parametric studies. Thus, optimal parameters, such as the frequency tuning ratio and damping ratio of the TMD, need to be determined to achieve the best performance. Studies on the applicability of PTMDs for seismic applications by Villaverde (1985) show that a TMD performed best when the first two complex modes of vibration of the combined structure and damper have approximately the same damping ratios as the average of the damping ratios of the structure, ξ_1, and TMD, ξ_2 as defined:

$$\xi_{avg} = (\xi_1 + \xi_2)/2 \tag{5-3}$$

To achieve this, Villaverde (1985) found that the TMD should be in resonance with the main structure and its damping ratio should satisfy the equation given by:

$$\xi_2 = \xi_1 + \Phi\sqrt{\mu} \tag{5-4}$$

where Φ is the amplitude of the mode shape at the TMD location and μ is the mass ratio of the TMD to the generalised mass of the structure in a given mode of vibration. Both Φ and μ are computed for a unit modal participation factor.

However, numerical results show that this formulation does not result in equal damping in the first modes of vibration, especially when utilizing large mass ratios. To solve the problem for large mass ratios of over 0.5%, Sadek et al. (1997) proposed another procedure to achieve equal damping in the two vibration modes. They found that the optimum values are determined when the difference between each of the two damping ratios is the smallest and that the optimum TMD parameters result in approximately equal damping ratios greater than $(\xi_1 + \xi_2)/2$, and equal modal frequencies.

For design purposes, Sadek et al. presented the optimum TMD parameters by simple equations using curve-fitting methods. Meanwhile, Miranda (2005) presented a theoretically approximate model for two degree of freedom mechanical systems based on their modal kinetic and modal strain energies. The model was subsequently used to determine optimum parameters that maximise the modal damping of TMDs to be placed at the upper level of buildings using an iterative procedure. For a selected range of mass ratios, it was shown that the model is capable of closely matching exact numerical results previously obtained by Sadek et al.

In this study, for the large mass ratios utilising in the concept presented, the equations from Sadek et al. are adopted to find the optimal parameters of frequency tuning and damping ratios. For high values of mass ratio, μ, it is likely that the TMD will not be an appendage added to the structure, but, as noted, a portion of the structure itself,

such as one or more upper storeys. According to Sadek et al., the equation of the optimal frequency tuning ratio, f_{2opt}, and the optimal damping ratio, ξ_{2opt}, of the TMD systems are thus defined:

$$f_{2opt} = \frac{1}{1+\mu}\left(1-\xi_1\sqrt{\frac{\mu}{1+\mu}}\right) \tag{5-5}$$

$$\xi_{2opt} = \frac{\xi_1}{1+\mu}+\sqrt{\frac{\mu}{1+\mu}} \tag{5-6}$$

For practical application, it is necessary to obtain the resulting optimal TMD stiffness, k_{2opt} and optimal damping coefficient, c_{2opt}. These parameters can be derived using f_{2opt} and ξ_{2opt}.

$$k_{2opt} = m_2\omega_1{}^2 f_{2opt}{}^2 = m_2\omega_1{}^2\left(\frac{1}{1+\mu}\right)^2\left(1-\xi_1\sqrt{\frac{\mu}{1+\mu}}\right)^2 \tag{5-7}$$

$$c_{2opt} = 2m_2\omega_1 f_{2opt}\xi_{2opt} = \frac{2m_2\omega_1}{1+\mu}\left(1-\xi_1\sqrt{\frac{\mu}{1+\mu}}\right)\left(\frac{\xi_1}{1+\mu}+\sqrt{\frac{\mu}{1+\mu}}\right) \tag{5-8}$$

where ω_1 is the frequency of the main system.

Figure 5-3 shows the optimum TMD tuning and damping ratio from Equations (5-5) and (5-6) respectively, plotted versus mass ratios ranging from 0 to 1, with different structural damping values (ξ_1=0, 0.02, 0.05 and 0.1) and a main structural mass (m_1) of 27.3kN-s^2/m. The figure indicates that the higher the mass ratio, the lower the tuning ratio and the higher the TMD damping ratio. The higher the damping ratio (ξ_1) of the main system, the lower is the tuning ratio and the higher the TMD damping ratio. Figures 5-4 and 5-5 show the optimum TMD stiffness and damping coefficient from Equations (5-7) and (5-8) for the three different periods of main system (T_1=1.19, 1.52 and 1.88) with the same structural damping, ξ_1. From the figures, as expected, the larger is the mass ratio and/or the shorter is the building period, the higher is the stiffness and damping coefficient required of the TMD to achieve optimal performances.

From these trends, it can be predicted that there is no more increase in the TMD stiffness when the mass ratio is over 1.0, which is an unrealistic value. The effects of the device damping on the performance behaviour of the building system become more pronounced with higher mass ration and lower building period (ie. higher building stiffness). A nearly linear increase in TMD damping coefficient is observed with increase in the mass ratio, and it is also observed that there is nearly no effect of the damping ratio of the main structure (ξ_1) on the TMD damping coefficient for the fundamental natural period examined. Figure 5-6 shows the resulting optimal design process for the 2-DOF TMD system. The parametric results from this design process will be used as the basic references for the MDOF verification study on TMD building systems.

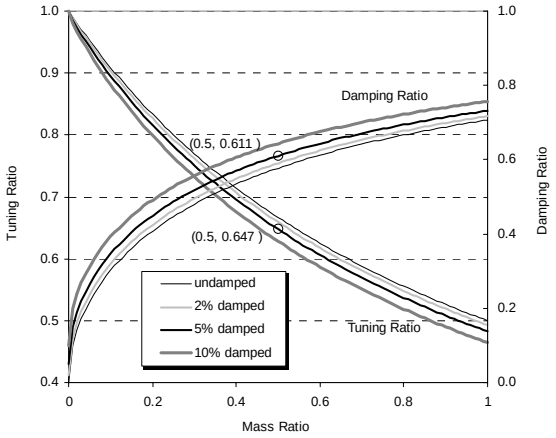

Figure 5-3 Optimum TMD tuning and damping ratios

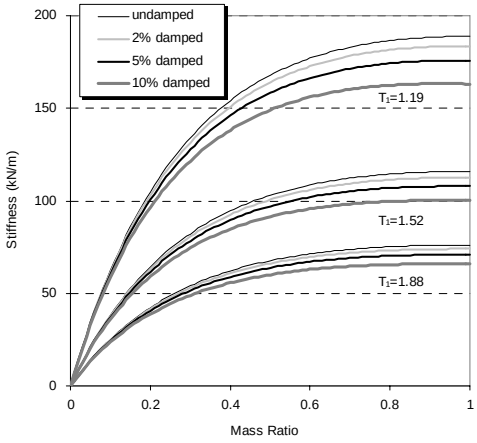

Figure 5-4 Optimum TMD stiffness (m_1=27.3kN-s^2/m)

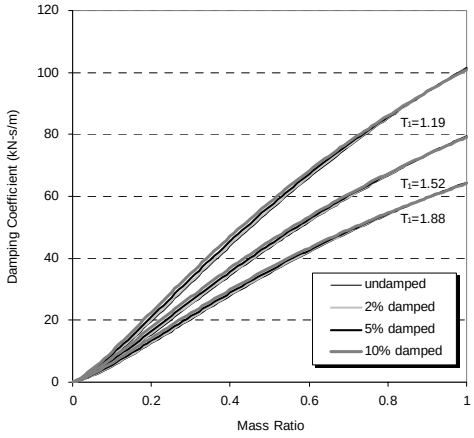

Figure 5-5 Optimum TMD damping coefficient (m_1=27.3kN-s^2/m)

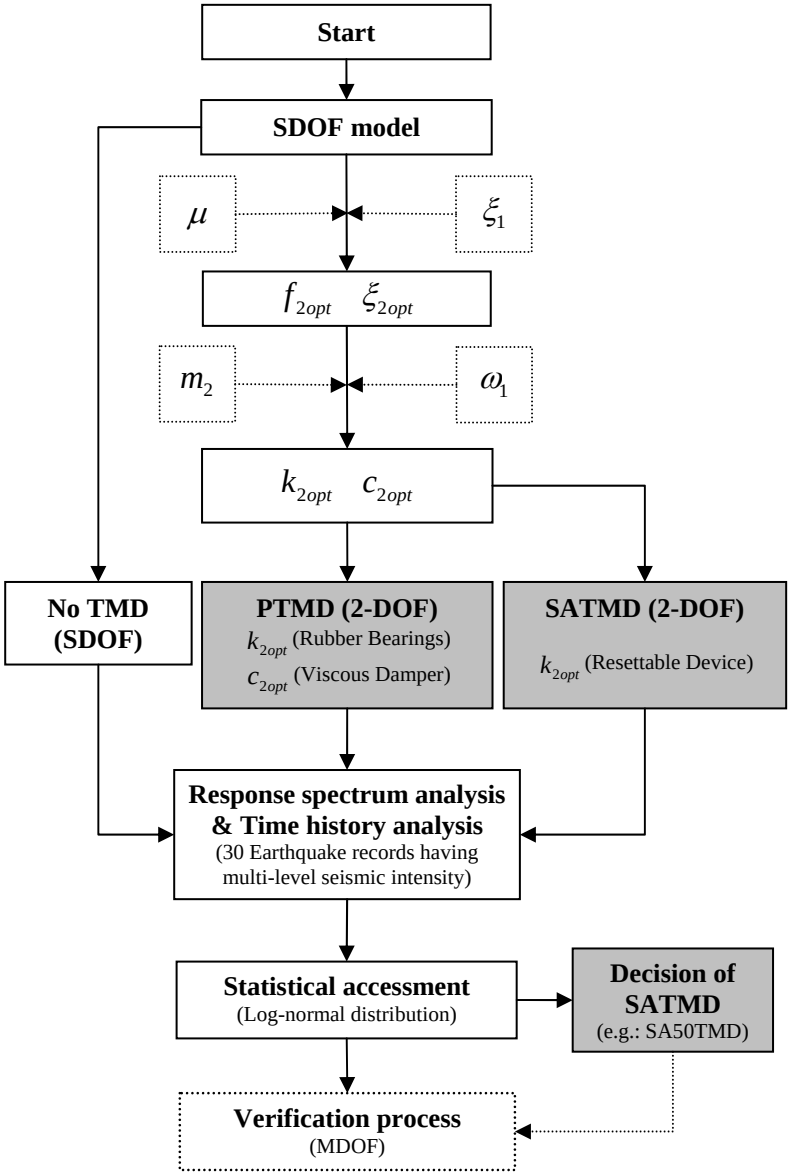

Figure 5-6 Design process for the TMD system

5.3 Response Spectrum Analysis

5.3.1 Analysis Methods

To demonstrate the proposed control methodology, 2-DOF linear models including 5% internal structural damping with natural periods of 1.19, 1.52 and 1.88 seconds are investigated. These periods span the seismically critical T=1.0-2.0 sec range and are obtained using the properties in Table 5-1. For these main systems, the mass ratio of 0.5 was used and this value is the mass ratio of the 1st modal mass of the TMD to the total mass of the main system. To assess the control effects of the resetable device, the percentage ratio of the resetable device stiffness to the total stiffness are selected as 25%, 50%, 75%, 100% and 33% (without rubber bearing) of k_{2opt}, the optimal value of the TMD stiffness. The TMD stiffness combinations of resetable device and rubber bearings are shown in Table 5-2.

Performance with No TMD, optimum PTMD (PTMD(on)), and off-optimum PTMD (PTMD(off)) are compared with the SATMD cases. For the off-optimum PTMD, the TMD damping ratio (ξ_2) of 0.15 was used, as this much lower value is a much more realistic figure compared to the optimum one of 0.611. As a result, a more realistic result will be obtained and the reliability of the optimum parameters can be estimated. In addition, this value represents the relatively maximum amount of damping that might be obtained practically, and is thus reasonable for broad comparison to various equally practical SATMD cases. The maximum force of 27.7kN is selected for the SA resetable device, representing 13.8% (Hunt 2002) of the total system weight of 402kN multiplied by mass ratio (μ=0.5). The TMD parameters used for each case obtained from Equations (6-5) to (6-8) are listed in Table 5-3.

Table 5-1 Dynamic properties of main system

Item	Value	Unit
Weight	268	kN
1st Modal Mass	27.3	kN-s^2/m
Natural period (Frequency)	1.19 (5.26) 1.52 (4.12) 1.88 (3.34)	sec (rad/sec)

Table 5-2 TMD stiffness combination of resetable device and rubber bearings

TMD	Resetable device (%)	Rubber bearing (%)	Total (%)
PTMD(off/on)	0	100	100
SA25TMD	25	75	100
SA50TMD	50	50	100
SA75TMD	75	25	100
SA100TMD	100	0	100
SA33TMD*	33	0	33

* without rubber bearings

Table 5-3 Parameters for TMD system (μ=0.5, ξ_1=0.05)

main system (sec)	TMD	f_{2opt}	ξ_{2opt}	k_{2opt} (kN/m)	c_{2opt} (kN-s/m)
1. 19	PTMD(off)	0.647	0.150	158.7	14.0
	PTMD(on)	0.647	0.611	158.7	56.9
	SATMDs	0.647	-	158.7	-
	SA33TMD*	0.647	-	52.8	-
1. 52	PTMD(off)	0.647	0.150	97.4	10.9
	PTMD(on)	0.647	0.611	97.4	44.6
	SATMDs	0.647	-	97.4	-
	SA33TMD*	0.647	-	32.4	-
1. 88	PTMD(off)	0.647	0.150	63.7	8.8
	PTMD(on)	0.647	0.611	63.7	36.0
	SATMDs	0.647	-	63.7	-
	SA33TMD*	0.647	-	21.2	-

* without rubber bearings

To demonstrate the relative control effects of the TMD systems, the performance measures are evaluated statistically from the individual structural responses for the 10 seismic records within each suite (low, medium and high). All controlled displacement and acceleration values are presented and reduction factors are created by normalising to the uncontrolled (No TMD) result. Reduction factors more clearly indicate effect and are more readily incorporated into performance-based design methods when using suites of probabilistically scaled events (Rodgers et al. 2007b). Thus, the response reduction factors for PTMD (off and on), SA33TMD* (without rubber bearing) and SATMDs for low, medium and high suites are presented.

To indicate the range of spread of results over a suite at a given natural period, the 16^{th}, 50^{th} and 84^{th} percentiles are used. The values of median (50^{th} percentile) and the width, which is the spread between the 16^{th} and 84^{th} percentiles, are taken for each period analysed. Thus, a specific system would be considered more robust to different ground motions and/or more effective over all if the width between the 16^{th} and 84^{th} percentile curves is reduced. Furthermore, the index of 'Standard error of control (SEC)' can be derived from the each width as a final result for band width reduction as follow

$$SEC = \frac{RF(84^{th}) - RF(16^{th})}{RF(50^{th})} \tag{5-9}$$

Finally, the TMD case with the best trade off between band width reduction and response reduction for a decision making can be determined from the collected results based on the designer's preference.

5.3.2 Analysis Results

Figures 5-7 to 5-12 show the median displacement and acceleration spectra for each suite. Figures 5-13 to 5-21 show the maximum response results for both displacement and acceleration of the main system models at the three natural periods. From these results, it is observed that the performance of the TMD (PTMD and SATMD) building systems is feasible. As expected, the No TMD case values coincide with each spectrum line. The off-optimum PTMD system showed reduced responses compared to the optimum PTMD system in terms of displacement, while the optimum PTMD building system presented reduced responses in acceleration due to the higher damping ratio under the all suites of earthquake intensity. Even though the control efficiency is not so different, the SATMD systems around SA50TMD (SA25TMD to SA75TMD) showed relatively better displacement reductions than other SATMD cases. Also, all the SATMD cases reduced the acceleration response of each main system. However, this reduction is less than those of the PTMD (both on and off), also due to the level of TMD damping contained.

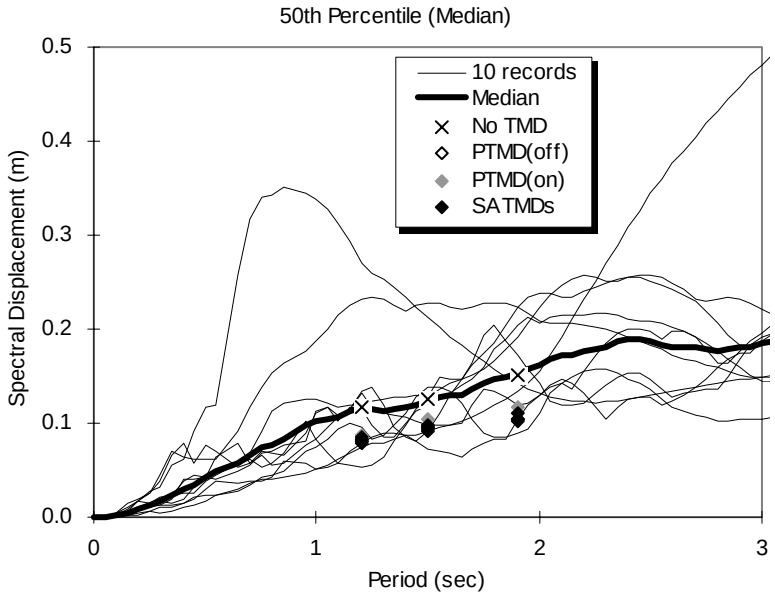

Figure 5-7 Response spectra of main system (Median displacement / Low suite)

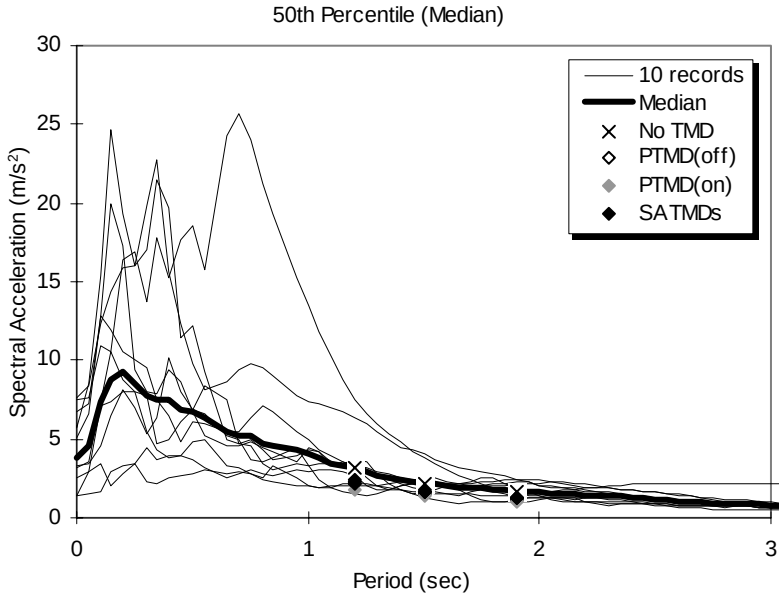

Figure 5-8 Response spectra of main system (Median acceleration / Low suite)

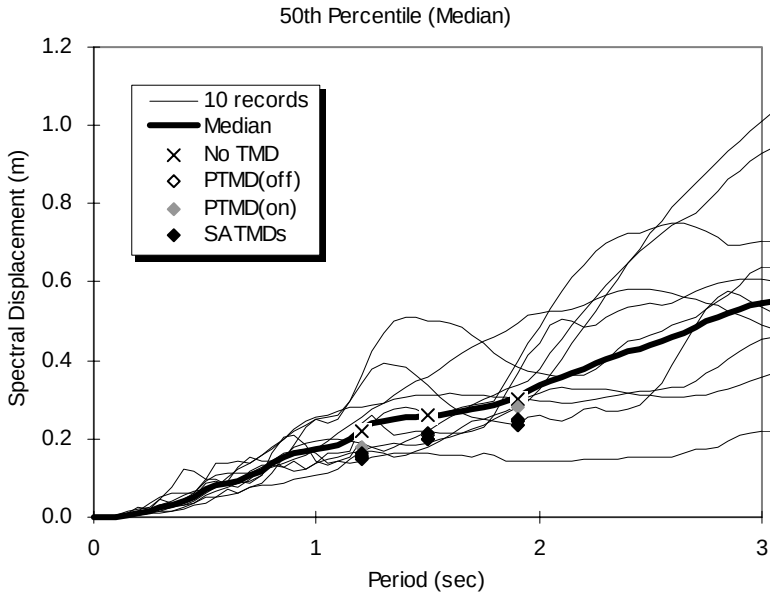

Figure 5-9 Response spectra of main system (Median displacement / Medium suite)

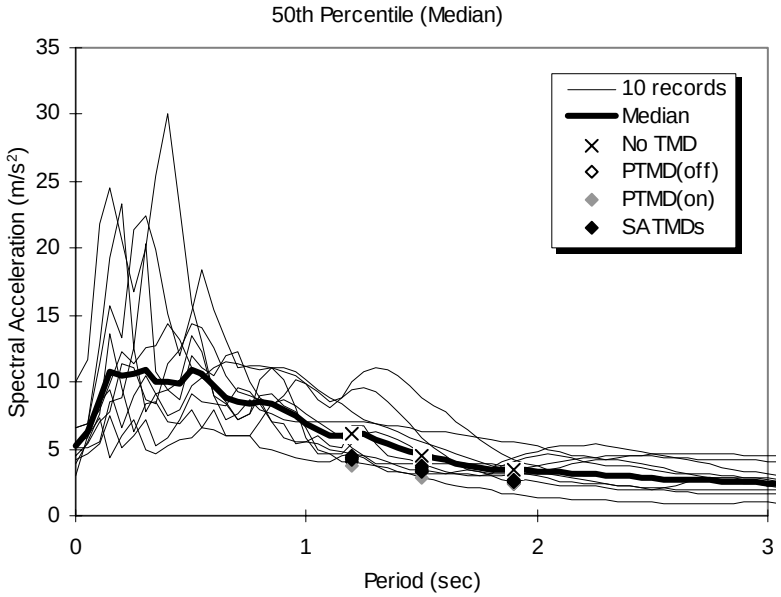

Figure 5-10 Response spectra of main system (Median acceleration / Medium suite)

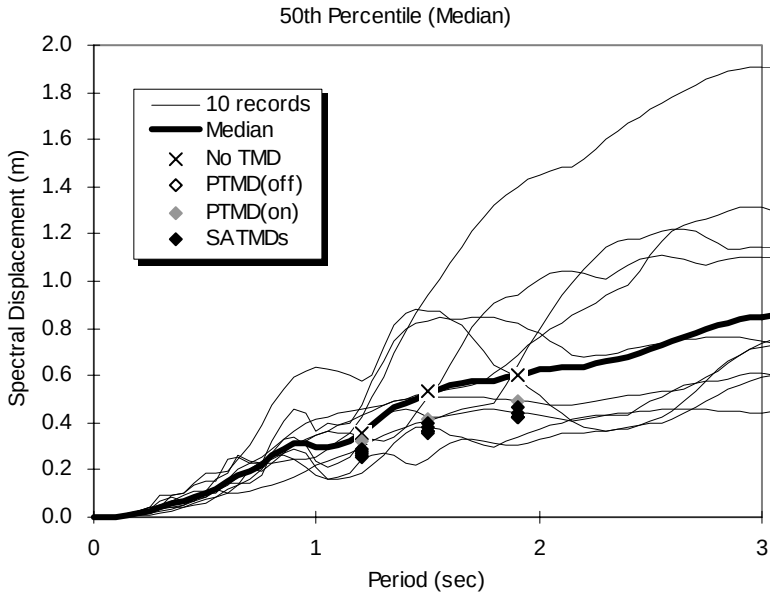

Figure 5-11 Response spectra of main system (Median displacement / High suite)

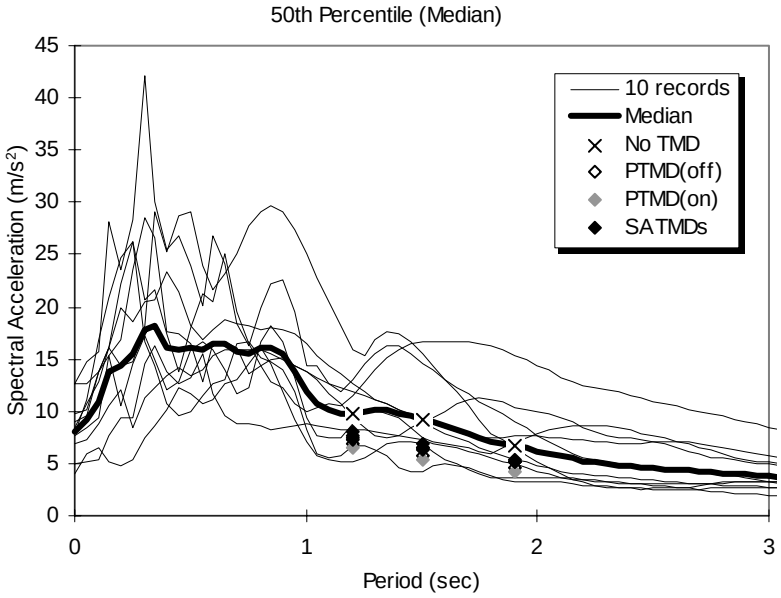

Figure 5-12 Response spectra of main system (Median acceleration / High suite)

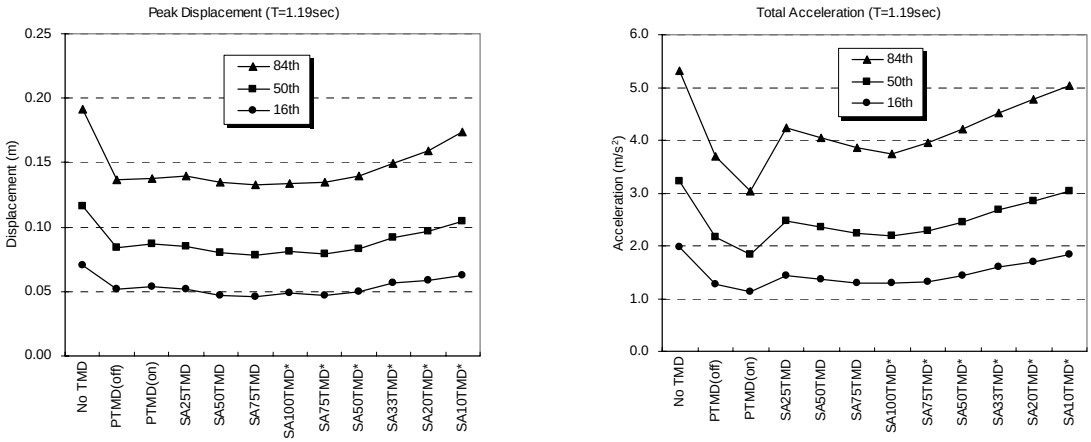

Figure 5-13 Maximum response of main system by TMD systems (T=1.19sec / Low suite)

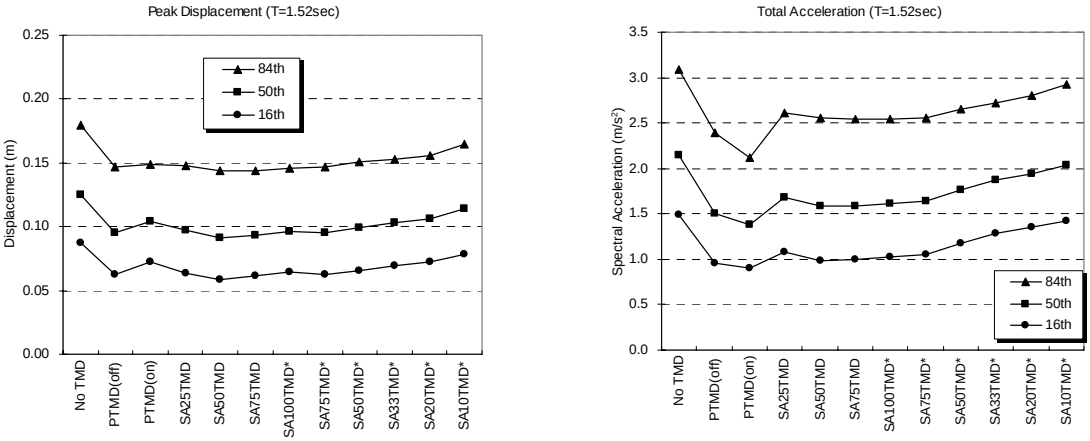

Figure 5-14 Maximum response of main system by TMD systems (T=1.52sec / Low suite)

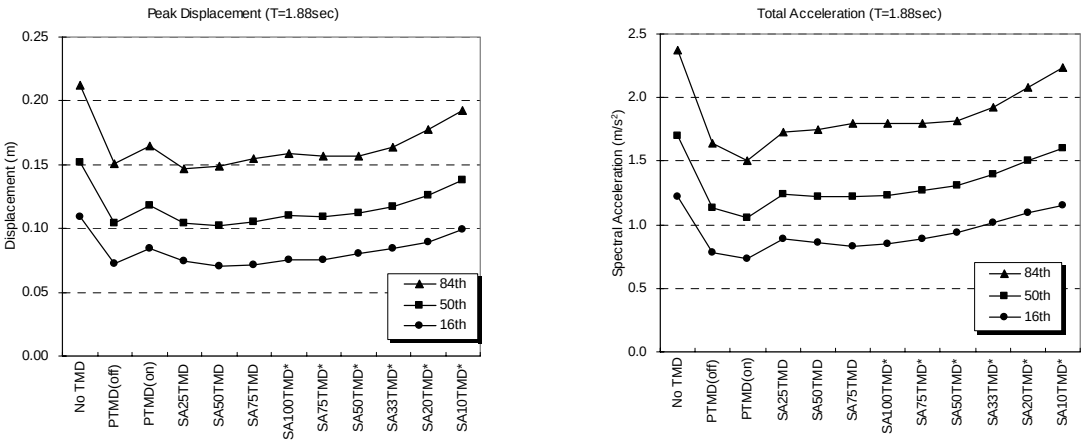

Figure 5-15 Maximum response of main system by TMD systems (T=1.88sec / Low suite)

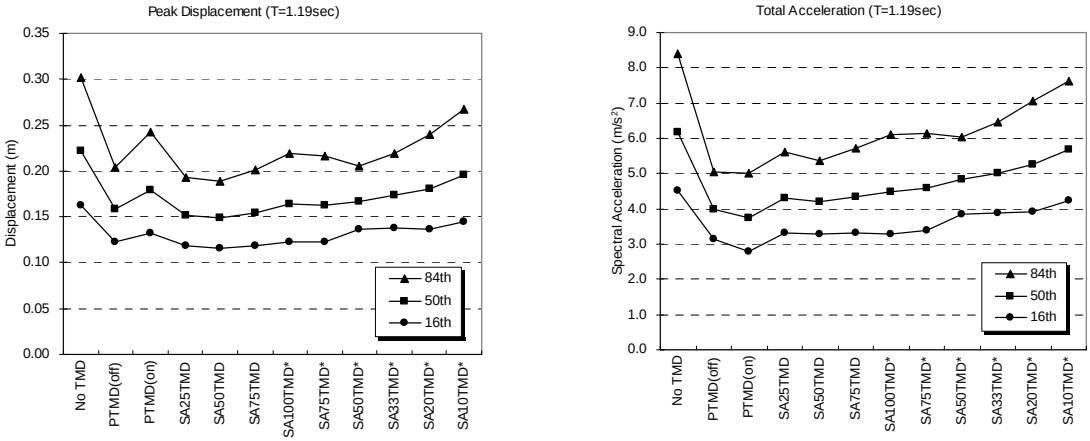

Figure 5-16 Maximum response of main system by TMD systems (T=1.19sec / Medium suite)

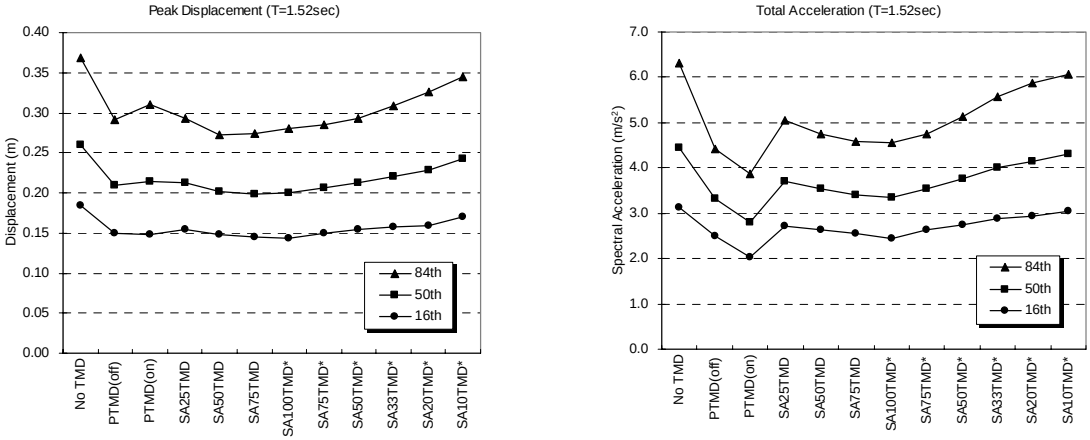

Figure 5-17 Maximum response of main system by TMD systems (T=1.52sec / Medium suite)

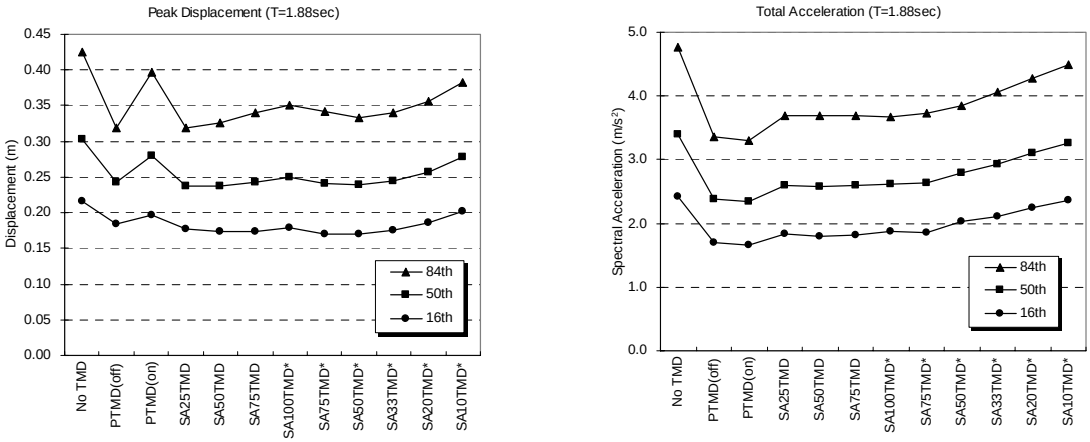

Figure 5-18 Maximum response of main system by TMD systems (T=1.88sec/Medium suite)

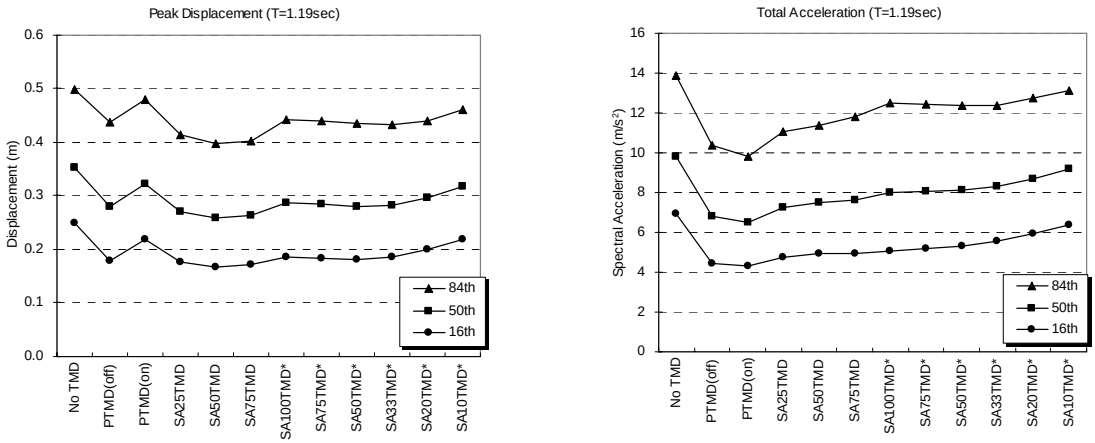

Figure 5-19 Maximum response of main system by TMD systems (T=1.19sec / High suite)

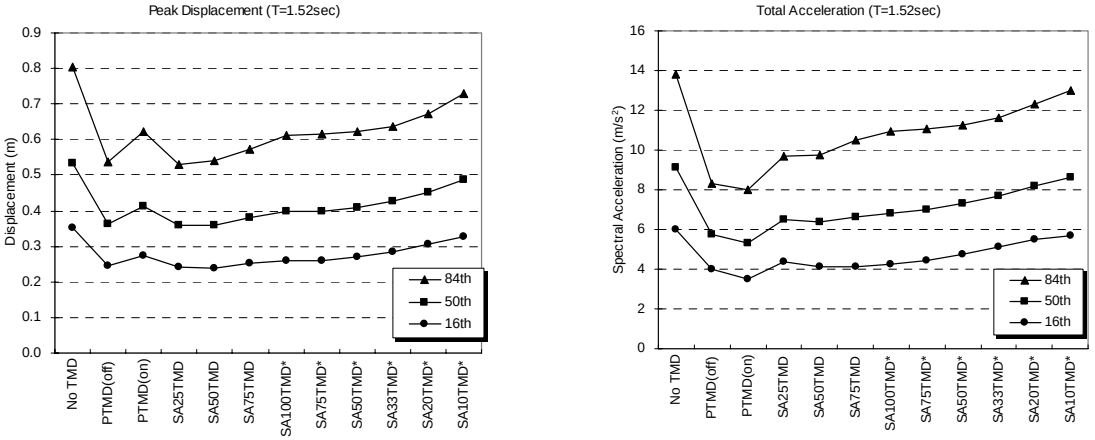

Figure 5-20 Maximum response of main system by TMD systems (T=1.52sec / High suite)

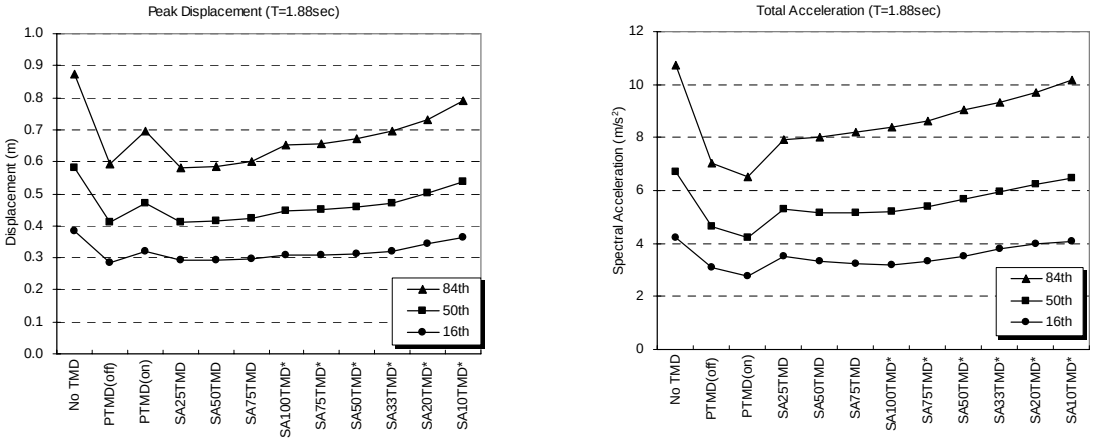

Figure 5-21 Maximum response of main system by TMD systems (T=1.88sec / High suite)

Figures 5-22 to 5-39 present the response (displacement and acceleration) reduction factors relative to the uncontrolled case for each main system for each of the different earthquake suites. Note that the solid lines represent the reduction factors, while the grey lines represent the standard error of control. Note that there are three solid curves for each set of results where the upper, central and lower curves represent the 84^{th}, 50^{th} and 16^{th} percentiles, respectively.

Each suite shows similar results with the SA33TMD* system having a much smaller band width (or level of uncertainties) and SEC value than the any other TMD system indicating an improvement in performance and more predictable response of the system and this statistical properties are clear for higher intensity of suites and in terms of displacement reduction. These results show that even if the PTMD system is perfectly tuned for the structural system the SA33TMD* system has a better overall performance with smaller band widths.

In reality, tuning a PTMD system to perfection would be very difficult, if not impossible due to insufficient structural information and changes in the structure over time. Hence, the SATMD system without rubber bearings offers a suitable alternative as it is easier to design with a certain resetable stiffness, a value that does not have to be exact for the system to have an improved performance.

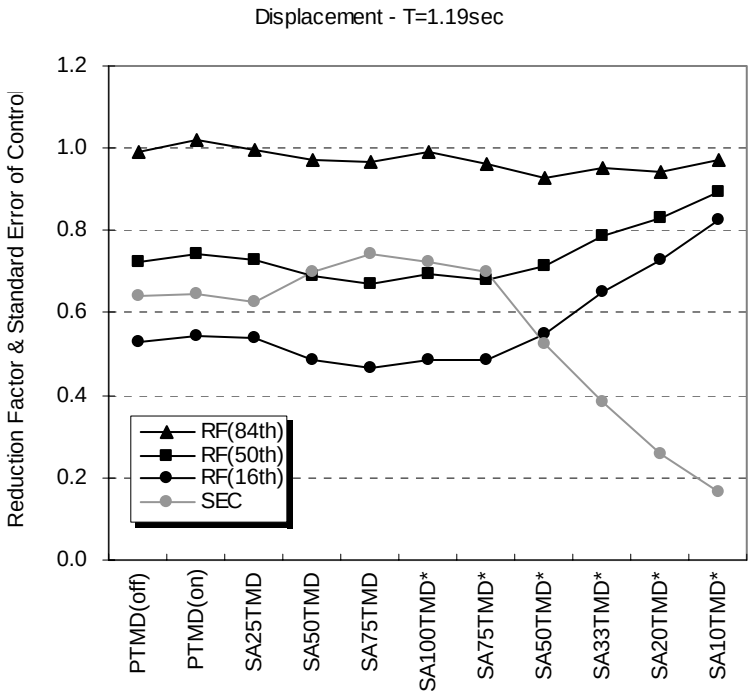

Figure 5-22 Displacement reduction factor and standard error of control (T=1.19sec/Low suite)

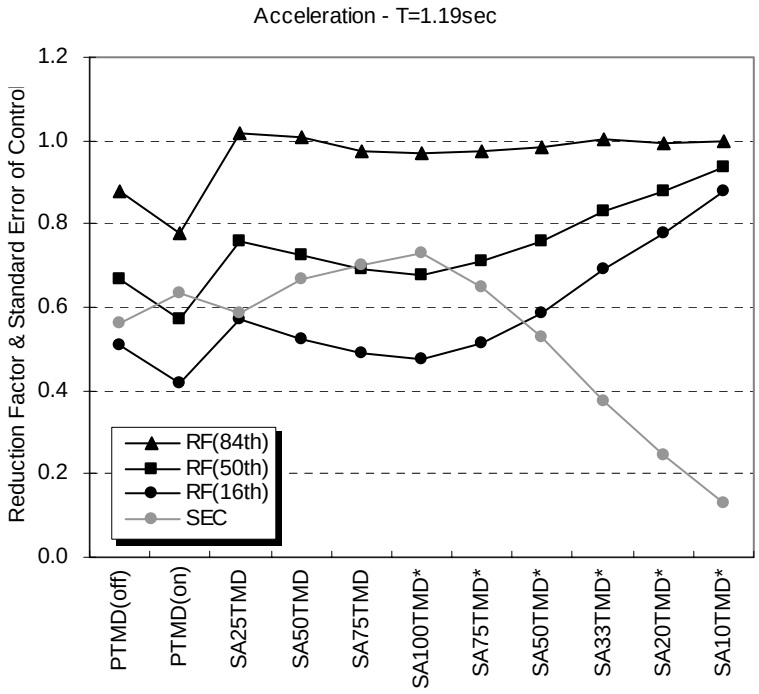

Figure 5-23 Acceleration reduction factor and standard error of control (T=1.19sec/Low suite)

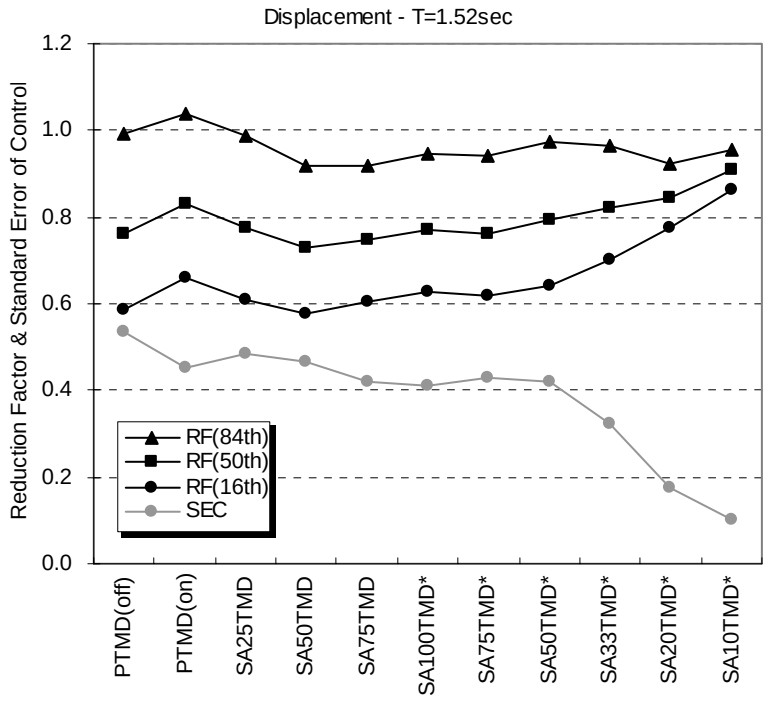

Figure 5-24 Displacement reduction factor and standard error of control (T=1.52sec/Low suite)

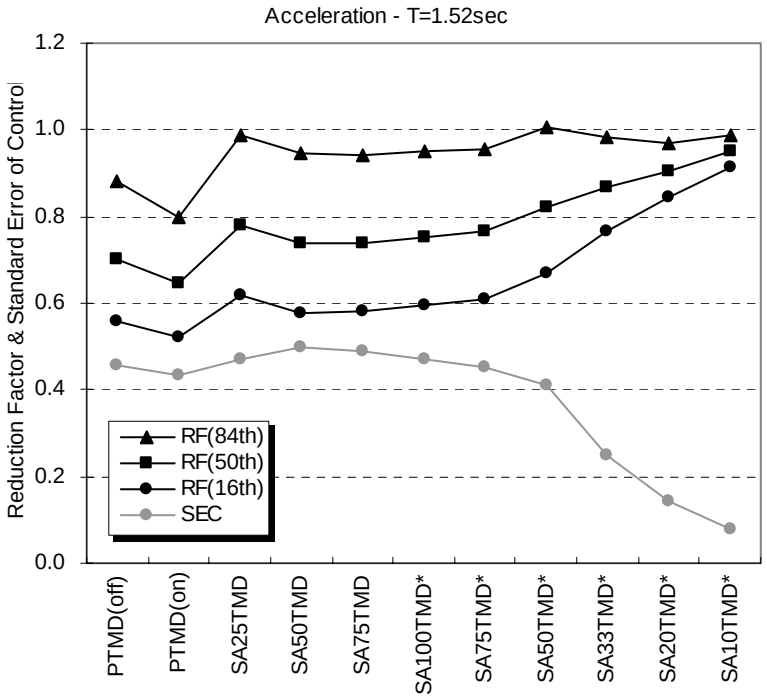

Figure 5-25 Acceleration reduction factor and standard error of control (T=1.52sec/Low suite)

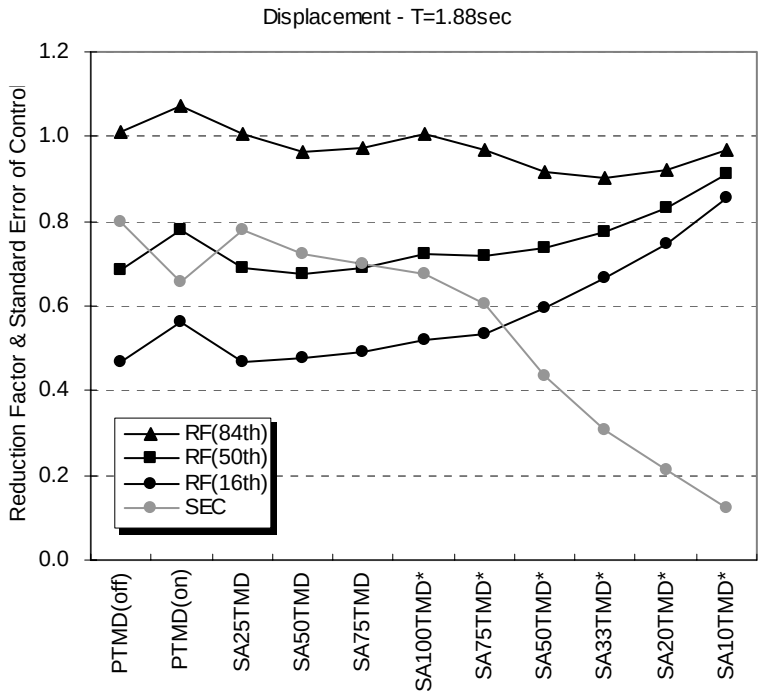

Figure 5-26 Displacement reduction factor and standard error of control (T=1.88sec/Low suite)

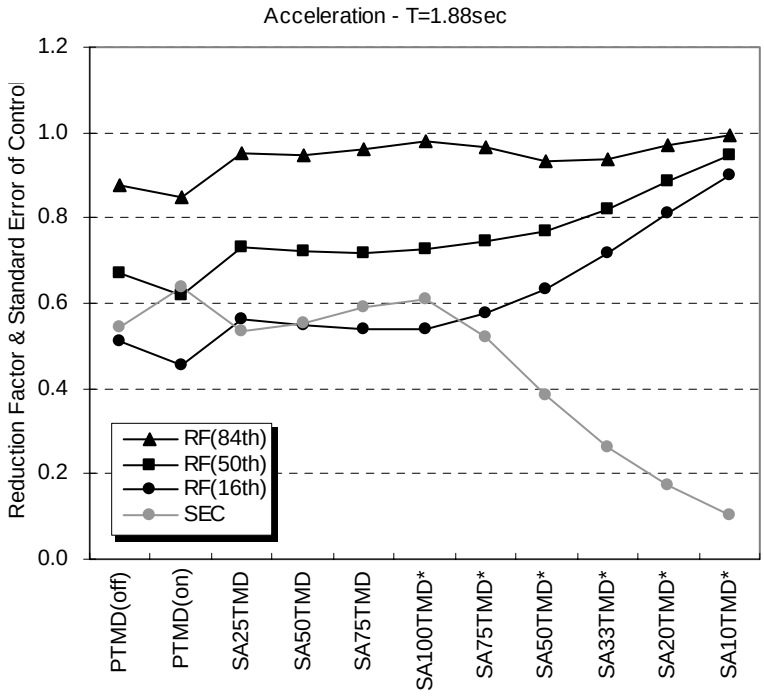

Figure 5-27 Acceleration reduction factor and standard error of control (T=1.88sec/Low suite)

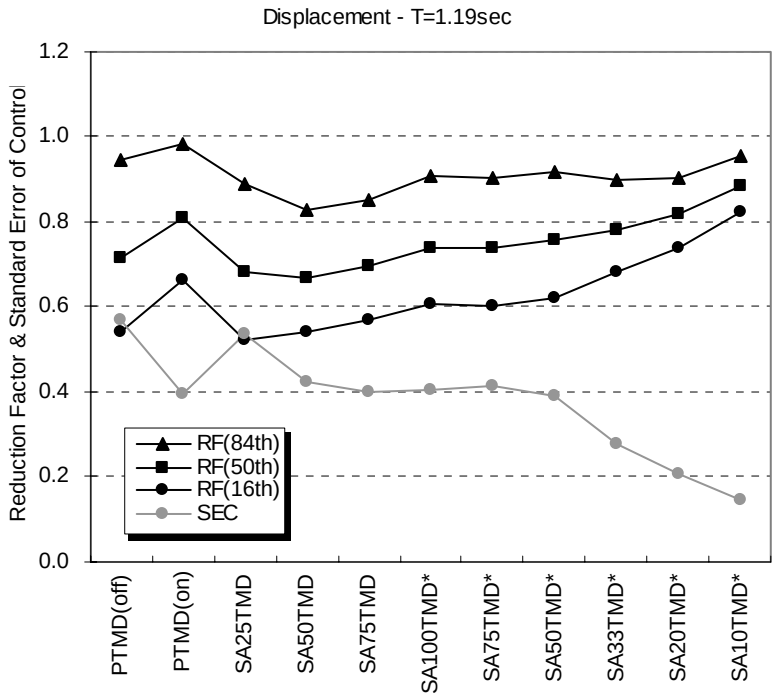

Figure 5-28 Displacement reduction factor and standard error of control (T=1.19sec/Medium suite)

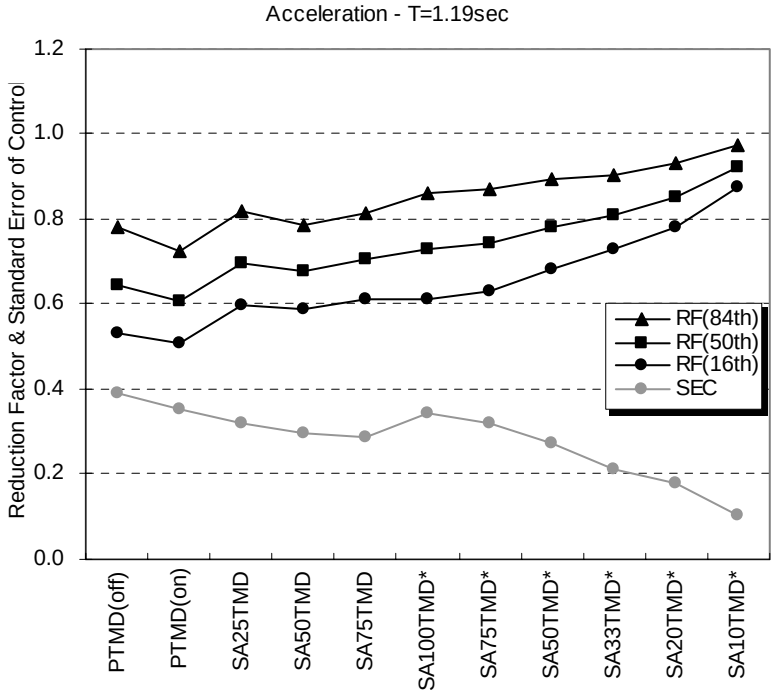

Figure 5-29 Acceleration reduction factor and standard error of control (T=1.19sec/Medium suite)

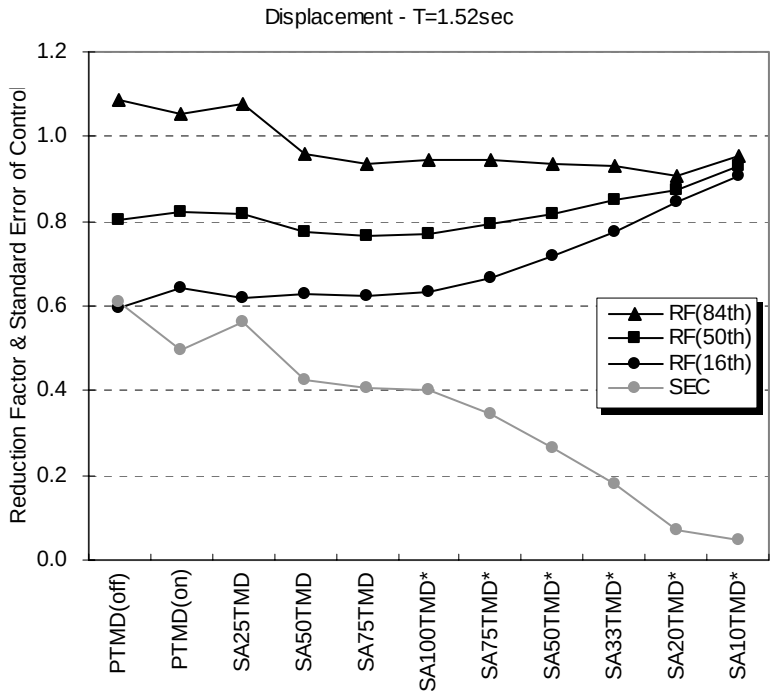

Figure 5-30 Displacement reduction factor and standard error of control (T=1.52sec/Medium suite)

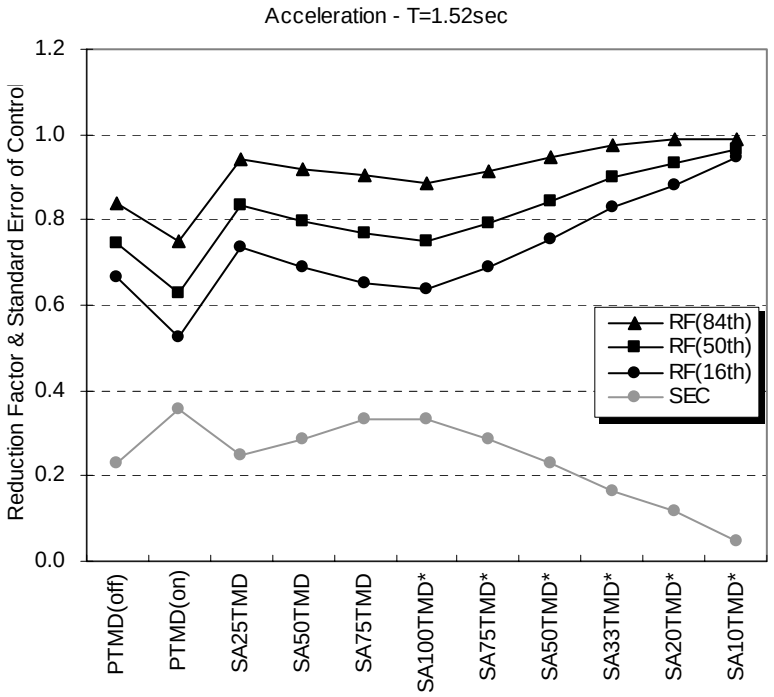

Figure 5-31 Acceleration reduction factor and standard error of control (T=1.52sec/Medium suite)

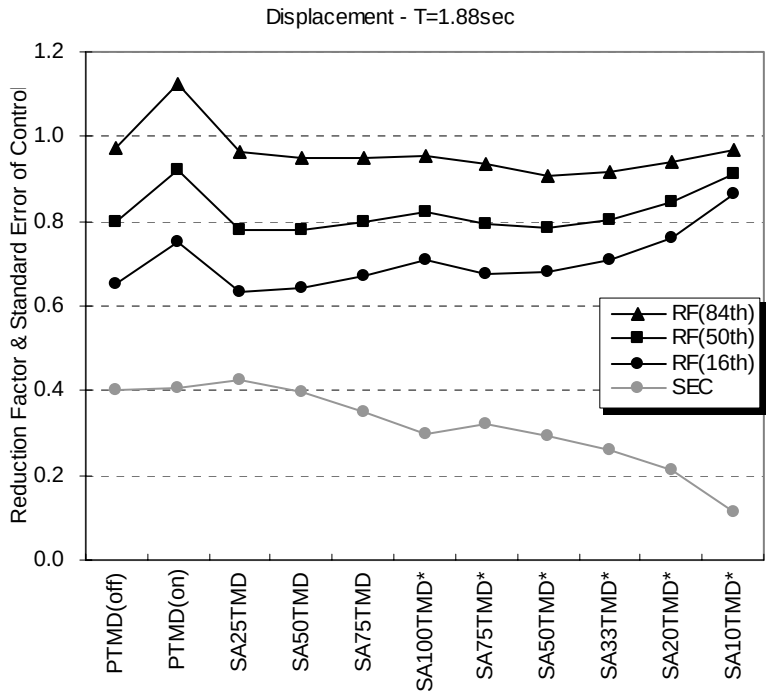

Figure 5-32 Displacement reduction factor and standard error of control (T=1.88sec/ Medium suite)

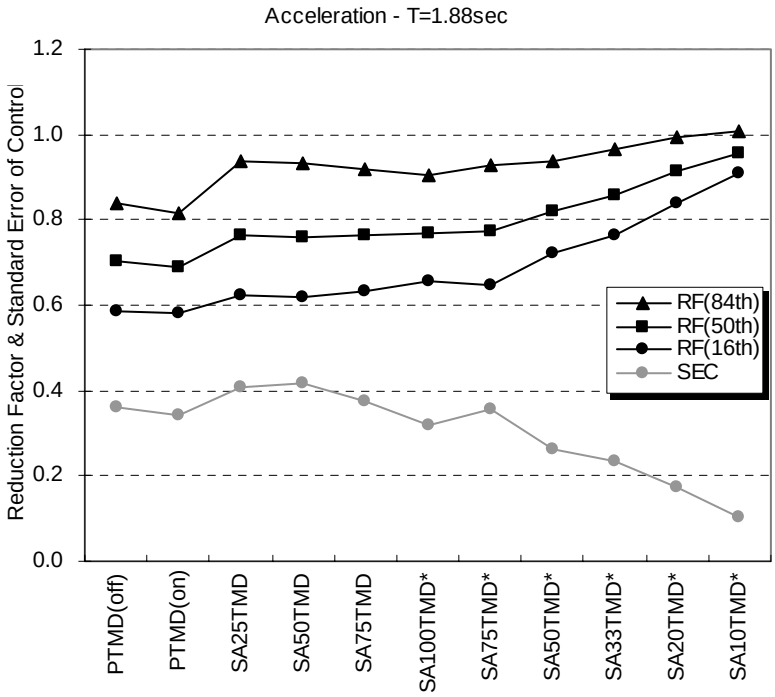

Figure 5-33 Acceleration reduction factor and standard error of control (T=1.88sec/ Medium suite)

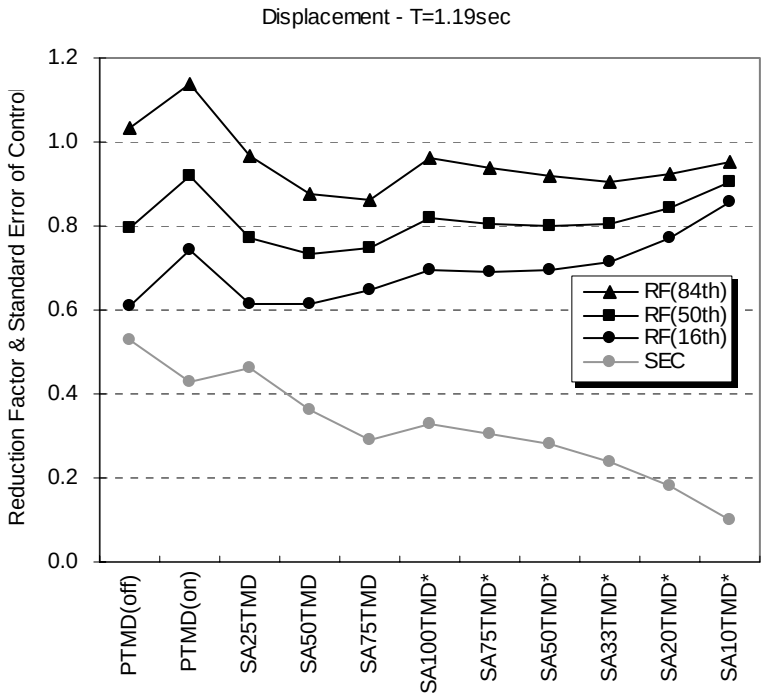

Figure 5-34 Displacement reduction factor and standard error of control (T=1.19sec/Hgih suite)

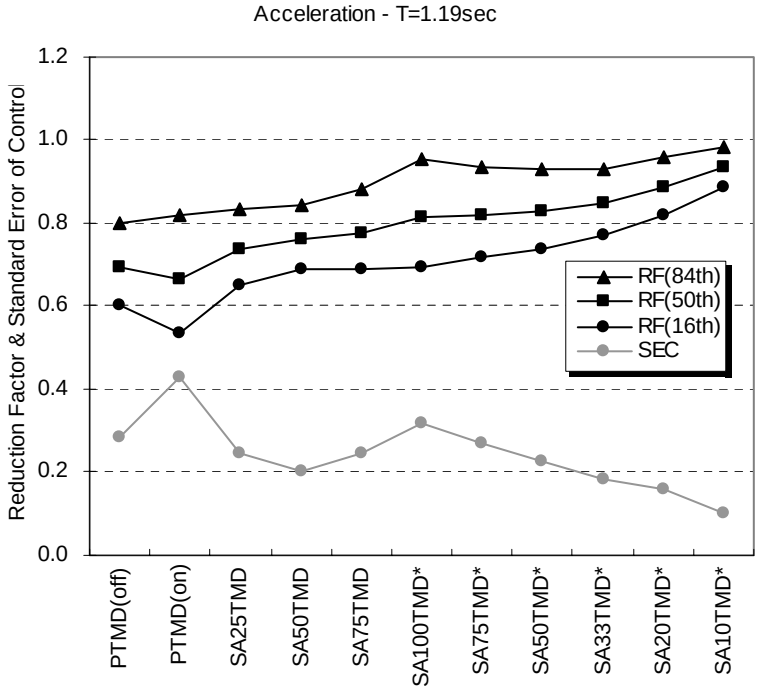

Figure 5-35 Acceleration reduction factor and standard error of control (T=1.19sec/High suite)

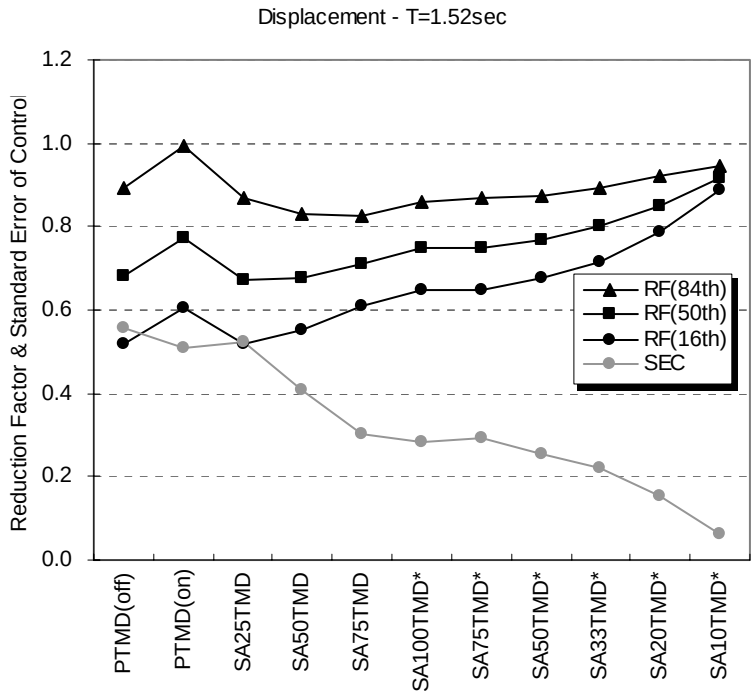

Figure 5-36 Displacement reduction factor and standard error of control (T=1.52sec/High suite)

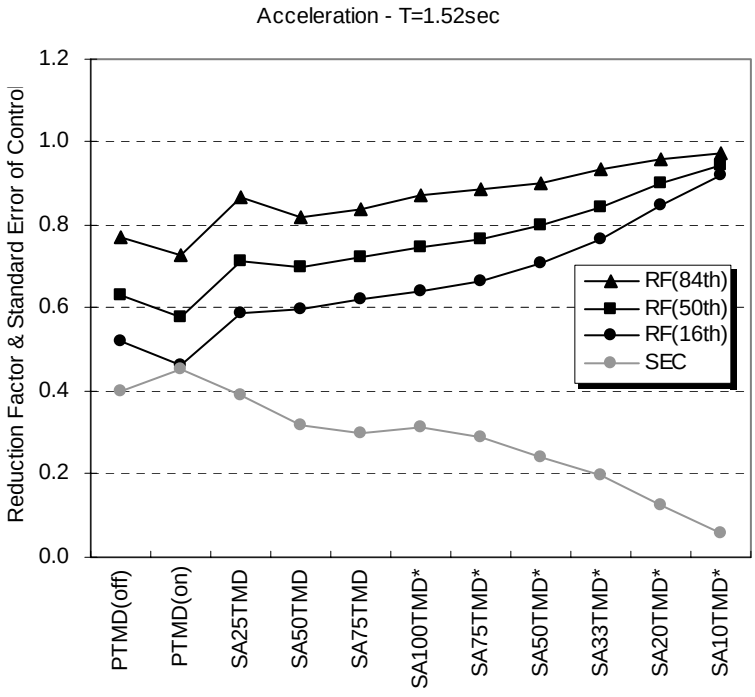

Figure 5-37 Acceleration reduction factor and standard error of control (T=1.52sec/High suite)

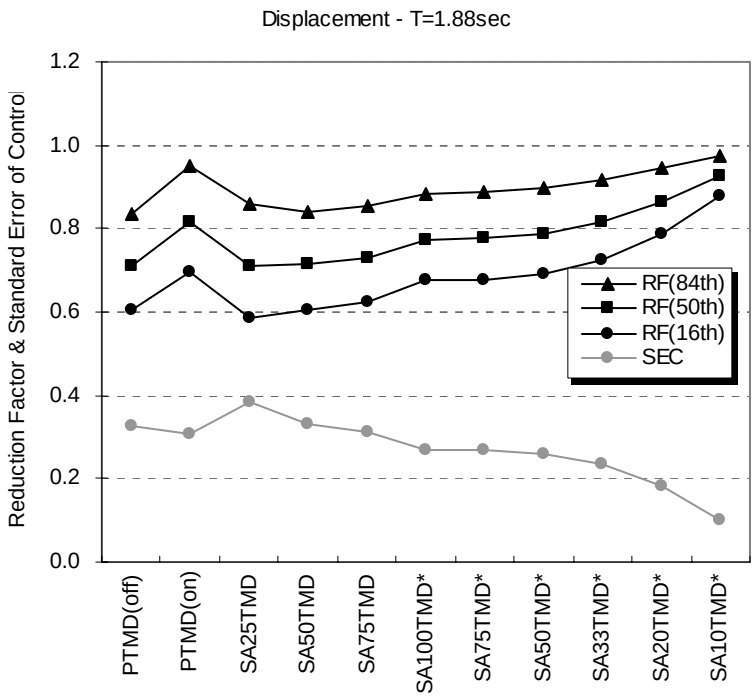

Figure 5-38 Displacement reduction factor and standard error of control (T=1.88sec/High suite)

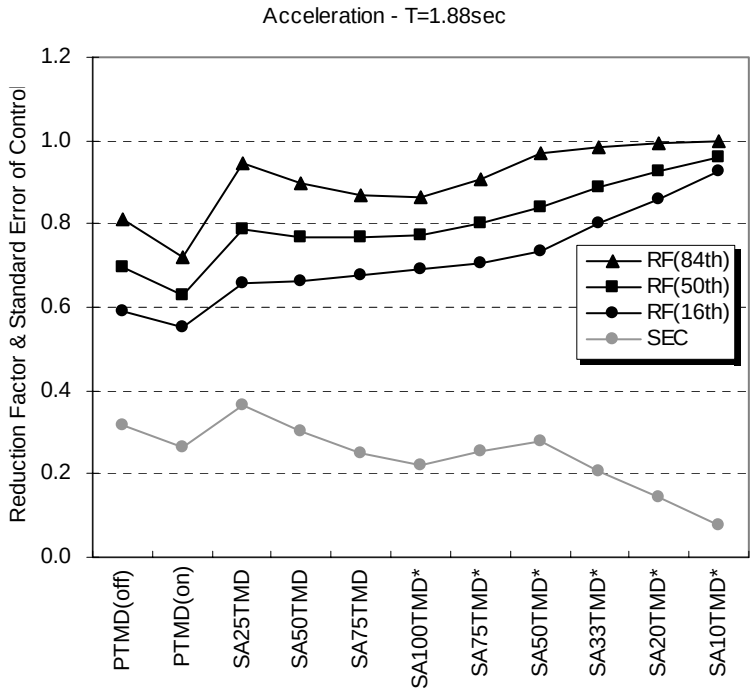

Figure 5-39 Acceleration reduction factor and standard error of control (T=1.88sec/High suite)

Tables 5-4 and 5-5 list the final outcomes for the displacement and acceleration response reduction factors. For the SATMD, in these tables, the case showing the best response reduction factor based on 50^{th} percentile is listed for each natural period of main system. For example, the most effective SATMD control schemes for the main system of 1.19 second period are the SA75TMD (RF=0.672) under the low suite, the SA50TMD (RF=0.670) under medium suite and the SA50TMD (RF=0.733) under high suite respectively. However, over all the TMD systems, the values of SEC for the SA33TMD* systems shows remarkably small values compared to any other cases, for the indicating the potential of this differently tuned system.

From the results, the most effective SATMD for 5 of the total 9 cases is the SA50TMD design, and they also show good reduction values for the rest of the cases. This consistent result shows both the independency of the excitation suites used and that the balanced stiffness between the resetable device (50%) and the rubber bearings (50%) could be a reasonable design strategy for these TMD systems, where the design stiffness matches k_{2opt}.

Table 5-4 Reduction factor of TMD (Displacement)

Suite	Period (sec)	TMD	Reduction Factor (Displacement)		Standard Error of Control
			50^{th}	[16^{th} 84^{th}]	
Low	1. 19	PTMD(off)	0.723	[0.527 0.990]	0.640
		PTMD(on)	0.744	[0.542 1.022]	0.645
		SA75TMD	0.672	[0.467 0.967]	0.744
		SA33TMD*	0.788	[0.651 0.953]	0.382
	1. 52	PTMD(off)	0.762	[0.584 0.993]	0.537
		PTMD(on)	0.829	[0.662 1.038]	0.454
		SA50TMD	0.729	[0.578 0.918]	0.466
		SA33TMD*	0.823	[0.701 0.966]	0.322
	1. 88	PTMD(off)	0.687	[0.466 1.013]	0.796
		PTMD(on)	0.777	[0.563 1.073]	0.656
		SA50TMD	0.677	[0.476 0.963]	0.721
		SA33TMD*	0.773	[0.664 0.900]	0.305
Medium	1. 19	PTMD(off)	0.713	[0.539 0.945]	0.569
		PTMD(on)	0.809	[0.665 0.985]	0.396
		SA50TMD	0.670	[0.543 0.826]	0.422
		SA33TMD*	0.783	[0.681 0.899]	0.279
	1. 52	PTMD(off)	0.804	[0.596 1.084]	0.608
		PTMD(on)	0.823	[0.673 1.052]	0.498
		SA75TMD	0.764	[0.624 0.935]	0.407
		SA33TMD*	0.849	[0.775 0.929]	0.231
	1. 88	PTMD(off)	0.799	[0.654 0.975]	0.402
		PTMD(on)	0.921	[0.753 1.126]	0.405
		SA50TMD	0.782	[0.643 0.951]	0.395
		SA33TMD*	0.805	[0.707 0.916]	0.260
High	1. 19	PTMD(off)	0.795	[0.612 1.033]	0.530
		PTMD(on)	0.918	[0.741 1.136]	0.430
		SA50TMD	0.733	[0.612 0.877]	0.362
		SA33TMD*	0.805	[0.715 0.906]	0.237
	1. 52	PTMD(off)	0.679	[0.517 0.893]	0.554
		PTMD(on)	0.774	[0.602 0.995]	0.507
		SA25TMD	0.671	[0.518 0.871]	0.525
		SA33TMD*	0.800	[0.716 0.894]	0.222
	1. 88	PTMD(off)	0.711	[0.604 0.836]	0.325
		PTMD(on)	0.814	[0.698 0.950]	0.309
		SA25TMD	0.710	[0.586 0.861]	0.386
		SA33TMD*	0.814	[0.724 0.916]	0.235

Table 5-5 Reduction factors of TMD (Acceleration)

Suite	Period (sec)	TMD	Reduction Factor (Acceleration)		Standard Error of Control
			50^{th}	[16^{th} 84^{th}]	
Low	1. 19	PTMD(off)	0.668	[0.507 0.881]	0.559
		PTMD(on)	0.569	[0.417 0.777]	0.632
		SA100TMD	0.678	[0.475 0.968]	0.728
		SA33TMD*	0.833	[0.691 1.003]	0.375
	1. 52	PTMD(off)	0.703	[0.560 0.881]	0.457
		PTMD(on)	0.645	[0.520 0.800]	0.433
		SA75TMD	0.739	[0.581 0.941]	0.487
		SA33TMD*	0.869	[0.769 0.984]	0.249
	1. 88	PTMD(off)	0.669	[0.511 0.875]	0.543
		PTMD(on)	0.620	[0.453 0.848]	0.638
		SA75TMD	0.719	[0.538 0.962]	0.589
		SA33TMD*	0.821	[0.720 0.937]	0.265
Medium	1. 19	PTMD(off)	0.645	[0.531 0.782]	0.389
		PTMD(on)	0.608	[0.510 0.725]	0.354
		SA50TMD	0.680	[0.586 0.787]	0.296
		SA33TMD*	0.811	[0.730 0.902]	0.211
	1. 52	PTMD(off)	0.747	[0.666 0.839]	0.231
		PTMD(on)	0.629	[0.527 0.750]	0.356
		SA100TMD	0.751	[0.624 0.935]	0.335
		SA33TMD*	0.900	[0.829 0.967]	0.162
	1. 88	PTMD(off)	0.703	[0.588 0.840]	0.359
		PTMD(on)	0.689	[0.581 0.817]	0.342
		SA50TMD	0.760	[0.618 0.934]	0.416
		SA33TMD*	0.860	[0.765 0.966]	0.233
High	1. 19	PTMD(off)	0.695	[0.603 0.801]	0.285
		PTMD(on)	0.663	[0.536 0.821]	0.431
		SA25TMD	0.738	[0.653 0.833]	0.244
		SA33TMD*	0.847	[0.772 0.928]	0.184
	1. 52	PTMD(off)	0.634	[0.519 0.773]	0.400
		PTMD(on)	0.580	[0.463 0.725]	0.452
		SA50TMD	0.698	[0.596 0.818]	0.319
		SA33TMD*	0.846	[0.767 0.933]	0.196
	1. 88	PTMD(off)	0.694	[0.593 0.812]	0.316
		PTMD(on)	0.631	[0.554 0.719]	0.262
		SA75TMD	0.768	[0.678 0.869]	0.250
		SA33TMD*	0.887	[0.800 0.983]	0.207

5.4 Summary

PTMD and SATMD building concepts have been presented and implemented in a design simulation. The suggested system is the synthesis model of the TMD control and segmental building system using purposely separated seismic masses of a structure itself. A 2-DOF model explores the efficacy of these modified control system and the validity of the optimal parameters was demonstrated.

To avoid erroneous conclusions being drawn due to a typical performance for a single earthquake, the log-normal median response values were defined under three earthquake suits from the Los Angeles SAC project representing multi-level seismic hazard. For the parametric study, the efficacy of a stiffness mixture of resetable devices and rubber bearings was illustrated. Based upon the investigation described in this chapter, the following summary conclusions can be drawn:

- SATMD systems with a proper combination of TMD parameters is a relatively better control strategy than PTMD system, especially if the optimum stiffness of TMD (k_{2opt}) is not ideal due to degradation or mis-modelling of the building. Thus, more effective parameter combinations may be available beyond the scope of this initial parametric analysis.
- Semi-active solutions are not constrained to k_{2opt} and its control ability is improved when a lower semi-active stiffness is used, providing robust and effective seismic energy management. Thus, the SATMD system is also easier to design as the tuning of the system to the structure, by altering the stiffness value, is not as critical as for the PTMD system where slight "out-of-tuning" can have a detrimental effect on the structural response. In particular, the use of 100% semi-active control (without passive control) achieves a small control bandwidth over a wide range of ground motions and levels of earthquake intensity.
- There is thus very good potential for the SATMD building concept, especially in retrofit where lack of space constrains future urban development to expand upward. It would be beneficial when additional stories are added to an existing structure as these stories become part of a structural control system,

thus alleviating the necessity for additional mass that is redundant for the majority of the time and has no other use. For example, a 12+2 or 12+4 storey structural concept can be utilised to control 12-storey structures.

The numerical results from the 2-DOF design cases herein can therefore be used as the basic design guideline reference for the design of multistorey applications. Furthermore, the control concept presented here is also amenable to base-isolation (Chase et al. 2007) and hybrid (the TMD with base-isolation building system) control of structures.

6 Prototype Structural Modelling

6.1 Structural Model

A 12-storey, two-bay reinforced concrete framed structure is used to demonstrate the potential and beneficial effects of TMD building systems. This model was designed originally by Jury (1978) according to the New Zealand Loadings Code (NZS4203 1976) based on the concept of capacity design. Its strengths were then revised following the changes to NZS4203 made in 1992 (NZS4203 1992). It was assumed that the frame would be required to resist the component of earthquake motion in the plane of the frame only. No torsional effects for the building as a whole were taken into account. The distance between frames is a consistent 9.2m for the entire building structure.

According to the NZS Code for beam design, all frames share in carrying gravity and seismic-induced loads. Moment redistribution is then carried out using a method developed by Paulay (1976). An effort was made during moment redistribution to allow the full utilisation of beam sections by equalising, if possible, the demand for top and bottom flexural steel at the column face. Thomson (1991) increased the dimensions according to data reported by Paulay (1979), because the original design (Jury 1978) called for overtly high reinforcement ratios. The columns above the first level were specified to remain elastic in accordance with the strong column–weak beam concept.

A width of the floor slab equal to 12 times its thickness was considered to contribute to the elastic stiffness of the beams. The slab thicknesses were 120mm for the framed structure. The building dimensions adopted in this study are shown in Figure 6-1 and the detailed frame data, including yield moments used in the analyses can be found in the Appendix A.

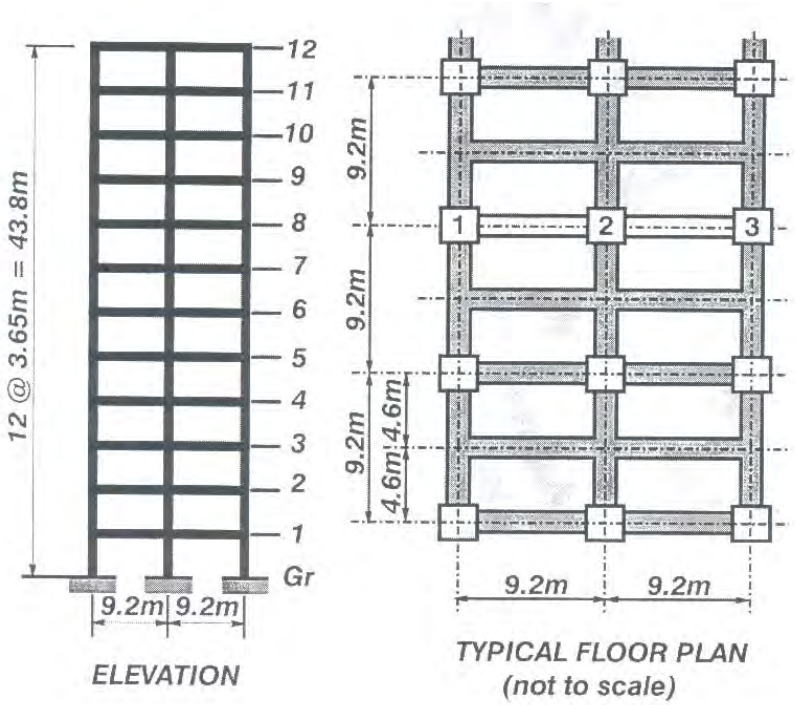

Figure 6-1 Modelling of 12-storey two-bay reinforced concrete frame (Jury 1978)

The member sizes adopted in this study are shown in Table 6-1. The dynamic properties of the frame, such as the natural frequency, modal effective mass, modal damping ratios, and participation factors, are calculated and listed in Table 6-2. It was noted that under the considered structural properties and ground excitations, the displacement response due to the first mode constitutes approximately 80%-90% of the total displacement response. Thus, the first mode was selected for the design of the TMD systems considered.

Table 6-1 Member sizes of the frame structure

Members	Level	Dimensions (mm)
Beams	1 – 6	900 × 400
	7 – 8	850 × 400
	9-12	800 × 400
Exterior Columns	1 – 6	775 × 500
	7 – 8	750 × 500
	9-12	650 × 500
Interior Column	1 – 6	800 × 800
	7 – 8	725 × 725
	9-12	675 × 675

Table 6-2 Dynamic properties of 12-storey building, as modelled

Item	12-storey	Unit
Weight	19,190	kN
1st Modal Mass	1,514	kN-s^2/m
Natural period	1.880	sec
Frequency	3.34	rad/sec
Damping Ratio	0.05	-
1st Modal Amplitude	1.366	-

The assumptions used in this study for the frame include:

- It was assumed that fame is fully fixed at the base.
- To allow for cracking, the second moment of inertia of the beams and columns were taken as 75% of the gross moment of inertia. The cross sectional area of beams and columns was taken as 50% of the gross area.
- Plastic hinge lengths of all members were taken as 70% of the overall depth of the relevant section.
- Rigid end blocks of the beams were assumed as one half the appropriate column width and those of the columns were one half the appropriate depths.
- A value of 5% of critical damping was assumed for each of two normal modes in each structure.
- The initial gravity loading on each structure was assumed to be D+L/3, where D is the dead load and L is the maximum live load.

6.2 Mathematical Modelling and Computational Method

6.2.1 Introduction

Building codes generally prescribe design static lateral loads that are considerably lower than those determined from elastic dynamic analysis. Under earthquake

excitation, the response of building structure is often assumed to be inelastic, rather than elastic. Intensive research on the inelastic behaviour of subassemblages of structural members has been carried out over the past few decades. In the inelastic analysis of reinforced concrete building structures, several fundamental nonlinear effects have been identified to obtain a realistic analysis. These problems include modelling of the inelastic behaviour of the reinforced concrete members, degradation of the stiffness, identifying the shape of the hysteresis loops, P-delta effects, damping of the structural systems, rigid zones at the joints and plastic hinge lengths, and the selection of critical ground motions.

Since inelastic dynamic analysis requires a more refined technique, it is important to select a numerical integration technique that provides both the necessary accuracy and stability (Bathe and Wilson 1973; Wilson et al. 1973). In addition, it is important to create a model that reduces the gap between the analytical results and true behaviour of the structure, as much as possible. However, it is also important to avoid too complex a model. Hence, a delicate balance must be created between realistic nonlinear effects and minimal complexity.

6.2.2 Frame Member

The modelling of frame member elements and their hysteresis loop has been a major discussion point among civil engineers. In inelastic analysis, the modelling is much more critical than in the equivalent elastic analysis. One of difficulties is that while a designer may have a reasonable idea of the stiffness required for a structure prior to carrying out the elastic dynamic analyses, an inelastic analysis is not always practical until the structure has been designed and the member strengths are known. In addition, while the elastic behaviour is reasonably well understood, the representation of the inelastic behaviour of the member is still open to considerable debate and uncertainty, depending upon many potential variables.

Under a large earthquake, concrete structural members may undergo large inelastic deformations followed by the developing of member-end plastic hinges. There is also

a type of inelastic deformation that is associated with transverse cracking along the length of the member, where the inelastic deformation does not concentrate in a critical location (Otani 1980). For the analytical models used here, the simplest member type is introduced based on the idea that the member may be represented as an assemblage of sub-members, where hinges are modelled as the ends of the members.

In this study, the Giberson one-component model (Carr 2004), which consists of a single elastic member with independent inelastic springs at each member-end, was used to model the beam members. Each of the springs is assigned the resistance deformation behaviour of the plastic hinge at the member-end, as illustrated in Figure 6-2. This member has a possible plastic hinge at one or both ends of the elastic central length of the member. The stiffness of the hinge is controlled by the tangent stiffness of the current point on the appropriate hysteresis rule.

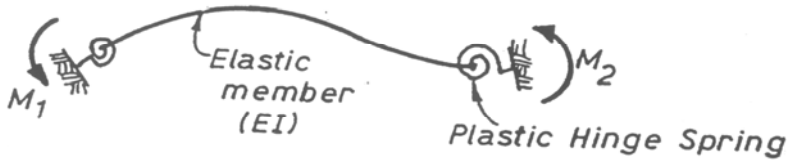

Figure 6-2 Gilberson one component beam model (Carr 2004)

In this model, the inelastic deformations at the member-ends are independent, which means that the inelastic deformation of a member-end is not affected by the moment acting upon the other member-end. Hence, any flexural hysteresis loop can be assigned to the inelastic spring, which constitutes the primary advantage of this model. The disadvantage of this model is that the member-end deformation should depend on the moment acting at both member-ends. This approach means that the deformation at either end is a function of the moment at the other end. Furthermore, it is not always appropriate for all of the inelastic deformation to be modelled as lumped at the member-ends (Otani 1980).

6.2.3 Stiffness Modelling

In reinforced concrete buildings, every member usually has a constant cross section along its length. Even though the degree of cracking could differ along the length of member, it is modelled with a constant cross section. This choice is made for simplicity in formulating the member flexural rigidity, *EI*. Simplifying assumptions are then made for modelling of concrete member flexural rigidities. The simplest modelling assumption takes a fraction of the gross section of concrete member flexural rigidigy, E_cI_e. For the concrete modulus of elasticity, E_c, Paulay and Priestley (1992) recommended the typical values of effective member moment of inertia, I_e.

For symmetrical T beams resisting stresses from flexure, NZS3101 (1982) recommends that the effective width should not exceed one-quarter of the span length of the beam. In addition, its overhanging width on each side of the web should not exceed 8 times the slab thickness or one-half of the clear distance to the next beam. For beams having a flange on one side only, the effective overhanging flange width should not exceed 1/12 of the span length of the beam, or 6 times the slab thickness, or half the clear distance to the next beam.

The effective width of monolithic T-beams gives both an additional stiffness and strength to beams. The effective relative stiffness of the T and L concrete members may therefore be expressed (Paulay and Priestley 1992):

$$K_{eb} = f\left(\frac{E_c I_e}{L_s}\right) \tag{6-1}$$

Where K_{eb} is an effective relative stiffness for T and L beams, L_s, is the beam span, f is a coefficient for the moment of inertia of the flange sections.

6.2.4 Column Moment-Axial Load Interaction

The most popular philosophies in seismic design suggest that the critical sections of columns be provided along the overstrength. The overstrength is designed to be sufficiently large to ensure that virtually all the frame's plastic hinges form in the beam members. However, there is the possibility, especially for the frames where high overturning moments are retained, that the variation of axial loads in columns will cause significant fluctuations of the ultimate strength on some sections during an earthquake.

For common building materials, the relationship between the axial load and ultimate moments of a section is far from linear. Hence, an approximation must be sought to enable a simple numerical representation to be made. The beam-column members used for the base columns in the frame were modelled to allow for interaction between the axial force and bending moment yield states. The interaction was governed by an interaction diagram, as shown in Figure 6-3.

In accordance with accepted principles used in New Zealand, the chosen structural system consists of strong columns and weak beams. Therefore, the strength of a subframe with respect to overturning moments of any kind was designed to be limited by the beam strength. This concept led the behaviour of beams to be inelastic and the columns, except for the first floor, to be elastic for this study.

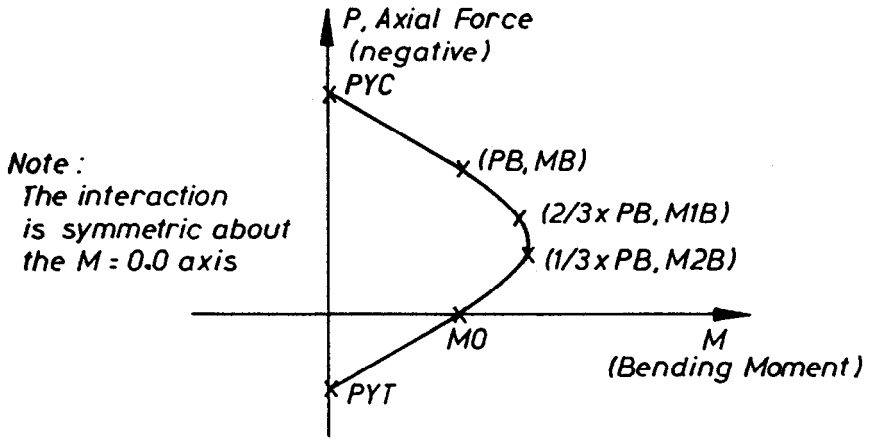

Figure 6-3 Concrete beam-column yield interaction surface (Carr 2004)

6.2.5 Rigid End-Blocks and Plastic Hinge Lengths

The joint at the intersection between the beam and columns performs a very important role in generating the stiffness of moment resisting frame structures. Such joints are usually taken to be rigid so that they can accommodate all of the forces acting on the beams and columns without any joint deformation. There is some evidence from past earthquakes that some structural damage was primarily caused by column failures due to shear failure or inadequate column lateral confinement (Paulay and Priestley 1992).

The usual earthquake resistant design philosophy for ductile moment resisting frame structures allows the formation of beam plastic hinges to be adjacent to the beam-column joints. The internal forces transmitted from these beams or column members result in joint shear forces in both vertical and horizontal directions leading to the diagonal compression and tension stresses within the joint core. However, the New Zealand Standard (NZS3101 1982) states that the joint strength should not normally govern during the development of the full strength of adjoining members and that energy dissipation within the joint core is undesirable. This approach means that during moderate earthquakes the joints should not show any strength degradation.

If the joint remains rigid the beam rigid-zone length can be measured from the centre-line to face of column. Assumptions for the rigid-zone of members can have a significant effect on the stiffness of a frame, its natural frequencies of free vibration and on the response of the structure to dynamic excitation. Some analyses have indicated a decrease in the natural periods of the order of 10% to 20% when member rigid end-blocks were included (Carr 1994).

In this case, natural period decreased by 16% for the 12 storey structure used in this research. Thus, when a member connects into large joins, a rigid end-block effect should be considered for the analysis. The modelling technique of the rigid-zone therefore provides a considerable enhancement in computational effort for this study.

However, results of some laboratory tests showed that after a few cycles of beam plastic hinging, it is not possible to prevent some inelastic deformation from occurring

within the beam-column joints (Al-Haddad and Wight 1988; Paulay and Priestley 1992). Therefore, some design effort is required to relocate plastic hinges away from the column face even when maximum moments occur at there. Some researchers have investigated this relocation of the plastic hinges (Abdel-Fattah and Wight 1987; Al-Haddad and Wight 1988; Park and Paulay 1987), even though this approach causes an increase in the beam curvature ductilities.

The plastic hinge length, L_p, has a direct bearing on the curvature and displacement ductility. Various empirical expressions have been proposed by investigators for the length of the plastic hinge L_p. Several studies (Chai et al. 1991; Priestley and Park 1987) carried out several laboratory tests to determine the approximate plastic hinge length and suggested an expression of the basic form:

$$L_p = 0.08L + 6d_b \tag{6-2}$$

Where L is the distance from the point of contra-flexure of the column to the section of maximum moment, and d_b is the longitudinal bar diameter.

For typical beam and column proportions, it was recommended that the approximate average value of the member plastic hinge be defined (Paulay and Priestley 1992; Priestley and Park 1987):

$$L_p \approx 0.50d_m \tag{6-3}$$

where d_m is the depth of the concrete member.

In this study, the plastic hinge lengths were taken as 70% of the overall depth of the relevant section.

6.2.6 Mass and Damping

For any seismic analysis, the inertia properties of a structure need to be modelled by assigning appropriate mass values to selected degrees of freedom. In this study, the weights of the structure are converted to masses internally within the program

Ruaumoko. Generally, for building models, masses are typically lumped at the floor levels. These floor masses are then distributed to the different load resisting frames on the basis of the frames tributary areas. The mass used in this study was a lumped mass matrix where contributions are made to the diagonal terms associated with the two translational degrees of freedom at each end of the member, with no mass contribution to the rotational degrees of freedom.

The critical damping of the structure should also be considered, since the damping forces contribute to the equation of dynamic equilibrium. The damping can thus affect the displacement of the structure, as well as the following inelastic displacements of the members. For direct integration of the equations of motion, a Rayleigh type representation of damping is very popular as a damping model because it uses the mass and stiffness matrices that are already computed within the analysis. In this study, the Rayleigh or Proportional damping model was used. The damping matrix [C] is thus defined as a linear combination of the mass [M] and stiffness [K] matrices.

$$[C] = \alpha[M] + \beta[K] \tag{6-4}$$

There are only two tuning parameters, α and β, that can be varied to give the desired amounts of damping at two different frequencies. The coefficients α and β are specified or computed by specifying the fraction of critical damping for two user specified modes. The selection of values for the constants α and β may be guided by knowledge and/or experience of these modal damping properties. For example, if the fractions of critical damping, ξ_1 and ξ_2, associated with two different modes of vibration having the respective frequencies ω_1 and ω_2, are known, then the constants α and β in Equation (6-4) can be determined. It should be realized that the Rayleigh damping model permits the prescription of damping ratios for ξ_1 and ξ_2 for only the two selected frequencies, as shown in Figure 6-4, where it is seen that the amount of damping increases almost linearly along with frequency as the natural frequency increases above ξ_2. The amount of damping at all other frequencies is then prescribed by the following equation:

$$\lambda_n = \frac{1}{2}\left(\frac{\alpha}{\omega_n} + \beta\omega_n\right) \tag{6-5}$$

where λ_n is the fraction of critical damping at nth mode of free vibration, and ω_n is the natural circular frequency at nth mode of free vibration.

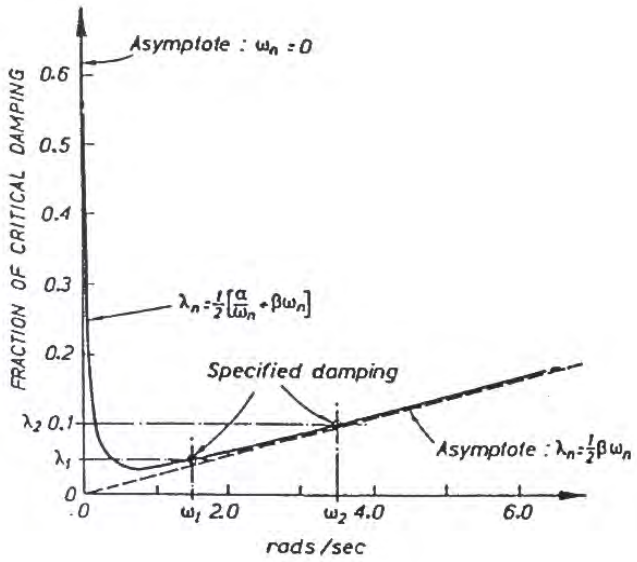

Figure 6-4 Rayleigh or Proportional Damping Model (Carr 2004)

Rayleigh damping can be modelled as proportional to the tangent or initial stiffness matrices. In this study, the initial stiffness matrix was used and 5% critical damping was specified for the 1st and 9th modes of the 12 storey framed structure.

When the TMD is added to the structure, the first mode is affected by the response of the TMD itself. The previously determined 1st and 9th modal damping values for the structure without the TMD were used for the 2nd and 10th modes with the TMD. Thus, the modal characteristics of the structure without the TMD can be transferred to the structure with TMD to create a more equal comparison.

6.3 Summary

This chapter introduced a prototype 12-storey framed structure used for the practical design analysis of multi-storey TMD building systems. This model is strong but close to the current practical design requirements. More specifically, it was designed

according to the New Zealand Loadings Code (NZS4203 1992) based on the concept of capacity design.

In dynamic analysis it is important to set up a proper mathematical model that reduces the gap between the analytical results and the true behaviour of structure during an earthquake. Thus, the detailed member and dynamic properties of the frame have been presented, along with the mathematical modelling and computational method. The modelling technique associated with this model has been developed by the inelastic time-history analysis program, RUAUMOKO (Carr 2004). Overall, it is a realistic nonlinear structure that is broadly representative of tall framed structures in New Zealand and internationally.

7 10+2 and 8+4 Storey TMD Building Systems

7.1 Introduction

In prior Chapter 5, 2-DOF PTMD and SATMD building models were presented and implemented in a system design simulation, and the efficacy of these modified control system and the validity of the optimal designs were demonstrated as the design reference for MDOF verification. Therefore, in this chapter, analyses are extended to the response of MDOF systems through a series of linear time history analyses.

A method for explicitly accounting for the optimum TMD parameter for MDOF TMD systems is suggested and the performance results of the expected seismic demands of MDOF TMD building structures are carried out. This MDOF analysis examines multi-storey SATMD systems that use segregated upper some storeys as a relatively very large tuned mass and a semi-active resetable device to provide robust adaptability to broader ranges of structural response. For this study, the performance of 12-storey SATMD building system models are compared with those from the corresponding No TMD and PTMD building systems, over suites of probabilistically scaled ground motions. Results are presented using appropriate log-normal statistics so that results could be put into standard hazard and design frame works. It is also observed that the expected seismic demands of the structures can be estimated by using modal properties of PTMD and SATMD building systems. Finally, the goal is a proof of concept MDOF analysis of the overall robustness and efficacy of this SATMD design concept in comparison to equivalent, well-accepted PTMD system.

7.2 Modelling

To demonstrate the effects of the SATMD building system, realistic 12-storey two-bay reinforced concrete framed structure models have been developed in *Ruaumoko* (Carr 2004). For SATMD and large mass PTMD systems, the upper two and four storeys are isolated respectively. The resulting retrofitted structures are thus modelled as ‘10+2’ storey and ‘8+4’ storey structures, as shown in Figure 7-1. Figure 7-2

shows the schematic description of isolation layer including rubber bearings and viscous damper or resetable device.

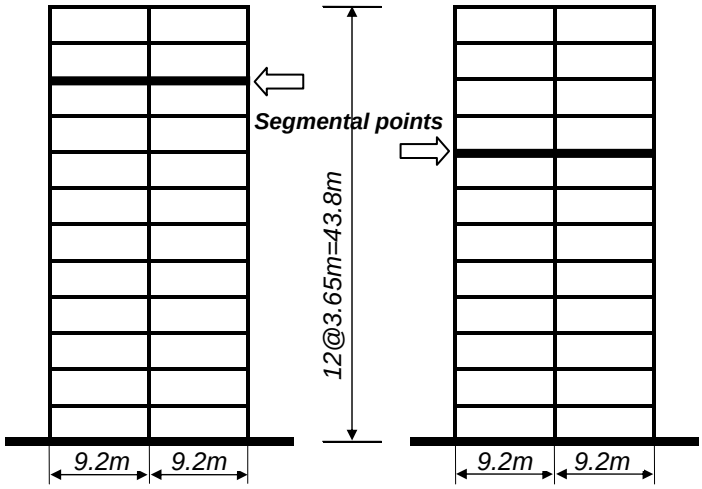

(a) '10+2' model **(b) '8+4' model**

Figure 7-1 '10+2' and '8+4' models of 12-storey two-bay reinforced concrete frames

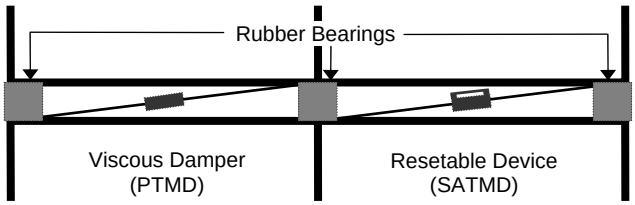

Figure 7-2 Schematic description of isolation layer

The building dimensions and member sizes adopted in these models are shown in Table 6-1. The natural period of the lower part of the each frame model is 1.52sec for the 10-storey structure and 1.19sec for the 8-storey structure respectively. The structural damping ratio of each structure is assumed to be 5% of critical damping. The total weight of the TMD building structures (10+2 and 8+4 structures) is 19,190kN. The dynamic properties of the un-isolated lower frames, including modal characteristics, are listed in Table 7-1.

Table 7-1 Dynamic properties of 8-storey and 10-storey buildings

Item	8-storey	10-storey	Unit
Weight	12,940	16,080	kN
1st Modal Mass	1,072	1,301	kN-s^2/m
Natural period	1.187	1.518	sec
Frequency	5.30	4.14	rad/sec
Damping Ratio	0.05	0.05	-
1st Modal Amplitude	1.309	1.343	-

It was assumed that the frame would be required to resist the component of earthquake motion in the plane of the frame only. No torsional effects for the building as a whole were taken into account. The columns above the first level were specified to remain elastic in accordance with the strong column-weak beam concept. A width of the floor slab equal to 12 times its thickness was considered to contribute to the elastic stiffness of the beams. The slab thicknesses were 120mm for the framed structure.

Figures 7-3 to 7-5 show the force-displacement loops for a modelled, ideal SATMD under three different levels of earthquake intensity. The maximum device forces are set at 644kN and 1,573kN, which represent the value of 13.8% (Hunt 2002) of the structural weight multiplied by mass ratios of 0.244 (10+2) and 0.594 (8+4), respectively. The force-displacement loops show that the force grows linearly with displacement until the maximum displacement is reached for a given cycle. At this point, the force drops indicating that the device has reset. The force then decreases linearly with decreasing displacement until the minimum is reached at which the force jumps to zero again showing that the device has once again reset. These loops represent basic, idealised resetable device operations (Barroso et al. 2003; Bobrow et al. 2000; Carr 2004; Carr 2005; Hunt 2002; Jabbari and Bobrow 2002).

New results in resetable devices can provide highly customised hysteresis loops (Chase et al. 2006; Rodgers et al. 2007b). For this standard case, devices with up to 1.7MN are already in use in limited numbers of commercial structures (Kurino et al. 2006; Shmizu et al. 2006). Hence, the devices for this approach may be assumed to be either available or within the possibility to design.

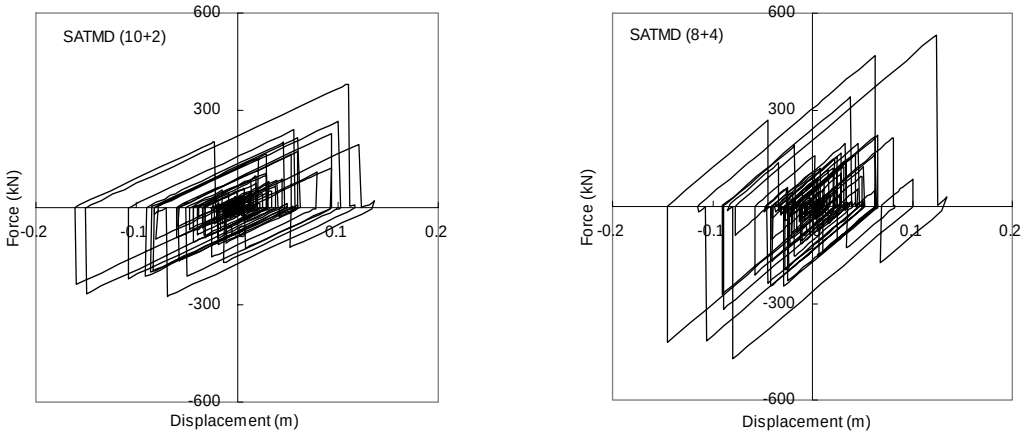

Figure 7-3 Hysteresis behaviour of resetable device (Kern County / Low Suite)

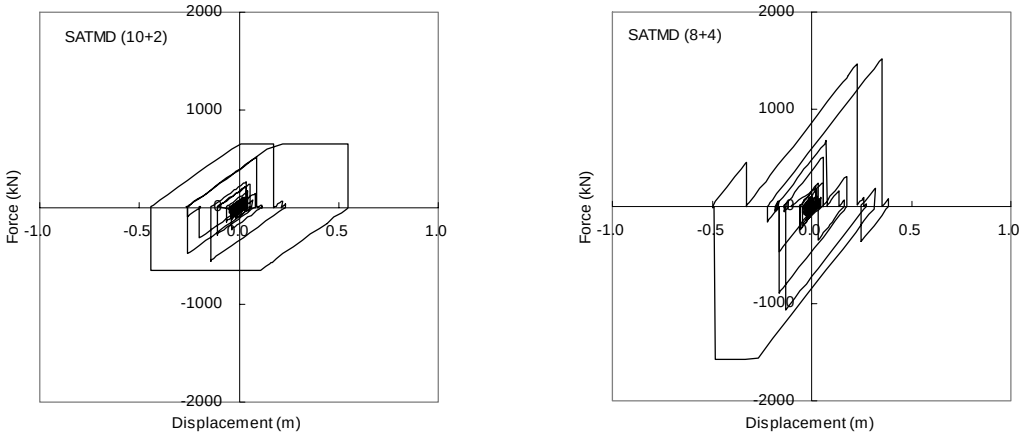

Figure 7-4 Hysteresis behaviour of resetable device (Imperial Valley / Medium Suite)

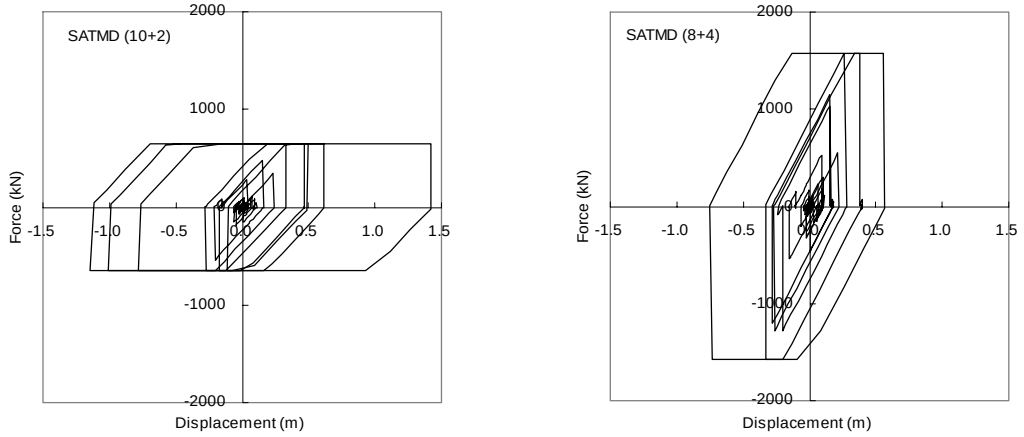

Figure 7-5 Hysteresis behaviour of resetable device (Kobe / High Suite)

For convenience, a flow diagram of optimal design of MDOF TMD building system by numerical optimisation is shown in Figure 7-6. From the diagram, it is seen that the TMD parameters are based on the results of the 2-DOF design process in Chapter 5. The modified TMD parameters for the MDOF system are applied to the multi-storey structures. The dynamic characteristics of the controlled systems are analysed by modal analysis. Finally, time history analyses using suites of ground motions supplies the individual performance values for the final statistical performance assessment, since the use of a probabilistic format allows for a consideration of structural response over a range of seismic hazards.

It was noted that given the structural properties and ground excitations considered, the linear displacement response due to the first mode constitutes approximately 80%~90% of the total displacement response. Thus, the first mode is selected for the design of both the PTMD and SATMD systems.

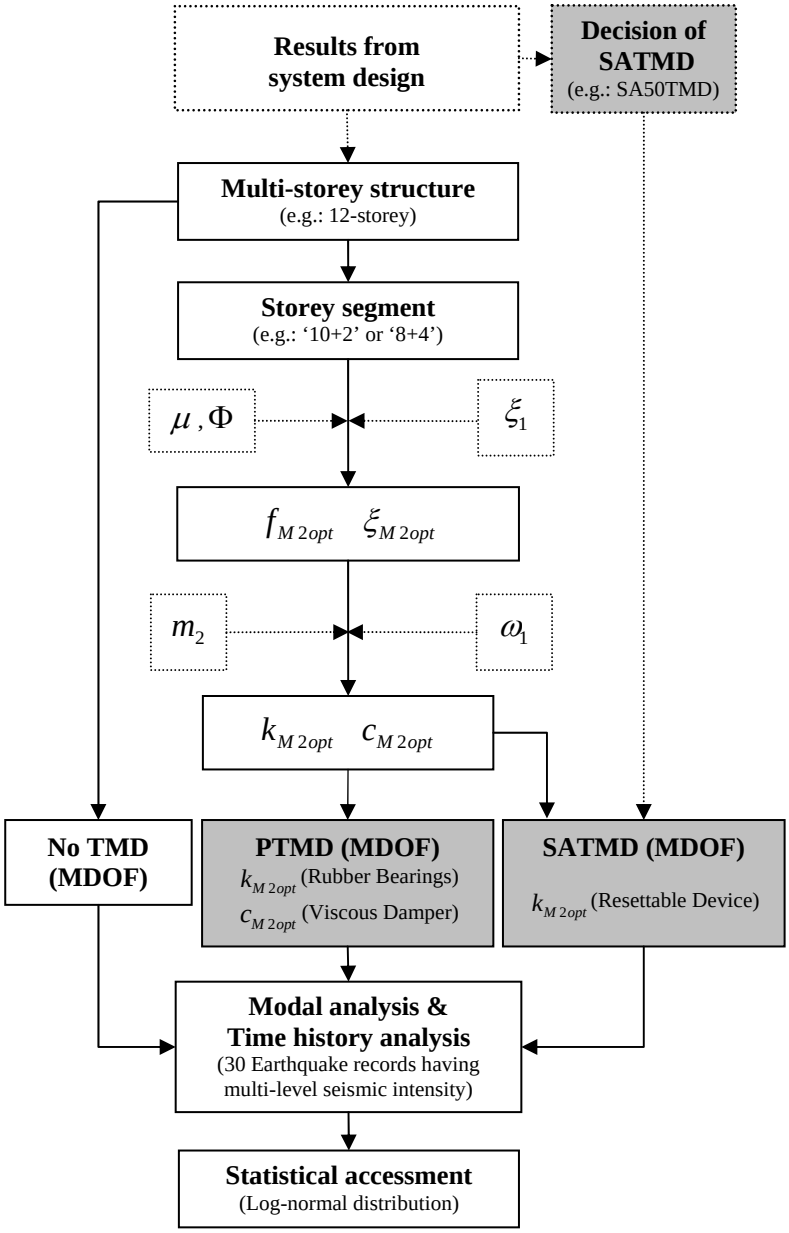

Figure 7-6 Verification process for the TMD building system

7.3 Parametric Optimisation

For a MDOF structure, the mass ratio is computed as the ratio of the TMD mass to the generalised mass for the fundamental mode for a unit modal participation factor

$$\mu = \frac{m}{\phi_1^T [M] \phi_1} \tag{7-1}$$

where [*M*] is the mass matrix and ϕ_1 is the fundamental mode shape normalised to have a unit participation factor. A procedure similar to that for 2-DOF TMD systems is used to determine the optimum parameters that would result in approximately equal frequencies and damping ratios in the first two modes.

For the optimum TMD parameters, it was found that the tuning ratio for a MDOF TMD system is nearly equal to the tuning ratio for a 2-DOF TMD system for a mass ratio of $\mu\Phi$, where Φ is the amplitude of the first mode of vibration for a unit modal participation factor computed at the location of the TMD, i.e. $f_{M2opt}(\mu) = f_{2opt}(\mu\Phi)$ (Sadek et al. 1997). The equation for the tuning ratio is obtained from the equation for the 2-DOF TMD system by replacing μ by $\mu\Phi$. Thus:

$$f_{M\,2opt} = \frac{1}{1+\mu\Phi}\left(1 - \xi_1\sqrt{\frac{\mu\Phi}{1+\mu\Phi}}\right) \tag{7-2}$$

The TMD damping ratio is also found to correspond approximately to the damping ratio computed for a 2-DOF TMD system multiplied by Φ, $\xi_{M2opt}(\mu) = \Phi\xi_{2opt}(\mu)$. The equation for the damping ratio is therefore obtained by multiplying the equation for the 2-DOF TMD system by Φ, as defined:

$$\xi_{M\,2opt} = \Phi\left(\frac{\xi_1}{1+\mu} + \sqrt{\frac{\mu}{1+\mu}}\right) \tag{7-3}$$

For MDOF structures, the practical parameters of the optimal TMD stiffness and the optimal damping coefficient can be thus derived:

$$k_{M2opt} = m_2 \omega_1^{\,2} f_{M2opt}^{\,2} = \frac{m_2 \omega_1^{\,2}}{(1+\mu\Phi)^2}\left(1-\xi_1\sqrt{\frac{\mu\Phi}{1+\mu\Phi}}\right)^2 \quad (7\text{-}4)$$

$$c_{M2opt} = 2m_2\omega_1 f_{M2opt}\xi_{M2opt} = \frac{2m_2\omega_1}{1+\mu\Phi}\left(1-\xi_1\sqrt{\frac{\mu\Phi}{1+\mu\Phi}}\right)\left(\frac{\xi_1}{1+\mu}+\sqrt{\frac{\mu}{1+\mu}}\right) \quad (7\text{-}5)$$

Figure 7-7 shows the optimum TMD tuning and damping ratios versus mass ratio values ranging from 0 to 1, with 5% of internal damping for 10+2 and 8+4 storey models. The optimum values for the 10+2 and 8+2 models have been marked by small squares on the lines at the mass ratios of 0.244 and 0.594 respectively. For the 10+2 and 8+4 models, the weights of the primary structures are 16,080kN (10-storey) and 12,940kN (8-storey), and the amplitude of the first modal vibration, Φ, of 1.343 and 1.309 are adopted respectively. Figure 7-8 shows the optimum TMD stiffness and damping coefficient for the models of 10+2 and 8+4 cases. It can be seen that the gaps between the optimum TMD stiffness lines for the two models increase with increasing mass ratio. However, only relatively small gaps can be found between the optimum TMD damping coefficients for the two models.

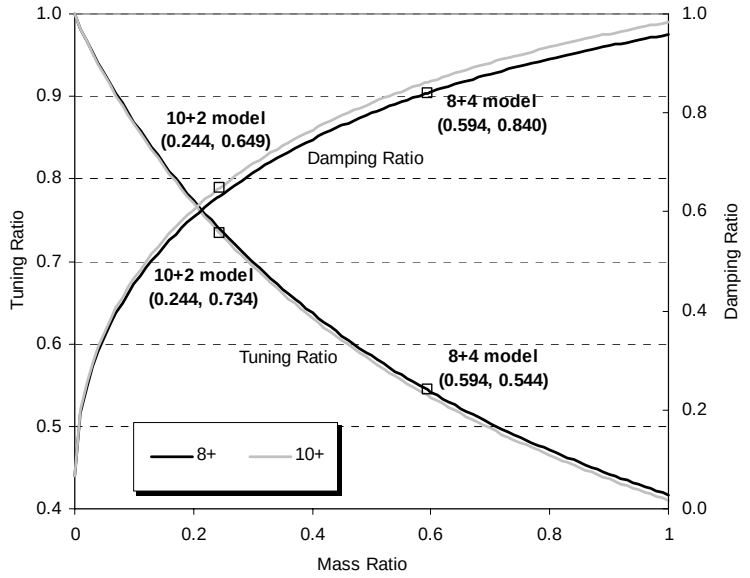

Figure 7-7 Optimum TMD tuning and damping ratios (5% of critical damping)

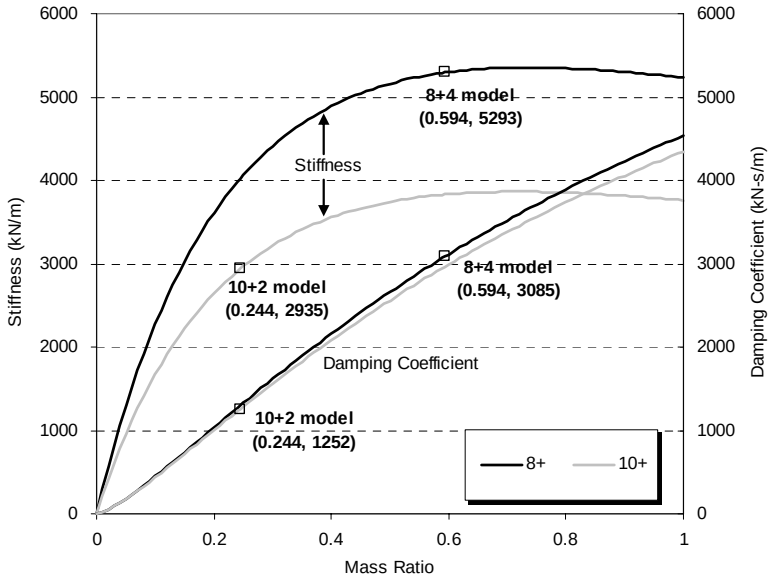

Figure 7-8 Optimum TMD stiffness and damping coefficient (5% of critical damping)

The resulting optimum parameters are listed in Table 7-2. The total value of k_{M2opt} is allocated to rubber bearing stiffness and the stiffness of the SA resetable device. According the results from Chapter 5 for the 2-DOF analysis (system design), the SATMD having same stiffness values of the resetable device and the rubber bearings has been chosen and adopted for each structure and earthquake suite. This equivalent combined stiffness was chosen for simplicity and may not represent an optimal SATMD design (Mulligan 2006a), where much lower stiffness values may be used.

Table 7-2 Parameters for TMD building systems

Model	μ	f_{M2opt}	ξ_{M2opt}	k_{M2opt} (kN/m)	c_{M2opt} (kN-s/m)	Device Force (kN)
PTMD(10+2)	0. 244	0. 734	0. 649	2,935	1,252	-
SATMD(10+2)	0. 244	0. 734	-	2,935	-	644
PTMD(8+4)	0. 594	0. 544	0. 840	5,293	3,085	-
SATMD(8+4)	0. 594	0. 544	-	5,293	-	1,573

7.4 Modal analysis

Modal analysis results using *Ruaumoko* are shown in Figures 7-9 to 7-11. The TMD building systems now offer two major modes of vibration instead of one in the 12-storey uncontrolled (No TMD) case. Despite having two major modes and thus a system susceptible to receiving larger amounts of input energy from an earthquake, a relatively large portion of the entrapped energy is concentrated in the isolation layer. For the SATMD building systems, the 1st mode dominates the upper storeys and a much smaller magnitude 2nd mode dominates the lower storey response. Thus, both the 1st and 2nd modes of the original structure are decoupled by the isolation layer.

These results indicate two different methods of dissipating energy. The PTMD dissipates energy via tuned absorption. However, the SATMD dissipates energy via enhanced relative motion obtained by decoupling the structural segments.

The modal participation factor for the i^{th} mode is defined as:

$$\Gamma_i = \frac{L_i}{M_i} \tag{7-6}$$

in which L_i is the earthquake excitation factor for the ith mode, and M_i is the generated modal mass of that mode. Another useful parameter for the modal response analysis is the mass participation factor.

$$\beta_i = \frac{M_{eff,i}}{M} = \frac{1}{M}\frac{L_i^2}{M_i} \tag{7-7}$$

in which $M_{eff,i}$ is the effective mass for the ith mode and M is the total mass of the building. Because the effective mass indicates the importance of the contribution of the ith mode to the total base shear acting on the structure, the mass participation factor can be an index showing how much of the total mass of the building will contribute in generating base shear in that mode. Thus, if the mass participation factor of the 1st mode is much higher than that of the 2nd mode, the 1st mode can be readily excited by base excitation.

Table 7-3 shows the numerical results of this modal analysis. Second modal participation factors of the SATMD (10+2 and 8+4) building systems are closer to those of the first mode and relatively larger than those of the second mode for the PTMD system. Furthermore, the second mass participation factors of the SATMD building systems are larger than those of the first modes. Therefore, in the SATMD building system, the interaction between the first and second modes is more pronounced and the relatively larger mode and mass participations of the second mode for the SATMD building system may contribute to the further reduction of the overall responses of displacement and base shear responses compared to the PTMD results.

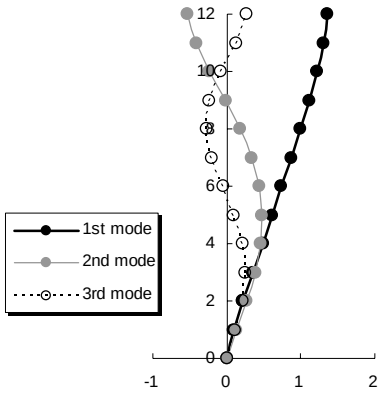

Figure 7-9 Modal analysis (No TMD)

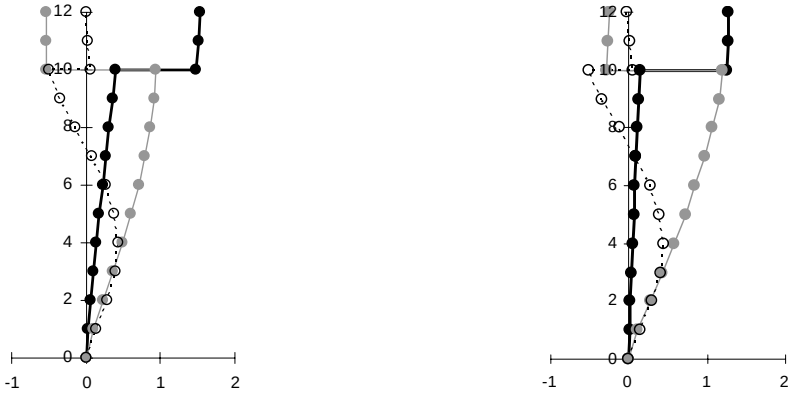

(a) PTMD **(b) SATMD**

Figure 7-10 Modal analysis of '10+2' model (PTMD and SATMD)

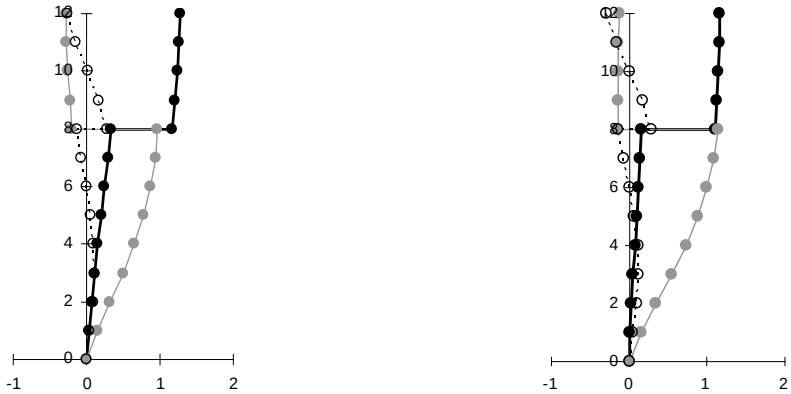

(a) PTMD **(b) SATMD**

Figure 7-11 Modal analysis of '8+4' model (PTMD and SATMD)

Table 7-3 Numerical results of modal analysis

TMD	Mode	Mass (kN-s^2/m)	Freq. (rad/sec)	Part-Fact	
				mode	mass
No TMD	1st	1514	0.53	1.37	0.805
	2nd	252	1.52	-0.53	0.134
	3rd	74	2.73	-0.27	0.039
PTMD (10+2)	1st	816	0.38	1.53	0.436
	2nd	812	0.74	0.94	0.434
	3rd	181	1.92	-0.50	0.097
SATMD (10+2)	1st	513	0.27	1.27	0.274
	2nd	1109	0.68	1.20	0.593
	3rd	187	1.90	-0.50	0.100
PTMD (8+4)	1st	1020	0.36	1.29	0.541
	2nd	697	0.96	0.97	0.370
	3rd	39	2.39	0.28	0.021
SATMD (8+4)	1st	834	0.27	1.17	0.442
	2nd	878	0.89	1.15	0.465
	3rd	47	2.33	-0.30	0.025

7.5 Performance Results

Figures 7-12 to 7-23 show the 50th percentile (median) and 84th percentile levels of several seismic response criteria of the No TMD, PTMD (10+2 and 8+4) and SATMD (10+2 and 8+4) are subjected to three suites of earthquakes. For comparison, the SATMD* (8+4), which used 33% of the optimum TMD stiffness is also presented. The maximum relative displacements, interstorey drift ratios, normalised storey shear forces (shear forces divided by structure weight) and total accelerations for all floors are calculated as control effectiveness indices.

Overall, the TMD (PTMD and SATMD) building systems show good response reduction quantities. Almost all results show the ability of the SA device and larger mass ratio reduce overall structural response measures. In particular, the reduction of seismic demands for these cases is most pronounced in the 84th percentile responses.

The maximum displacements of each level increase steadily over the height of the level and the control effects of the displacement are proportional as the height of the building. Large displacements can be found at the isolation layer, especially in the SATMD system. However, this tendency is expected based upon the modal properties of the almost separated modal responses and the increased participation factor of the 2nd mode. They also maximise the dissipative effect of the SA devices to best effect within this design.

The better control effects of the SATMD and the higher mass ratio (8+4) building structures, as compared to the PTMD building system, can be seen in the interstorey drift and shear force at mid and higher floor levels. This tendency is increased for the larger intensity, primarily near-field, high suite ground motions. For the interstorey drift, the low suite induces median interstorey drift demands, as a representative value of about 0.5%. This value increases to about 1% and 2% under the medium and high suites respectively.

For the No TMD structure, the location of peak interstorey drift occurs in the 9th floor. However, for the TMD building structures, the interstorey drifts are distributed constantly or proportionally over the floor level under the suites. From the statistical response of the interstorey drifts and storey shear forces, it is apparent that the upper storeys above the isolation interface of the SATMD building system are effectively controlled due to the proper interrupting function of the SA isolation system from the seismic energy. In contrast, the lower storeys of the PTMD building system are reduced more than those of the SATMD system due to the partially coupled modal responses of the 1st and 2nd modes.

The acceleration responses of the isolated storeys of the upper segment show a significant reduction in all cases. The reason for these reductions is that the upper segment is isolated from the main structure, so the base excitation is not transferred to the separated upper portion directly. However, the acceleration response at the isolation interface of the SATMD system is clearly increased due to the operation of resetable device and this point needs to be considered in this type of TMD design.

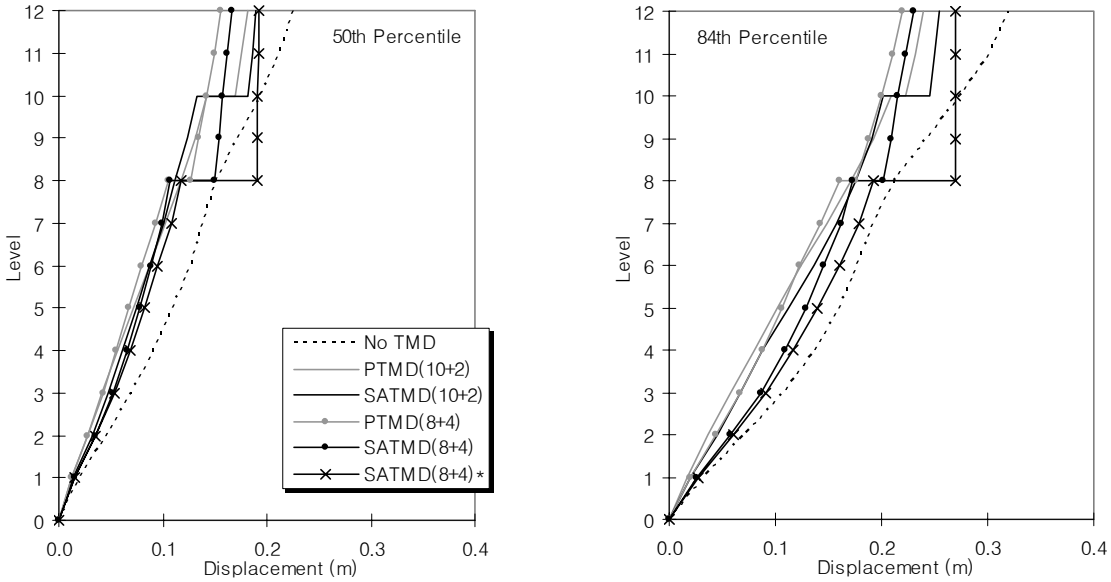

Figure 7-12 Maximum displacement of '10+2' and '8+4' models (Linear / Low suite)

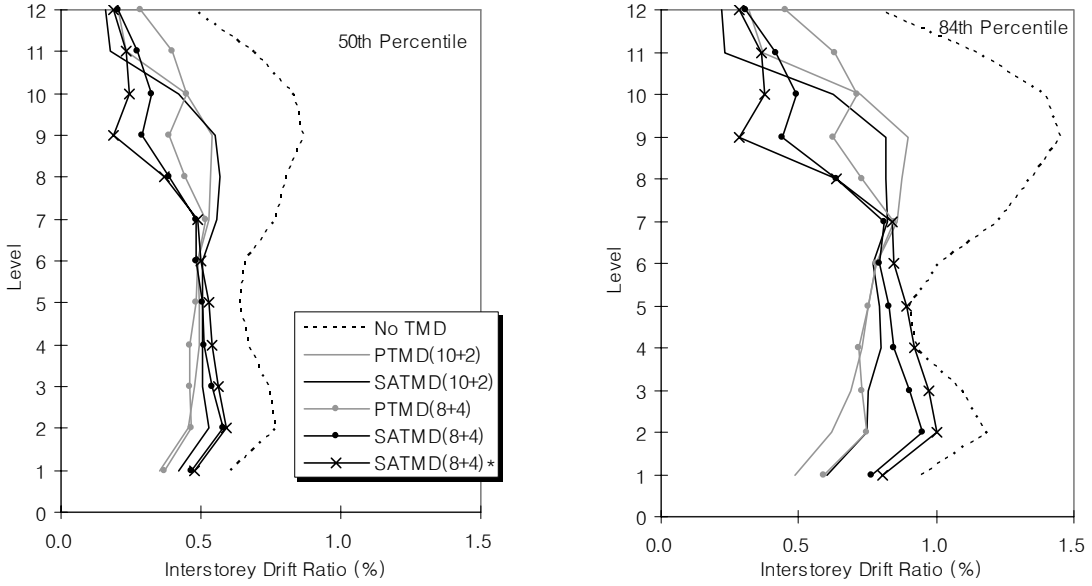

Figure 7-13 Interstorey drift of '10+2' and '8+4' models (Linear / Low suite)

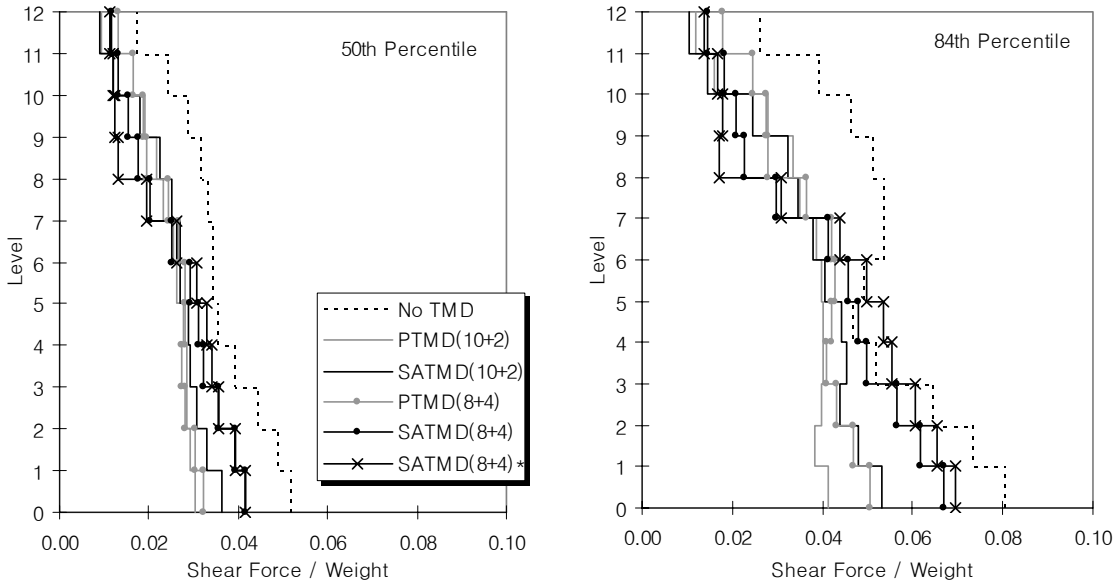

Figure 7-14 Storey shear force of '10+2' and '8+4' models (Linear / Low suite)

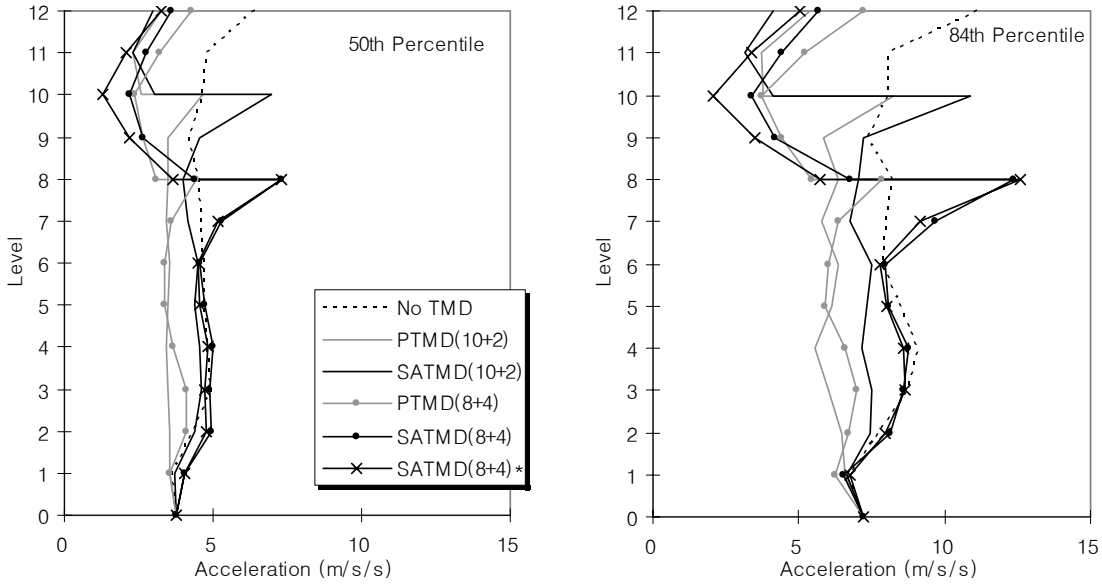

Figure 7-15 Total acceleration of '10+2' and '8+4' models (Linear / Low suite)

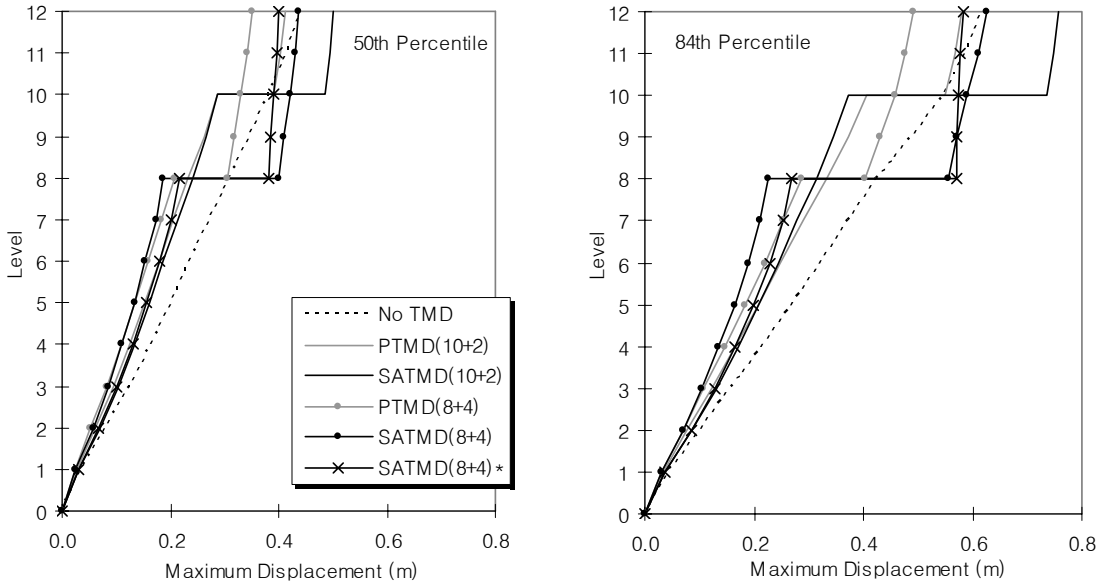

Figure 7-16 Maximum displacement of '10+2' and '8+4' models (Linear / Medium suite)

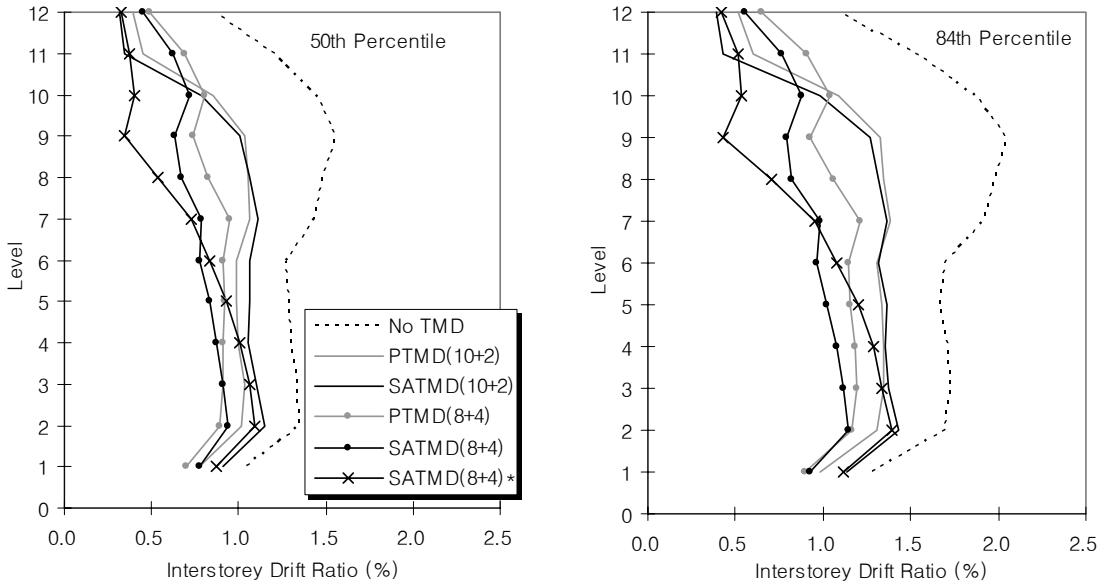

Figure 7-17 Interstorey drift of '10+2' and '8+4' models (Linear / Medium suite)

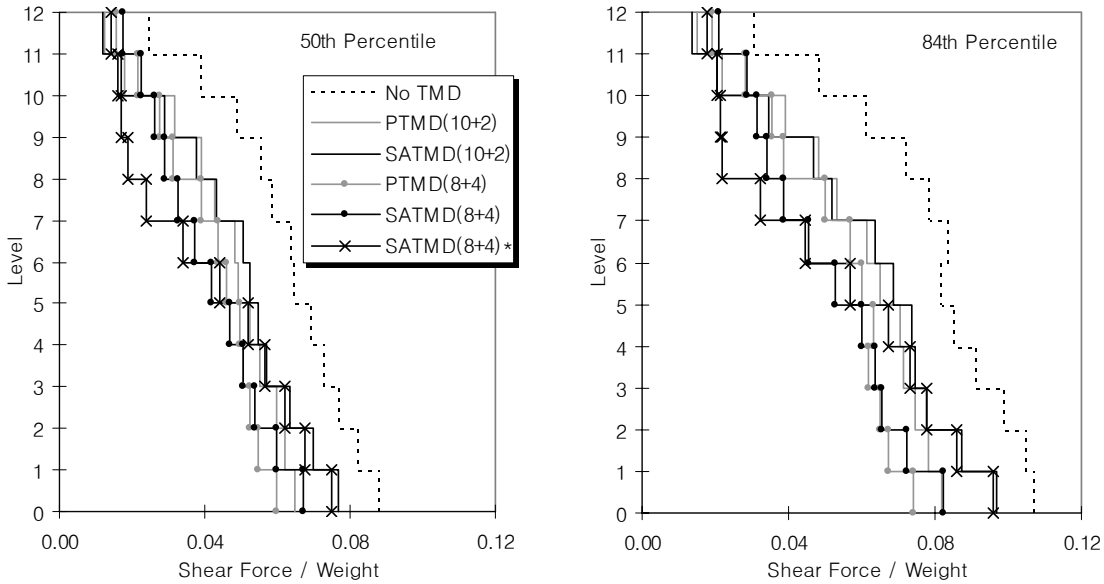

Figure 7-18 Storey shear force of '10+2' and '8+4' models (Linear / Medium suite)

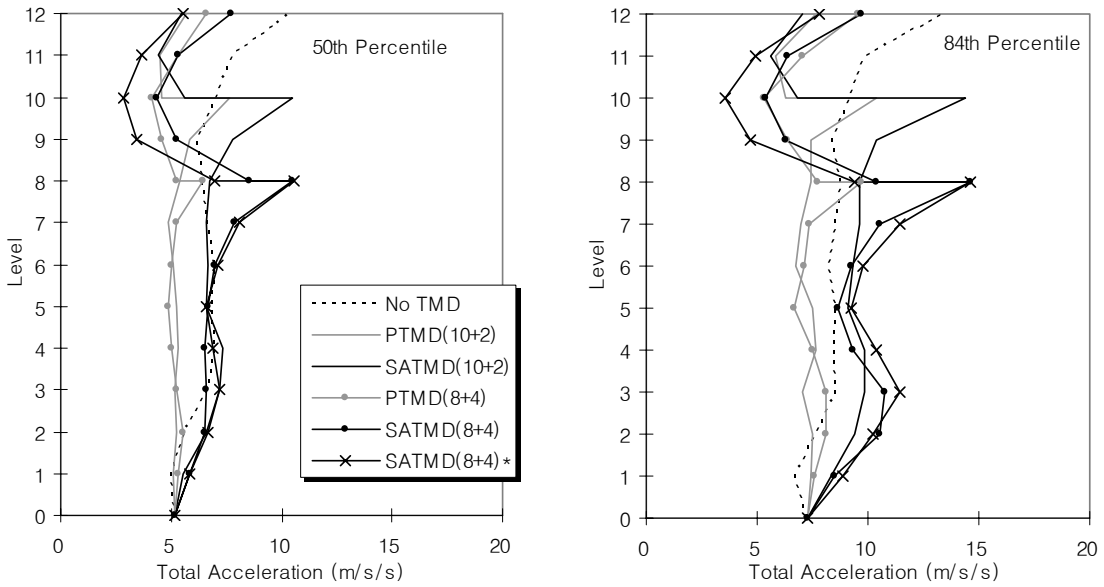

Figure 7-19 Total acceleration of '10+2' and '8+4' models (Linear / Medium suite)

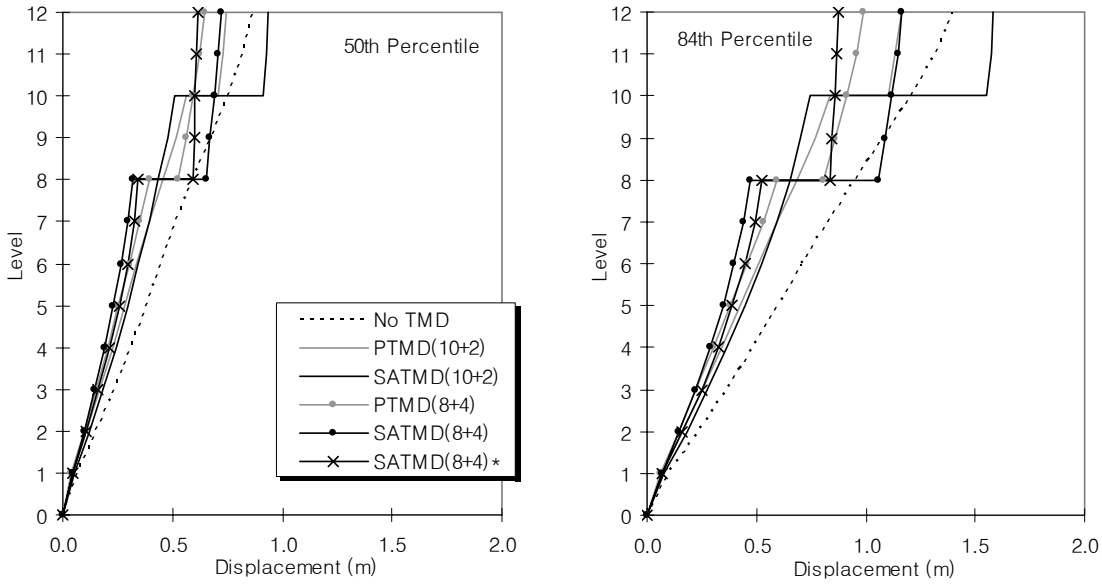

Figure 7-20 Maximum displacement of '10+2' and '8+4' models (Linear / High suite)

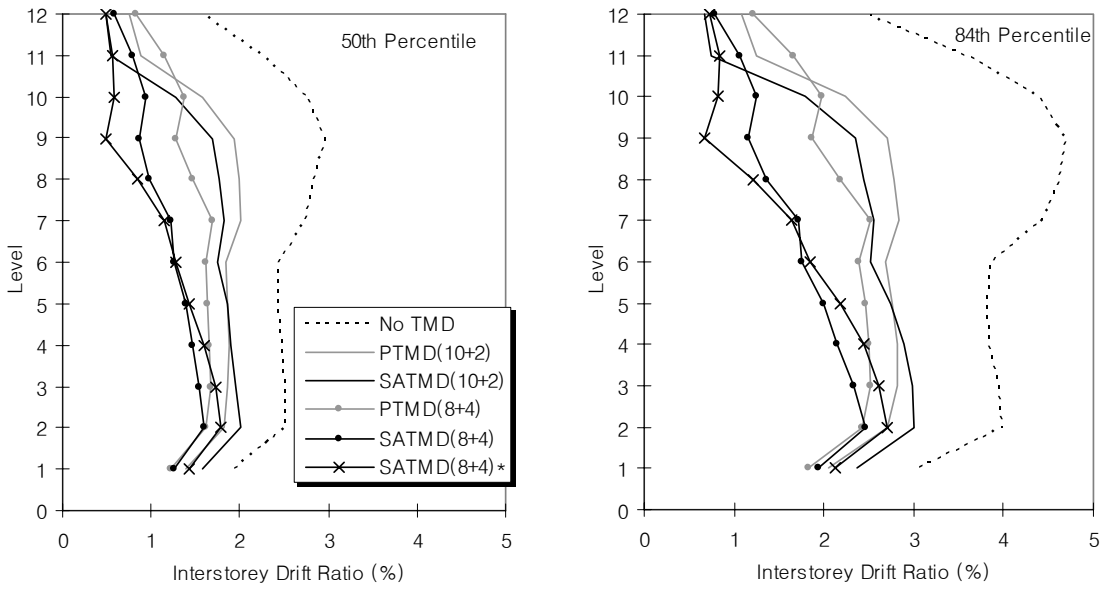

Figure 7-21 Interstorey drift of '10+2' and '8+4' models (Linear / High suite)

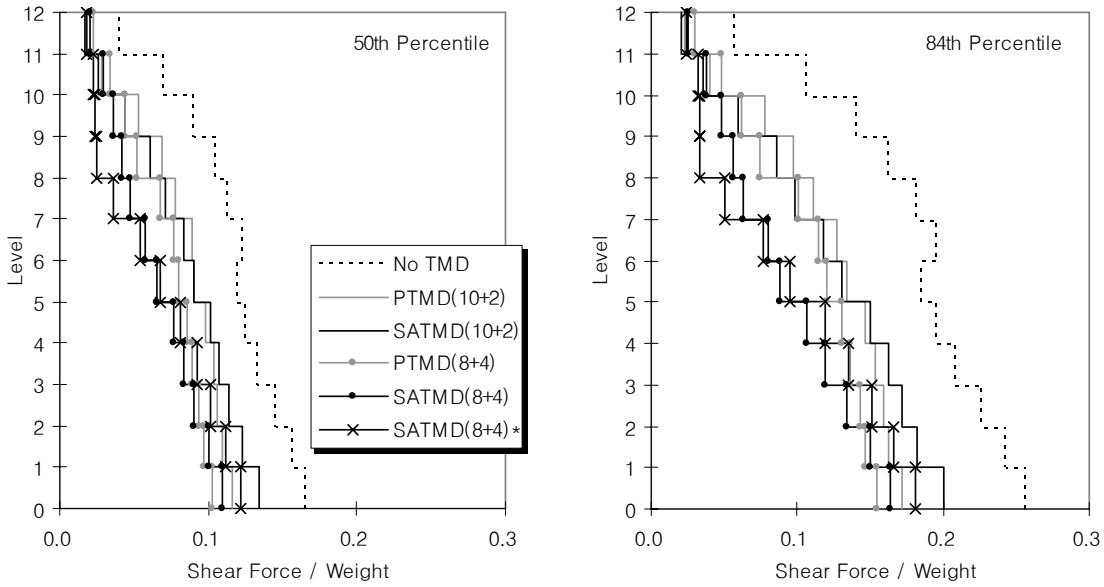

Figure 7-22 Storey shear force of '10+2' and '8+4' models (Linear / High suite)

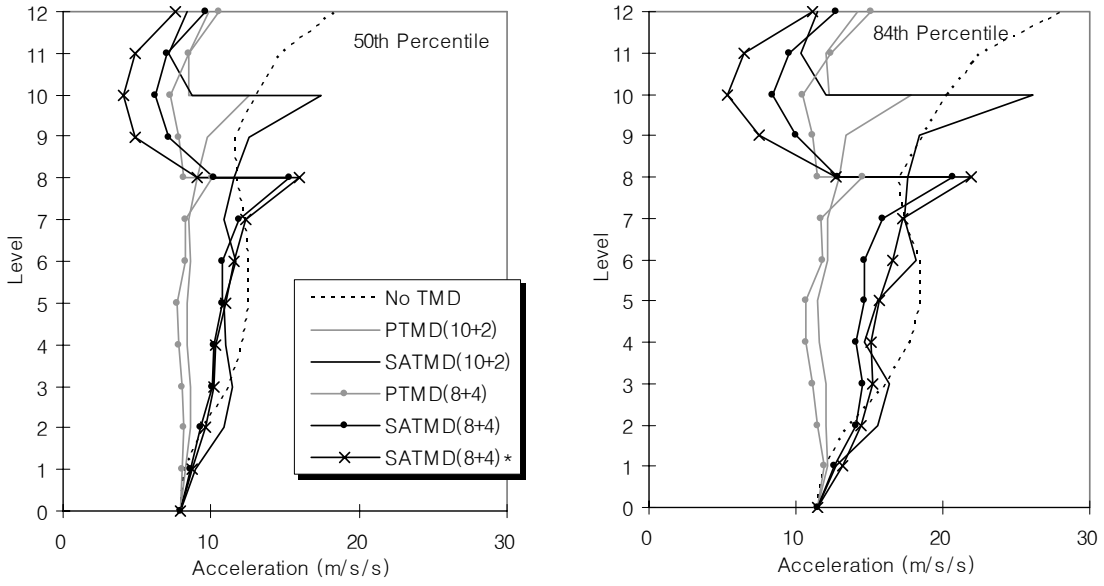

Figure 7-23 Total acceleration of '10+2' and '8+4' models (Linear / High suite)

To compare the relative ability of the different TMD building systems at reducing the seismic demands, the median and 84th percentile structural reduction factor profiles for each suite are generated for the PTMD (10+2 and 8+4) and SATMD (10+2 and 8+4) building systems in series of results presented in Figures 7-24 to 7-35. The multiplicative reduction factors shown in these figures are normalised to the corresponding uncontrolled (No TMD) floor response values. For the response performance indices presented, the reduction factor profiles indicate the advantage of the structural operation of the PTMD and SATMD building systems clearly. Again, these factors reflect the relative control abilities among the TMD systems compared.

For the displacement reduction factors, as seen in the previous performance results, the values of relatively large response behaviour are seen in the storeys above the isolation layer under the medium and high ground motion suites. However, since these large reduction factors of over 1.0 are affected by large displacements at the isolation layer, the displacement within each segment of the upper and lower storeys is relatively small. For the interstorey drifts and shear force reduction factors, the reduction factors of the isolated upper storeys clearly indicate the advantage of the structural operation of the SATMD building systems. For the lower storeys under the isolation layer, however, the reduction factors indicate that the SATMD system is not superior to the PTMD system and it's dependant on the suite used. However, this result may only be accurate for this comparison where both PTMD and SATMD systems have the same isolating stiffness, k_{2opt}. Other studies with different values optimased to each case have shown clearer differences, especially if the PTMD is not ideally or perfectly tuned (Mulligan 2006b).

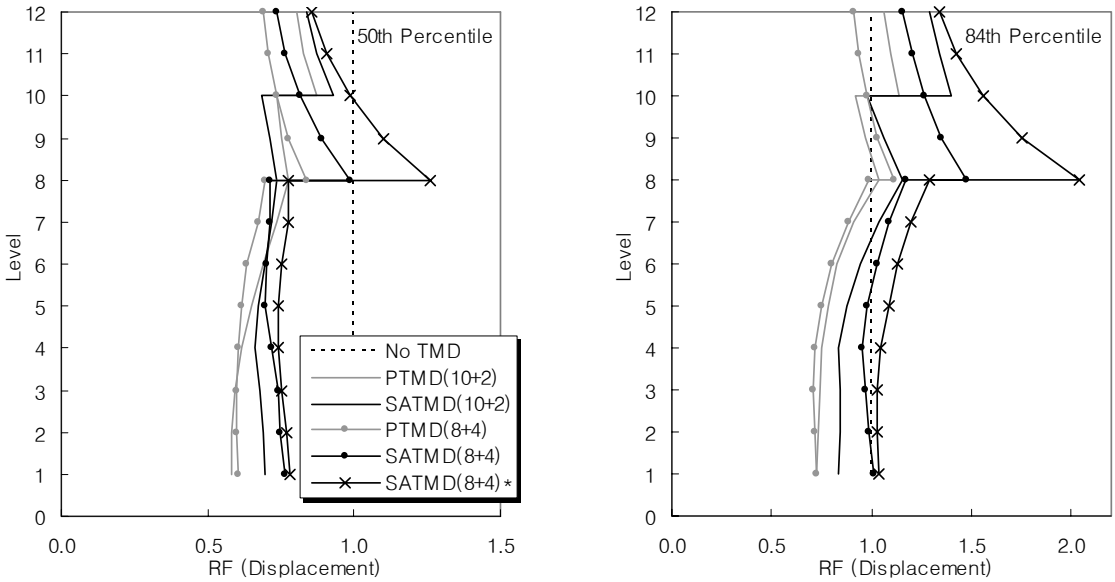

Figure 7-24 Displacement reduction factor of '10+2' and '8+4' models (Linear / Low suite)

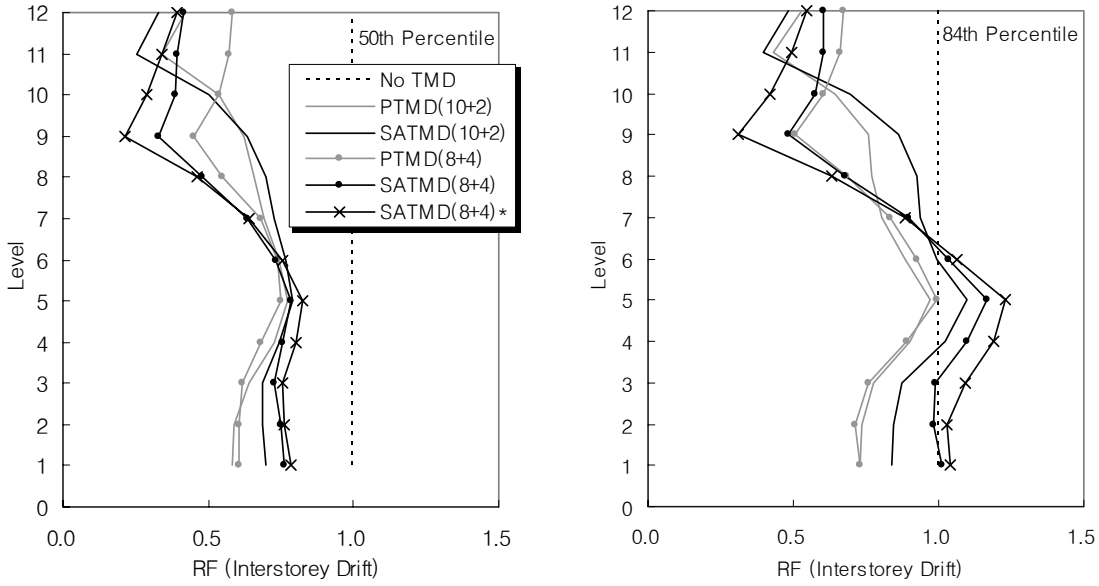

Figure 7-25 Interstorey drift reduction factor of '10+2' and '8+4' models (Linear / Low suite)

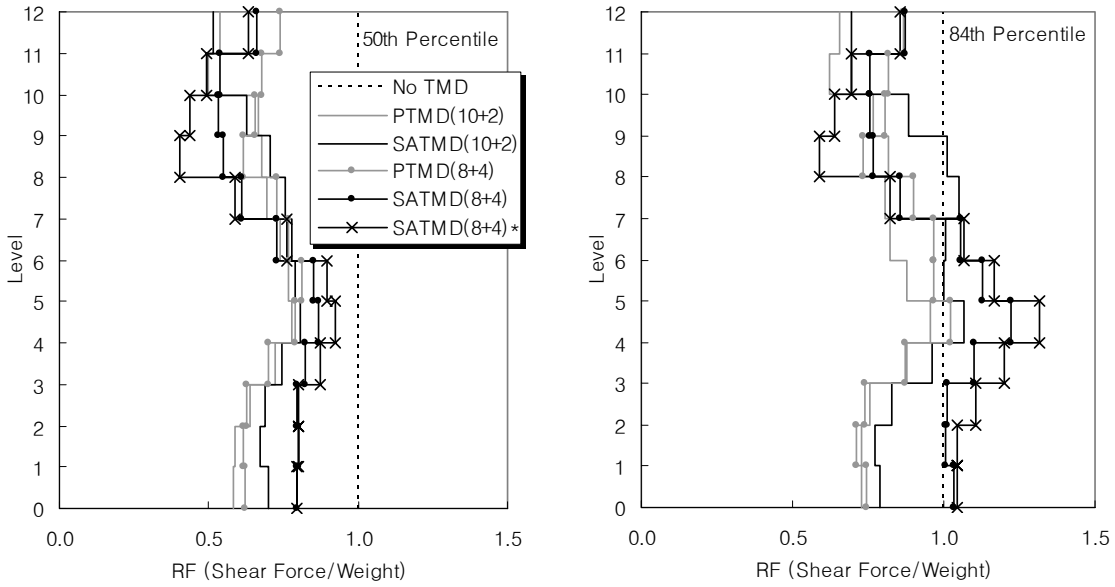

Figure 7-26 Storey shear force reduction factor of '10+2' and '8+4' models (Linear / Low suite)

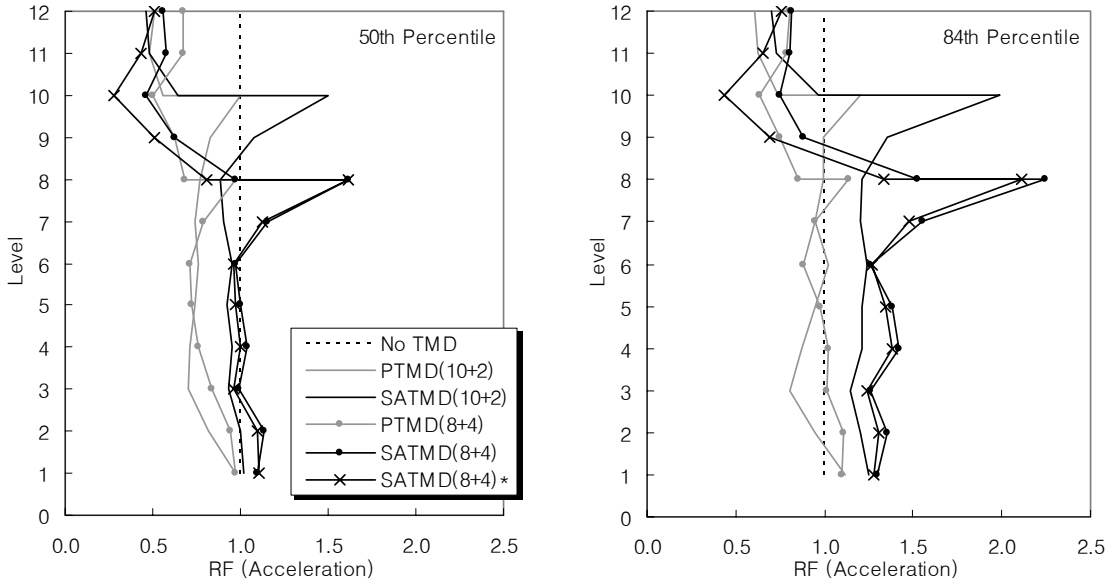

Figure 7-27 Total acceleration reduction factor of '10+2' and '8+4' models (Linear / Low suite)

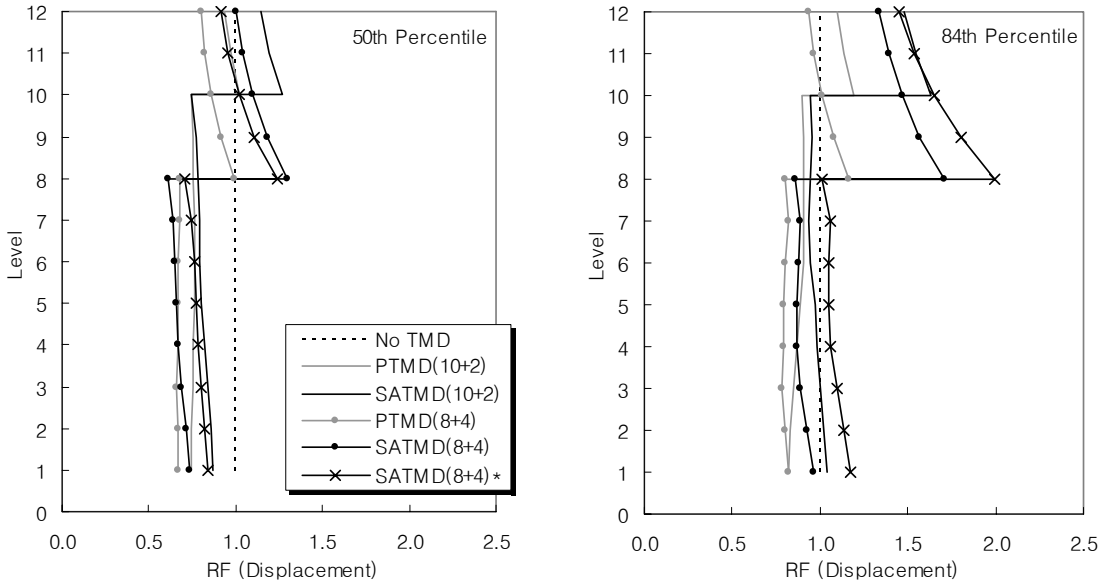

Figure 7-28 Displacement reduction factor of '10+2' and '8+4' models (Linear / Medium suite)

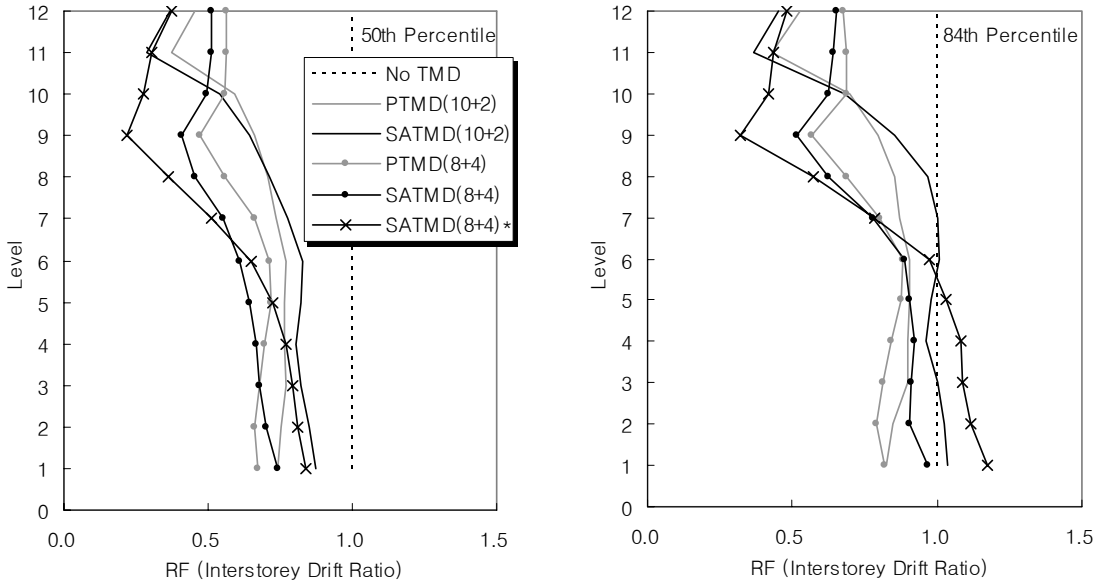

Figure 7-29 Interstorey drift reduction factor of '10+2' and '8+4' models (Linear/Medium suite)

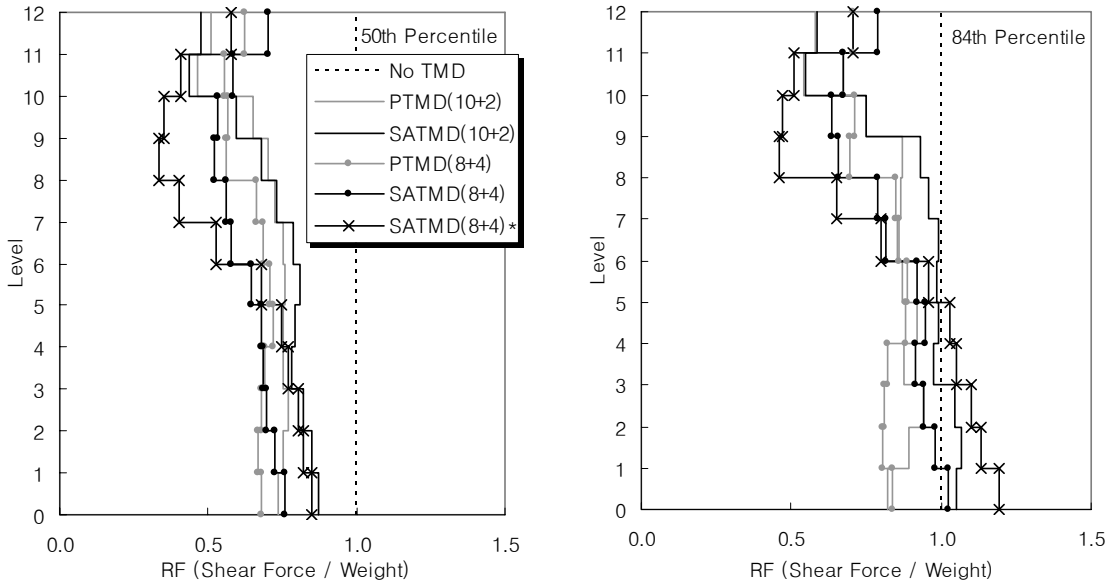

Figure 7-30 Storey shear force reduction factor of '10+2' and '8+4' models (Linear/Medium suite)

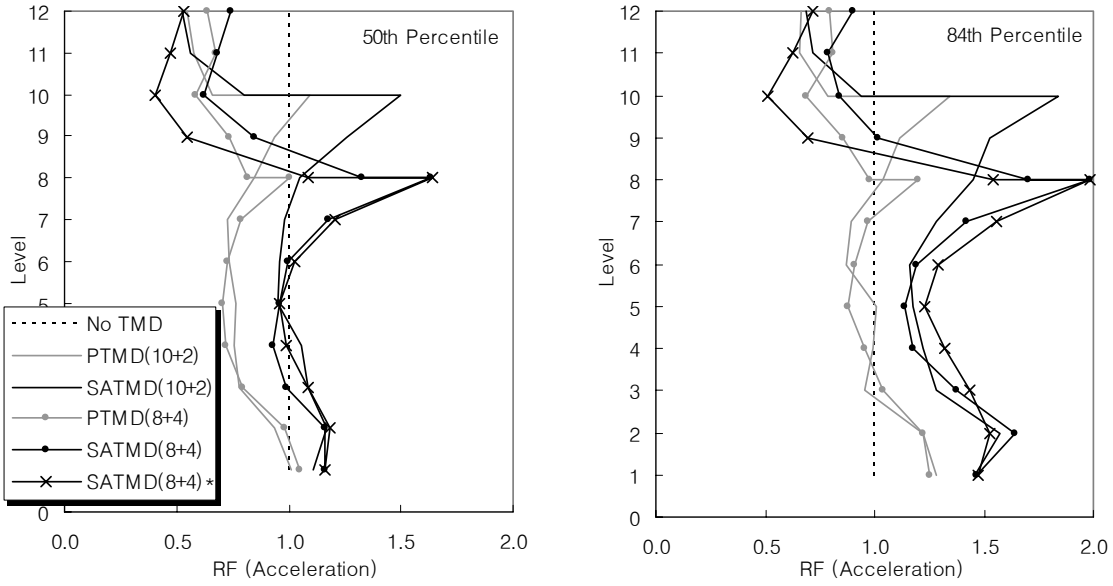

Figure 7-31 Total acceleration reduction factor of '10+2' and '8+4' models (Linear / Medium suite)

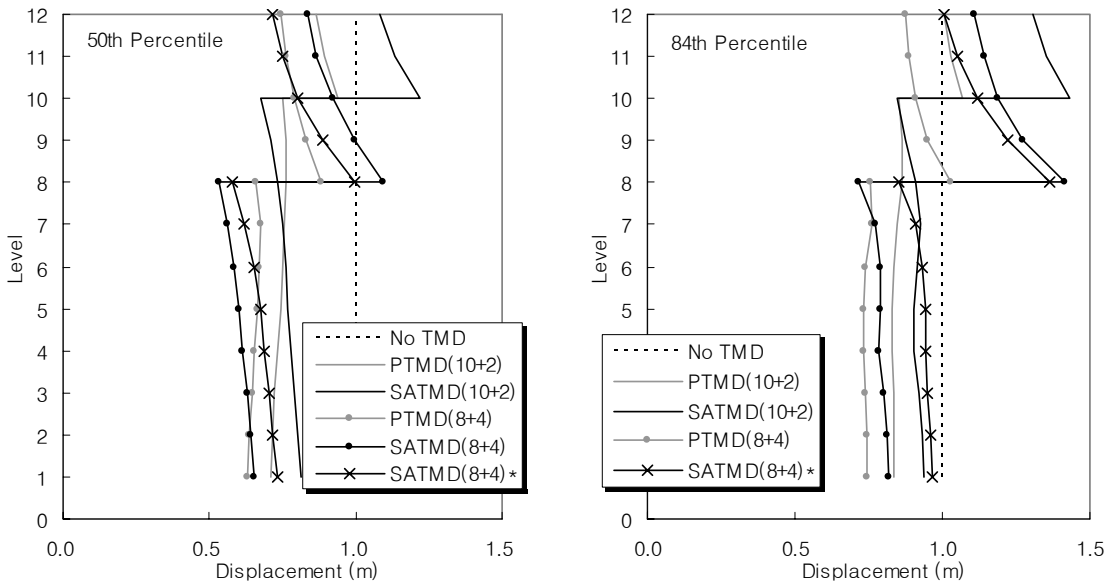

Figure 7-32 Displacement reduction factor of '10+2' and '8+4' models (Linear / High suite)

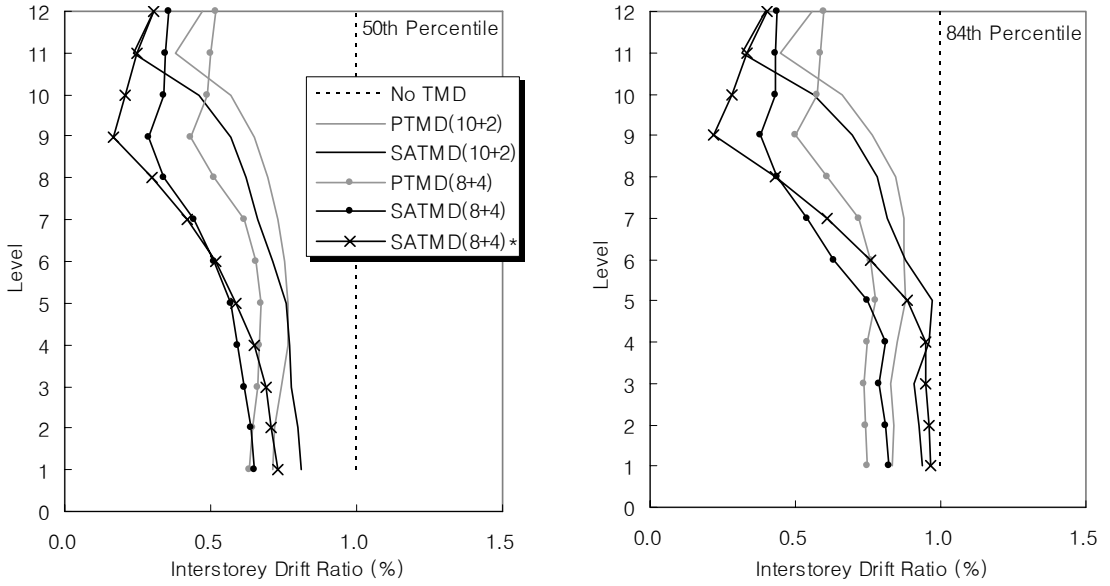

Figure 7-33 Interstorey drift reduction factor of '10+2' and '8+4' models (Linear / High suite)

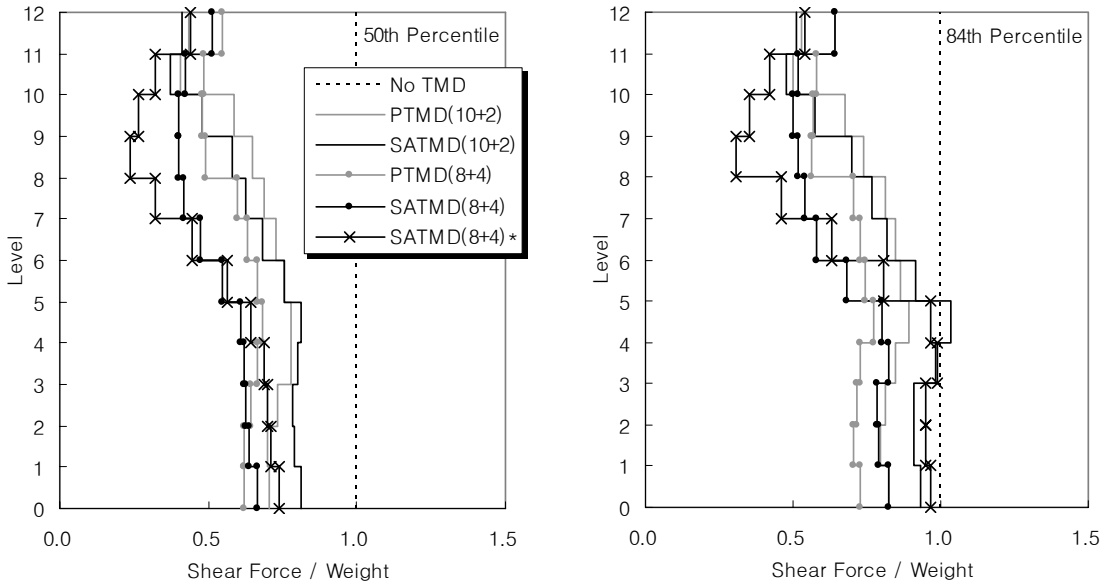

Figure 7-34 Storey shear force reduction factor of '10+2' and '8+4' models (Linear / High suite)

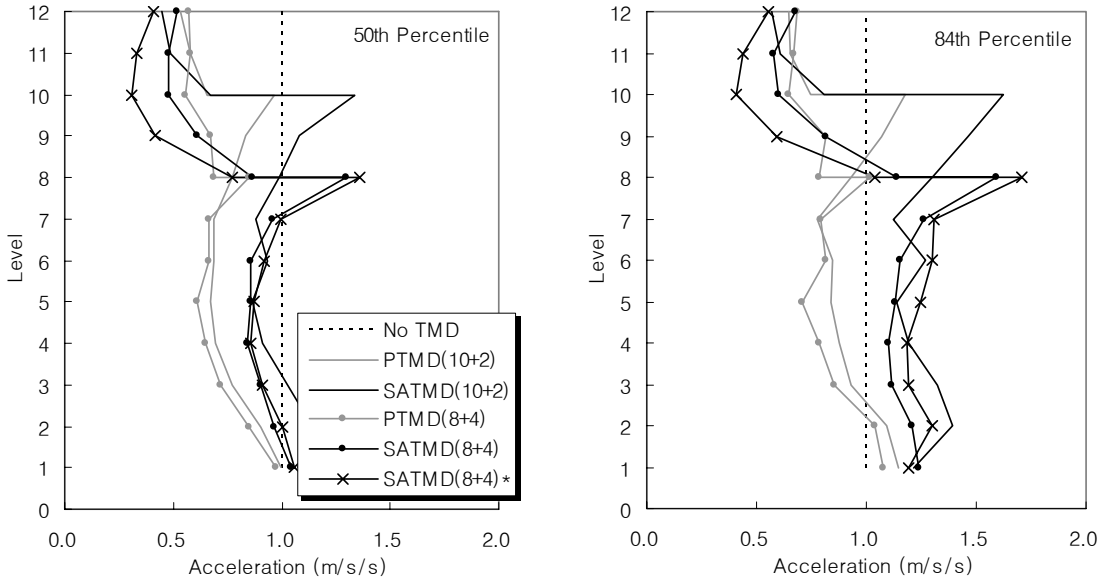

Figure 7-35 Total acceleration reduction factor of '10+2' and '8+4' models (Linear / High suite)

The three percentile (16^{th}, 50^{th} and 84^{th}) reduction factors and standard error of control (SEC) from each bandwidth (84^{th}–16^{th}) of the TMD (8+4) systems are compared in Tables 7-4 to 7-15. The shaded cells represent the isolated upper stories for each building system. In particular, it can be seen that the band width between 50^{th} and 84^{th} percentiles of SATMDs (8+4) is broader than for the PTMD (8+4) system.

However, it should be noted that the PTMD results are optimal, but not necessarily practical. Specifically, the 60-80% damping ratio might not be really achieved. Thus, similar SATMD results indicate that optimal level solutions can be obtained without resorting to unrealistically large non-linear viscous damper values.

Table 7-4 Displacement reduction factor and standard error of control of '10+2' and '8+4' TMD building systems (Low Suite)

TMD		PTMD(8+4)				SATMD(8+4)				SATMD(8+4)*			
Index		Maximum Displacement				Maximum Displacement				Maximum Displacement			
Percentile		50th	16th	84th	SEC	50th	16th	84th	SEC	50th	16th	84th	SEC
Level	12	0.69	0.52	0.91	0.56	0.74	0.47	1.16	0.93	0.85	0.55	1.34	0.92
	11	0.71	0.53	0.94	0.58	0.76	0.49	1.20	0.94	0.90	0.58	1.42	0.94
	10	0.73	0.55	0.97	0.57	0.81	0.52	1.26	0.91	0.99	0.62	1.56	0.95
	9	0.78	0.59	1.03	0.57	0.89	0.58	1.35	0.86	1.10	0.69	1.75	0.96
	8	0.70	0.49	0.99	0.71	0.71	0.43	1.17	1.04	0.78	0.47	1.29	1.06
	7	0.67	0.51	0.88	0.55	0.71	0.47	1.09	0.86	0.78	0.50	1.19	0.89
	6	0.64	0.50	0.80	0.47	0.70	0.48	1.02	0.78	0.75	0.51	1.13	0.82
	5	0.61	0.50	0.75	0.41	0.70	0.50	0.98	0.69	0.74	0.51	1.08	0.78
	4	0.60	0.51	0.72	0.35	0.72	0.54	0.96	0.58	0.74	0.53	1.05	0.70
	3	0.60	0.51	0.71	0.32	0.74	0.57	0.97	0.54	0.75	0.55	1.03	0.63
	2	0.60	0.50	0.71	0.35	0.75	0.57	0.99	0.56	0.77	0.58	1.03	0.58
	1	0.60	0.50	0.73	0.37	0.76	0.58	1.01	0.57	0.78	0.59	1.04	0.57

Table 7-5 Interstorey drift reduction factor and standard error of control of '10+2' and '8+4' TMD building systems (Low Suite)

TMD		PTMD(8+4)				SATMD(8+4)				SATMD(8+4)*			
Index		Interstorey Drift Ratio				Interstorey Drift Ratio				Interstorey Drift Ratio			
Percentile		50th	16th	84th	SEC	50th	16th	84th	SEC	50th	16th	84th	SEC
Level	12	0.58	0.50	0.67	0.30	0.42	0.29	0.60	0.77	0.39	0.28	0.54	0.68
	11	0.57	0.49	0.66	0.30	0.39	0.26	0.60	0.89	0.34	0.23	0.49	0.76
	10	0.54	0.47	0.61	0.25	0.38	0.26	0.58	0.84	0.29	0.20	0.42	0.77
	9	0.45	0.39	0.51	0.25	0.33	0.23	0.48	0.78	0.22	0.15	0.31	0.73
	8	0.55	0.44	0.69	0.44	0.48	0.34	0.68	0.71	0.46	0.33	0.63	0.65
	7	0.68	0.55	0.83	0.42	0.63	0.45	0.90	0.72	0.64	0.46	0.88	0.65
	6	0.74	0.59	0.92	0.45	0.73	0.52	1.03	0.70	0.76	0.54	1.06	0.69
	5	0.75	0.56	0.99	0.57	0.79	0.53	1.17	0.81	0.82	0.55	1.23	0.83
	4	0.68	0.52	0.89	0.54	0.76	0.52	1.10	0.76	0.80	0.54	1.19	0.81
	3	0.62	0.50	0.76	0.41	0.73	0.54	0.99	0.62	0.76	0.53	1.09	0.75
	2	0.60	0.51	0.71	0.33	0.75	0.57	0.98	0.55	0.76	0.57	1.03	0.61
	1	0.60	0.50	0.73	0.37	0.76	0.58	1.01	0.57	0.78	0.59	1.04	0.57

Table 7-6 Storey shear force/weight reduction factor and standard error of control of '10+2' and '8+4' TMD building systems (Low Suite)

TMD		PTMD(8+4)				SATMD(8+4)				SATMD(8+4)*			
Index		Shear Force / Weight				Shear Force / Weight				Shear Force / Weight			
Percentile		50th	16th	84th	SEC	50th	16th	84th	SEC	50th	16th	84th	SEC
Level	12	0.74	0.63	0.87	0.32	0.66	0.50	0.87	0.57	0.63	0.47	0.86	0.61
	11	0.68	0.56	0.82	0.38	0.54	0.38	0.76	0.69	0.49	0.35	0.69	0.71
	10	0.65	0.53	0.80	0.41	0.53	0.38	0.75	0.70	0.44	0.30	0.64	0.78
	9	0.62	0.52	0.73	0.35	0.55	0.39	0.77	0.69	0.40	0.28	0.59	0.78
	8	0.72	0.59	0.90	0.43	0.61	0.43	0.86	0.69	0.59	0.42	0.82	0.69
	7	0.77	0.61	0.96	0.46	0.73	0.50	1.06	0.77	0.76	0.54	1.07	0.69
	6	0.81	0.68	0.96	0.34	0.85	0.64	1.13	0.57	0.89	0.68	1.17	0.54
	5	0.79	0.61	1.02	0.51	0.87	0.62	1.22	0.69	0.92	0.65	1.32	0.72
	4	0.70	0.56	0.87	0.44	0.82	0.61	1.10	0.59	0.87	0.63	1.20	0.65
	3	0.63	0.53	0.74	0.33	0.79	0.63	1.01	0.48	0.80	0.58	1.10	0.66
	2	0.62	0.54	0.71	0.29	0.80	0.64	1.00	0.46	0.80	0.61	1.04	0.54
	1	0.62	0.52	0.74	0.37	0.79	0.61	1.04	0.54	0.80	0.60	1.05	0.56

Table 7-7 Acceleration reduction factor and standard error of control of '10+2' and '8+4' TMD building systems (Low Suite)

TMD		PTMD(8+4)				SATMD(8+4)				SATMD(8+4)*			
Index		Total Acceleration				Total Acceleration				Total Acceleration			
Percentile		50th	16th	84th	SEC	50th	16th	84th	SEC	50th	16th	84th	SEC
Level	12	0.67	0.56	0.81	0.38	0.56	0.39	0.82	0.77	0.51	0.34	0.76	0.82
	11	0.67	0.57	0.79	0.32	0.57	0.41	0.80	0.68	0.43	0.29	0.65	0.84
	10	0.50	0.39	0.64	0.49	0.47	0.29	0.75	0.99	0.28	0.18	0.43	0.90
	9	0.62	0.52	0.75	0.36	0.63	0.45	0.88	0.69	0.51	0.38	0.69	0.60
	8	0.97	0.84	1.13	0.30	1.61	1.16	2.24	0.67	1.61	1.24	2.11	0.54
	7	0.79	0.65	0.95	0.37	1.15	0.85	1.55	0.61	1.13	0.86	1.48	0.55
	6	0.71	0.57	0.88	0.43	0.97	0.75	1.26	0.52	0.96	0.73	1.27	0.57
	5	0.72	0.53	0.98	0.63	1.00	0.73	1.38	0.65	0.97	0.70	1.35	0.67
	4	0.76	0.56	1.03	0.62	1.04	0.76	1.42	0.64	1.00	0.73	1.39	0.66
	3	0.83	0.68	1.01	0.40	0.99	0.79	1.26	0.48	0.96	0.74	1.24	0.53
	2	0.95	0.81	1.11	0.32	1.14	0.95	1.35	0.36	1.10	0.92	1.31	0.35
	1	0.97	0.86	1.10	0.24	1.10	0.92	1.30	0.34	1.11	0.96	1.28	0.29

Table 7-8 Displacement reduction factor and standard error of control of '10+2' and '8+4' TMD building systems (Medium Suite)

TMD		PTMD(8+4)				SATMD(8+4)				SATMD(8+4)*			
Index		Maximum Displacement				Maximum Displacement				Maximum Displacement			
Percentile		50th	16th	84th	SEC	50th	16th	84th	SEC	50th	16th	84th	SEC
Level	12	0.80	0.69	0.93	0.31	1.00	0.75	1.34	0.59	0.92	0.58	1.45	0.96
	11	0.82	0.70	0.97	0.32	1.04	0.77	1.39	0.60	0.96	0.60	1.53	0.98
	10	0.86	0.73	1.01	0.32	1.10	0.82	1.47	0.59	1.02	0.63	1.65	1.00
	9	0.92	0.78	1.08	0.33	1.18	0.90	1.57	0.57	1.11	0.68	1.81	1.01
	8	0.67	0.56	0.81	0.36	0.61	0.43	0.86	0.71	0.71	0.50	1.01	0.73
	7	0.68	0.57	0.82	0.37	0.64	0.46	0.89	0.67	0.75	0.53	1.06	0.71
	6	0.67	0.56	0.80	0.35	0.65	0.48	0.88	0.62	0.76	0.55	1.05	0.66
	5	0.67	0.56	0.79	0.34	0.65	0.49	0.87	0.58	0.77	0.57	1.05	0.62
	4	0.66	0.56	0.79	0.35	0.66	0.50	0.87	0.55	0.79	0.58	1.06	0.61
	3	0.66	0.56	0.78	0.35	0.68	0.53	0.88	0.52	0.80	0.59	1.09	0.63
	2	0.67	0.55	0.80	0.38	0.71	0.55	0.93	0.53	0.82	0.59	1.14	0.66
	1	0.67	0.55	0.82	0.40	0.74	0.57	0.97	0.54	0.84	0.60	1.17	0.68

Table 7-9 Interstorey drift reduction factor and standard error of control of '10+2' and '8+4' TMD building systems (Medium Suite)

TMD		PTMD(8+4)				SATMD(8+4)				SATMD(8+4)*			
Index		Interstorey Drift Ratio				Interstorey Drift Ratio				Interstorey Drift Ratio			
Percentile		50th	16th	84th	SEC	50th	16th	84th	SEC	50th	16th	84th	SEC
Level	12	0.56	0.47	0.67	0.36	0.51	0.40	0.65	0.49	0.38	0.29	0.48	0.50
	11	0.56	0.46	0.69	0.40	0.51	0.41	0.64	0.47	0.31	0.21	0.44	0.73
	10	0.56	0.45	0.69	0.43	0.49	0.39	0.62	0.48	0.27	0.18	0.42	0.87
	9	0.47	0.39	0.57	0.37	0.41	0.32	0.51	0.48	0.22	0.15	0.32	0.77
	8	0.56	0.45	0.69	0.42	0.45	0.33	0.62	0.64	0.36	0.22	0.57	0.97
	7	0.66	0.54	0.80	0.39	0.55	0.39	0.78	0.71	0.51	0.33	0.79	0.89
	6	0.71	0.58	0.88	0.43	0.61	0.42	0.89	0.78	0.65	0.43	0.97	0.83
	5	0.72	0.59	0.88	0.41	0.65	0.46	0.90	0.68	0.72	0.51	1.03	0.72
	4	0.70	0.58	0.84	0.38	0.67	0.49	0.92	0.65	0.77	0.55	1.08	0.70
	3	0.68	0.57	0.82	0.36	0.68	0.50	0.91	0.60	0.79	0.58	1.09	0.65
	2	0.66	0.56	0.79	0.35	0.70	0.54	0.91	0.53	0.81	0.59	1.12	0.65
	1	0.67	0.55	0.82	0.40	0.74	0.57	0.97	0.54	0.84	0.60	1.17	0.68

Table 7-10 Storey shear force/weight reduction factor and standard error of control of '10+2' and '8+4' TMD building systems (Medium Suite)

TMD		PTMD(8+4)				SATMD(8+4)				SATMD(8+4)*			
Index		Shear Force / Weight				Shear Force / Weight				Shear Force / Weight			
Percentile		50th	16th	84th	SEC	50th	16th	84th	SEC	50th	16th	84th	SEC
Level	12	0.62	0.55	0.71	0.25	0.70	0.62	0.79	0.24	0.58	0.47	0.71	0.40
	11	0.56	0.46	0.67	0.38	0.58	0.50	0.68	0.29	0.41	0.33	0.51	0.44
	10	0.56	0.45	0.71	0.47	0.53	0.44	0.64	0.37	0.35	0.26	0.47	0.59
	9	0.56	0.45	0.69	0.43	0.52	0.42	0.66	0.46	0.34	0.24	0.46	0.65
	8	0.66	0.52	0.85	0.49	0.56	0.40	0.79	0.70	0.40	0.25	0.65	0.99
	7	0.68	0.54	0.86	0.47	0.58	0.41	0.82	0.70	0.53	0.35	0.80	0.86
	6	0.71	0.56	0.89	0.46	0.64	0.45	0.92	0.73	0.68	0.48	0.96	0.70
	5	0.72	0.58	0.88	0.42	0.68	0.48	0.95	0.69	0.75	0.54	1.03	0.65
	4	0.69	0.58	0.82	0.35	0.69	0.52	0.91	0.58	0.77	0.57	1.05	0.63
	3	0.68	0.57	0.81	0.35	0.69	0.51	0.94	0.62	0.81	0.59	1.10	0.64
	2	0.67	0.55	0.81	0.38	0.72	0.54	0.98	0.61	0.82	0.59	1.13	0.66
	1	0.68	0.55	0.84	0.42	0.76	0.56	1.02	0.61	0.85	0.61	1.19	0.69

Table 7-11 Acceleration reduction factor and standard error of control of '10+2' and '8+4' TMD building systems (Medium Suite)

TMD		PTMD(8+4)				SATMD(8+4)				SATMD(8+4)*			
Index		Total Acceleration				Total Acceleration				Total Acceleration			
Percentile		50th	16th	84th	SEC	50th	16th	84th	SEC	50th	16th	84th	SEC
Level	12	0.64	0.51	0.79	0.44	0.74	0.61	0.90	0.39	0.53	0.40	0.72	0.60
	11	0.68	0.57	0.81	0.35	0.68	0.59	0.79	0.29	0.47	0.35	0.62	0.58
	10	0.58	0.50	0.68	0.32	0.62	0.46	0.84	0.61	0.40	0.31	0.51	0.50
	9	0.73	0.63	0.86	0.32	0.85	0.70	1.02	0.37	0.55	0.43	0.69	0.47
	8	1.01	0.84	1.20	0.35	1.63	1.35	1.98	0.39	1.64	1.36	1.98	0.38
	7	0.79	0.64	0.97	0.43	1.18	0.97	1.42	0.38	1.21	0.94	1.56	0.51
	6	0.72	0.58	0.91	0.46	1.00	0.84	1.19	0.36	1.03	0.82	1.29	0.46
	5	0.71	0.57	0.87	0.43	0.96	0.81	1.14	0.34	0.96	0.74	1.23	0.51
	4	0.72	0.55	0.96	0.57	0.93	0.74	1.18	0.47	0.99	0.74	1.32	0.58
	3	0.79	0.60	1.04	0.55	0.99	0.71	1.38	0.67	1.09	0.82	1.44	0.57
	2	0.98	0.79	1.22	0.44	1.16	0.81	1.64	0.72	1.18	0.92	1.53	0.52
	1	1.05	0.89	1.25	0.35	1.16	0.92	1.47	0.47	1.16	0.91	1.47	0.49

Table 7-12 Displacement reduction factor and standard error of control of '10+2' and '8+4' TMD building systems (High Suite)

TMD		PTMD(8+4)				SATMD(8+4)				SATMD(8+4)*			
Index		Maximum Displacement				Maximum Displacement				Maximum Displacement			
Percentile		50th	16th	84th	SEC	50th	16th	84th	SEC	50th	16th	84th	SEC
Level	12	0.75	0.64	0.87	0.32	0.83	0.63	1.11	0.58	0.72	0.51	1.01	0.70
	11	0.76	0.66	0.89	0.30	0.87	0.66	1.14	0.56	0.75	0.53	1.05	0.69
	10	0.79	0.69	0.91	0.28	0.92	0.71	1.19	0.52	0.80	0.58	1.12	0.67
	9	0.83	0.72	0.95	0.28	1.00	0.78	1.27	0.50	0.89	0.64	1.22	0.66
	8	0.66	0.58	0.75	0.27	0.53	0.40	0.72	0.60	0.58	0.39	0.85	0.80
	7	0.67	0.60	0.76	0.24	0.56	0.41	0.77	0.64	0.62	0.42	0.91	0.78
	6	0.67	0.60	0.74	0.21	0.59	0.43	0.79	0.61	0.65	0.46	0.93	0.73
	5	0.66	0.60	0.73	0.20	0.60	0.46	0.79	0.56	0.67	0.48	0.94	0.68
	4	0.65	0.58	0.73	0.23	0.61	0.48	0.79	0.51	0.69	0.50	0.94	0.64
	3	0.65	0.56	0.74	0.27	0.63	0.49	0.80	0.49	0.70	0.52	0.95	0.62
	2	0.64	0.55	0.74	0.31	0.64	0.51	0.81	0.47	0.72	0.54	0.96	0.59
	1	0.63	0.53	0.75	0.34	0.65	0.52	0.82	0.46	0.73	0.55	0.97	0.56

Table 7-13 Interstorey drift reduction factor and standard error of control of '10+2' and '8+4' TMD building systems (High Suite)

TMD		PTMD(8+4)				SATMD(8+4)				SATMD(8+4)*			
Index		Interstorey Drift Ratio				Interstorey Drift Ratio				Interstorey Drift Ratio			
Percentile		50th	16th	84th	SEC	50th	16th	84th	SEC	50th	16th	84th	SEC
Level	12	0.52	0.45	0.60	0.29	0.36	0.30	0.43	0.38	0.30	0.23	0.40	0.58
	11	0.50	0.43	0.59	0.32	0.35	0.28	0.43	0.43	0.25	0.18	0.34	0.61
	10	0.49	0.42	0.57	0.32	0.34	0.26	0.43	0.50	0.21	0.15	0.28	0.62
	9	0.43	0.37	0.50	0.29	0.29	0.22	0.38	0.55	0.17	0.13	0.22	0.56
	8	0.51	0.43	0.61	0.34	0.34	0.27	0.44	0.49	0.30	0.20	0.43	0.78
	7	0.61	0.52	0.72	0.32	0.44	0.37	0.54	0.40	0.42	0.29	0.61	0.76
	6	0.66	0.57	0.76	0.29	0.51	0.42	0.63	0.42	0.52	0.35	0.76	0.79
	5	0.67	0.58	0.78	0.29	0.57	0.44	0.75	0.54	0.59	0.39	0.89	0.84
	4	0.67	0.60	0.75	0.23	0.59	0.43	0.81	0.63	0.65	0.44	0.95	0.78
	3	0.66	0.59	0.74	0.22	0.61	0.48	0.79	0.51	0.69	0.50	0.95	0.65
	2	0.64	0.56	0.74	0.29	0.64	0.50	0.81	0.49	0.71	0.52	0.96	0.61
	1	0.63	0.53	0.75	0.34	0.65	0.52	0.82	0.46	0.73	0.55	0.97	0.56

Table 7-14 Storey shear force/weight reduction factor and standard error of control of '10+2' and '8+4' TMD building systems (High Suite)

TMD		PTMD(8+4)				SATMD(8+4)				SATMD(8+4)*			
Index		Shear Force / Weight				Shear Force / Weight				Shear Force / Weight			
Percentile		50th	16th	84th	SEC	50th	16th	84th	SEC	50th	16th	84th	SEC
Level	12	0.55	0.47	0.64	0.32	0.51	0.41	0.64	0.45	0.44	0.36	0.54	0.41
	11	0.48	0.40	0.58	0.38	0.42	0.34	0.52	0.42	0.32	0.24	0.42	0.55
	10	0.48	0.41	0.57	0.33	0.40	0.32	0.50	0.44	0.26	0.20	0.35	0.60
	9	0.49	0.43	0.56	0.28	0.40	0.31	0.52	0.52	0.24	0.18	0.30	0.51
	8	0.60	0.51	0.70	0.34	0.42	0.32	0.54	0.52	0.32	0.22	0.46	0.75
	7	0.63	0.55	0.73	0.29	0.47	0.38	0.58	0.42	0.45	0.31	0.63	0.72
	6	0.67	0.60	0.75	0.23	0.55	0.44	0.68	0.44	0.56	0.39	0.81	0.75
	5	0.69	0.61	0.78	0.25	0.61	0.46	0.80	0.56	0.64	0.43	0.96	0.83
	4	0.67	0.61	0.73	0.18	0.62	0.47	0.82	0.57	0.69	0.48	0.99	0.73
	3	0.64	0.58	0.72	0.21	0.62	0.49	0.79	0.47	0.70	0.52	0.95	0.62
	2	0.62	0.55	0.71	0.26	0.64	0.52	0.79	0.43	0.71	0.53	0.95	0.58
	1	0.62	0.53	0.73	0.33	0.66	0.53	0.82	0.44	0.74	0.57	0.96	0.54

Table 7-15 Acceleration reduction factor and standard error of control of '10+2' and '8+4' TMD building systems (High Suite)

TMD		PTMD(8+4)				SATMD(8+4)				SATMD(8+4)*			
Index		Total Acceleration				Total Acceleration				Total Acceleration			
Percentile		50th	16th	84th	SEC	50th	16th	84th	SEC	50th	16th	84th	SEC
Level	12	0.57	0.47	0.69	0.38	0.52	0.40	0.68	0.54	0.41	0.31	0.56	0.61
	11	0.58	0.50	0.67	0.30	0.48	0.40	0.58	0.38	0.33	0.25	0.44	0.55
	10	0.56	0.48	0.65	0.29	0.48	0.38	0.60	0.46	0.31	0.24	0.41	0.55
	9	0.67	0.55	0.81	0.39	0.61	0.46	0.82	0.58	0.42	0.30	0.59	0.70
	8	0.85	0.72	1.01	0.34	1.30	1.06	1.59	0.41	1.36	1.08	1.71	0.46
	7	0.67	0.56	0.79	0.35	0.96	0.73	1.26	0.55	1.00	0.76	1.31	0.55
	6	0.66	0.54	0.82	0.42	0.86	0.64	1.15	0.61	0.92	0.66	1.30	0.70
	5	0.61	0.52	0.71	0.30	0.86	0.65	1.13	0.56	0.87	0.61	1.24	0.72
	4	0.65	0.54	0.78	0.38	0.84	0.64	1.10	0.54	0.86	0.62	1.19	0.67
	3	0.72	0.60	0.86	0.35	0.90	0.73	1.11	0.42	0.91	0.70	1.19	0.54
	2	0.85	0.70	1.04	0.40	0.97	0.78	1.20	0.44	1.01	0.78	1.30	0.52
	1	0.97	0.88	1.08	0.20	1.04	0.88	1.24	0.34	1.06	0.94	1.19	0.23

7.6 Summary

This Chapter presented a case study on the seismic response of linear multi-storey passive and semi-active tuned mass damper building systems under probabilistically scaled suites of earthquake records. Linear structure models give a good indication of the overall structure response without computational intensity of more realistic nonlinear studies. Hence, they provide good initial indications of the efficacy of any design approach. To demonstrate the effects of the PTMD and SATMD building systems, 10+2 and 8+4 storey, two-bay reinforced concrete framed structures were developed in *Ruaumoko*, and results were compared to results for structures with no control.

Based on the performance results of the previous 2-DOF study for the device design, the optimal parameters of the multi-degree of freedom structure were derived. From this value a stiffness allocations to the resetable device and rubber bearings were defined. The choice of the control parameters does not indicate an ideally optimum selection. Instead, they were chosen as reasonable values, based on design considerations and the values that gave the best response in a previous analysis.

Modal analysis showed that the TMD building systems have the unique modal features to isolate the structure to be controlled effectively and that the resetable device provides a more advanced control function by effectively anticipating the isolation layer response using sensor feedback. Specifically, the PTMD and SATMD response clearly showed a far different dominant structural period of response compared to the uncontrolled case. Hence, the modal response between the TMD systems used shows that the PTMD and SATMD designs developed reduce structural response by different mechanisms, which is an interesting and unique result of its own.

From the performance results over several response indices, time history analysis and normalised reduction factor results showed that the TMD building systems can provide significant reductions on the control indices for all seismic hazards at the cost of increasing the acceleration at the isolation interface. In this respect, the SATMD

and the higher mass ratio (8+4) building structures, as compared to the PTMD building system, have shown the best results.

From this chapter, the validity of the MDOF linear PTMD and SATMD building systems has been demonstrated. The response features obtained in this linear analysis could be used as the initial design reference for the further studies investigating inelastic seismic response for more realistic nonlinear structures. Even though this study does not provide exact design criteria, the aim of this analysis is to statistically quantify the fundamental qualitative benefit of these TMD systems by examining both the efficacy of the segregated structural configuration and the use of resetable devices in that approach.

8 12+2 and 12+4 Storey TMD Building Systems

8.1 Introduction

Based upon new and emerging findings in the area of seismic effects on buildings, an increasing number of existing structures are facing the necessity of seismic retrofit. There is not yet a practical method for a large number of buildings to improve their performances in the case of an earthquake event. In addition, there is an increasing desire to expand upwards due to lack of new land to develop. The TMD building system can be a great help for both cases because it does not require any major changes in existing buildings and, in some cases can be applied without significant interruption in their operation.

In an ideal case, it is possible to apply this technique on top of the structure simply by adding a few storeys as these storeys become part of the structure control system, alleviating the necessity for additional mass that is redundant for the majority of the time. This approach is considered as a quite lucrative retrofit approach in places where land for new buildings is expensive. As an example, a comparison between a 12-storey building and a 16-storey case retrofitted with a TMD on top of the 12^{th} floor can be performed. This case can be interpreted as adding four more storeys on top of the existing 12-storey structure.

8.2 Modelling

Again, a 12-storey, two-bay reinforced concrete framed structure is modelled in to investigate the effects of the TMD building systems. The dynamic properties of this frame are listed in Table 8-1. Two stories and four stories are added and isolated for the control of 12-storey models and these mean that 24% and 40% mass is added to the 12-storey structure creating ‘12+2’ storey and ‘12+4’ storey structures, respectively (Chey et al. 2006). These cases are shown schematically in Figure 8-1. The optimal parameters for TMD systems are based on the dynamic properties of the 12-storey frame and listed in Table 8-2.

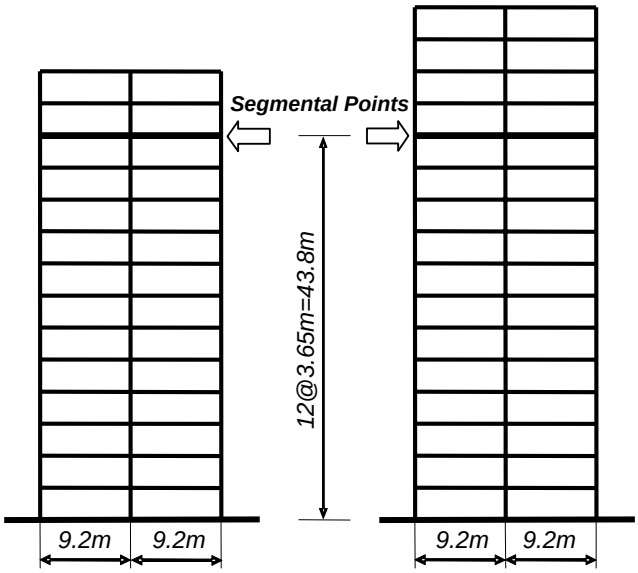

(a) 12+2 storey model **(b) 12+4 storey model**

Figure 8-1 '12+2' and '12+4' storey two-bay reinforced concrete framed structures

Table 8-1 Dynamic properties of 12-storey building

Item	12-storey	Unit
Weight	19,190	kN
1st Modal Mass	1,514	kN-s^2/m
Natural period	1.88	sec
Frequency	3.342	rad/sec
Damping Ratio	0.05	-
1st Modal Amplitude	1.36	-

Table 8-2 Parameters for TMD building systems

Model	μ	f_{M2opt}	ξ_{M2opt}	k_{M2opt} (kN/m)	c_{M2opt} (kN-s/m)	Device Force (kN)
PTMD(12+2)	0.31	0.684	0.716	2,448	1535	-
SATMD(12+2)	0.31	0.684	-	2,448	-	1,017
PTMD(12+4)	0.52	0.568	0.842	2,814	2489	-
SATMD(12+4)	0.52	0.568	-	2,814	-	1,914

Based on the design results from the 2-DOF analysis of Chapter 5, the SA50TMD was used for all of the ground motion suites. The total value of k_{M2opt} is allocated to rubber bearing stiffness and the stiffness of the resetable device for the given SATMD building systems. The maximum device force is set at 1,017kN for the '12+2' model and 1,914kN for the '12+4' model. For the PTMD building system, the value of c_{M2opt} is used as the damping coefficient of the viscous damper along with the value of k_{M2opt}, despite the potentially over-large damping provided by this optimal case.

8.3 Performance Results

The analytical results for the buildings described are obtained to check the performance of each structural control case. To investigate the efficiency of the applied control systems, the 50^{th} (median) and 84^{th} percentile responses of the No TMD, PTMD, and SATMD under the suites (low, medium and high) are compared over all floors and the response envelopes are presented in Figures 8-2 to 8-13. The peak relative displacements, total accelerations, interstorey drift ratios and storey shear forces for all floors are calculated as control effectiveness indices.

In addition, to compare the TMD systems developed, the summarised response values and those reduction factors to the No TMD system over 1^{st} to 12^{th} floor (original storeys) have been listed in Tables 8-3 to 8-5. This is a possible summarising approach, since the most of the response envelops are reasonably uniform or linear, and the distribution of the demands are fairly equivalent and the slight differences are apparent with TMD cases developed.

Overall, it is observed that the SATMD control provides satisfactory reductions and that control performance is clearly dependent on the specific earthquakes and suites. In addition, the control effects of the SATMD systems are not so influenced by the amount of added mass (12+2 vs. 12+4). As expected, the response differences between systems become more pronounced at the 84th percentile values. On average, the 12+2 or 12+4 storey TMD system received considerably more input energy than the original 12-storey building. However, the share of structural components of the

system from this energy remained small. Reductions in responses are fairly modest considering that the retrofitted structures have fourteen and sixteen storeys instead of the twelve of the original configuration. In addition, care must be taken not to assume that TMD strategies which reduce statistical values for the ground motion sets will reduce demands for all individual excitations. In a motion-by-motion comparison, occasionally the TMD systems do make performance worse.

The maximum displacements of each level increase steadily over the height of the level under the all suites in Figures 8-2, 8-6 and 8-10. All TMD (PTMD and SATMD) systems produce very similar displacements under the low suite (Figure 8-2). However, under the medium suite, the SATMD systems show greater more reductions, and the distribution of different displacement demands is fairly equivalent and apparent (Figure 8-6), while, under the high suite, the PTMD systems demonstrate more reduced and evenly distributed demands (Figure 8-10). The 50th percentile reduction factors of the maximum displacements by the SATMD systems are 0.65~0.78 under the suites, while 0.64~0.81 by PTMD systems, as shown in Tables 8-3 to 8-5.

The envelopes of the interstorey drifts are reasonably uniform, whereas the drifts are decreased over the 12th floor to the 16th floor. Though, under the low suite, the distributions of the drift demands are similar between the TMD systems, differences are apparent between the TMD systems for medium and high suites. In particular, the drift envelops of both PTMD systems (12+2 and 12+4) and SATMD systems (12+2 and 12+4) cross one another at the 9th floor under the high suite (Figure 8-11). Overall, the SATMD systems present more reliable and constant drift demands along the height of the original 12-storey structures. In the medium suite, for example, the SATMDs show the 50^{th} percentile drift demands close to 1.0% at most of the floors (Figure 8-7). The 50th percentile reduction factors of interstorey drifts by the SATMD systems are 0.71~0.77 under the suites, while 0.70~0.83 by PTMD systems, as shown in Tables 8-3 to 8-5. Again, the SATMDs prove to be more effective under the medium suite than any other suites.

The storey shear forces divided by total weight of the structure with the TMD systems also show good reductions based on the results from the maximum displacements

(Figures 8-4, 8-8 and 8-12). Under the all suites, the normalised shear force demands are reduced and, these response reductions are increased for 12+4 cases. In spite of adding 24% mass (12+2) and 40% mass (12+4) to the buildings, the method of construction that uses TMD (PTMD and SATMD) at the interface actually reduces the seismic demand in the storeys under the all suites of the earthquake records considered. The PATMD systems result in greater reductions of normalised shear force demands than the SATMD systems under the high suite (Figure 8-12). The 50th percentile reduction factors of normalised storey shear forces by the SATMD systems are 0.52~0.63 under the suites, while 0.48~0.64 by PTMD systems, as shown in Tables 8-3 to 8-5.

The acceleration responses of the isolated stories of the upper segment have a significant reduction in all cases. The reason for these reductions is again that the upper segment is isolated from the main structure, so base excitation is not directly transmitted to the separated upper portion of the TMD as discussed in Chapter 7. As seen in Figures 8-5, 8-9 and 8-13, the acceleration distributions over the height are fairly similar and the PTMD systems show more reduced demands under the all suites. Added viscous dampers of the PTMD systems have the benefit of being capable of reducing the acceleration demands on the structure while resulting in more even distributions over the height of the structures. The SATMD systems, in contrast, produce less effective acceleration demands over the original 12-storey structures due to semi-active control operations. However, the isolated upper storeys of the SATMD systems are more effectively controlled than the PTMD systems, and these reflect the effective interruption of energy flows between both upper and lower segments of the structures. The 50th percentile reduction factors of accelerations by the SATMD systems are 0.87~0.91 under the suites, while 0.64~0.76 by PTMD systems, as shown in Tables 8-3 to 8-5.

In all cases, it should be noted that PTMD results represent optimal exact tuning. Such exact tuning may not be practically possible due to construction or load variability, as well as degradation over time. Hence, the SATMD results would appear much better given their broad control band and adoptability.

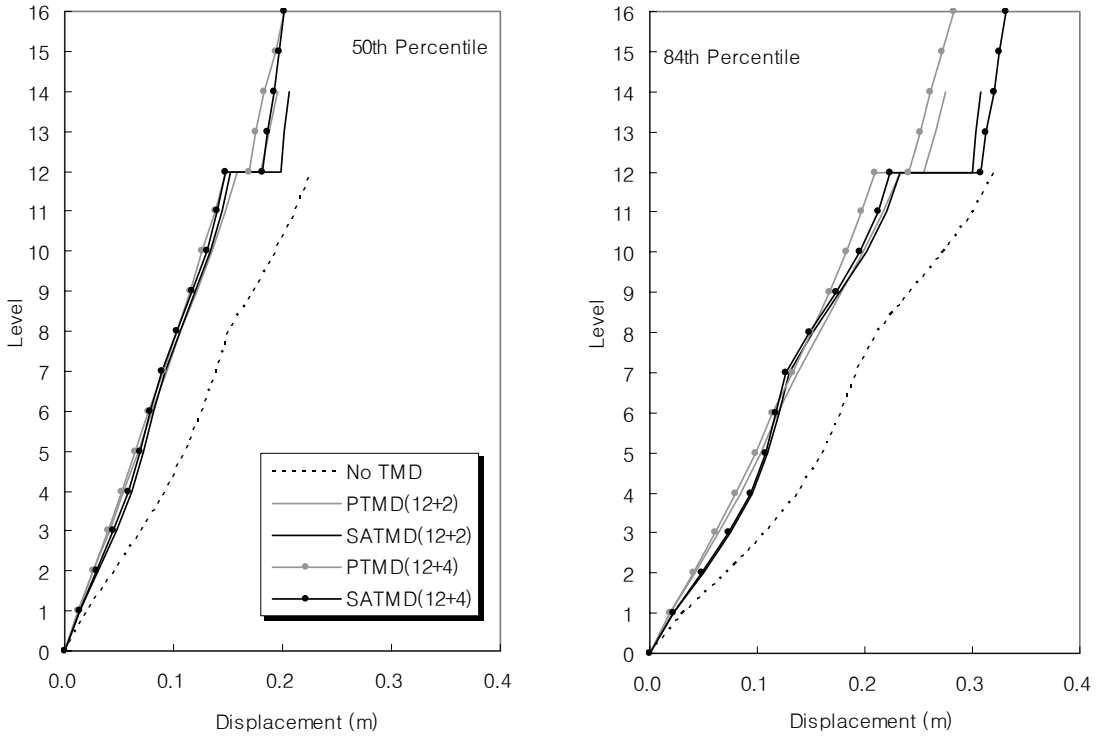

Figure 8-2 Maximum displacement of '12+2' and '12+4' models (Linear / Low suite)

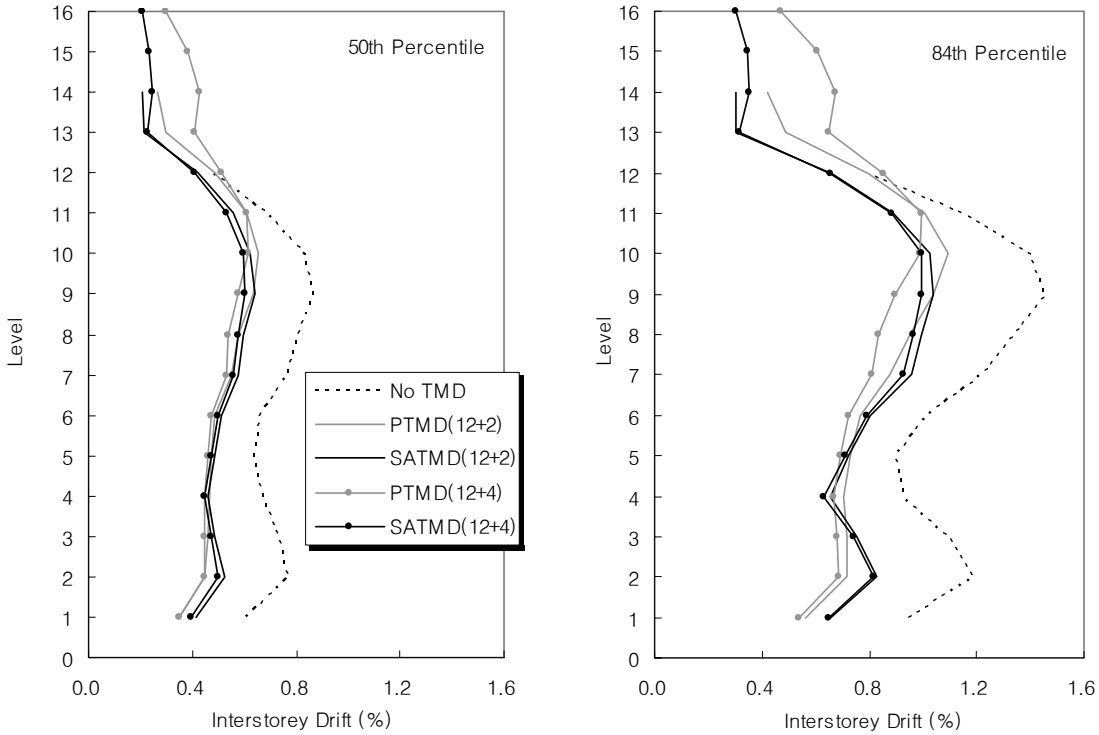

Figure 8-3 Interstorey drift of '12+2' and '12+4' models (Linear / Low suite)

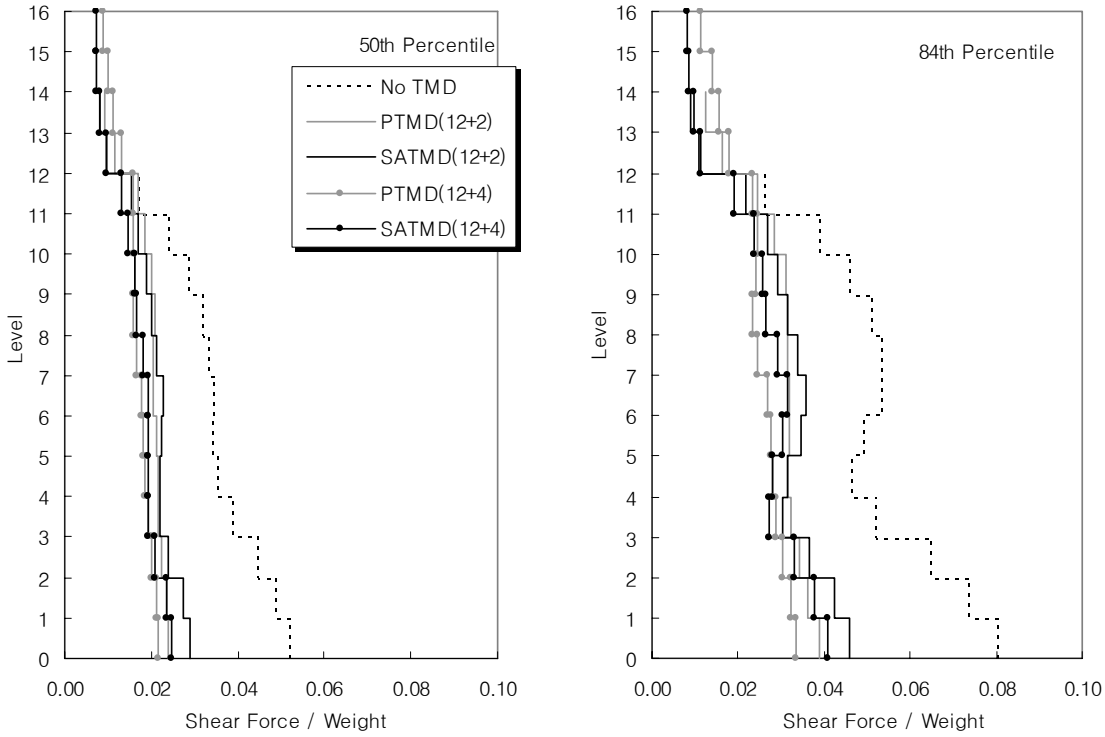

Figure 8-4 Storey shear force of '12+2' and '12+4' models (Linear / Low suite)

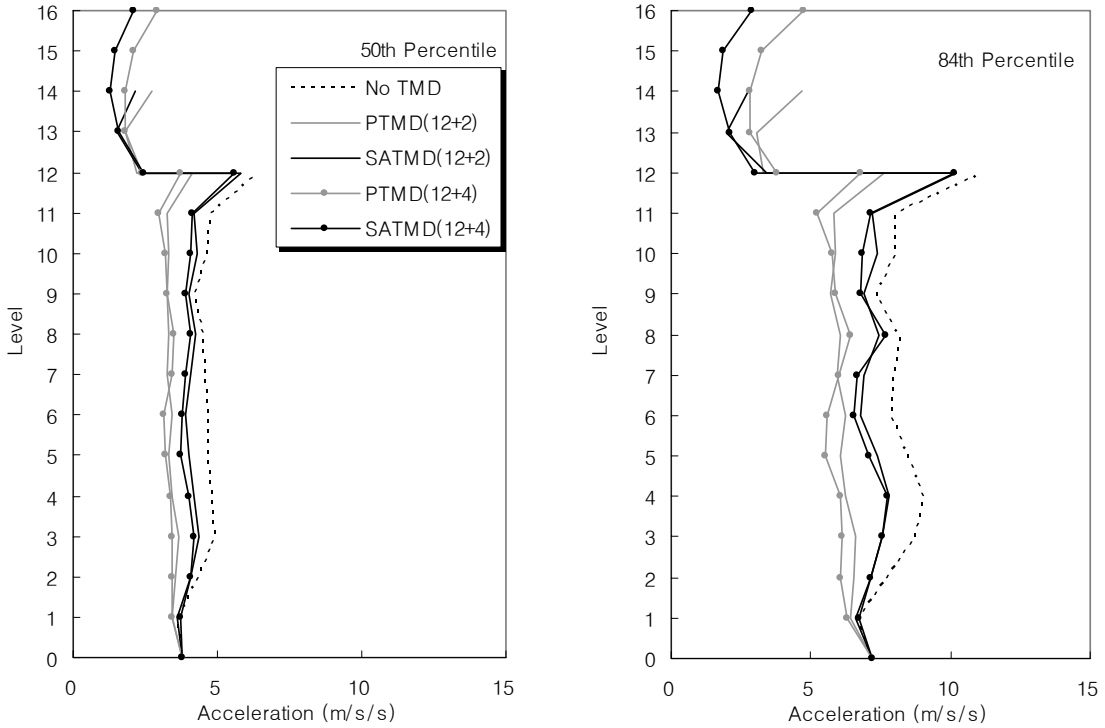

Figure 8-5 Total acceleration of '12+2' and '12+4' models (Linear / Low suite)

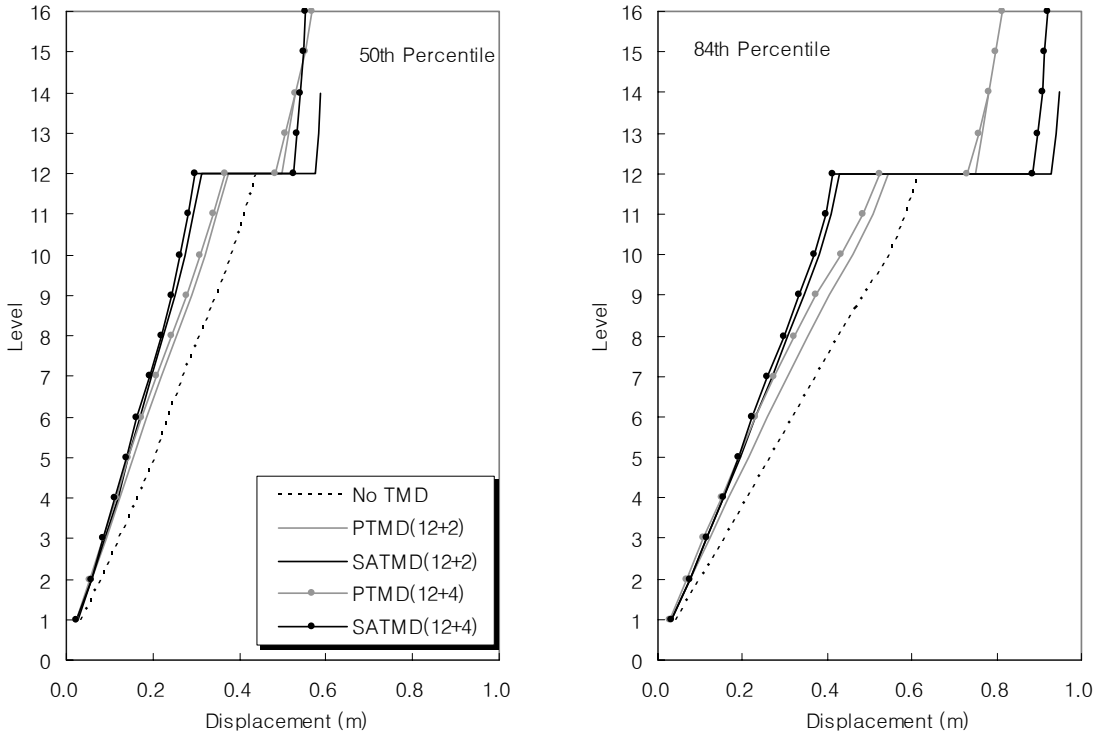

Figure 8-6 Maximum displacement of '12+2' and '12+4' models (Linear / Medium suite)

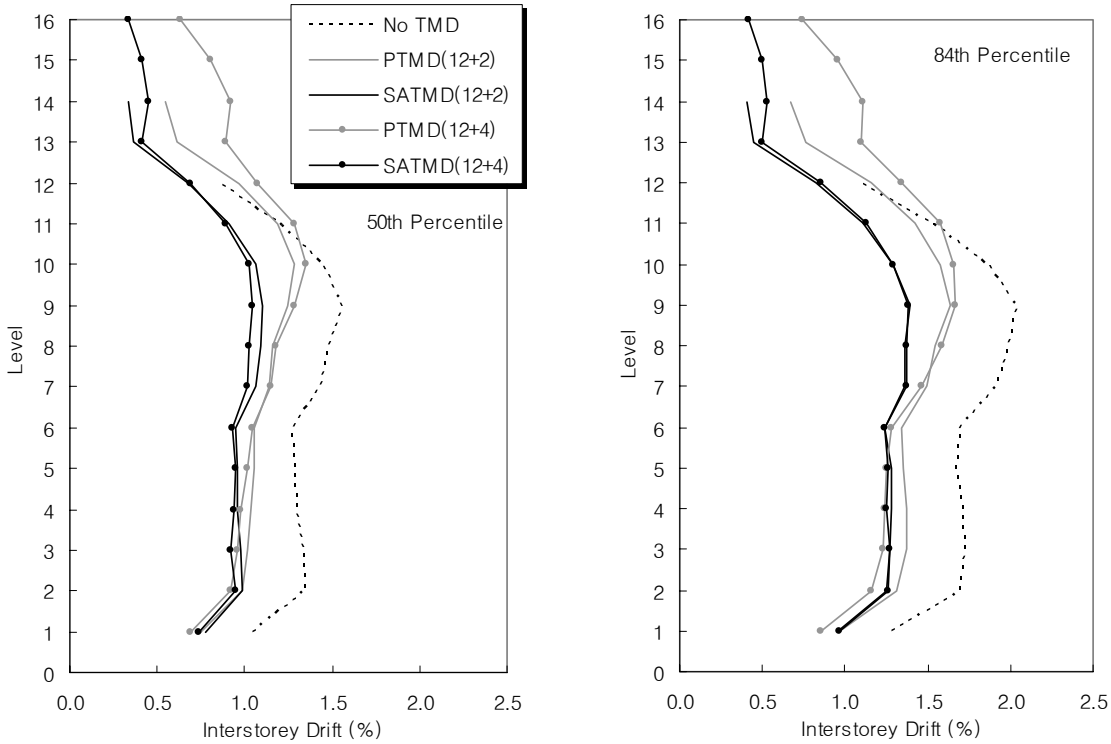

Figure 8-7 Interstorey drift of '12+2' and '12+4' models (Linear / Medium suite)

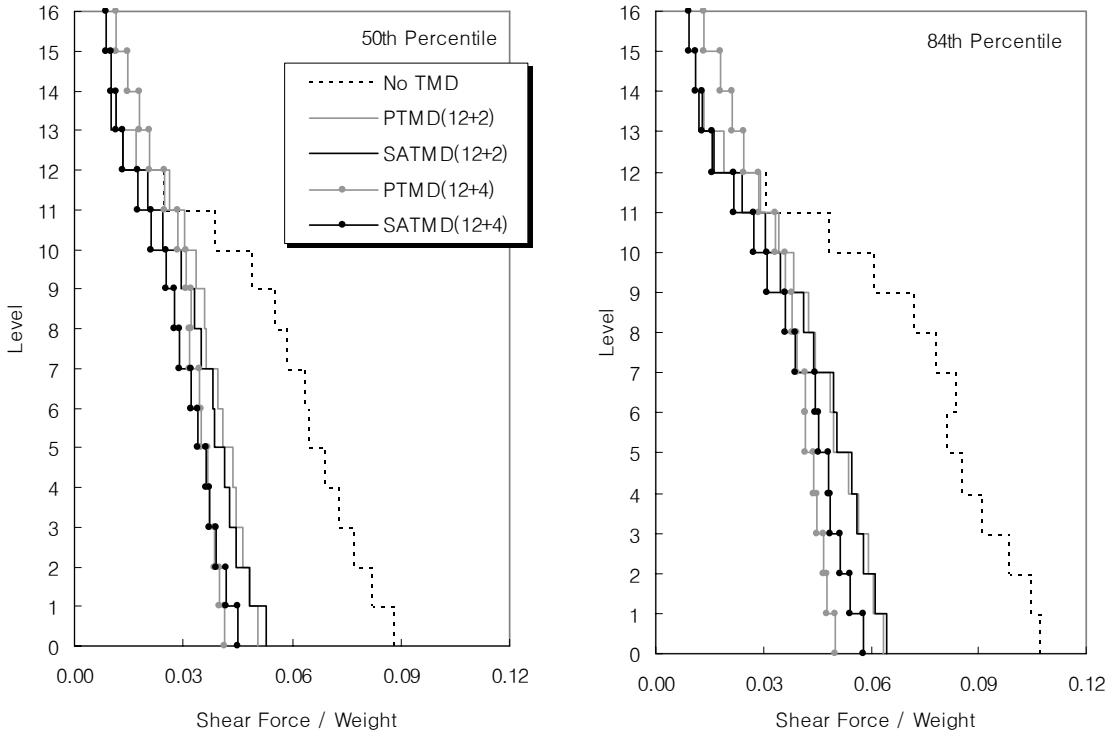

Figure 8-8 Storey shear force of '12+2' and '12+4' models (Linear / Medium suite)

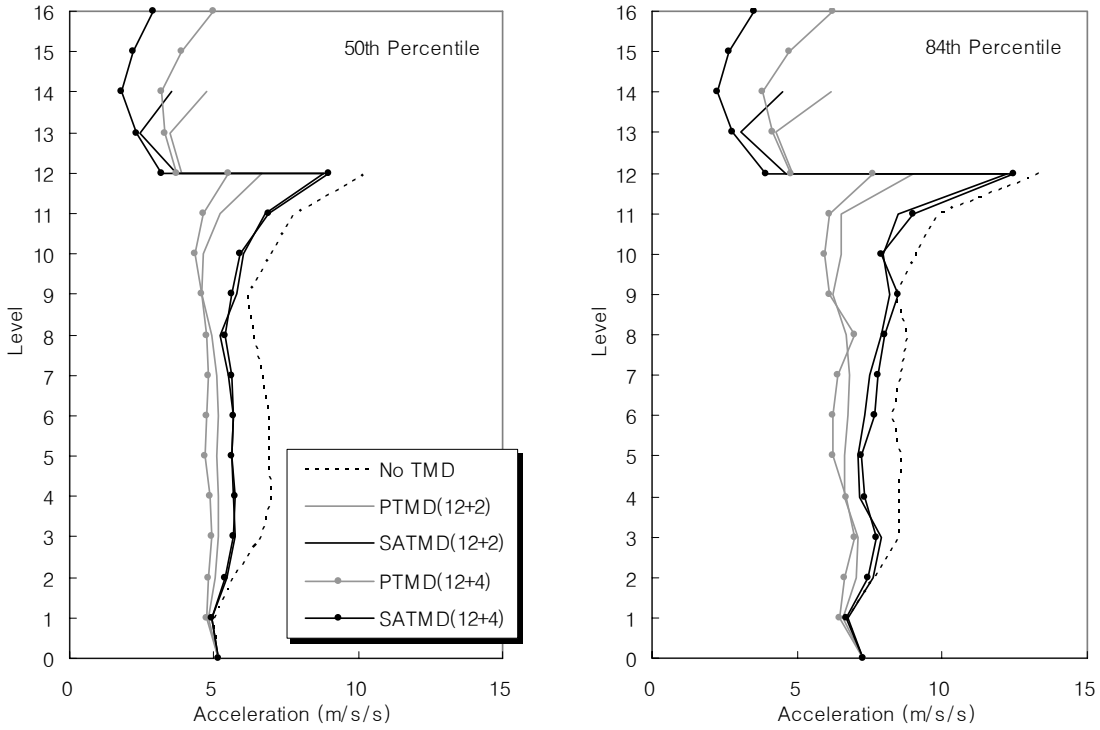

Figure 8-9 Total acceleration of '12+2' and '12+4' models (Linear / Medium suite)

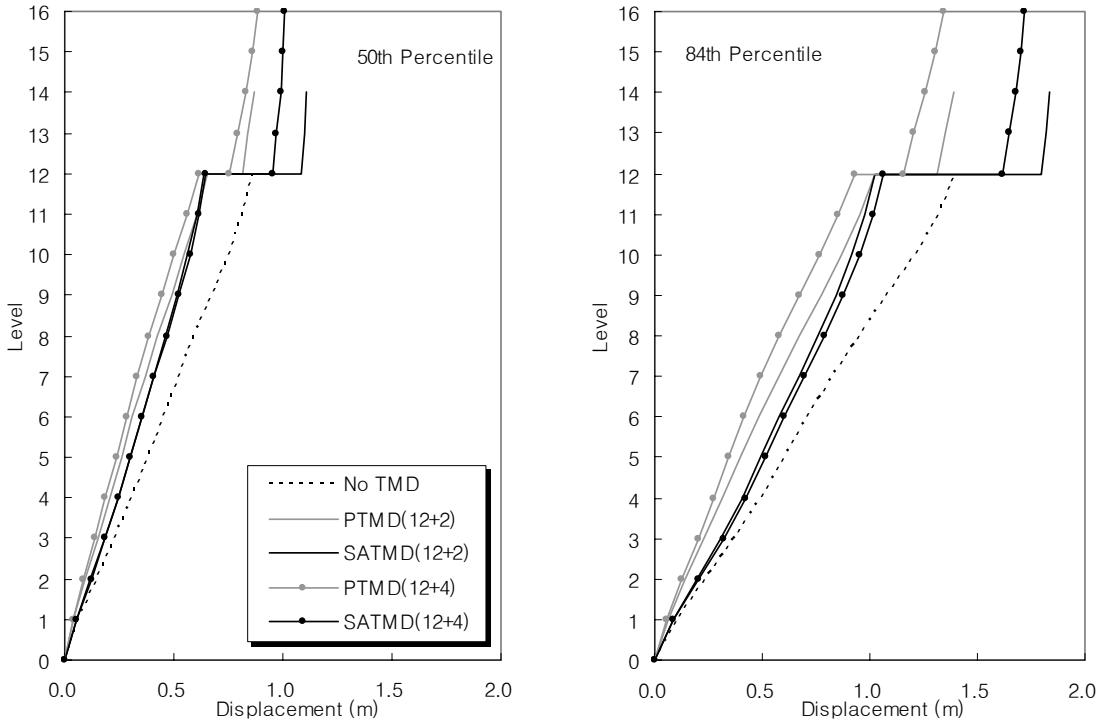

Figure 8-10 Maximum displacement of '12+2' and '12+4' models (Linear / High suite)

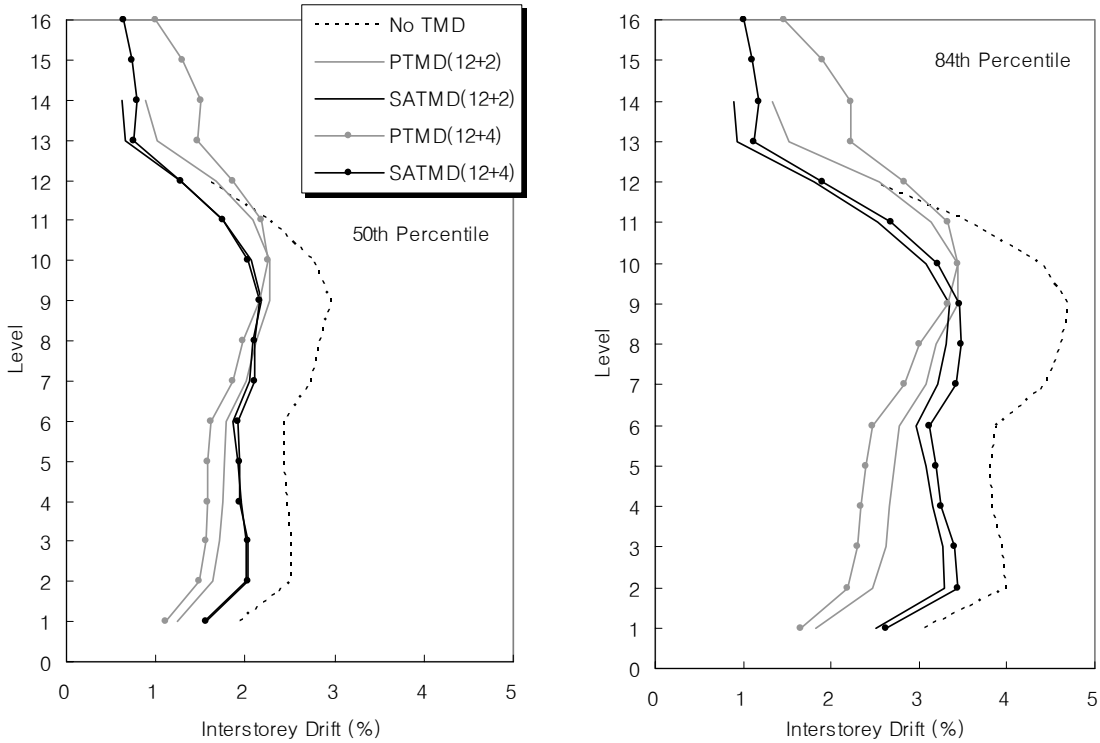

Figure 8-11 Interstorey drift of '12+2' and '12+4' models (Linear / High suite)

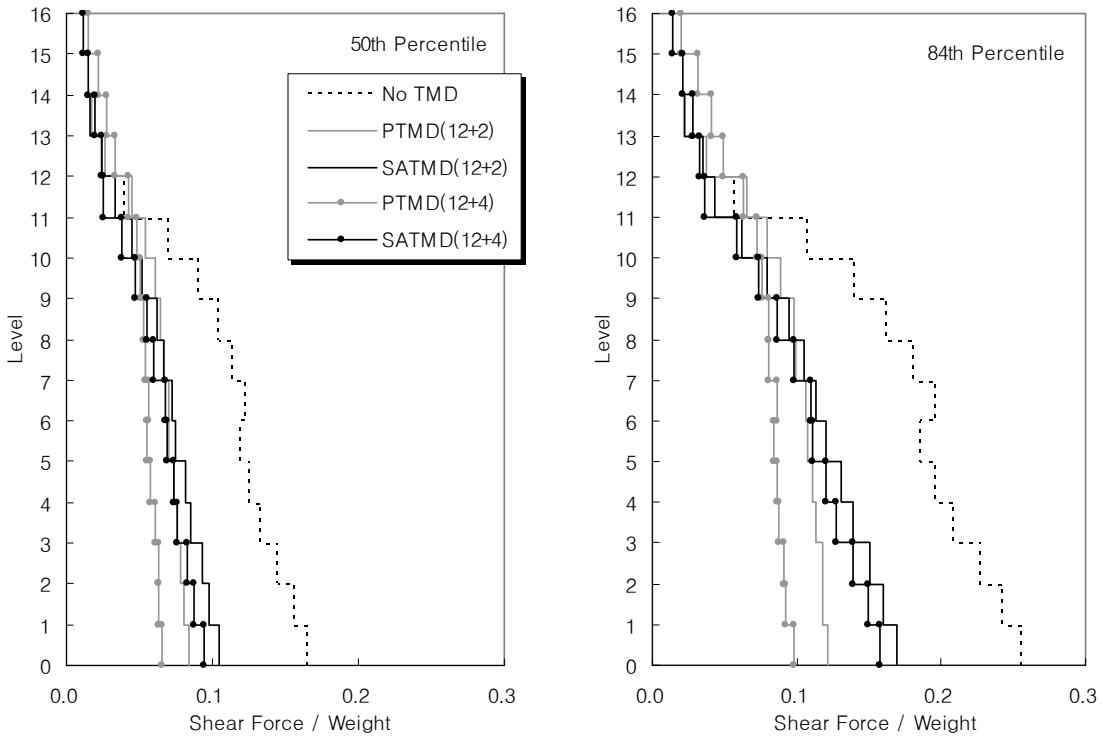

Figure 8-12 Storey shear force of '12+2' and '12+4' models (Linear / High suite)

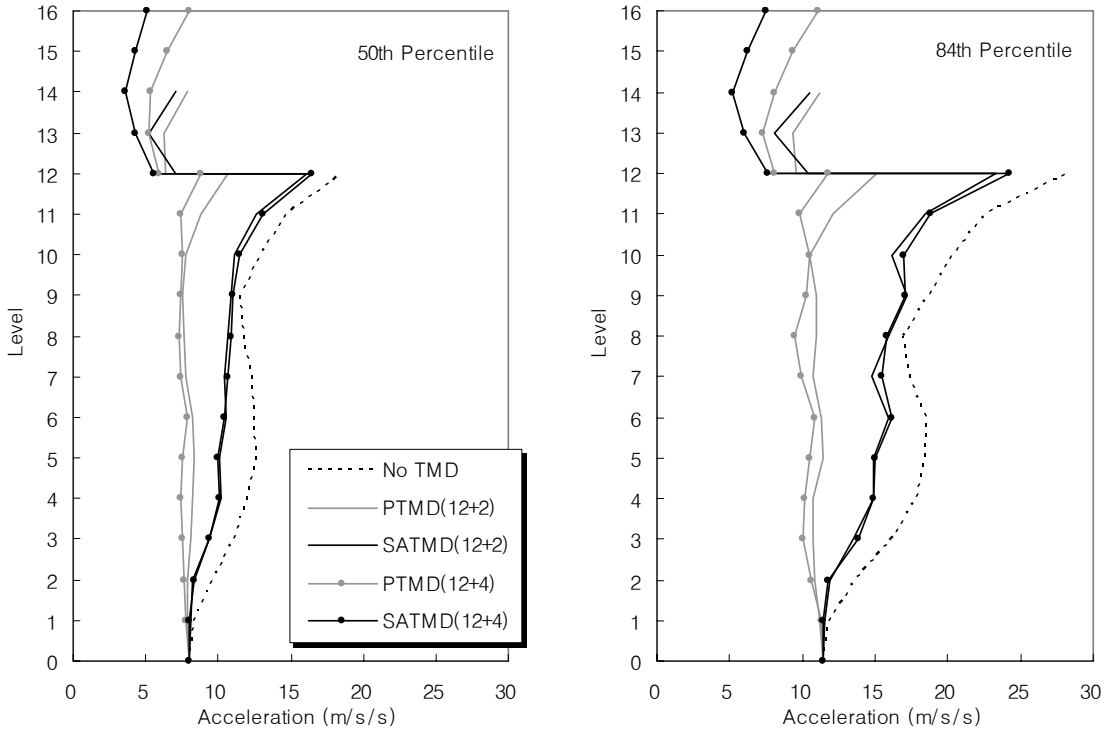

Figure 8-13 Total acceleration of '12+2' and '12+4' models (Linear / High suite)

Table 8-3 Seismic demands and reduction factors over 1st to 12th floor of PTMD(12+2 and 12+4) and SATMD(12+2 and 12+4) building systems (low suite)

Index >	Maximum Displacement		Interstorey Drift Ratio		Shear Force / Weight		Total Acceleration	
Percentile >	50th	84th	50th	84th	50th	84th	50th	84th
No TMD	0.130	0.186	0.713	1.123	0.035	0.053	4.62	8.22
PTMD(12+2)	0.087	0.130	0.516	0.830	0.021	0.032	3.47	6.33
[RF]	[0.67]	[0.70]	[0.72]	[0.74]	[0.60]	[0.60]	[0.75]	[0.77]
SATMD(12+2)	0.088	0.132	0.525	0.833	0.022	0.033	4.20	7.42
[RF]	[0.68]	[0.71]	[0.74]	[0.74]	[0.63]	[0.62]	[0.91]	[0.90]
PTMD(12+4)	0.083	0.121	0.501	0.780	0.018	0.027	3.38	6.07
[RF]	[0.64]	[0.65]	[0.70]	[0.69]	[0.51]	[0.51]	[0.73]	[0.74]
SATMD(12+4)	0.085	0.128	0.504	0.812	0.019	0.029	4.06	7.34
[RF]	[0.65]	[0.69]	[0.71]	[0.72]	[0.54]	[0.55]	[0.88]	[0.89]

Table 8-4 Seismic demands and reduction factors over 1st to 12th floor of PTMD(12+2 and 12+4) and SATMD(12+2 and 12+4) building systems (medium suite)

Index >	Maximum Displacement		Interstorey Drift Ratio		Shear Force / Weight		Total Acceleration	
Percentile >	50th	84th	50th	84th	50th	84th	50th	84th
No TMD	0.250	0.345	1.303	1.689	0.062	0.079	6.76	8.76
PTMD(12+2)	0.203	0.287	1.075	1.378	0.040	0.048	5.14	6.91
[RF]	[0.81]	[0.83]	[0.82]	[0.82]	[0.64]	[0.61]	[0.76]	[0.79]
SATMD(12+2)	0.180	0.244	0.959	1.217	0.037	0.047	5.87	7.96
[RF]	[0.72]	[0.71]	[0.74]	[0.72]	[0.60]	[0.60]	[0.87]	[0.91]
PTMD(12+4)	0.195	0.265	1.077	1.358	0.034	0.041	4.81	6.60
[RF]	[0.78]	[0.77]	[0.83]	[0.80]	[0.55]	[0.52]	[0.71]	[0.75]
SATMD(12+4)	0.173	0.238	0.926	1.220	0.032	0.042	5.89	8.08
[RF]	[0.69]	[0.69]	[0.71]	[0.72]	[0.52]	[0.53]	[0.87]	[0.92]

Table 8-5 Seismic demands and reduction factors over 1st to 12th floor of PTMD(12+2 and 12+4) and SATMD(12+2 and 12+4) building systems (high suite)

Index >	Maximum Displacement		Interstorey Drift Ratio		Shear Force / Weight		Total Acceleration	
Percentile >	50th	84th	50th	84th	50th	84th	50th	84th
No TMD	0.484	0.775	2.467	3.907	0.116	0.180	12.0	17.9
PTMD(12+2)	0.347	0.540	1.860	2.824	0.068	0.102	8.2	11.4
[RF]	[0.72]	[0.70]	[0.75]	[0.72]	[0.59]	[0.57]	[0.68]	[0.64]
SATMD(12+2)	0.371	0.604	1.892	2.964	0.072	0.114	10.5	15.4
[RF]	[0.77]	[0.78]	[0.77]	[0.76]	[0.62]	[0.63]	[0.87]	[0.86]
PTMD(12+4)	0.316	0.476	1.769	2.676	0.056	0.083	7.7	10.5
[RF]	[0.65]	[0.61]	[0.72]	[0.69]	[0.48]	[0.46]	[0.64]	[0.59]
SATMD(12+4)	0.376	0.628	1.905	3.099	0.065	0.105	10.6	15.6
[RF]	[0.78]	[0.81]	[0.77]	[0.79]	[0.56]	[0.59]	[0.88]	[0.87]

8.4 Summary

This Chapter shows the response characteristics for extended linear TMD building systems when new stories are added as the tuned mass. Overall, the results are quite promising, but may not look convincing. Intuitively, adding more storeys to the existing building is primarily an attempt to control the 1st mode of vibration of the original structure by a damping mechanism located on the top of the building. Therefore, from a structural point of view, the additional storeys are solely meant to be a support for the reaction of the damping mechanism. In the new system, the mass of added storeys contributes mostly to the 1st mode of vibration, which is properly isolated by a long natural period. The 2nd mode of the structure, which has the mass of the original building, is now accompanied by a large damping ratio as was intended, by design thus describing how energy and force transmitted to the system are reduced.

9 Nonlinear MDOF TMD Building Systems

9.1 Introduction

In order to predict the actual seismic responses of a building for possible earthquake excitations, the inelastic characteristics of the structural behaviours should be understood. Also, the prediction of inelastic seismic responses and the evaluation of seismic performance of a building structure are very important subjects in performance-based design. A compromise between accuracy and efficiency is usually necessary, requiring a determination of the level of modelling and type of analysis required for this purpose. However, linear models can overestimate the effectiveness of the structural system when comparing controlled performance with uncontrolled response. Thus, a reliable evaluation of the effect of nonlinear behaviour on the demands resulting from time history analyses is required and, finally leads to accurate evaluation of the seismic performance not only for the global nonlinear behaviour of a building but also for its local nonlinear seismic responses.

Previous control evaluation research into the effect of nonlinear aspects has highlighted the necessity to include two main types of nonlinear effects if models are to accurately represent real and actual structural demands (Barroso 1999; Breneman 2000). The inclusion of the effect of geometric nonlinear P-delta effects of flexural stiffness is the one of these aspects, while the other is a nonlinear hysteretic model to account for structural energy dissipation and yielding during large motions.

The structural vibration procedure under earthquake excitation is actually an energy transferring process in nature. Energy is released by the collision of underground plates, and the movement of the ground transfers part of energy to the buildings to induce structural vibrations. The input energy is then transformed into other types of energy, such as strain energy and kinetic energy. Therefore, the energy dissipation in a building is the capacity of the structural member to dissipate energy through hysteretic behaviour. An element has a limited capacity to dissipate energy in this manner prior to failure. As a result, the amount of energy dissipated serves as an indicator of how much damage has occurred during seismic loading.

In addition, detection of damage to structures has recently received considerable attention from the view point of maintenance and safety assessment. In this respect, the vibration characteristics of buildings have been applied consistently to obtain a damage index of the local and whole building. Capturing the accumulation of damage sustained during dynamic loading is of particular interest to structural engineers. This process is usually accomplished through a low-cycle fatigue formulation or calculation of the energy absorbed by the system during loading. In both those cases, inelastic behaviour is assumed before any damage is considered.

In order to demonstrate the accurate and valid controlled performances of the SATMD building systems, in this chapter, the inelastic time history analyses based on nonlinear structural models including the main types of nonlinear effects are used. In addition, dissipated hysteretic energy and weighted damage values are evaluated as performance indices as well as some traditional response performance indicators as previously discussed in Chapters 7 and 8.

9.2 Modelling

9.2.1 P-delta Effects

In most analyses, the first order moments and deflections are determined on the assumption of linear elastic behaviour. However, as the frame sways laterally the vertical loads acting through the deflected shape cause additional moments and deflections. These added moments and deflections are second order effects that are not predicted by the first order analysis, but may be important in large structural responses. More specifically, these effects produce a second order stiffness called the geometric stiffness, which may be assigned to augment the first order stiffness.

When large deflections are present, the strain-displacement equations contain nonlinear terms that must be included in calculating the stiffness matrix *k*. The

nonlinear terms in the equations modify the element stiffness matrix *k* so that the total stiffness is defined:

$$k = k_E + k_G \tag{9-1}$$

where k_E is the standard elastic stiffness matrix and k_G is the geometric stiffness matrix.

The geometric stiffness matrix, k_G , is presented in Equation (9-2) where the formulation was based on the lateral deformation shape along the beam being a cubic function of the position along the length.

$$k_G = \begin{bmatrix} V_1 \\ M_1 \\ V_2 \\ M_2 \end{bmatrix} = \frac{P}{L} \begin{bmatrix} \frac{6}{5} & \frac{L}{10} & -\frac{6}{5} & \frac{L}{10} \\ \frac{L}{10} & \frac{2L^2}{15} & -\frac{L}{10} & -\frac{L^2}{30} \\ -\frac{6}{5} & -\frac{L}{10} & \frac{6}{5} & -\frac{L}{10} \\ \frac{L}{10} & -\frac{L^2}{30} & -\frac{L}{10} & \frac{2L^2}{15} \end{bmatrix} \begin{bmatrix} \delta_1 \\ \theta_1 \\ \delta_2 \\ \theta_2 \end{bmatrix} \tag{9-2}$$

where *P* is the axial fore, θ is the stability coefficient and *L* is the member length.

Instead of using the cubic function, a linear function was used in this study, as seen in Figure 9-1. The net effect is the same as subtracting the geometric stiffness from the member stiffness, but is computationally more efficient. This is based on the assumption that the same displacement as the cubic function, δ, is a function of shear force, *V*, and the member force, *L*. Such an assumption implies the use of an average slope over the whole length of the structure. When this assumption is used, the simplified geometric stiffness matrix is defined:

$$k_G = \begin{bmatrix} V_1 \\ M_1 \\ V_2 \\ M_2 \end{bmatrix} = \frac{P}{L} \begin{bmatrix} 1 & 0 & -1 & 0 \\ 0 & 0 & 0 & 0 \\ -1 & 0 & 1 & 0 \\ 0 & 0 & 0 & 0 \end{bmatrix} \begin{bmatrix} \delta_1 \\ \theta_1 \\ \delta_2 \\ \theta_2 \end{bmatrix} \tag{9-3}$$

The above geometric stiffness matrix of Equation (9-3) is usually referred to as the string stiffness.

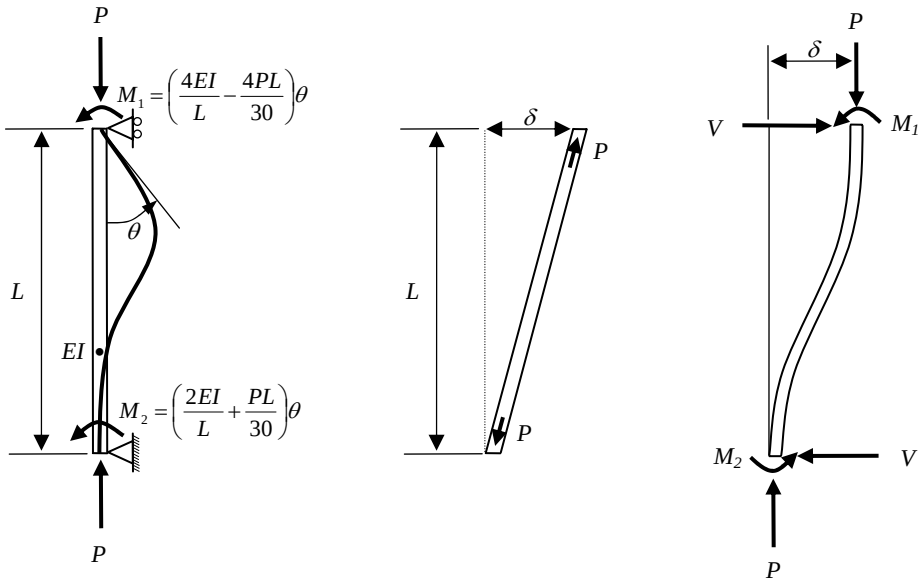

Figure 9-1 Configurations of slope in calculating the geometric stiffness

To represent the second order effects due to the lateral displacement of the gravity loads, the simplified P-delta option was used in *Ruaumoko* (Carr 2004). Here, the displacements are assumed to be small and the coordinates are unchanged, but the beam and column stiffnesses are adjusted for the axial forces from the static analysis. This allows for the lateral softening of the columns due to the gravity loads. The P-delta effect is assumed to be constant as the increase in stiffness on one side of the structure is matched by a decrease in stiffness on the other side of the structure under lateral loading, where the sum of the vertical forces is assumed to be constant.

9.2.2 Hysteresis Models

In the inelastic analysis of structures, the force-deformation relationship of members observed in a laboratory test must be idealised into an analytical moment-curvature hysteresis model. One of the general hysteretic characteristic is the stiffness change due to cracking of the concrete and the yielding of the reinforcement. It has been

shown from previous studies that these stiffness changes can have a significant effect on the response amplitude, response waveform, residual displacement, and hysteresis loop shape.

9.2.2.1 Elasto-Plastic and Bilinear Models

At the initial development stage of the nonlinear dynamic analysis, the elasto-perfectly plastic hysteresis model (elasto-plastic), shown in Figure 9-2, was used. This model is intended for perfectly elasto-plastic materials. The primary curve consists of a bi-linear relationship, which also defines member stiffness during loading, unloading and reloading. Accordingly, the elastic slope represents the effective stiffness of reinforced concrete prior to yielding, including the effect of cracking. The same stiffness is also used during unloading and reloading beyond the elastic rage between the yield loads in two directions. Upon reaching the yield load, the member is assumed to have zero stiffness until unloading begins. It can thus be defined by only three rules, defining the regime of stiffness changes for loading and load reversal (Saiidi 1982).

The primary curve of the Bilinear model, shown in Figure 9-3, also consists of two segments as in the Elasto-Plastic model. The Bilinear model has a finite positive slope that is assigned to the stiffness after yielding to simulate the strain hardening characteristics of the reinforced concrete member. The unloading stiffness after yielding is equal to the initial elastic stiffness. The post-yield stiffness, rk_0, as seen in Figure 9-3, is the effect of the strain hardening and is usually expressed as a fraction, r, of the initial stiffness, k_0. In a similar manner to the Elasto-Plastic model, the Bilinear model is easy to formulate and can be described by only three rules.

These two models do not represent the degradation of unloading and reloading stiffnesses due to inelastic deformation, which is a characteristic feature of reinforced concrete. The energy dissipation during small amplitudes is also not modelled. These two models are thus not fully appropriate for a refined nonlinear analysis of a reinforced concrete framed structure (Otani 1981; Saiidi 1982). However, they have

been widely used because of the simplicity because of the simplicity and reasonable approximation they offer.

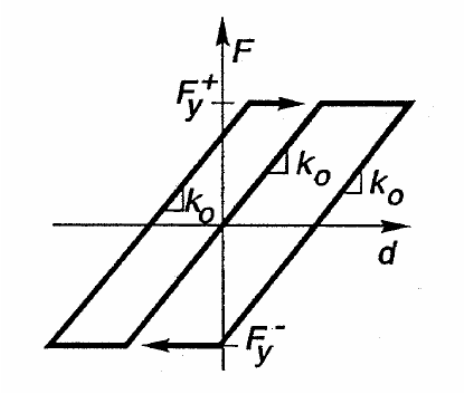

Figure 9-2 Elasto-plastic hystresis

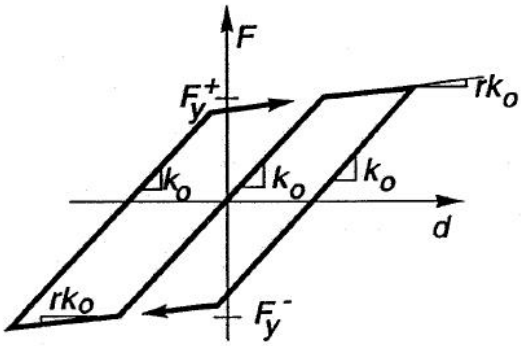

Figure 9-3 Bilinear hystresis

9.2.2.2 Degrading Bilinear and Clough Degrading Stiffness Models

The degrading bilinear model is similar to the bilinear rule except that the loading and unloading stiffness degrade with the previous maximum displacement (Nielsen and Imbeault 1971), shown in Figure 9-4. The degraded stiffness can be defined:

$$K_u = K_0 \left(\frac{d_y}{d_m} \right)^{\alpha} \tag{9-4}$$

where α : unloading stiffness degrading parameter ($0 < \alpha < 1$)

K_0 : initial elastic stiffness

d_y : yielding displacement

d_m : previously attained maximum displacement in any direction

The unloading stiffness remains constant until the response displacement amplitude exceeds the previous maximum displacement in either direction. If the value of α is chosen to be zero, the unloading stiffness will not degrade with yielding and the degrading bilinear model reverts to the bilinear model. A smaller value of α tends to produce a larger residual displacement. Like the Elasto-Plastic and Bilinear models, this model does not dissipate hysteretic energy until yield occurs.

The Clough Degrading Stiffness Model (Clough and Penzien 1966), shown in Figure 9-5, was the first degrading stiffness rule to represent reinforced concrete membdr hysteretic behaviour. The rule is the same as the modified Takeda rule when the parameters α and β are both equal to zero. The unloading stiffness after yielding is kept equal to the initial elastic stiffness. The response point during reloading moves toward the previous maximum response point.

The Clough model has two areas of deficiency. First, the model does not consider the degradation of the unloading stiffness, which is one of the characteristic features of reinforced concrete members. Second, the model may overestimate the softening of the reloading stiffness for the subsequent cycles of small inelastic excursion after a large inelastic excursion. However, in a global sense, when considering both the unloading and reloading paths, an effective cyclic reduction of stiffness is observed.

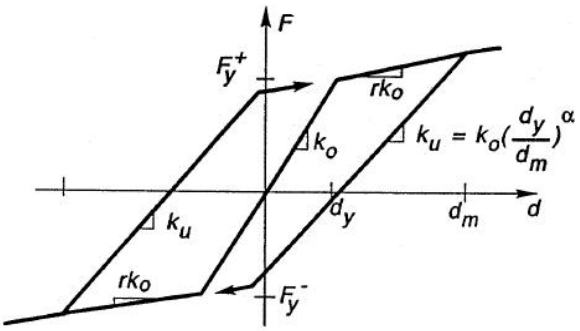

Figure 9-4 Degrading bilinear hystresis

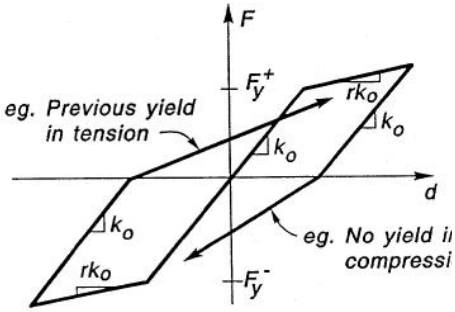

Figure 9-5 Clough degrading hystresis

9.2.2.3 Modified Takeda Model

The Takeda model includes stiffness changes at flexural cracking and yielding, hysteresis rules for small cycle inner hysteresis loops inside the outer loop, and unloading stiffness degradiation with deformation. When compared to the Bilinear Hysteresis Model, this model is more complicated, but also more realistic in simulating the nonlinear behaviour of reinforced concrete members.

However, the disadvantage of this hysteretic model is the complexity of the rules. The primary curve of the Takeda model has therefore been modified by Otani (Otani 1974) to be bilinear, by choosing the yield point to be the origin of the hysteretic loop instead of original tri-linear back-bone. Such a model is called as the "bilinear Takeda" model, as shown in Figure 9-6, where α is an unloading stiffness degrading factor and β is a reloading stiffness degrading factor. Increasing α decreases the unloading stiffness, and increasing β increases the reloading stiffness. The unloading stiffness after yielding is $(d_y/d_m)^{\alpha}$ times the initial elastic stiffness, k_0, which is similar to the approach used by Emori and Schnobrich (1978). The response point during reloading moves toward the point, whose displacement is $(d_m-\beta d_p)$, where d_m is the displacement of the previously maximum inelastic response point. α usually ranges from 0.0 to 0.5, while β is from 0.0 to 0.6. An alternative that is modelled on the Drain-2D program (Kanaan and Powell 1973) for the unloading stiffness is available in the program *Ruaumoko* (Carr 2004).

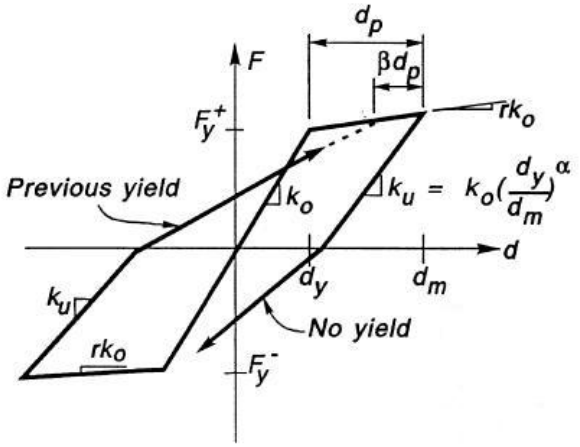

Figure 9-6 Modified Takeda hystresis

For post 1970's structures, where typical hysteresis loops are available, it is suggested that the Modified Takeda model be used. The equivalent unloading and reloading stiffness degradation parameters α and β should be determined for the experimental hysteresis loops of the similar members, as shown in Equations (9-5) and (9-6).

$$\alpha = \ln\frac{K_u}{K_0} \Big/ \ln\frac{d_y}{d_m} \tag{9-5}$$

$$\beta = \frac{\beta d_p}{d_p} \tag{9-6}$$

where K_0 and K_u are the initial and degraded unloading stiffness at maximum displacement, d_m respectively, and d_y is the yield displacement. Finally, $d_p = d_m - d_y$ and βd_p refer to the definitions in Figure 9-6.

9.2.2.4 Recommended Hysteresis Model

Considering that the Modified Takeda hysteresis model is able to use different unloading and reloading stiffness degrading parameters, and better represents realistic hysteretic behaviour of reinforced concrete members, this hysteresis model is recommended when carrying out inelastic time history analysis for computing damage indices for members, storeys and structures. The main problem is to identify the unloading and reloading stiffness degradation parameters α and β, especially the unloading stiffness degradation parameters, α, due to its greater sensitivity in the overall structural prediction. The unloading and reloading stiffness degradation parameters α and β can be identified by comparing with experimental hysteresis loops for the same or similar members to those in the modelled structures under evaluation.

Varying the unloading stiffness degradation parameter α from 0.0 to 0.3 and the reloading stiffness degradation parameter β from 0.0 to 0.6 does not significantly affect the predicted storey and structural damage indices for the Modified Takeda hysteresis model. The larger the unloading stiffness degradation parameter α ($0.3<\alpha<0.5$), the larger the predicted overall structural damage indices. For the Park et al. (1987) member damage indices, the maximum variation in the structural damage index by increasing the unloading stiffness degradation parameters α ($0.3<\alpha<0.5$) can be up to 1.25.

For post 1970's structures, if the hysteresis loops from laboratory tests for the members or similar members of structures to be analysed are unavailable, the Modified Takeda ($\alpha=0.5$, $\beta=0.0$) may be used for the damage evaluation. Using the

Modified Takeda hysteresis model, in this research, the inelastic dynamic time history is carried out.

9.3 Seismic Energy Demand

9.3.1 Introduction

It is well known that seismic damage to a multistorey frame is not only caused by maximum response, such as force or lateral displacement. Inelastic excursions below the maximum response can still cause significant damage to structures (McCabe and Hall 1992). This duration-related damage, which can be expressed as the energy absorbed in a structure, should also be considered in the evaluation of structural performance (Akiyama 1985; Leelataviwar et al. 1999).

Meanwhile, new trends in the seismic design methodologies are oriented to the definition of performance-based methods for the design of new facilities and for the assessment of the seismic capacity of existing facilities. In this field, using energy concepts allows optimisation of the design and detailing. It also enables the optimised selection of strategies and techniques for innovative control or protective systems, such as base isolation and passive energy dissipation devices (Bertero 1997).

To extend the energy-based analysis method to multistorey frames, a procedure for the estimation of energy demand in a multi-degree-of freedom (MDOF) system is needed. In the last few years this approach has been largely accepted (Fajfar and Fischinger 1990; Uang and Bertero 1990; Zahrah and Hall 1984) and it has been introduced in advanced seismic codes, such as the Japanese code (Akiyama 1985). In particular, the energy criterion postulates that the structure collapses when it is demanded to dissipate, through inelastic deformations, an amount of energy larger than that supplied.

The energy approach remains a powerful tool, because it is simple to use and has a large experimental background. Moreover, if the allowable energy is assumed to be

equal to the energy dissipated under monotonic loads, the energy criterion represents a lower limit of the response capacity of the structure (Cosenza et al. 1993). Therefore, its application is on the safe side leading to a conservative design.

9.3.2 Hysteretic Energy Index

The input energy due to a ground motion depends mainly on the elastic period of the structure and on the seismic record, while it is much less dependent on the viscous damping and characteristics of the plastic response like the hysteresis and the ductility (Akiyama 1985; Fajfar and Vidic 1992; Uang and Bertero 1990; Zahrah and Hall 1984). Hence, the assessment of the input energy represents a good starting point to develop a seismic design method based on energy criteria. However, even though the input energy demand can be considered a good indicator of the damage potential of the earthquake (Bertero and Uang 1992; Conte et al. 1990), it must be noted that only a small percentage of the input energy dissipated as hysteretic energy related to seismic structural damage.

Ductile moment resisting framed structures of reinforced concrete designed using the capacity design philosophy allow energy to be dissipated at any of the beam ends at any level, as well as at the base of the first storey columns, via inelastic hysteretic behaviour. The hysteretic energy dissipation capacity of a member can be expressed by a hysteretic energy dissipation index, E_h, witch can be obtained from Equation (9-7) with the hysteretic model for the member (Otani 1981). The index, E_h, is defined to be the amount of hysteretic energy dissipated $\Delta\omega$ per cycle during a displacement cycle of equal amplitudes in the positive and negative directions divided by $2\pi F_m d_m$, where $2\pi F_m d_m$ is the critical viscous damping energy of an equivalent elastic member of stiffness $k_{eq}=F_m/d_m$.

$$E_h = \frac{\Delta\omega}{2\pi F_m d_m} \tag{9-7}$$

where F_m is the resistance at the peak displacement d_m, shown in Figure 9-7. The value of the index is equal to the equivalent viscous damping ratio of a linearly elastic

system which is capable of dissipating an amount of energy, $\Delta\omega$, in one cycle under "resonant steady-state" oscillation. The fore, *F* could be concentrated force and bending moment. The displacement, *d*, could be deflection, rotation and curvature. In this research, all of the forces and displacements related to hysteresis models refer to bending moment and curvature.

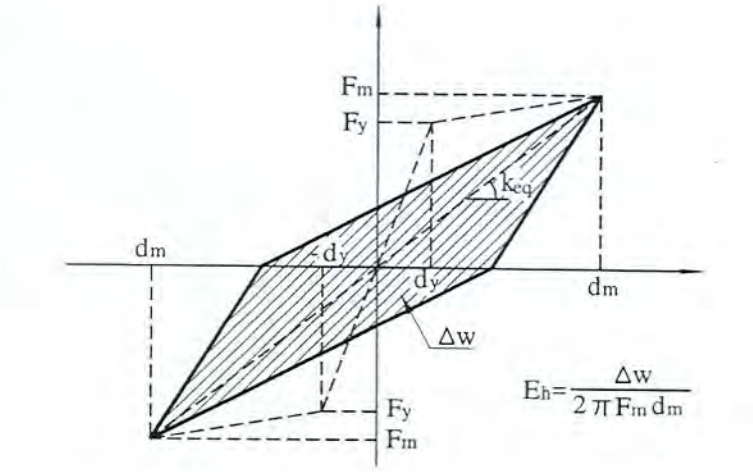

Figure 9-7 Hysteretic Energy Dissipation Index (Otani 1981)

The hysteretic energy dissipation index of the Modified Takeda Model is defined:

$$E_h = \frac{1}{2\pi}\left\{2-[R_p(\beta-2)(\mu-1)-2]\mu^{\alpha-1}+\frac{2\beta(\mu-1)R_p}{1+R_p(\mu-1)}+\beta\left(1-\frac{1}{\mu}\right)\right\} \quad (9\text{-}8)$$

where R_p : ratio of post-yield stiffness to initial stiffness

α : unloading stiffness degradation parameter

β : reloading stiffness degradation parameter

μ : ductility factor (ratio of maximum displacement to the initial yield displacement)

The energy index is a function of the unloading and reloading stiffness degradation parameters, the ratio of post-yielding stiffness to the initial elastic stiffness, and the curvature ductility factor, as shown in Figure 9-8.

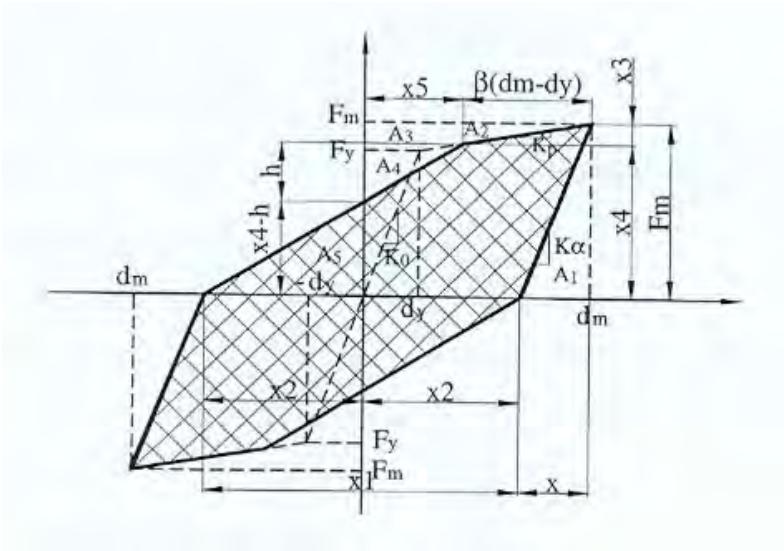

Figure 9-8 Hysteretic energy dissipation Index of the modified Takeda model

9.4 Seismic Damage Assessment

9.4.1 Introduction

The structural ductility factor indicates the maximum deflection of the structure under earthquake excitation. This deformation of the structure is strongly related to the damage of the structure. Hence, the damage of the structure is not evaluated only by the dissipated energy, number of cycles, stiffness deterioration and so on.

Degrees of damage are usually quantified using damage indices. In the past, many analyses have used the member ductility factors as a crude measure of damage potential. However, a realistic damage index for seismic damage assessment requires capturing not only the maximum response values, but also the total dissipated energy. Figure 9-9 shows two different inelastic displacement (curvature) histories of the same maximum response value that could be experienced by one structural member. The degrees of damage implied for the two curvature time histories will be same if only the maximum curvature ductility is used as the damage measure. This method ignores the effect of the accumulated dissipated hysteretic energy or the number of inelastic excursions on the accumulated damage in the member. However, it is

obvious that the displacement (curvature) history (b) will result in larger accumulated dissipated energy and much more damage in the member than that for history (a).

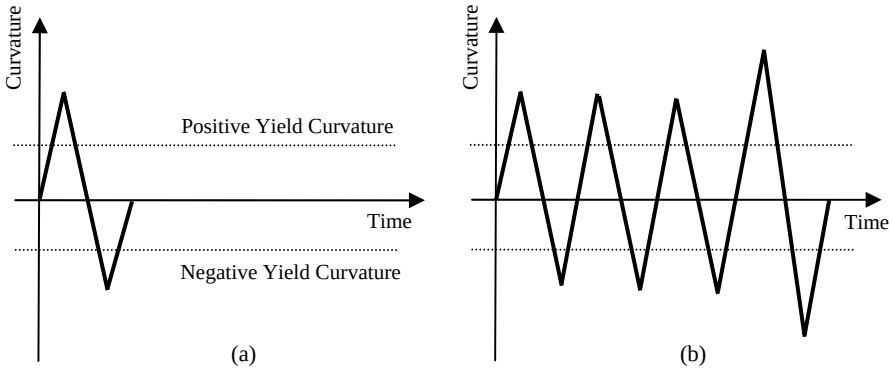

Figure 9-9 Two different inelastic displacement (curvature) histories (Dong 2003)

The degree of seismic damage for the member, the storeys, or the whole structure can thus be predicted or evaluated using damage models. Such models are used in order to either adjust the preliminary structural design under the design level earthquake, make an engineering decision to demolish or repair an existing structure after an extreme or moderate earthquake excitation, or to access the potential damage to a structure in a future earthquake. Damage models for reinforced concrete members are generally divided into five main categories. These categories are maximum ductility, normalised energy (Bracci et al. 1989), ductility and energy (Banon and Veneziano 1982; Park and Ang 1985; Park et al. 1985), a modified version of Miner's Hypothesis (Chung et al. 1987), and a stiffness degraded method (Roufaiel and Meyer 1987). Meanwhile, the global damage index may take three forms, the weighted average of the local member damage indices, the weighted average of all the storey damage indices, and the softening global damage index.

9.4.2 Member, Storey and Structure Ductility

Member ductility can be expressed as a function of either rotation or curvature at the member end. The member curvature ductility is defined as a ratio of maximum curvature to the yield curvature. The yield curvature can be obtained from the static moment-curvature relationship.

$$\mu_{\max} = \frac{\phi_{\max}}{\phi_y} \tag{9-9}$$

where $\mu_{\max}$: maximum member curvature ductility
$\phi_{\max}$: maximum curvature at the member end
ϕ_y : yield curvature

The beam members are carefully designed and detailed according to New Zealand codes and it needs to be able to sustain a curvature ductility of up to 30, which just meets the required member ductility demands. Thus, a beam curvature ductility of 30 is used in this research. For the column members, the ultimate curvature ductility of 20, which was used for the original 12-storey Jury frames (Jury 1978), is used for all the columns in the first storeys of the structure as part of the input data or the member damage indices.

The storey ductility, μ_s, is defined as the ratio of the maximum interstorey drift to the yield interstorey drift which can be determined using a pushover analysis or by the Carr and Tabuchi approach (Carr and Tabuchi 1993):

$$\mu_s = \frac{d_s}{d_{sy}} \tag{9-10}$$

where d_s : maximum interstorey drift
d_{sy} : yield interstorey drift

The structural ductility, μ_t, is defined as the ratio of the maximum top-level displacement to the yield top-level displacement.

$$\mu_t = \frac{d_t}{d_{ty}} \tag{9-11}$$

where d_t : maximum top-level displcement
d_{ty} : top-level displcement at yield

9.4.3 Damage indices

In evaluating seismic damage in a reinforced concrete, ductile framed structure, the damage indices for the structure and storeys are regarded as more rational indicators than the structure and storey ductilities. Although the structural and storey displacement ductilities are strongly related to the overall damage in the structure and storeys, they cannot reflect the contribution of the dissipated energy due to inelastic cyclic behaviour and the stiffness deterioration in members to the overall damage in the structure and in its storeys. There is a linear relationship between the structural damage indices and the structural displacement ductilities (Carr and Tabuchi 1993; Dong 2003). This relationship may alter for long durations of strong shaking due to large number of cycles of inelastic behaviour giving larger accumulated energy dissipation to the structural damage index.

From the inelastic step-by-step integration time history analyses, the member damage indices for every inelastic member end can be obtained. From this data the storey and structural damage indices are calculated as the energy weighted average of all inelastic member ends a storey and in the whole structure respectively.

9.4.3.1 Member Damage Index

The damage index for the member is calculated at each member end. The original equation of Park and Ang's damage index is represented as a linear combination of the maximum deformation and the total dissipated energy caused by repeated cyclic loading (Park and Ang 1985; Park et al. 1985). The index is expressed:

$$DI = \frac{\delta_m}{\delta_u} + \frac{\beta}{Q_y \times \delta_u} \int dE \qquad (9\text{-}12)$$

where δ_m: maximum response deformation under an earthquake
δ_u: ultimate deformation capacity under monotonic loading
Q_y: calculated yield strength
dE: incremental dissipated hysteretic energy
$\int dE$: total dissipated hysteretic energy
β: experimental constant (=0.05 for reinforced concrete members).

The first term in Equation (9-12) represents the damage due to maximum deformation experienced during seismic loading, and the second term reflects the influence of the total absorbed hysteretic energy on the local or member damage.

The constant parameter β=0.05 is found experimentally. According to Park et al., β was determined using a regression equation obtained from experimental results with 400 reinforced concrete columns and beams. The value of β obtained by Park et al. (1985) was 0.05 for reinforced concrete members, and this value is used in this study.

For reinforced concrete structures, an equivalent form of the Park and Ang's damage index is modified to use the member curvature (Charng 1998) that is obtained from the program *Ruaumoko* (Carr 2004). The damage index for the plastic hinge locations at the ends of a member is defined:

$$DI_m = \frac{\phi_m}{\phi_u} + \frac{\beta}{M_y \times \phi_u} \int dE \qquad (9\text{-}13)$$

where ϕ_m: maximum positive or negative curvature
ϕ_u: ultimate curvature capacity under monotonic loading
M_y: calculated yield moment
dE: incremental dissipated hysteretic energy
$\int dE$: total dissipated hysteretic energy
β: experimental constant model parameter (=0.05 in this study).

The member damage index is represented by the index DI_m with $DI_m \geq 1.0$ representing failure of the member. The ultimate curvature ductility of a member under monotonic loading has a strong influence on the member damage index and is

an indicator of the curvature deformation capacity. Hence, it is very important to accurately evaluate the ultimate curvature capacity for the designed member. However, it should be noted that it can be difficult to define the ultimate state of a given member.

The curvature ductility for reinforced concrete members depends strongly on the confinement in the plastic hinge region of the member. The curvature ductility is about four times the deflection ductility (Carr and Tabuchi 1993). Therefore, in this research, the ultimate curvature ductility was assumed to be 30 for all beam members and 20 for column members at 1st floor.

9.4.3.2 Storey and Structural Damage Indices

The damage index for a storey or a whole structure is used to quantify the degree of damage to the storey or to the overall structure. A storey is defined as all the beams at the level under consideration and all the columns just below that level. The damage index for a storey can be obtained by calculating a weighted average of the local damage indices at all the inelastic member ends in this storey. Park and Ang (1985) proposed a damage index for the storeys in which the dissipated energy is used in calculating the weighting factors for every member end.

There are three ways for computing the structural (global) damage index. The first is to calculate a weighted average of the local damage indices at member ends over the whole structure. The second is to calculate a weighted average of the damage indices for all storeys. The last method is by considering some variation in the overall characteristic of the structure, such as the lower modal periods of free-vibration and is called the softening global index.

Damaged structures typically show degradation in stiffness when compared with undamaged structures. This change implies a variation in the natural periods of free vibration in every time step during the earthquake. The history of the degree of damage for the overall structure can thus be expressed by the history of variation in

the stiffness (Mork 1992; Nielsen et al. 1992) or period of free-vibration (DiPasquale and Cakmak 1990) etc. The maximum damage index in this history can then be regarded as the overall damage index.

Park and Ang (1985) proposed a global damage index defined as a weighted average of the local damage indices for all components of a structure. The weighting factor for each end of a member is proportional to the dissipated energy at the corresponding end in the element. The global damage index DI_g is thus defined:

$$DI_g = \sum_{i=1}^{n} (\lambda_i \times DI_i) \tag{9-14}$$

where

$$\lambda_i = \frac{E_i}{\sum_{i=1}^{n} E_i} \tag{9-15}$$

n: number of member ends of whole structure where the local damage index is computed

E_i: dissipated energy at end i of a member

The storey-level damage index is also obtained from Equation (9-12). The only difference is that the number of members is limited to these in the storey under consideration.

According to the damage assessment carried out by Park and Ang (1985) for a prototype structure, the global structural damage index can be interpreted as follows:

$DI_g \leq 0.4$	Repairable damage
$DI_g > 0.4$	Damage beyond repair
$DI_g \geq 1.0$	Total collapse

For context, a global damage index equal to zero denotes that the structure remains in the elastic region during the excitation.

9.4.3.3 Damage Index for Assessment in this Study

The Park & Ang (1985) structural damage index was used in evaluating overall structural damage when the structural displacement ductility is near the design structural ductility. Because the damage indices for the members, storeys and structure is available, and the interpretation of the overall structural damage indices for the degree of damage for this damage model is also available, this damage model is to be recommended for computing the damage indices. Furthermore, it is the only damage index calibrated from laboratory tests (Park and Ang 1985; Park et al. 1985).

Damage analyses were carried out in this research for the prototype structures using the results obtained from nonlinear time history analyses. As the storey damage indices are weighted by the dissipated energy, the damage part in the structure is more sensitive to the storey damage index than the maximum storey ductility factor. The maximum storey ductility factor cannot reflect the member contribution to the whole structure for the seismic resistance capacity. Therefore, the storey damage index is more suitable for the damage evaluation of the structure (Carr and Tabuchi 1993) in this case.

Furthermore, attention is focused on overall structural damage indices because these parameters summarily lump all existing damage in members in a single value that can be easily correlated to single-value seismic parameters. For this purpose, the programme *Ruaumoko* uses a modified damage index. In this slightly modified damage model, the global damage is obtained as a weighted average of the local damage at the ends of each element, with the dissipated energy as the weighting function.

9.5 Performance of 10+2 and 8+4 Storey TMD Building Systems

It is known that the critical effects of secondary moments due to the gravity load upon ductile reinforced concrete frames emerge only when large inelastic deflections occur. To understand the impact of PTMD and SATMD building systems, the seismic

demands for the controlled and uncontrolled systems need to be investigated. After a series of dynamic nonlinear analyses of the structures under the three earthquake suites, a number of response parameters were developed. The maximum relative displacement, the maximum interstorey drift, the storey shear force divided by structure weight, and the total acceleration for all levels of structure are thus evaluated.

In addition, hysteretic energy distributions and storey damage distributions along the height of the structures were developed. Furthermore, these indices are summed (hysteretic energy distributions) and averaged (storey damage distributions) to the structural energy and structural damage indices respectively as representative performance parameters. Again, the response performance of 10+2 and 8+4 storey PTMD and SATMD building systems are compared, and the SA50TMD cases are used for the SATMD systems, based on the results of Chapter 5.

The performance results of 12+2 and 12+2 storey nonlinear TMD building systems have been presented in APPENDIX C.

9.5.1 Maximum Displacement

The maximum displacement at a floor has been commonly used in inelastic analysis since this response quantity is directly related to the structural stiffness. Figures 9-10, 9-18 and 9-26 show the envelopes of the maximum displacement in the No TMD, PTMD, and SATMD systems.

As expected, the isolation layer produces large relative displacement between adjacent storeys and this storey separation is increased for the SATMD system due to the absence of viscous damping. From Figure 9-10, it can be seen that the floor responses below the isolation interface are reduced more than that for the uncontrolled (No TMD) system. However, the reduction quantities are not so different for the TMD cases developed and the SATMD (8+4) system produced the larger 84^{th} percentile of the displacement responses. The envelopes in the TMD building systems under the medium and high suites (especially under the medium suite) show the clear reduction

of displacement responses and this control effectiveness is pronounced for the SATMD and '8+4' storey systems, as shown in Figures 9-18 and 9-26. Referring to the maximum displacements observed, it is worth noting that all suites of motion show reasonably controlled response values compared to the uncontrolled responses.

9.5.2 Interstorey Drift Ratio

The intertorey drift ratio (the interstorey drift normalised by the storey height) has been developed as a response parameter that characterises the architectural damage. This value relates well with observed architectural damage after severe earthquakes. A wide consensus exists in the earthquake engineering community that for moment resisting frames the interstorey drift demand is the best indicator of expected damage. As a global parameter, interstorey drift is much more appropriate than the roof drift because in individual storeys it may exceed the latter by a factor of two or more (Gupta and Krawinkler 2000; Krawinkler and Gupta 1998). Figures 9-11, 9-19 and 9-27 show the maximum interstorey drift ratios resulting from the analyses.

For the low suite, the 50^{th} percentile drifts of No TMD system are reasonably uniform over the height of the structure and the peak drift occurs in the 9^{th} storey. However, the TMD systems reduced the response of the isolated upper storeys, as well as the lower storeys. The location of the 84^{th} percentile of the peak drift has migrated to the 3^{rd} storey for the '8+4' structures and to the 7^{th} or 8^{th} storey for the '10+2' structures, as seen in Figure 9-11.

Meanwhile, a different behaviour is presented in the controlled structures, where the lines for the different TMD systems cross one another in 4^{th} floor. Figure 9-11 clearly reflects the systematic advantage of the SATMD systems. Though increasing the level of seismic hazard increases the interstorey drift, the increased ratios of the drift in the isolated upper storeys are still small and again the peak drift locations are shifted to the lower storeys, as seen in Figures 9-19 and 9-27. For the low and medium sets of motion, all the drift demands of the TMD systems are less than the life

safety limit of 2.5% for the numerical time history analysis specified in NZS4203 (1992).

9.5.3 Storey Shear Force

To ensure that shear will not inhibit the desired ductile behaviour of the systems and that shear effects will not significantly reduce energy dissipation during hysteretic response, it must not be allowed to control strength. Therefore, an estimate must be made for the maximum shear force that might need to be sustained by the system during extreme seismic response. The goal is to ensure that energy dissipation can be confined primarily to yielding.

The normalized shear forces are not so different between the uncontrolled and both TMD systems under the three sets of ground motions. The values of the shear forces are decreased constantly along the height of the structure regardless of increasing the hazard level. However, increasing the hazard level has minor impact on the improving the control effectiveness of the TMD systems. As a result of the nonlinearity of the structures, the shear force results under PTMD and SATMD control are very different to those for linear structures, as might be expected.

9.5.4 Total Acceleration

Acceleration demands are of concern for the nonstructural components of the building. In general, added seismic control systems have the benefit of being capable reducing the acceleration demands on the structure, while also reducing drift demands. More traditional methods, such as increasing the building stiffness, cannot achieve this behaviour motivating these more enhanced control approaches.

From Figures 9-13, 9-21 and 9-29, it can be seen that the accelerations at the isolated upper floors are clearly reduced. In contrast, the accelerations at the isolation layer show an abrupt increase. These performance properties are similar to those observed

in terms of the displacement response. To achieve the reductions in drift desired, the TMD system sacrifices floor accelerations at the isolation layer.

Under the low suite of ground motions, shown in Figure 9-13, the PTMD(10+2 and 8+4) and SATMD(10+2 and 8+4) systems produce 50th percentile floor accelerations similar to the uncontrolled (No TMD) system at the lower floors. The accelerations for the SATMD(10+2 and 8+4) systems are slightly higher than those of the uncontrolled system. However, only the SATMD(8+4) system slightly increases the 50th percentile floor accelerations at the lower floors under the medium suite of motions, as shown in Figure 9-21. For the high suite of ground motions, it is difficult to find the virtual control effectiveness of the acceleration responses at the lower floors under the isolation layer. Meanwhile, the PTMD(10+2 and 8+4) systems reduce the floor accelerations of the upper floors below those of the SATMD systems under the medium suite of ground motions, as shown in Figure 9-21 and a similar pattern is observed in the high suite of ground motions, as seen in Figure 9-29.

9.5.5 Storey and Structural Hysteretic Energy

While peak interstorey drift provides a good indication of performance, the resulting information is incomplete as it does not take into account the cumulative damage to the structure. Experimental investigations have demonstrated that structural damage is a function of both peak as well as cumulative values. As hysteretic energy provides a good indication of cumulative damage in structures, median and 84th percentile values of hysteretic energy are compared for the TMD systems for each set of ground motions.

The hysteretic energy dissipated by the frame members at each floor along the height of the structures are developed in Figures 9-14, 9-22 and 9-30. As expected from increasing storey drift demands, as the severity of ground motions increases, the amount of hysteretic energy dissipated by the structure members increases. The comparison of these figures shows that the higher level of hazard produces high

energy demands in the lower storeys and the energy distribution patterns correspond to the drift demands of the structure.

In particular, clearly lower energy demands at upper storeys which are above the isolation layer can be found due to its interception of the energy flow up from the base. This structural property produces the reduced energy demands of the lower stories too. In other words, the amount of transferred energies from the base was decreased by splitting the lump of overall structural mass and, therefore, the dissipated energy along the height is reduced. In the low suite of motions, the energy curves of the isolated upper structures lie along the y-axis, as they are successful in isolating and maintaining the upper structure within the limits of elastic behaviour as seen in Figure 9-14. In the medium and high suites of motions, the TMD systems are still successful at keeping the response essentially linear, as indicated by very low values of hysteretic energy indices as shown in Figures 9-22 and 9-30.

Finally, as a representative energy value, all of the dissipated energy values along the height are summed to establish a total structural hysteretic dissipated energy index, as seen in Figures 9-15, 9-23 and 9-31. Again, the control effects are shown to become significant for the larger mass ratio (8+4) and the SATMD system, and the control effectiveness difference is pronounced from the PTMD(10+2) to the SATMD(8+4) systems. This result shows that the combined operation of the semi-active device and large TMD mass contributes greatly to the effectiveness of the overall TMD control system compared to typical and optimal passive design. Overall, all the TMD systems were successful in reducing the seismic hysteretic energy demands at all hazard levels.

9.5.6 Storey and Structural Damage

The distribution of storey damage indices are shown in Figures 9-16, 9-24 and 9-32. Storey damage indices are based on the member damage indices in a level. It can be said that the distribution of storey damage has a similar pattern to that of storey dissipated energy, which is used as a weighting factor for the calculation of the

damage index. The only difference between these two indices is from the part of structural deformation.

From the figures it can be seen that all of the TMD systems suffer insignificant repairable storey damage up to the 50th percentile of the medium suite. Only the 1st level of the TMD systems suffers significant damage for the 84th percentile of the high suite, which gives damage indices over 1.0. The figures also show that the damage indices of the upper isolated storeys for every suite are less than 0.4 at each level, which indicates again the effective interception of energy flow at the isolation layer. Overall, it seems that the main benefits of the reduced damage demands are on the upper storeys for each suite, rather than for the lower storeys.

The structural damage indices, which indicate the damage of the whole structure, are summarised in Figures 9-17, 9-25 and 9-33. The structural damage indices are obtained as a weighted average of the local damage at the ends of each element, with the dissipated energy as the weighting function. The structural damage indices for all suites are less than 0.4 except for the 84th percentile of the high suite. Hence, all of the TMD systems are repairable for those suites. Even for the 84th percentile of the high suite, the structural damage indices are under 1.0, which indicates that the structures can survive with damage beyond repair under the high suite. The SATMD(8+4) system proves to be more effective than any other type of TMD system in terms of structural damage indices and this effectiveness becomes more pronounced for the lower hazard suites.

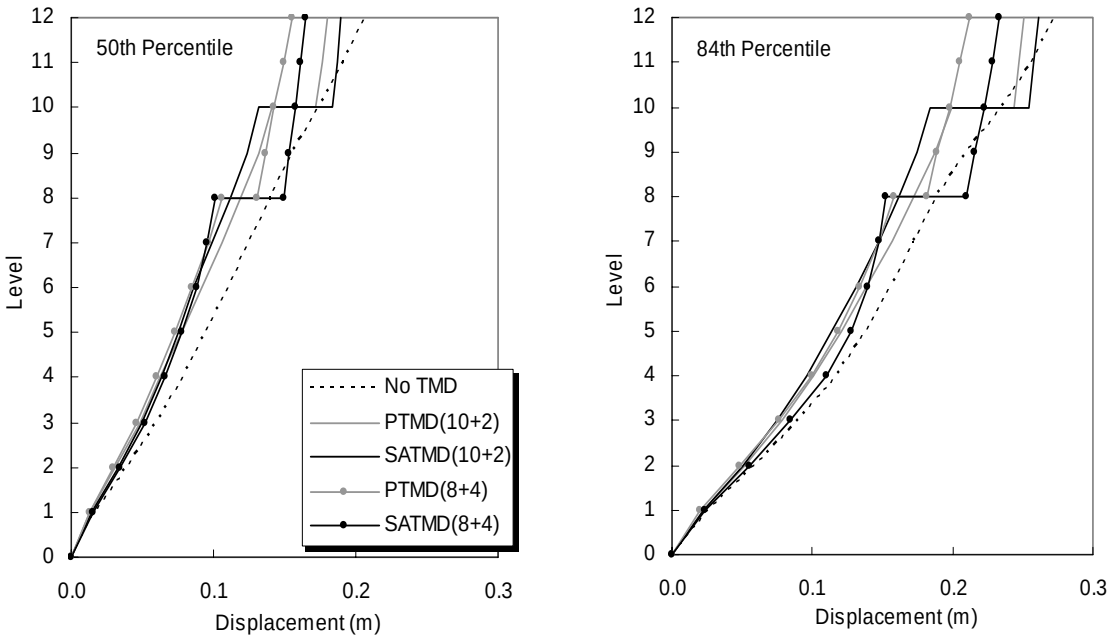

Figure 9-10 Maximum displacement of '10+2' and '8+4' models (Nonlinear / Low suite)

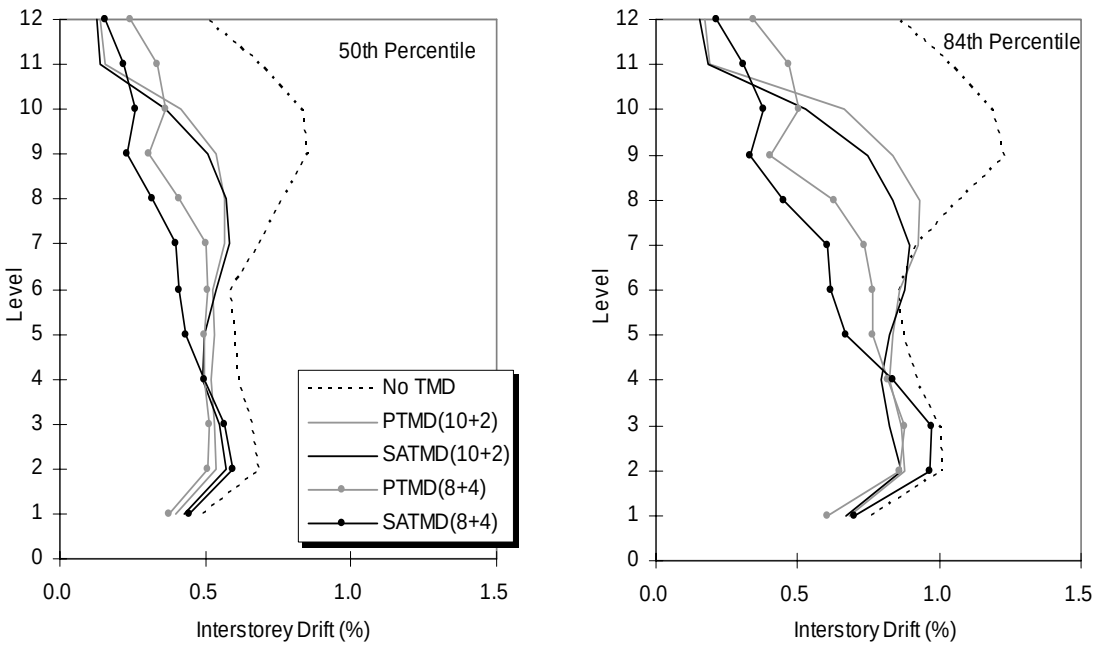

Figure 9-11 Interstorey drift of '10+2' and '8+4' models (Nonlinear / Low suite)

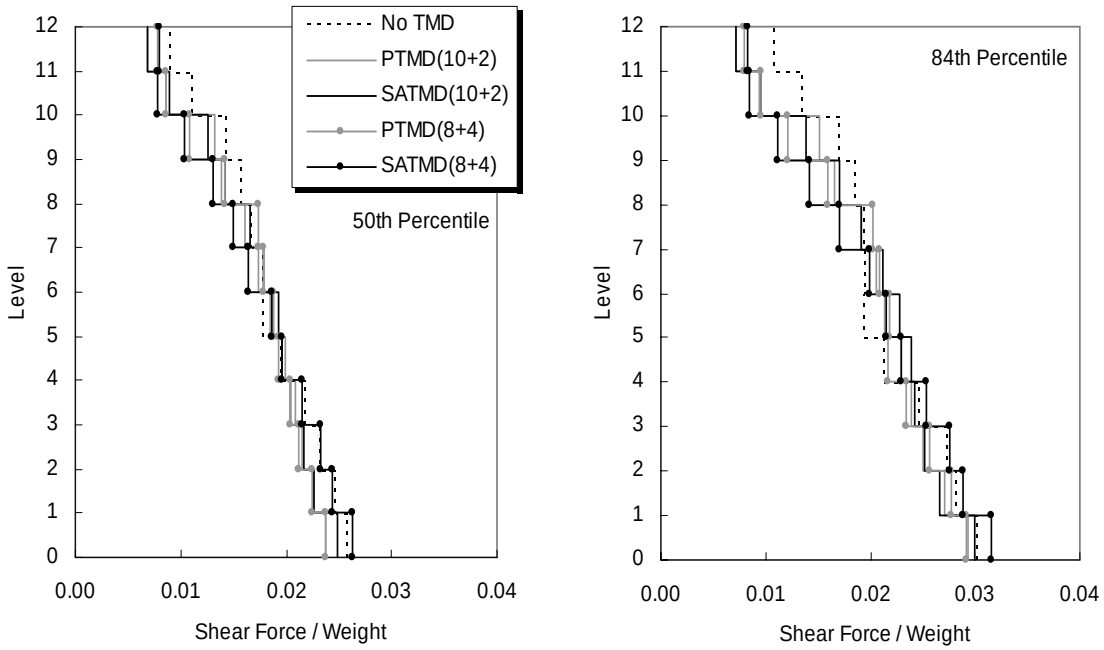

Figure 9-12 Storey shear force of '10+2' and '8+4' models (Nonlinear / Low suite)

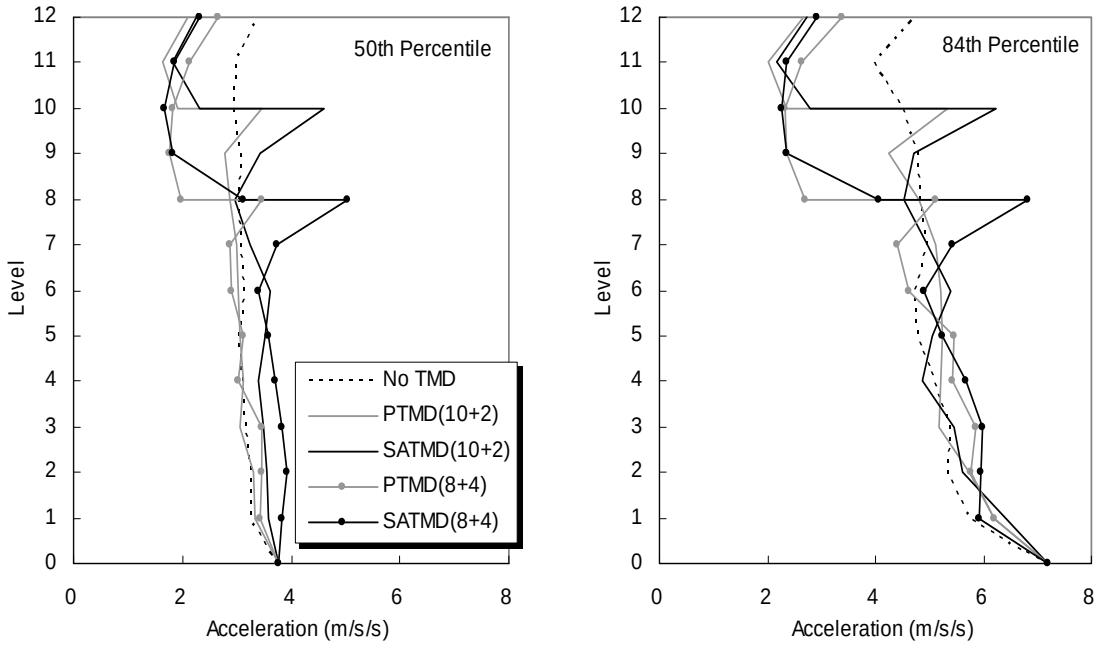

Figure 9-13 Total acceleration of '10+2' and '8+4' models (Nonlinear / Low suite)

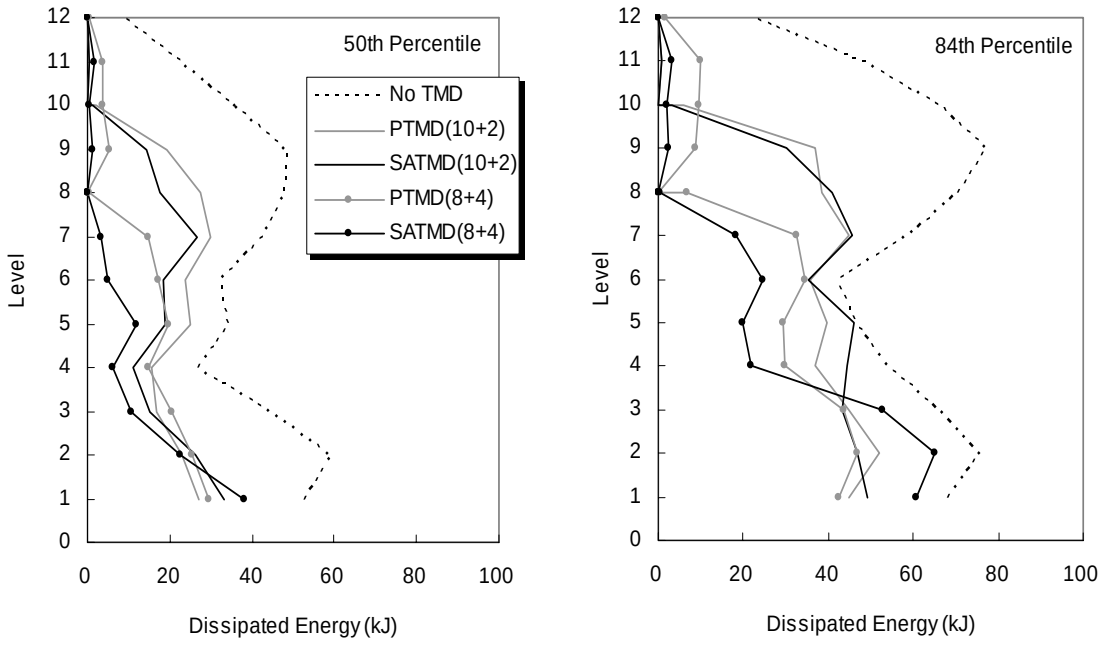

Figure 9-14 Storey dissipated energy of '10+2' and '8+4' models (Nonlinear / Low suite)

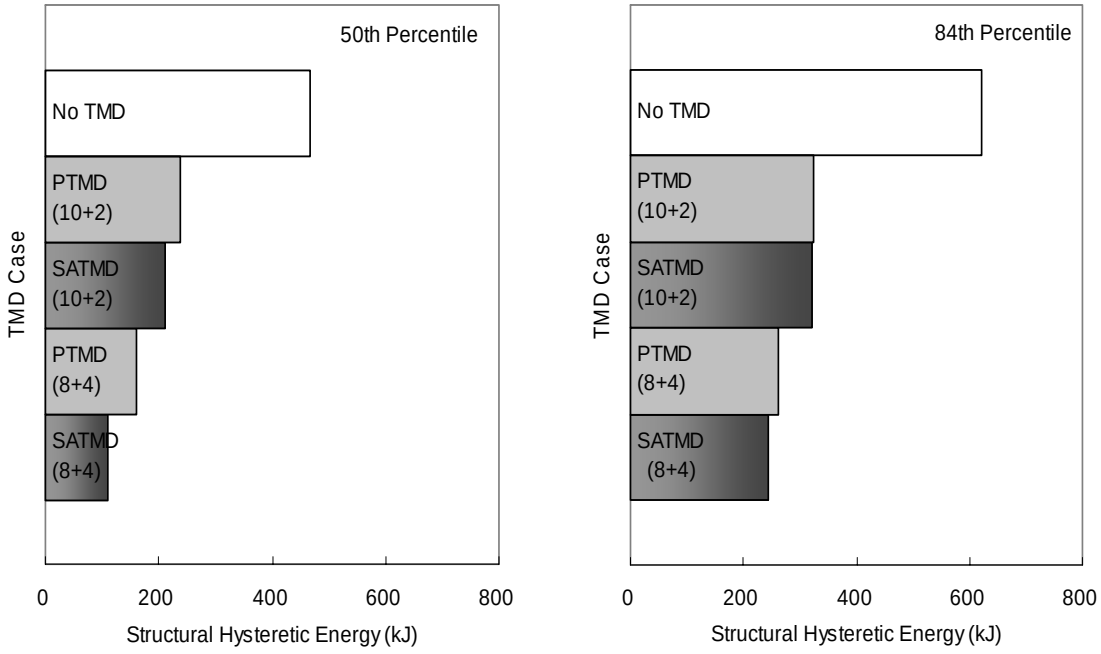

Figure 9-15 Structural hysteritic energy of '10+2' and '8+4' models (Nonlinear / Low suite)

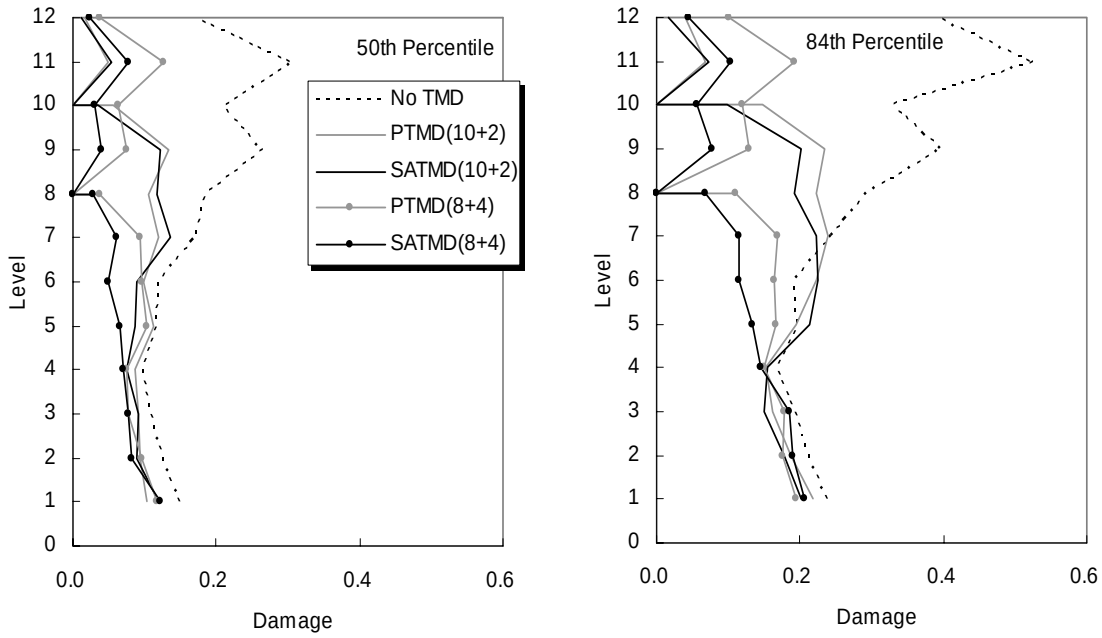

Figure 9-16 Storey damage index of '10+2' and '8+4' models (Nonlinear / Low suite)

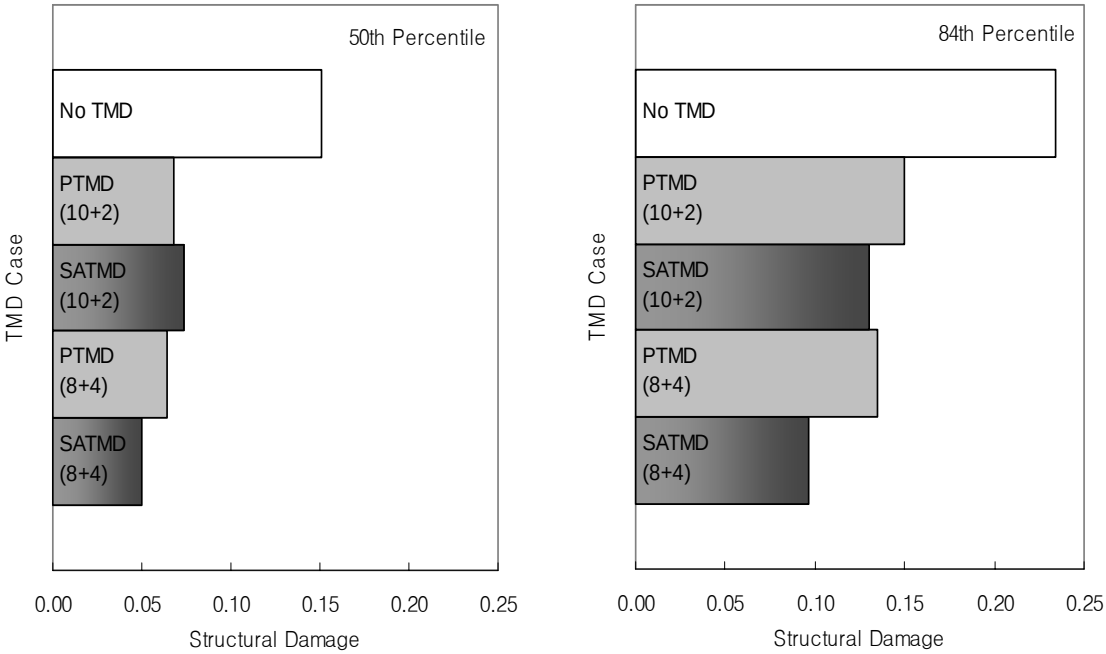

Figure 9-17 Structural damage index of '10+2' and '8+4' models (Nonlinear / Low suite)

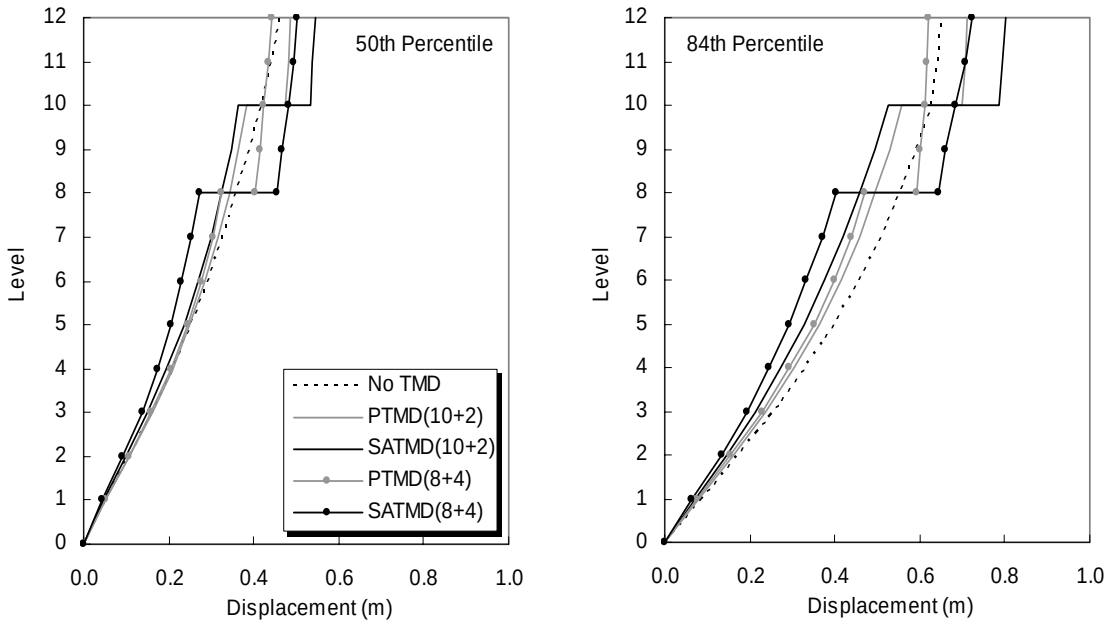

Figure 9-18 Maximum displacement of '10+2' and '8+4' models (Nonlinear / Medium suite)

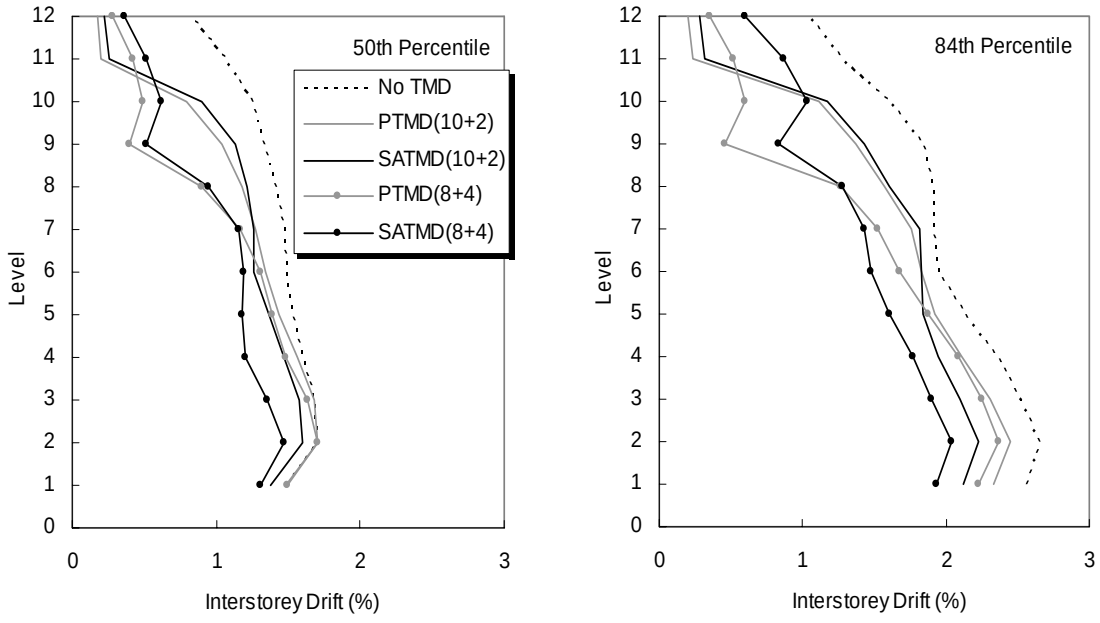

Figure 9-19 Interstorey drift of '10+2' and '8+4' models (Nonlinear / Medium suite)

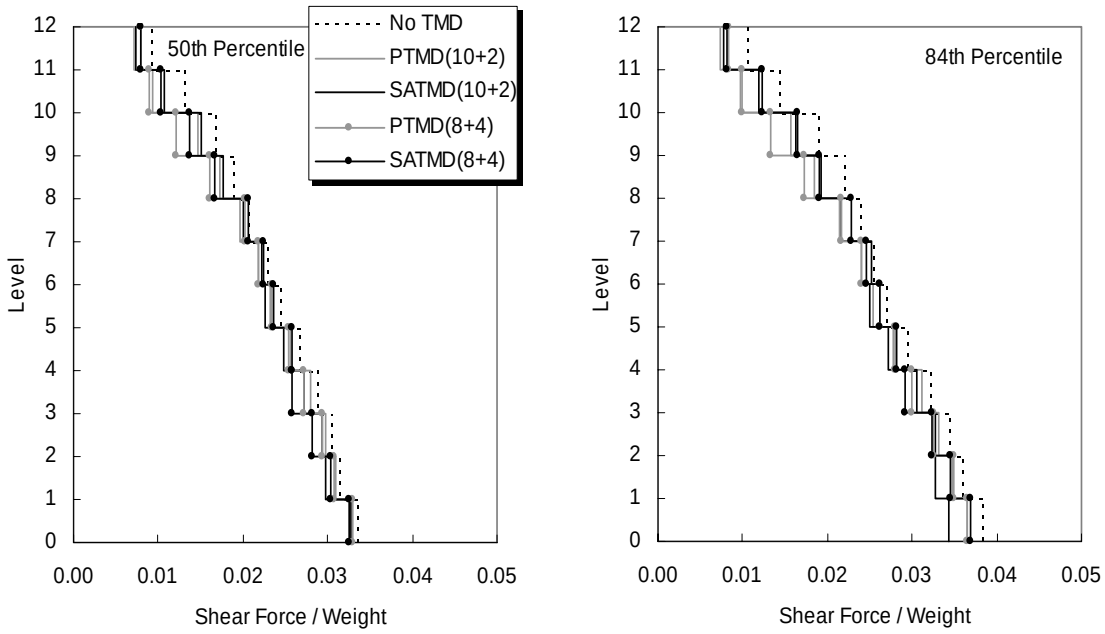

Figure 9-20 Storey shear force of '10+2' and '8+4' models (Nonlinear / Medium suite)

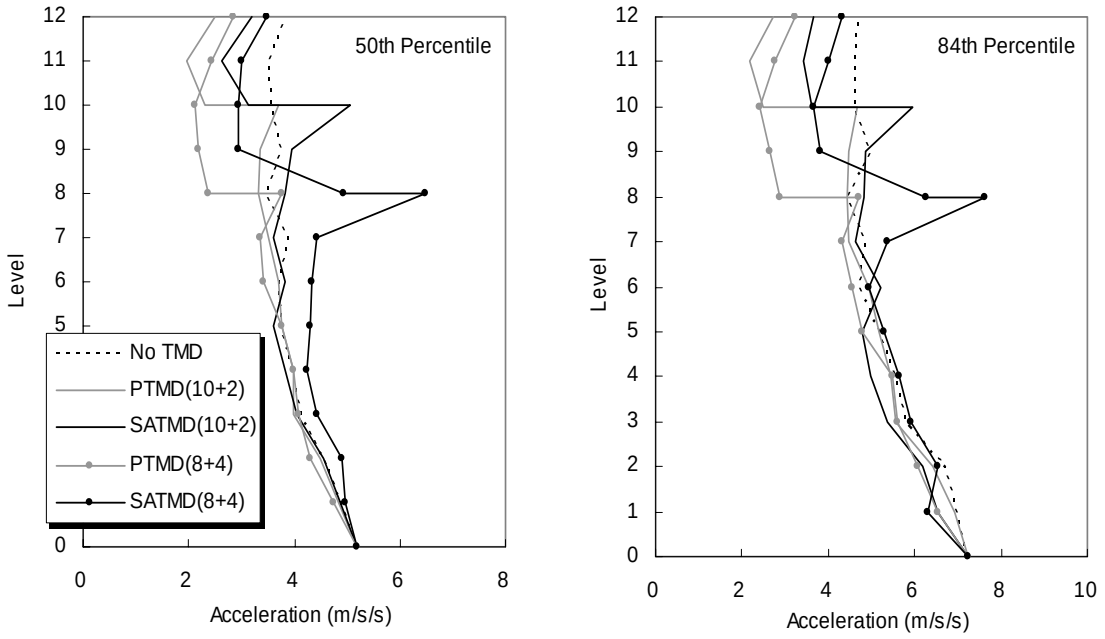

Figure 9-21 Total acceleration of '10+2' and '8+4' models (Nonlinear / Medium suite)

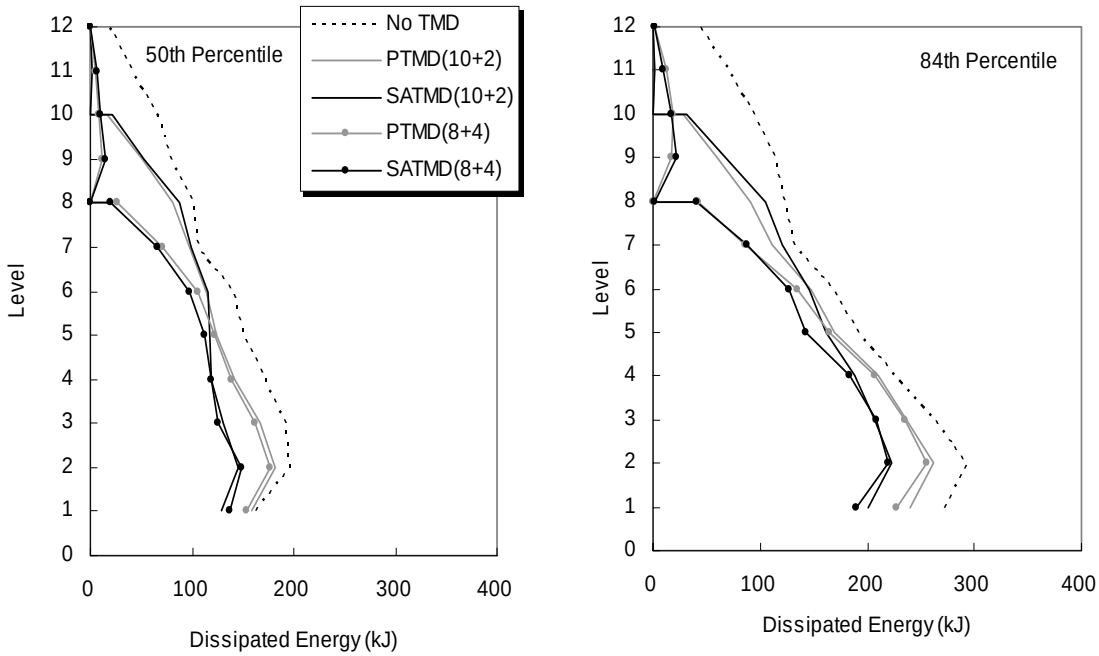

Figure 9-22 Storey dissipated energy of '10+2' and '8+4' models (Nonlinear / Medium suite)

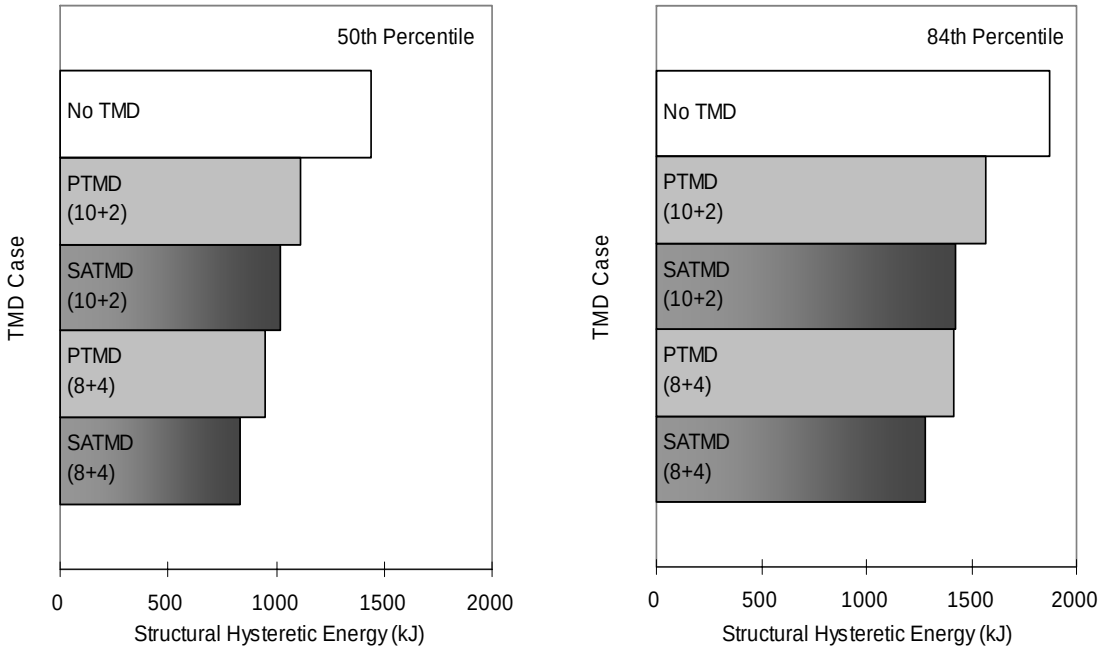

Figure 9-23 Structural hysteritic energy of '10+2' and '8+4' models (Nonlinear / Medium suite)

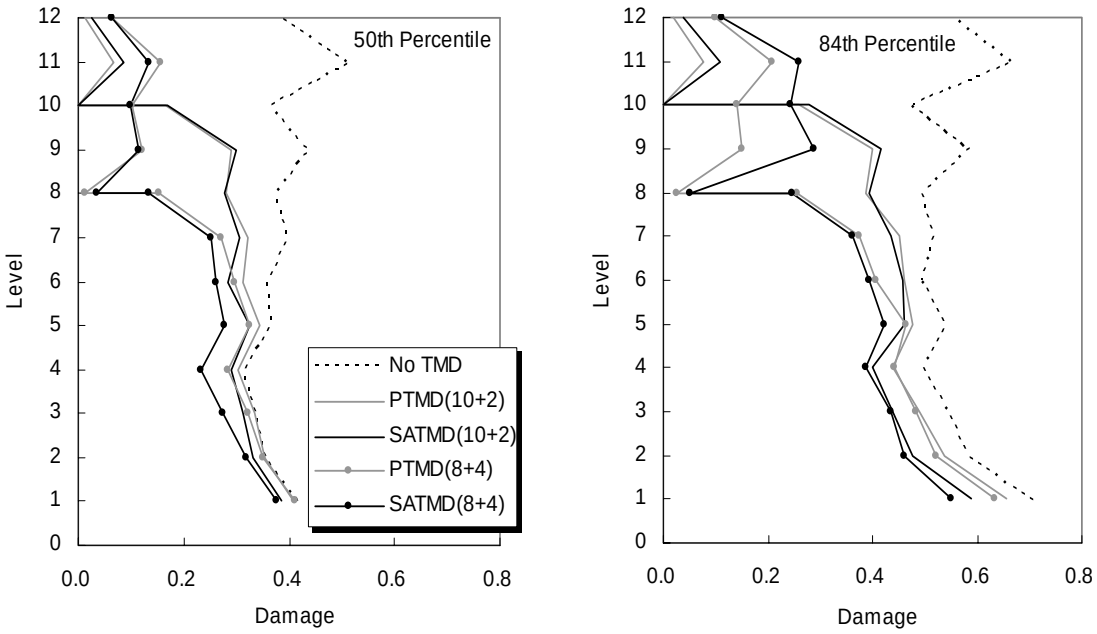

Figure 9-24 Storey damage index of '10+2' and '8+4' models (Nonlinear / Medium suite)

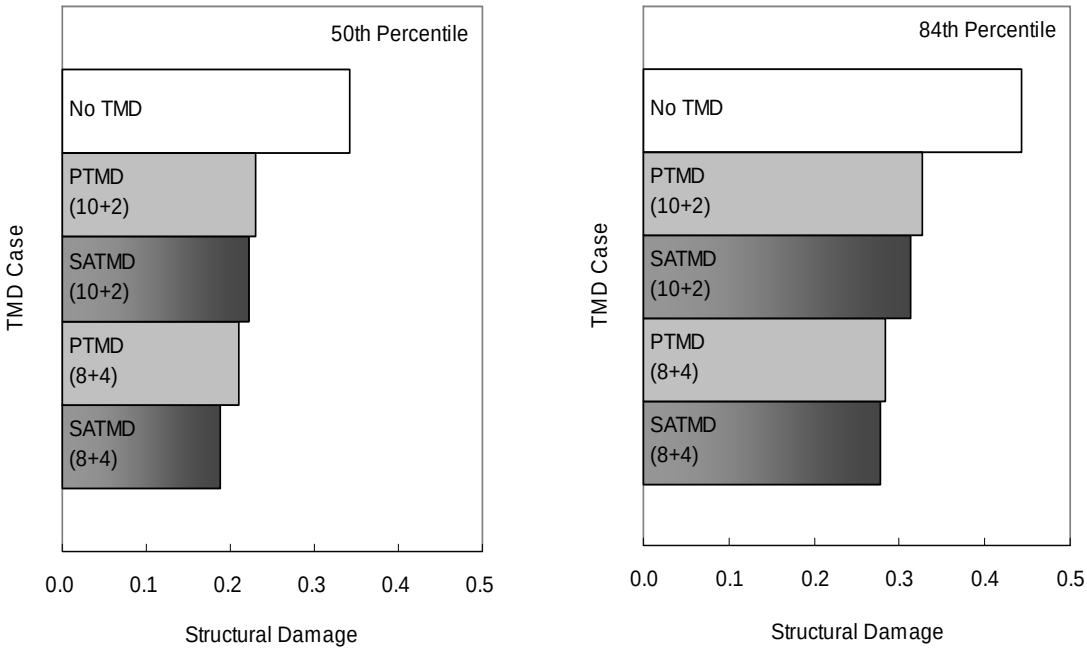

Figure 9-25 Structural damage index of '10+2' and '8+4' models (Nonlinear / Medium suite)

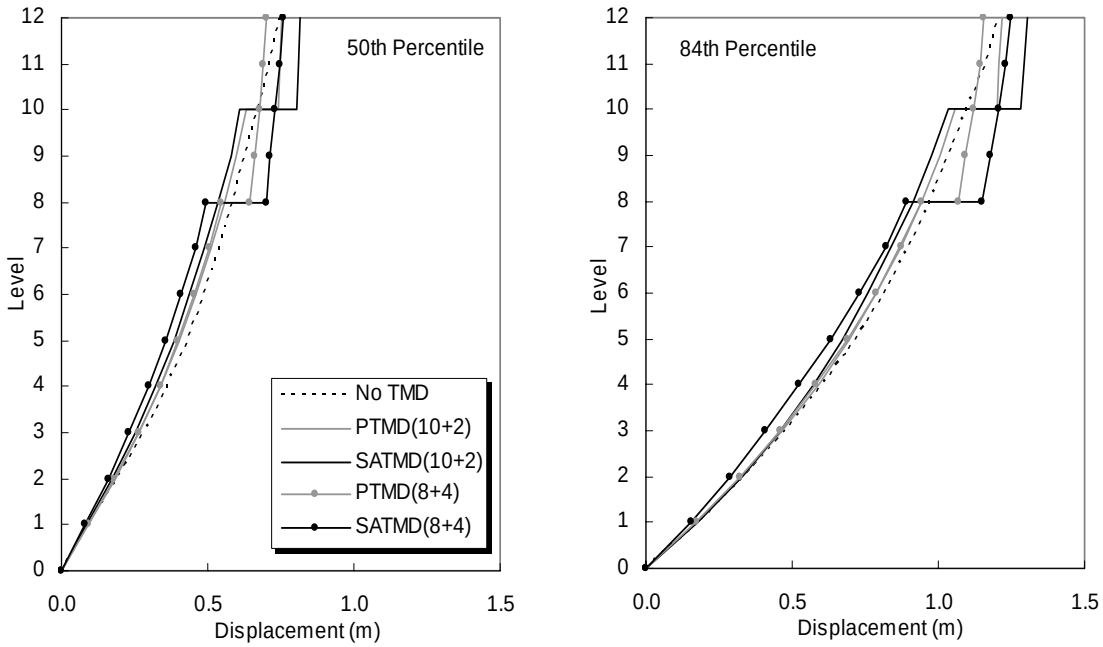

Figure 9-26 Maximum displacement of '10+2' and '8+4' models (Nonlinear / High suite)

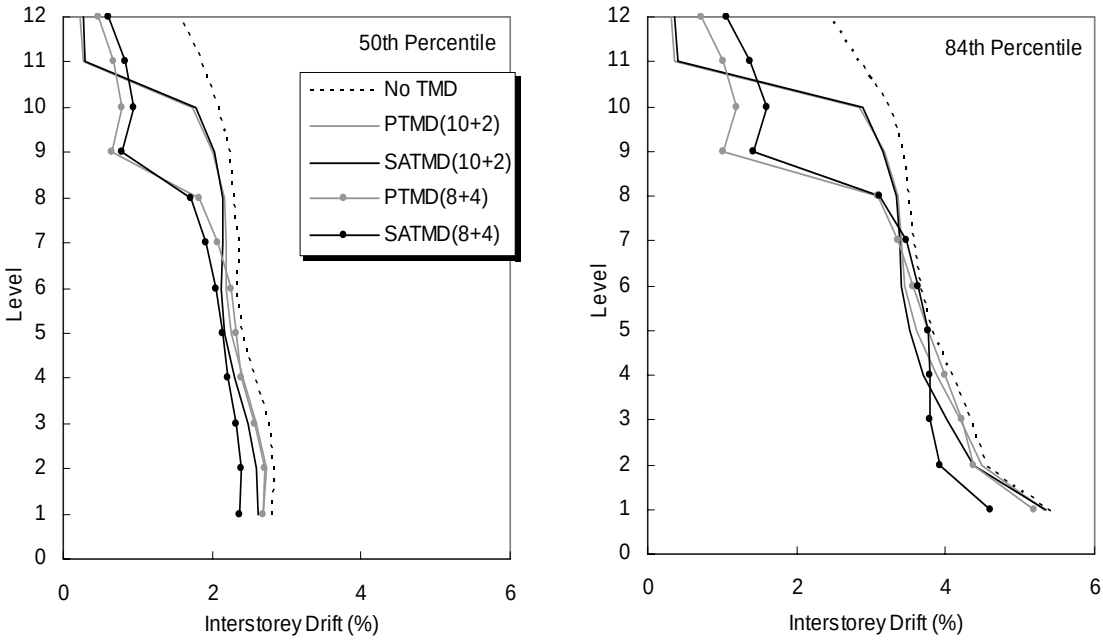

Figure 9-27 Interstorey drift of '10+2' and '8+4' models (Nonlinear / High suite)

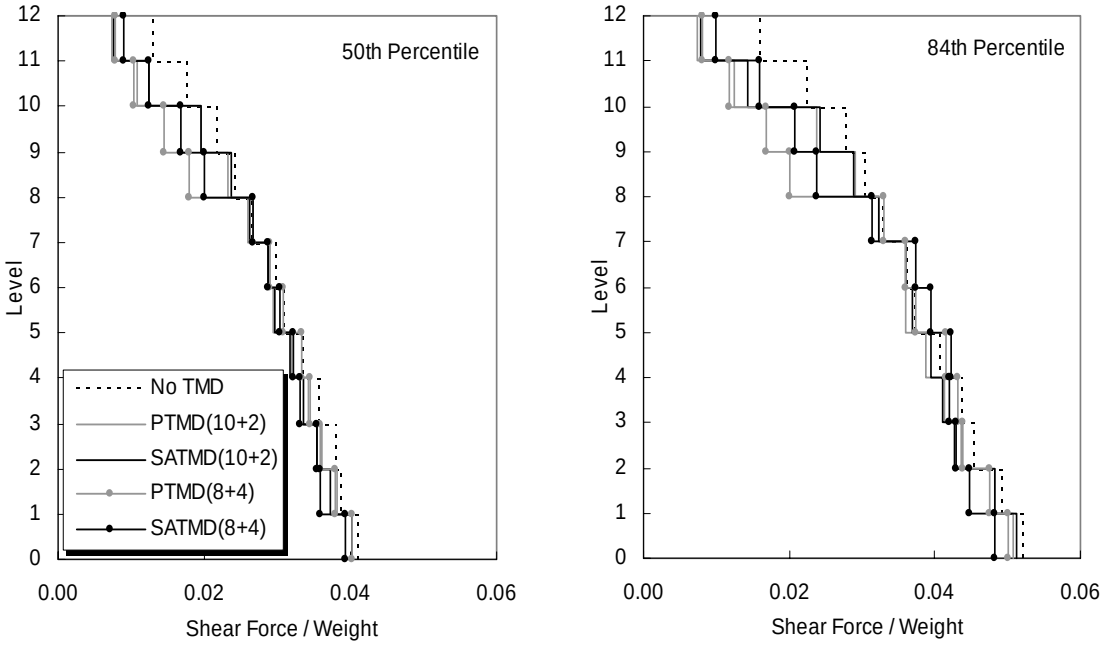

Figure 9-28 Storey shear force of '10+2' and '8+4' models (Nonlinear / High suite)

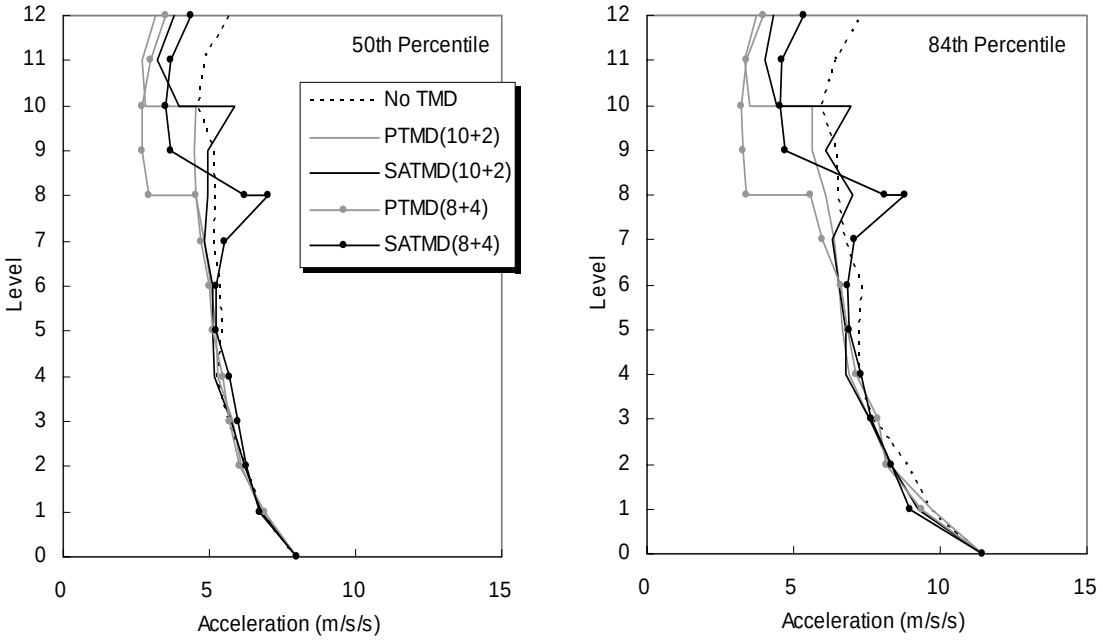

Figure 9-29 Total acceleration of '10+2' and '8+4' models (Nonlinear / High suite)

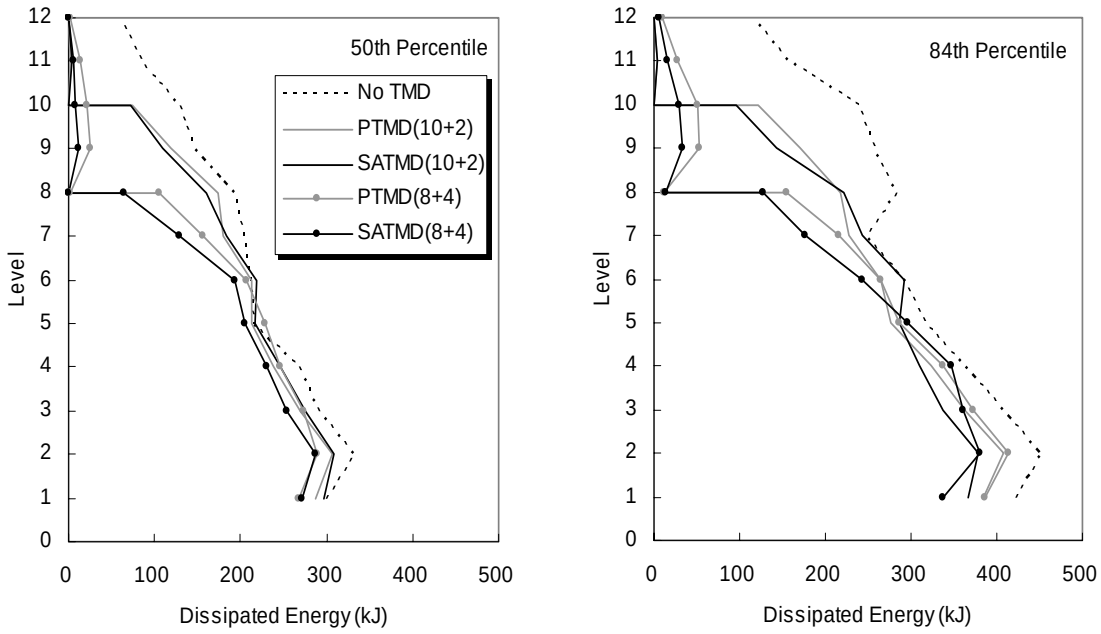

Figure 9-30 Storey dissipated energy of '10+2' and '8+4' models (Nonlinear / High suite)

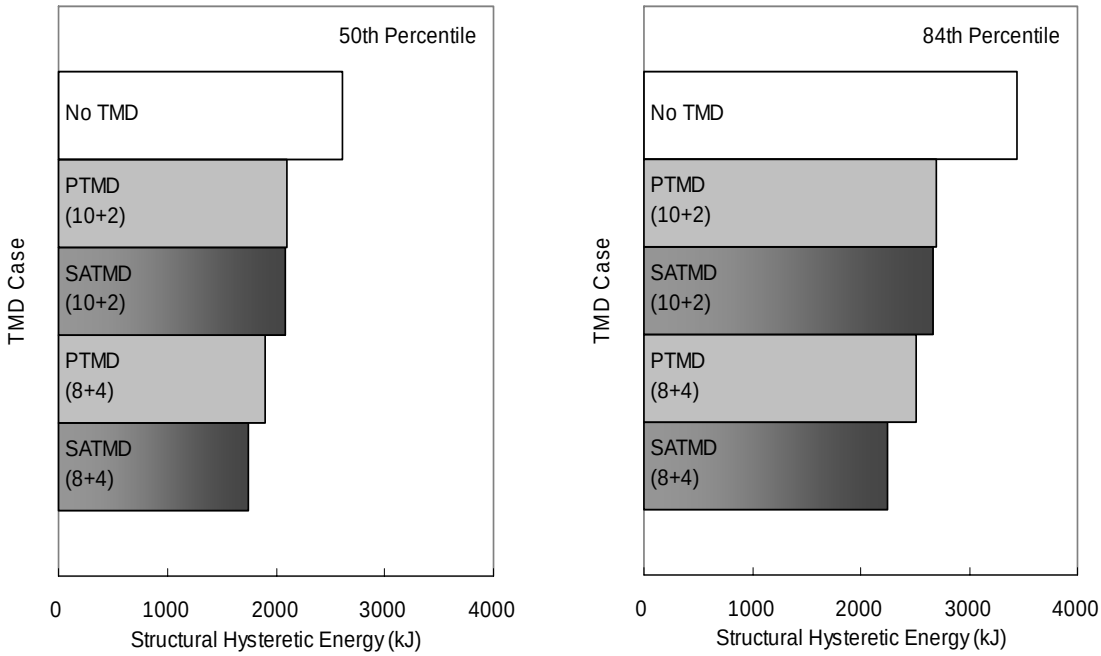

Figure 9-31 Structural hysteritic energy of '10+2' and '8+4' models (Nonlinear / High suite)

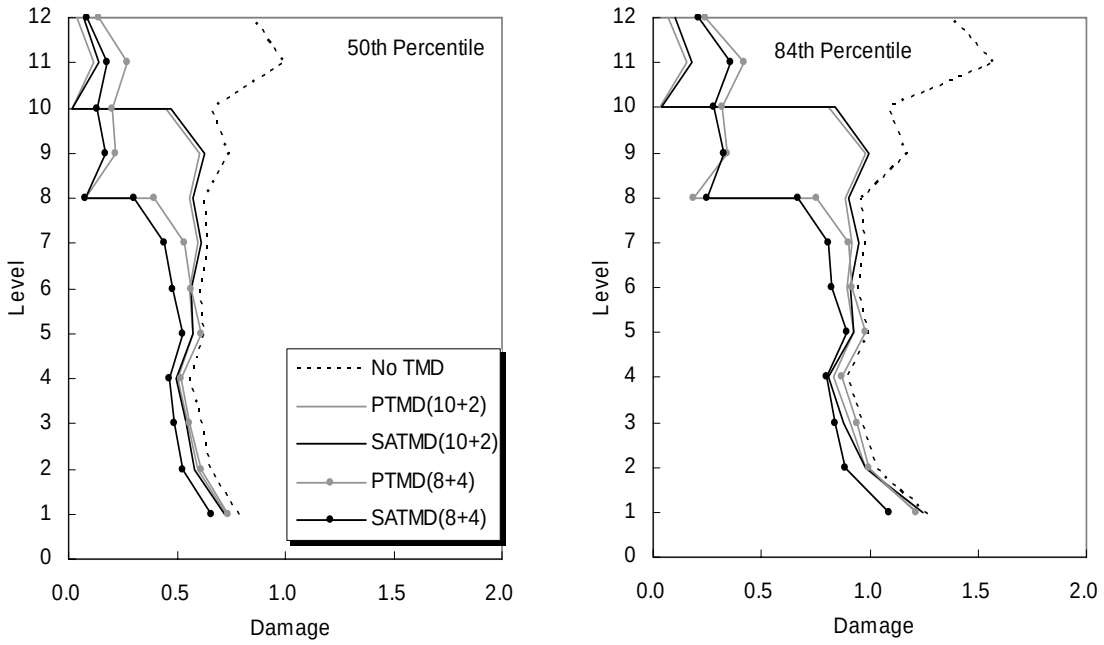

Figure 9-32 Storey damage index of '10+2' and '8+4' models (Nonlinear / High suite)

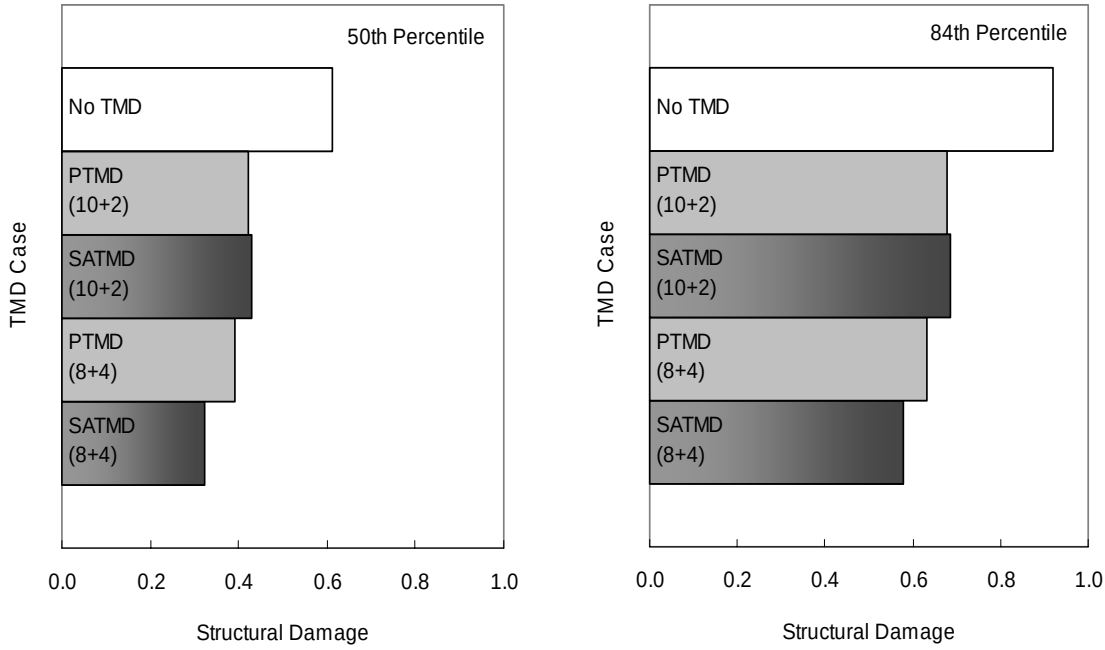

Figure 9-33 Structural damage index of '10+2' and '8+4' models (Nonlinear / High suite)

9.6 Summary

As a better approximation of realistic structures, this chapter compares the performance of five different nonlinear TMD building systems (No TMD, PTMD (10+2 and 8+4) and SATMD (10+2 and 8+4)) over three probabilistically scaled suites of earthquake records. The seismic demands were based on several assumptions concerning structural parameters and modelling, including P-delta effects, modified Takeda hysteresis, and several others.

Performance comparisons were based on statistically calculated maximum displacement, interstorey drift ratio, storey shear force, total acceleration, storey/structural hysteretic energy and storey/structural damage demands. Peak responses alone do not describe the possible damage incurred by the structure as cumulative damage can often result from several smaller cycles into or near the inelastic range. Thus, more accurate evaluations involved consideration of the dissipated hysteretic energy. Particularly, in contrast to the previous linear analyses of Chapters 7 and 8, hysteretic dissipated energy and practical damage assessments were developed to provide information regarding the cumulative damage to the structure, which may be more important in evaluating potential damage and degradation.

Finally, in this chapter, realistic and inelastic response effectiveness of PTMD and SATMD systems were presented as comprehensive results of suggested novel building systems over a range of seismic hazards. TMD building systems were successful in reducing the seismic demands in statistical point of view for both new designs (10+2 and 8+4) and retrofitted systems (12+2 and 12+4). Overall, the SATMD system provided more robust response mitigation over a range of ground motions within each suite. Thus, it might be concluded, as in chapter 5, that the SATMD is the better choice for the seismic case where future input motions are unknown.

10 Conclusions and Future Works

10.1 Conclusions

10.1.1 TMD Building Systems

Passive and Semi-Active Tuned Mass Damper (SATMD) building systems are proposed to mitigate structural response due to seismic loads. As an alternative approach, a structure's upper portion itself plays the role of the tuned mass saving excessive non-functional added weight. This configuration supplies reaction forces to the main structure, generated by the relative motion between the structure and the segregated upper portion. A viscous damper of some form is typically used and assumed for the Passive TMD (PTMD) systems examined in this thesis. Further, it was proposed to replace the passive spring damper with semi-active resetable devices, creating more adoptive resetable device based SATMD systems. This semi-active system use of feedback control to alter or manipulate the reaction forces, effectively retunes the system depending on the (often nonlinear) structural response. The semi-active system therefore offers a broader more adaptable solution than passive tuning. Overall, this proposal combines emerging semi-active devices with existing concepts of tuned mass dampers and base isolation to create extended applications for seismic response mitigation.

10.1.2 Semi-Active Resetable Device

A specific prototype resetable device design was introduced and detailed. Semi-active resetable devices, as described, are relatively simple and thus reliable devices, which can act autonomously. Described fundamentally as a non-linear pneumatic or hydraulic spring element, the equilibrium position or rest length can be reset to obtain maximum energy dissipation from the structural system. They thus offer a unique highly controllable energy dissipating solution and the ability to sculpt hysteretic

behaviour with the novel independent chamber controlled device presented and used in this study.

10.1.3 2-DOF Spectral Analysis of SATMD and PTMD Building Systems

Two-degree-of-freedom (2-DOF) analytical studies are employed to design the prototype structural system, specify its element characteristics and determine its effectiveness for seismic response mitigation, including defining the resetable device dynamics. For the PTMD system, realistic 15% and much higher optimal TMD damping ratios are compared. For the SATMD system the stiffness of the resetable device design is combined with and without rubber bearing stiffness. From the parametric results, the most effective SATMD system is derived and then adopted as a practical control scheme. Log-normal statistical spectrum results, using three suites of probabilistically scaled earthquake records from the SAC phase II project, are presented to compare the SATMD scheme to an uncontrolled (No TMD) and an ideal, optimal passive tuned mass damper (PTMD) building system.

Both TMD systems (PTMD and SATMD) were successful in reducing the seismic demands. The response results of the time history spectrum analysis and those normalised reduction factor results showed the response reductions for all seismic hazards. The SATMD system provided a better, more robust overall control strategy than PTMD systems, especially if the optimum stiffness of TMD is not ideal or perfectly tuned. Note that, more optimal SATMD parameter combinations may be available, but one beyond the scope of this initial spectral parametric analysis.

Semi-active solutions are also not constrained by the optimum tuning stiffness for the TMD like the passive case. In fact, their control ability is improved when a stiffness lower than the optimal value is used, providing a more robust and effective seismic energy management. Thus, the SATMD system is easier to design as no tuning is required. In contrast, slight “out-of-tuning” in the passive PTMD case can have a significant detrimental effect on the controlled response.

Overall, there is thus good potential for SATMD building concepts, especially in retrofit where lack of space constrains development to expand upward. The results from this design analysis research have then been utilised to assess the linear and non-linear seismic response of realistic multi-degree-of-freedom (MDOF) structures. Hence, this first analysis provides the fundamental design guidelines to be verified in realistic structural case study analyses.

10.1.4 MODF Analysis of SATMD and PTMD Building Systems

The seismic performances of multi-storey passive and semi-active tuned mass damper (PTMD and SATMD) linear and nonlinear building systems have been investigated for 12-storey two-bay reinforced concrete moment resisting framed structures modelled as '10+2' storey and '8+4' storey in *Ruaumoko*. Segmented upper stories (2 and 4) of the structure are isolated as a tuned mass, and passive viscous dampers or semi-active resetable devices are adopted for energy dissipation. Optimum TMD control parameters and appropriate matching SATMD configurations are adopted from previously analysed design results from the simplified 2-DOF system. Thus, large SATMD systems can effectively manage seismic response for MDOF systems across a broad range of ground motions in comparison to passive solutions.

Modal analysis showed that both types of TMD building systems utilise unique modal features to isolate the superstructure to be controlled effectively. In particular, the semi-active resetable devices of the SATMD systems provide a more advanced control function by anticipating the motion of the isolation layer. The time history analysis and normalised reduction factor results showed that both TMD building systems present significant reductions in all of the control indices considered for all seismic hazards. However, the cost included is an increase in the accelerations at the isolation interface, which may or may not necessarily be detrimental. Nonlinear modelling of the MDOF structures results in more realistic structural response. The difference in response between the No TMD, PTMD and SATMD is not as pronounced as it was for the linear structures. However, the fundamental changes in structural period and control action are still evident for both TMD systems.

From the results of additional 12+2 and 12+4 storey retrofit case studies, SATMD systems show significant promise for application of structural control where extra storeys might be added. They offer unique advantages over PTMD systems in obtaining consistent response reductions over broad ranges and types of ground motions at realistic seismically important structural natural frequencies. They are thus more robust to ground motion variation, as they provide tighter ranges across each suite.

10.1.5 Concluding Remarks

Structural control provides an extra mechanism to improve seismic structural performance. For maximum effectiveness, minimal control effort is required to achieve the desired performance goals. Based on this point of view, this research has demonstrated the validity of the realistic PTMD and SATMD building systems for consideration in future design and construction.

The details and results of a set of comparative studies are used to assess the feasibility and effectiveness of such isolation systems. From the results of this comparative study, it is found that the proposed scheme may significantly reduce the seismic response of a structure, even if the structure is nonlinear. In view of these findings, and the fact that they might be relatively easy to construct using these emerging SA devices, it is concluded that the proposed SATMD building system has the potential to become a practical and effective way to reduce earthquake damage. Thus, these systems merit further studies to examine their advantages and to further develop experimental validation and design solutions, leading eventually to practical initial designs.

The development of designs suitable for implementing SATMD energy management systems ensure the proposed research remains focused on outcomes that are immediately useful. All such outcomes will advance the state of the art by providing additional knowledge and capability from which structural designers can draw in

developing new structures or retrofitting existing structures. Finally, these outcomes ensure that the overall goal of taking semi-active energy management systems from a status of zero, or occasional highly specialised implementations, to a state where regular implementation may be more immediately practicable.

A trend towards widespread application of seismic isolation in civil engineering is underway. The concept of TMD systems can be equally well utilised for both segmented structure and traditional additional mass systems. Furthermore, the segregated TMD building concept appears to hold the promise of modifying the structural configuration of irregular structures that result from non-uniform mass, stiffness, strength, structural form, or a combination. It also extends the technique of base isolation to taller buildings and other types of seismic isolation-based control strategy.

10.2 Future Works

Further improvement of the SATMD and PTMD techniques presented requires detailed investigation on the stability margin of flexible frames. Additional study is also required on the passive and semi-active combined control system, to improve the performance of this technique in reducing earthquake effects in a variety of buildings. Future structural control research, particularly using resetable devices, should begin from the base point of optimising the control system to the demands of each individual structural system considered, and these TMD designs are no different in this regard.

More specifically, having two movable parts in a structure can lead to a series of architectural and technical problems that need to be addressed in detail. To have all utilities connected throughout the vibration process, to prevent the occurrence of rocking modes of the structure, and to transmit the gravity loads, an adequate design link including its flexible connection between its two isolated parts is required as introduced in previous research (Charng 1998). Thus, it is believed that more detailed and reliable solutions are required to solidify the safe features of isolation layer. Hence, future work may include an investigation to analyse the impact that the system might have on the architectural features of a building such as its water proofing, pipes and ducts, and stairways and elevators.

Semi-active resetable devices have significant promise as ‘smart’ dampers in existing structural control methods. Even though, the 1-4 resetable devices have been used for the SATMD systems in this research, structural hysteretic response manipulation resulting from other resetable device control laws (1-3 or 2-4) enable response improvements for more than a single response metric. In addition, these various types of resetable devices can be matched and adopted to a series of structural/isolation configurations. Finally, such device control laws may even be changed during an event to create more novel, extended solutions (Mulligan 2007). To bring these structural control systems to full-scale implementation, further studies focusing on a qualitative analysis are required, starting with hybrid testing.

The devices in this research use air as the working fluid, which eliminates the need for complex external plumbing systems. Device response forces can feasibly be altered by using a different hydraulic working fluid or pre-pressurising the device (Mulligan et al. 2006; Mulligan 2007). However, full-scale implementation of these devices is still limited due to moderate forces produced in comparison to the device size. Further work in this direction is required to achieve efficient, economic and flexible structural control designs. In addition, future work should include experimental tests with a small to full-scale model to verify the control effects of the suggested TMD building systems.

REFERENCES

Abdel-Fattah, B., and Wight, J. K. (1987). "Study of Moving Beam Hinging Zones for Earthquake-Resistant Design of R/C Buildings." *ACI Structural Journal*, January-February, 31-39.

Abdel-Rohman, M. (1984). "Optimal design of active TMD for buildings control." *Building and Environment*, 19(3), 191-195.

Abe, M. (1996). "Semi-active tuned mass dampers for seismic protection of civil structures." *Earthquake Engineering & Structural Dynamics*, 25(7), 743-749.

Akbay, Z., and Aktan, H. M. (1990). "Intelligent energy dissipation devices." *Proceedings of the US National Conference on Earthquake Engineering*, 427.

Akbay, Z., and Aktan, H. M. (1991). "Actively regulated friction slip braces." *Proceedings of the Canadian Conference on Earthquake Engineering*, 367.

Akira Nishitani, Y. I. (2001). "Overview of the application of active/semiactive control to building structures in Japan." *Earthquake Engineering & Structural Dynamics*, 30(11), 1565-1574.

Akiyama, H. (1985). *Earthquake Resistant Limit-State Design for Buildings*, University of Tokyo Press.

Al-Haddad, and Wight, J. K. (1988). "Relocating Beam Plastic Hinge Zones for Earthquake-Resistant Design of Reinforced Concrete Buildings." *ACI Structural Journal*, March-April, 122-133.

Aldemir, U. (2003). "Optimal control of structures with semiactive-tuned mass dampers." *Journal of Sound and Vibration*, 266(4), 847-874.

Andriono, T., and Carr, A. J. (1990). "Seismic resistant design of base isolated multistorey structures," PhD Thesis, University of Canterbury, Christchurch, New Zealand.

Andriono, T., and Carr, A. J. (1991a). "Reduction and Distribution of Lateral Seismic Forces on Base Isolated Mutli-Storey Structures." *Bulletin of the New Zealand National Society for Earthquake Engineering*, 24(3), 225-237.

Andriono, T., and Carr, A. J. (1991b). "A Simplified Earthquake Resistant Design Method for Base Isolated MultiStorey Buildings." *Bulletin of the New Zealand National Society for Earthquake Engineering*, 24(3), 238-250.

Annaka, T., and Yashiro, H. "Uncertainties in a probabilistic model for seismic hazard analysis in Japan." Bologna, Italy, 369-378.

Aref, A. J., and Jung, W.-Y. (2006). "Advanced composite panels for seismic and vibration mitigation of existing structures." *Journal of Engineering Materials and Technology, Transactions of the ASME*, 128(4), 618-632.

Arnold, C. (1984). "Building Configuration: The Architecture of Seismic Design." *Bulletin of the New Zealand National Society for Earthquake Engineering*, 17(2), 83-89.

Arnold, C., and Reitherman, R. (1982). *Building Configration and Seismic Design*, John Wiley.

Bakre, S. V., and Jangid, R. S. (2006). "Optimum parameters of tuned mass damper for damped main system." *Structural Control and Health Monitoring*, (in Press).

Balendra, T., Wang, C. M., and Rakesh, G. (1998). "Vibration control of tapered buildings using TLCD." *Journal of Wind Engineering and Industrial Aerodynamics*, 77-78, 245-257.

Banon, H., and Veneziano, D. (1982). "Seismic Safety of Reinforced Concrete Members and Structures." *Earthquake Engineering & Structural Dynamics*, 10, 179-193.

Barbat, A. H., Rodellar, J., Ryan, E. P., and Molinares, N. (1995). "Seismic performance of a new nonlinear active base isolation system." *Proceedings of the 10th European Conference on Earthquake Engineering*, Vienna, Austria, 2781.

Barroso, L. R. (1999). "Performance Evaluation of Vibration Controlled Steel Structures under Seismic Loading," PhD Thesis, Stanford University.

Barroso, L. R., Chase, J. G., and Hunt, S. (2003). "Resettable smart dampers for multi-level seismic hazard mitigation of steel moment frames." *Journal of Structural Control*, 10(1), 41-58.

Bathe, K. J., and Wilson, E. L. (1973). "Stability and Accuracy Analysis of Direct Integration Methods." *Earthquake Engineering & Structural Dynamics*, 1, 283-291.

Bernal, D. "Influence of ground motion characteristics on the effectiveness of tuned mass dampers." *Eleventh World Conference on Earthquake Engineering*, Acapulco, Mexico, Paper No. 1455.

Bertero, V. V. (1997). "In Seismic Design Methodologies for the Generation of Codes." Performance-based seismic engineering: a critical review of proposed guidelines, H. Fajfar P. and Krawinkler, ed., Balkema, Rotterdam, 1-32.

Bertero, V. V., and Uang, C. M. (1992). "Issues and future directions in the use of an energy approach for the seismic-resistant of design structures." Nonlinear Seismic Analysis and Design of Reinforced Concrete Buildings, H. Fajfar P. and Krawinkler, ed., Elsevier Applied Science, Amsterdam, 3-22.

Bobrow, J. E., and Jabbari, F. (1997). "A High-performance Semi-active Controller for Structural Vibration Suppression." *Smart Structures and Materials, SPIE*, 3041.

Bobrow, J. E., Jabbari, F., and Thai, K. (2000). "A new approach to shock isolation and vibration suppression using a resetable actuator." *Journal of Dynamic Systems, Measurement and Control, Transactions of the ASME*, 122(3), 570-573.

Bolt, B. A. (1997). "Discussion of Enduring lessons and opportunities lost from the San Fernando earthquake of February 9, 1971' by Paul C. Jennings." *Earthquake Spectra*, 13(3), 545-547.

Bracci, J. M., Reihorn, A. M., Mander, J. B., and Kunnath, S. K. (1989). "Deterministic Model for Seismic Damage Evaluation of Reinforced Concrete

Structures." *Technical Report NCEER-89-0033*, National Centre for Earthquake Engineering Research, State University of New York at Buffalo.

Breneman, S. E. (2000). "Design of Active Control Systems for Multi-Level seismic Resistance," PhD Thesis, Stanford University.

Carr, A. J. (1994). "Dynamic Aanalysis of Structures." *Bulletin of the New Zealand National Societ for Earthquake Engineering*, 271(2), 129-146.

Carr, A. J. (2004). "RUAUMOKO." Computer Program Library, Department of Civil Engineering, University of Canterbury.

Carr, A. J., and Tabuchi, M. (1993). "The Structural Ductility and the Damage Index for Reinforced Concrete Structure under Seismic Excitation." *Prodeedings of the Second European Conference on Structural Dynamics: EURODYN'93*, 1, 169-176.

Chai, Y. H., Priestley, M. J. N., and F., S. (1991). "Seismic Retrofit of Circular Bridge Column for Enhanced Flexural Response." *ACI Structural Journal*, September-October, 573-584.

Challa, V. R. M., and Hall, J. F. (1994). "Earthquake collapse analysis of steel frames." *Earthquake Engineering & Structural Dynamics*, 23(11), 1199-1218.

Chang, C. C., and Yang, H. T. Y. (1995). "Control of buildings using active tuned mass dampers." *Journal of Engineering Mechanics*, 121(3), 355-366.

Chang, J. C. H., and Soong, T. T. (1980). "Structural control using active tuned mass dampers." 106(6), 1091-1098.

Charng, P.-H. (1998). "Base isolation for multistorey building structures," PhD Thesis, University of Canterbury, Christchurch.

Chase, J., Mulligan, K., Gue, A., Mander, J., Alnot, T., Deam, B., Rodgers, G., Cleeve, L., and Heaton, D. (2005a) "Resetable Devices with Customised Performance for Semi-Active Seismic Hazard Mitigation of Structures." *Proc of NZ Society for Earthquake Engineering (NZSEE)*, Wairakei, New Zealand, 11-13.

Chase, J. G., Barroso, L. R., and Hunt, S. (2003). "Quadratic jerk regulation and the seismic control of civil structures." *Earthquake Engineering & Structural Dynamics*, 32(13), 2047-2062.

Chase, J. G., Barroso, L. R., and Hunt, S. (2004a). "The impact of total acceleration control for semi-active earthquake hazard mitigation." *Engineering Structures*, 26(2), 201-209.

Chase, J. G., Barroso, L. R., and Hunt, S. (2004b). "A semi-active acceleration-based control for seismically excited civil structures including control input impulses." *Structural Engineering and Mechanics*, 18(3), 287-301.

Chase, J. G., Hwang, K. L., Barroso, L. R., and Mander, J. B. (2005b). "A simple LMS-based approach to the structural health monitoring benchmark problem." *Earthquake Engineering & Structural Dynamics*, 34(6), 575-594.

Chase, J. G., Mulligan, K. J., Gue, A., Alnot, T., Rodgers, G., Mander, J. B., Elliott, R., Deam, B., Cleeve, L., and Heaton, D. (2006). "Re-shaping hysteretic behaviour using semi-active resettable device dampers." *Engineering Structures*, 28(10), 1418-1429.

Chase, J. G., Wodgers, G. W., Mulligan, K. J., Mander, J. B., and Dhakal, R. P. (2007) "Probablistic Analysis and Non-Linear Semi-Active Base Isolation Spectra for Aseismic Design." *8th Pacific Conference on Earthquake Engineering, Dec. 5 - 7,* Singapore.

Chen, G., Chen, C., and Cheng, F. Y. (2000a). "Soil-structure interaction effect on active control of multi-story buildings under earthquake loads." *Structural Engineering and Mechanics*, 10(6), 517-532.

Chen, G., Wu, J., Chen, C., and Lou, M. (2000b). "Recent development in structural control including soil-structure interaction effect." *Proceedings of SPIE - The International Society for Optical Engineering*, 3988, 229-242.

Chey, M. H. (2000). "Parametric control of structures using a tuned mass damper system under earthquake excitations," ME Thesis, University of Canterbury, Christchurch, New Zealand.

Chey, M. H., Chase, J. G., Mander, J. B., and Carr, A. J. (2007) "Design of semi-active tuned mass damper building systems using resetable devices." *8th Pacific Conference on Earthquake Engineering, Dec. 5 - 7,* Singapore, Paper No. 066.

Chey, M. H., Mander, J. B., Carr, A. J., and Chase, J. G. (2006) "Multi-storey semi-active tuned mass damper building system." *19th Australasian Conference on the Mechanics of Structures and Materials, Nov. 29 - Dec.1, Christchurch*, Paper No. 089.

Cho, S.-W., Kim, B.-W., Jung, H.-J., and Lee, I.-W. (2005). "Implementation of Modal Control for Seismically Excited Structures using Magnetorheological Dampers." *Journal of Engineering Mechanics*, 131(2), 177-184.

Choi, J.-S., Lee, J.-S., and Yun, C.-B. (2004). "Identification of the soil-structure interaction system using earthquake response data." *Journal of Engineering Mechanics*, 130(7), 753-761.

Chung, Y. S., Meyer, C., and Shinozuka, M. (1987). "Seismic Damage Assessment of Reinforced Concrete Members." *Technical Report NCEER-87-0022*, National Centre for Earthquake Engineering Research, State University of New York at Buffalo.

Clough, R. W., and Penzien, J. (1966). "Effect of Stiffness Degradation on Earthquake Ductility Requirements." *Report 66-16*, Structural and Materials Research, Structural Engineerig Laboratory, University of California, Berkeley.

Conte, J. P., Pister, K. S., and Mahin, S. A. (1990). "Influence of the earthquake ground motion process and structural properties on response characteristics of simple structures." *UBC-EERC Report 90/90*, Earthquake Engineering Research Center, Berkeley.

Cosenza, E., Manfredi, G., and Ramasco, R. (1993). "The use of damage functionals in earthquake engineering: a comparison between different methods." *Earthquake Engineering and Structural Dynamics*, 22, 855-868.

Cousins, W. J., and Porritt, T. E. (1993). "Improvements to lead-extrusion damper technology." *Bulletin of the New Zealand National Society for Earthquake Engineering*, 26(3), 342-348.

Cousins, W. J., Robinson, W. H., and McVerry, G. H. (1992). "Recent developments in devices for seismic isolation." *Bulletin of the New Zealand National Society for Earthquake Engineering*, 25(3), 167.

Crandall, S. H., and Mark, W. D. (1963). *Random vibration in mechanical systems*, Academic Press, New York.

Den Hartog, J. P. (1956). *Mechanical vibrations*, McGraw-Hill, New York.

DiPasquale, E., and Cakmak, A. S. (1990). "Seismic damage assessment using linear models." *Soil Dynamics and Earthquake Engineering*, 9(4), 194-215.

Djajakesukma, S. L., Samali, B., and Nguyen, H. (2002). "Study of a semi-active stiffness damper under various earthquake inputs." *Earthquake Engineering and Structural Dynamics*, 31(10), 1757-1776.

Dong, P. (2003). "Effect of varying hysteresis models and damage models on damage assessment of R/C structures under standard design level earthquakes obtained using a new scaling method." Ph.D. Thesis, University of Canterbury, Christchurch, New Zealand.

Dowrick, D. J., Cousins, W. J., Robinson, W. H., and Babor, J. (1992). "Recent developments in seismic isolation in New Zealand." *10th World Conference on Earthquake Engineering, Madrid*, Spain, 2305.

Dyke, S. J., and Spencer, B. F. (1996). "Modelling and Control of Magneto-Rheological Dampers for Seis-mic Response Reduction." *Smart Materials and Structures*, 5, 565-575.

Dyke, S. J., Spencer, B. F., Jr., Sain, M. K., and Carlson, J. D. (1996). "New semi-active control device for seismic response reduction." *Proceedings of the Engineering Mechanics*, Fort Lauderdale, FL, USA, 886-889.

Dyke, S. J., Spencer, B. F., Sain, M. K., and Carlson, J. D. (1996b). "Modeling and control of magnetorheological dampers for seismic response reduction." *Smart Materials and Structures*, 5(5), 565-575.

Emori, K., and Schnobrich, W. C. (1978). "Analysis of Reinforced Concrete Frame-Wall Structures for Strong Motion Earthquakes." *Structural Research Series, No. 434*, University of Illinois at Urbana Champaign, Urbana, Illinois.

Fajfar, P., and Fischinger, M. (1990). "A seismic procedure including energy concept." *Proceedings of IX ECEE*, Moscow, 312-321.

Fajfar, P., and Vidic, T. (1992). "On energy demand and supply in SDOF systems." Nonlinear Seismic Analysis of RC Buildings, P. Fajfar and H. Krawinkler, eds., Amstardam, 41-61.

Feng, M. Q. "Innovative base isolation system for buildings." (1993). *Proceedings of the Symposium on Structural Engineering in Natural Hazards Mitigation*, Irvine, CA, USA, 772-776.

Feng, M. Q., and Mita, A. (1995). "Vibration control of tall buildings using mega subconfiguration." *Journal of Engineering Mechanics*, 121(10), 1082-1088.

Feng, M. Q., and Shinozuka, M. (1992). "Friction controllable bearings for sliding base isolation systems." *Proceedings of the 24th Joint Meetings on Wind and Seismic Effects*. Gaithersburg, MD, USA, 189-198.

Frankel, A., Mueller, C., Perkins, D., Barnhard, T., Leyendecker, E., Safak, E., Hanson, S., Dickman, N., and Hopper, M. (1996). "New USGS seismic hazard maps for the United States." *Proceedings of the Conference on Natural Disaster Reduction*, Washington, DC, USA, 173-174.

Franklin, G., Powell, J. D., and Emami-Naeini, A. (1994). "Feedback control of dynamic systems." *Proceedings of the International Mechanical Engineering Congress and Exposition*, Chicago, IL, USA, Nov. 6-11, 1053-1054.

Fujino, Y., and Abe, M. (1993). "Design formulas for tuned mass dampers based on A perturbation technique." *Earthquake Engineering & Structural Dynamics*, 22(10), 833-854.

Fujino, Y., Sun, L., Pacheco, B. M., and Chaiseri, P. (1992). "Tuned liquid damper (TLD) for suppressing horizontal motion of structures." *Journal of Engineering Mechanics*, 118(10), 2017-2030.

Ghosh, A., and Basu, B. (2006). "A closed-form optimal tuning criterion for TMD in damped structures." *Structural Control and Health Monitoring*, (in Press).

Gordaninejad, F., Saiidi, M., Hansen, B. C., Ericksen, E. O., and Chang, F. K. (2002). "Magneto-rheological fluid dampers for control of bridges." *Journal of Intelligent Material Systems and Structures*, 13(2-3), 167-180.

Gu, Y. X., Zhao, G. Z., Zhang, H. W., Kang, Z., and Grandhi, R. V. (2000). "Buckling design optimization of complex built-up structures with shape and size variables." *Structural and Multidisciplinary Optimization*, 19(3), 183-191.

Gupta, A., and Krawinkler, H. (2000). "Estimation of seismic drift demands for frame structures." *Earthquake Engineering & Structural Dynamics*, 29(9), 1287-1305.

Hall, J. F., Heaton, T. H., Halling, M. W., and Wald, D. J. (1995). "Near-Source Ground Motion and its Effects on Flexible Buildings." *Earthquake Spectra*, 11(4), 569-605.

He, W.-L., and Agrawal, A. K. (2007). "Passive and hybrid control systems for seismic protection of a benchmark cable-stayed bridge." *Structural Control and Health Monitoring*, 14(1), 1-26.

Heaton, T. H., Hall, J. F., Wald, D. J., and Halling, M. W. (1995). "Response of Highrise and Base-Isolated Buildings to a Hypothetical M(W)7.0 Blind Thrust Earthquake." *Science*, 267(5195), 206-211.

Hoang, N., and Warnitchai, P. (2005). "Design of multiple tuned mass dampers by using a numerical optimizer." *Earthquake Engineering & Structural Dynamics*, 34(2), 125-144.

Housner, G. W., Bergman, L. A., Caughey, T. K., Chassiakos, A. G., Claus, R. O., Masri, S. F., Skelton, R. E., Soong, T. T., Spencer, B. F., and Yao, J. T. P. (1997). "Structural Control: Past, Present, and Future." *Journal of Engineering Mechanics*, 123(9), 897-971.

Hrovat, D., Barak, P., and Rabins, M. (1983). "Semi-active versus passive or active tuned mass damper for structural control." *Journal of Engineering Mechanics Division, ASCE*, 109, 691-705.

Huang, X., Elliott, S. J., and Brennan, M. J. (2003). "Active isolation of a flexible structure from base vibration." *Journal of Sound and Vibration*, 263(2), 357-376.

Hunt, S. J. (2002). "Semi-active smart-dampers and resetable actuators for multi-level seismic hazard mitigation of steel moment resisting frames," ME Thesis, University of Canterbury, Christchurch, New Zealand.

Inman, D. J. (2001). "Smart structures and materials 2001: Damping and isolation." *Proceedings of SPIE - The International Society for Optical Engineering*, Newport Beach, CA, 493.

Ioi, T., and Ikeda, K. (1978). "Dynamic Vibration Damped Absorber of Vibration System." *Bulletin of the Jsme-Japan Society of Mechanical Engineers*, 21(151), 64-71.

Jabbari, F., and Bobrow, J. E. (2002). "Vibration suppression with resettable device." *Journal of Engineering Mechanics*, 128(9), 916-924.

Jagadish, K. S., Prasad, B. K. R., and Rao, P. V. (1979). "Inelastic vibration absorber subjected to earthquake ground motions." 7(4), 317-326.

Jalihal, P., Utku, S., and Wada, B. K. (1994). "Active base isolation in buildings subjected to earthquake excitation." *Proceedings of the International Mechanical Engineering Congress and Exposition*, Chicago, IL, USA, Nov. 6-11, 381-388.

Jangid, R. S. (1999). "Optimum multiple tuned mass dampers for base-excited undamped system." *Earthquake Engineering & Structural Dynamics*, 28(9), 1041-1049.

Jansen, L. M., and Dyke, S. J. (2000). "Semiactive Control Strategies for MR Dampers: Comparative Study." *Journal of Engineering Mechanics*, 126(8), 795-803.

Jimmy, L. (1990). "Optimal weight absorber designs for vibrating structures exposed to random excitations." *Earthquake Engineering & Structural Dynamics*, 19(8), 1209-1218.

Johnson, E. A., Ramallo, J. C., Spencer, B. F., Jr., and Sain, M. K. (1998). "Intelligent Base Isolation Systems." *Proceedings of the Second World Conference on Structural Control*.

Jung, H. J., Park, K. S., Spencer Jr, B. F., and Lee, I. W. (2004). "Hybrid seismic protection of cable-stayed bridges." *Earthquake Engineering and Structural Dynamics*, 33(7), 795-820.

Jury, R. D. (1978). "Seismic load demands on columns of reinforced concrete multistorey frames." *Masters Thesis*, University of Canterbury, Christchurch, New Zealand.

Kanaan, A. E., and Powell, G. H. (1973). "General Purpose Computer Program for Inelastic Dynamic Response of Plane Structures." *Report No. EERC 73-6*, University of California at Berkeley.

Kao, G. C. (1998). "Design and shaking table tests of a four-storey miniature structure built with replaceable plastic hinges : a thesis submitted in partial fulfillment

of the requirements for the degree of Master of Civil Engineering in the University of Canterbury."

Kawabata, S., Ohkuma, T., Kanda, J., Kitamura, H., and Ohtake, K. (1990). "Chiba Port Tower. Full-scale measurement of wind actions Part 2. Basic properties of fluctuating wind pressures." *Journal of Wind Engineering and Industrial Aerodynamics*, 33(1-2), 253-262.

Kawamura, S., Sugisaki, R., Ogura, K., Maezawa, S., Tanaka, S., and Yajima, A. (2000). "Seismic isolation retrofit in Japan." *12th World Conference on Earthquake Engineering*, Auckland, New Zealand, Paper No. 2523.

Kelly, J. M. (1990). "Base Isolation: Linear Theory and Design." *Earthquake Spectra*, 6, 223-244.

Kelly, J. M., Skinner, R. I., and Heine, A. J. (1972). "Mechanisms of energy absorption in special devices for use in earthquake resistant structures." *Bulletin of Environmental Contamination and Toxicology*, 5(3), 63-73.

Kennedy, R. P., Cornell, C. A., Campbell, R. D., Kaplan, S., and Perla, H. F. (1980). "Probabilistic Seismic Safety Study of an Existing Nuclear-Power Plant." *Nuclear Engineering and Design*, 59(2), 315-338.

Khan, F. R. (1983). "100 Storey John Hancock Center, Chicago: A case study of the design process." *Engineering Structures*, 5(1), 10-14.

Kircher, C. A. (1997). "Guidelines for the seismic rehabilitation of buildings: Seismic isolation and energy dissipation applications with existing buildings." *Proceedings of the 15th structures Congress*, Part 2(of 2), Portland, OR, USA, 1234-1238.

Krawinkler, H., and Gupta, A. (1998). "Story Drfit Demands for Steel Moment Frame Structures in Different Seismic Region." *Proceedings of the 6th U.S. National Conference on Earthquake Engineering*.

Kurino, H., Yamada, T., Matsunaga, Y., and Tagami, J. (2006). "Switching Oil Damper with Automatic Valve Operation System for Structural Control." *4th World Conference on Structural Control and Monitoring*, University of California, San Diego, July 11-13.

Kwok, K. C. S., and Macdonald, P. A. (1990). "Full-scale measurements of wind-induced acceleration response of Sydney tower." *Engineering Structures*, 12(3), 153.

Kwok, K. C. S., and Samali, B. (1995). "Performance of Tuned Mass Dampers under Wind Loads." *Engineering Structures*, 17(9), 655-667.

Lagorio, H. J. (1990). *EARTHQUAKES An Architec's Guide to Non-Structural Seismic Hazard*, John Wiley & Sons, Inc.

Leelataviwar, S., Goel, S. C., and Stojadinovie, B. (1999). "Toward performance-based seismic design of structures." *Earthquake Spectra*, 15(3), 435-461.

Li, C., Liu, Y., and Wang, Z. (2003). "Active multiple tuned mass dampers: A new control strategy." *Journal of Structural Engineering*, 129(7), 972-977.

Limpert, E., Stahel, W. A., and Abbt, M. (2001). "Log-normal distributions across the sciences: Keys and clues." *Bioscience*, 51(5), 341-352.

Lin, M., Burns, S. A., and Wen, Y. K. (2005). "Multiobjective optimization for performance-based seismic design of steel moment frame structures." *Earthquake Engineering & Structural Dynamics*, 34(3), 289-306.

Loh, C.-H., and Chang, C.-M. (2006). "Vibration control assessment of ASCE benchmark model of cable-stayed bridge." *Structural Control and Health Monitoring*, 13(4), 825-848.

Lukkunaprasit, P., and Wanitkorkul, A. (2001). "Inelastic buildings with tuned mass dampers under moderate ground motions from distant earthquakes." *Earthquake Engineering & Structural Dynamics*, 30(4), 537-551.

Mackie, K. R., and Stojadinovic, B. (2006). "Fourway: Graphical Tool for Performance-Based Earthquake Engineering." *Journal of Structural Engineering*, 132(8), 1274-1283.

Mar, D., and Tipping, S. (2000). "Story Isolation: A New High-Performance Seismic Technology." 9th U.S.-Japan Workshop on the Improvement of Structural Design and Construction Practices, Victoria, British Columbia, Canada.

May, B. S., and Beck, J. L. (1998). "Probabilistic control for the active mass driver benchmark structural model." *Earthquake Engineering & Structural Dynamics*, 27(11), 1331-1346.

Mayes, R. L., Buckle, I. G., Kelly, T. R., and Jones, L. (1992). "AASHTO Seismic Isolation Design Requirements for Highway Bridges." *Journal of the Structural Division, ASCE*, 118(1), 284-304.

McCabe, S. L., and Hall, W. J. (1992). "Damage and reserve capacity evaluation of structrures subjected to strong earthquake ground motion." *Proceedings of the 10th World Conference on Earthquake Engineering*, Madrid, Spain, 3653-3658.

McNamara, R. J. (1977). "Tuned mass dampers for buildings." 103(9), 1785-1798.

Mehrain, M., and Krawinkler, H. "Guidelines for the seismic rehabilitation of buildings: New analysis procedures developed specifically for application with existing buildings." *Proceedings of the 15th structures Congress*, Part 2(of 2), Portland, OR, USA, 1229-1233.

Miranda, J. C. (2005). "On tuned mass dampers for reducing the seismic response of structures." *Earthquake Engineering and Structural Dynamics*, 34(7), 847-865.

Miyama, T. (1992). "Seismic response of multi-story frames equipped with energy absorbing story on its top." *10th World Conference of Earthquake Engineering*, 4201-4206.

Moehle, J. P. (1992). "Displacement-based design of RC structures subjected to earthquakes." *Earthquake Spectra*, 8(3), 403.

Moncarz, P. D., McDonald, B. M., and Caligiuri, R. D. (2001). "Earthquake failures of welded building connections." *International Journal of Solids and Structures*, 38(10-13), 2025-2032.

Mork, K. J. (1992). "Stochastic analysis of reinforced concrete frames under seismic excitation." *Soil Dynamics and Earthquake Engineering*, 11(3), 145-161.

Mulligan, K., Chase, J., Gue, A., Alnot, T., Rodgers, G., Mander, J., Elliott, R., Deam, B., Cleeve, L., and Heaton, D. (2005). "Large Scale Resetable Devices for

Multi-Level Seismic Hazard Mitigation of Structures." *Proc. 9th International Conference on Structural Safety and Reliability (ICOSSAR)*, Rome, Italy, 19-22.

Mulligan, K., Chase, J., Gue, A., Mander, J., Alnot, T., Deam, B., Rodgers, G., Cleeve, L., and Heaton, D. (2005). "Resetable Devices with Customised Performance for Semi-Active Seismic Hazard Mitigation of Structures." *Proc of NZ Society for Earthquake Engineering Conference (NZSEE), March 11-13, 2005*, Wairakei, New Zealand.

Mulligan, K., Chase, J., Mander, J., and LElliot, R. (2007). "Semi-active Resetable Actuators Incorporating a High Pressure Air Source." *Proc of NZ Society for Earthquake Engineering Conference (NZSEE)*, Palmerston North, New Zealand.

Mulligan, K., Chase, JG, Mander, JB, Fougere, M, Deam, BL, Danton, G and Elliott, RB. (2006). "Hybrid experimental analysis of semi-active rocking wall systems." *Proc New Zealand Society of Earthquake Engineering Conference (NZSEE)*, Napier, New Zealand.

Mulligan, K., Miguelgorry, M, Novello, V, Chase, JG, Mander, JB, Rodgers, GW, Carr, AJ, Deam, BL and Horn, B. (2006). "Semi-active Tuned Mass Damper Systems." *19th Australasian Conference on Mechanics of Structures and Materials (ACMSM)*, Christchurch, New Zealand.

Mulligan, K. J. (2007). "Experimental and Analytical Studies of Semi-Active and Passive Structural Control of Buildings," *PhD Thesis*, University of Canterbury, Christchurch, New Zealand.

Murakami, K., Kitamura, H., Ozaki, H., and Teramoto, T. (2000). "Design and analysis of a building with the middle-story isolation structural stystem." *12th World Conference of Earthquake Engineering*, Auckland, New Zealand, 0857, 1-8.

Murudil, M. M., and Mane, S. M. (2004). "Seismic Effectiveness of Tuned Mass Damper (TMD) for Different Ground Motion Parameters." *13th World Conference on Earthquake Engineering, Paper No. 2325*, Vancouver, Canada.

Naeim, F., and Kelly, J. M. (1999). *Design of seismic isolated structures : from theory to practice*, John Wiley, New York.

Nagarajaiah, S., and Varadarajan, N. (2001). "Smart variable stiffness control systems." *Proceedings of SPIE*, Newport Beach, CA, 345-353.

Nagashima, I. (2001). "Optimal displacement feedback control law for active tuned mass damper." *Earthquake Engineering and Structural Dynamics*, 30(8), 1221-1242.

Nagashima, I., Maseki, R., Asami, Y., Hirai, J., and Abiru, H. (2001). "Performance of hybrid mass damper system applied to a 36-storey high-rise building." *Earthquake Engineering & Structural Dynamics*, 30(11), 1615-1637.

Narasimhan, S., and Nagarajaiah, S. (2005). "A STFT semiactive controller for base isolated buildings with variable stiffness isolation systems." *Engineering Structures*, 27(4), 514-523.

Nielsen, N. N., and Imbeault, F. A. "Validity of Various Hysteretic Systems." *Prodeedings of the Third Japan National Conference on Earthquake Engineering*, 435-433.

Nielsen, S. R. K., Koyluoglu, H. U., and Calmak, A. S. (1992). "One and two-dimensional maximum softening damage indicators for reinforced concrete structures under seismic excitation." *Soil Dynamics and Earthquake Engineering*, 11(8), 435-443.

NZS3101. (1982). "New Zealand Standard; Code and Practice for the design of Concrete Structure ", Standards Association of New Zealand (SANZ).

NZS4203. (1976). "New Zealand Standard; Code of Practice for General Structural Design and Design Loadings for Buildings." Standards Association of New Zealand (SANZ).

NZS4203. (1992). "New Zealand Standard; Code of Practice for General Structural Design and Design Loadings for Buildings." Standards Association of New Zealand (SANZ).

Obtake, K., Mataki, Y., Ohkuma, T., Kanda, J., and Kitamura, H. (1992). "Full-scale measurements of wind actions on Chiba Port Tower." *Journal of Wind Engineering and Industrial Aerodynamics*, 43(pt 3), 2225-2236.

Ohkubo, S., and Asai, K. (1992). "Hybrid optimal synthesis method for truss structures considering shape, material and sizing variables." *International Journal for Numerical Methods in Engineering*, 34(3), 839-851.

Ohtori, Y., Christenson, R. E., Spencer, B. F., and Dyke, S. J. (2004). "Benchmark control problems for seismically excited nonlinear buildings." *Journal of Engineering Mechanics-Asce*, 130(4), 366-385.

Otani, S. (1974). "SAKE, A Computer Program for Inelastic Response of R/C Frames to Earthquakes." *Report UILU-Egn-74-2029*, Civil Engineering Studies, University of Illinois at Urbana Champaign, Urbana, Illinois.

Otani, S. (1980). "Nonlinear Dynamic Analysis of Reinforced Concrete Building Structures." *Canadian Journal of Civil Engineering*, 7(2), 333-344.

Otani, S. (1981). "Hysteresis Models of Reinforced Concrete for Earthquake Response Analysis." *Journal of the Faculty of Engineering, University of Tokyo*, 34(3), 407-441.

Pan, T.-C., Ling, S.-F., and Cui, W. (1995). "Seismic response of segmental buildings." *Earthquake Engineering & Structural Dynamics*, 24(7), 1039-1048.

Pan, T. C., and Cui, W. (1998). "Response of segmental buildings to random seismic motions." *ISET Journal of Engineering Technology*, 35(4), 105-112.

Park, R., and Paulay, T. (1987). "Joints in Reinforced Concrete Frames Designed for Earthquake Resistance." Research Report No. 84-9, Department of Civil Engineering, University of Canterbury, New Zealand.

Park, S. W. "Rheological modeling of viscoelastic passive dampers." *Proceedings of SPIE*, Newport Beach, CA, 343-354.

Park, Y.-J., and Ang, A. H. S. (1985). "Mechanistic seismic damage model for reinforced concrete." *Journal of Structural Engineering*, 111(4), 722-739.

Park, Y.-J., Ang, A. H. S., and Wen, Y. K. (1985). "Seismic damage analysis of reinforced concrete buildings." *Journal of Structural Engineering*, 111(4), 740-757.

Park, Y. J., Ang, A. H. S., and Wen, Y. K. (1987). "Damage-limiting aseismic design of buildins." *Earthquake Spectra*, 3(1), 1-26.

Parulekar, Y. M., Reddy, G. R., Vaze, K. K., and Kushwaha, H. S. (2004). "Lead extrusion dampers for reducing seismic response of coolant channel assembly." *Nuclear Engineering and Design*, 227(2), 175-183.

Paulay, T. (1976). "Moment redistribution in continuous beams of eqrthquake resistant multistorey reinforced concrete frames." *Bulletin of the New Zealand National Society of Earthquake Engineering*, 9(4), 205-212.

Paulay, T. (1979). "Developments in the Design of Ductile Reinforced Concrete Frames." *Proceedings of the 2nd South Pacific Regional Conference on Earthquake Engineering*, Wellington, New Zealand, 605-623.

Paulay, T., and Priestley, M. J. N. (1992). *Seismic Design of Reinforced Concrete and Masonry Buildings*, John Wiley & Sons, Inc.

Pieplow, K. (2006). "New chances with high-strength materials - constructions with CFRP." *Responding to Tomorrow's Challenges in Structural Engineering IABSE Symposium*, Sep. 13-15, Budapest, Hungary, 284-5.

Pinkaew, T., and Fujino, Y. (2001). "Effectiveness of semi-active tuned mass dampers under harmonic excitation." *Engineering Structures*, 23(7), 850-856.

Priestley, M. J. N. (2000). "Performance based seismic design." *Bulletin of the New Zealand National Society for Earthquake Engineering*, 33(3), 325-346.

Priestley, M. J. N., and Park, R. (1987). "Strength and Ductility of Concete Bridge Columns under Seismic Loading." *ACI Structural Journal*, January-February, 61-76.

Randall, S. E., Halsted, D. M., and Taylor, D. L. (1981). "Optimum Vibration Absorbers for Linear Damped Systems." *Journal of Mechanical Design - Transactions of the ASME*, 103(4), 908-913.

Refice, A., and Capolongo, D. (2002). "Probabilistic modeling of uncertainties in earthquake-induced landslide hazard assessment." *Computers and Geosciences*, 28(6), 735-749.

Ricciardelli, F., Occhiuzzi, A., and Clemente, P. (2000). "Semi-active Tuned Mass Damper control strategy for wind-excited structures." *Journal of Wind Engineering and Industrial Aerodynamics*, 88(1), 57-74.

Ricciardelli, F., Pizzimenti, A. D., and Mattei, M. (2003). "Passive and active mass damper control of the response of tall buildings to wind gustiness." *Engineering Structures*, 25(9), 1199-1209.

Robinson, D., Dhu, T., and Schneider, J. (2006). "SUA: A computer program to compute regolith site-response and estimate uncertainty for probabilistic seismic hazard analyses." *Computers and Geosciences*, 32(1), 109-123.

Robinson, W. H., and Greenbank, L. R. (1975). "Properties of an extrusion energy absorber." *Bulletin of the New Zealand Society for Earthquake Engineering*, 8(3), 187-191.

Rodgers, G., Mander, J., Chase, J., Mulligan, K., Deam, B., and Carr, A. (2006). "Re-Shaping Hysteretic Behaviour Using Resetable Devices to Customise Structural Response and Forces." *8th US National Conference on Earthquake Engineering (8NCEE)*, San Francisco, USA.

Rodgers, G. W., Chase, J. G., Mander, J. B., Leach, N. C., and Denmead, C. S. (2007a). "Experimental development, tradeoff analysis and design implementation of high force-to-volume damping technology." *Bulletin of the New Zealand Society for Earthquake Engineering*, 40(2), 35-48.

Rodgers, G. W., Mander, J. B., Chase, J. G., Mulligan, K. J., Deam, B. L., and Carr, A. (2007b). "Re-shaping hysteretic behaviour - Spectral analysis and design equations for semi-active structures." *Earthquake Engineering & Structural Dynamics*, 36(1), 77-100.

Roufaiel, M. S. L., and Meyer, C. (1987). "Analytical Modelling of Hysteetic Behaviour of R/C Frames." *Journal of the Structural Division, ASCE*, 113(3), 429-457.

Ruiz, S. E., and Esteva, L. (1995). "About the effectiveness of tuned mass dampers on nonlinear systems subjected to earthquakes." Proceedings of the 1996 1st International Conference on Earthquake Resistant Engineering Structures, ERES 96, Oct 30-Nov 1 1996, Computational Mechanics Publ, Southampton, Engl, Thessaloniki, Greece, 311-320.

Saadatmanesh, H. (1997). "Extending service life of concrete and masonry structures with fiber composites." *Construction and Building Materials*, 11(5-6), 327-335.

Sabouni, A.-R. R. (1995). "Expert system for the preliminary design of earthquake resistant buildings." *Congress on Computing in Civil Engineering*, Atlanta, GA, USA, 1188-1195.

Sadek, F., Mohraz, B., Taylor, A. W., and Chung, R. M. (1997). "A method of estimating the parameters of tuned mass dampers for seismic applications." *Earthquake Engineering & Structural Dynamics*, 26(6), 617-635.

Saiidi, M. (1982). "Hysteresis Models for Reinforced Concrete." *Journal of Structural Division, ASCE*, 116(ST5), 1077-1087.

Samali, B., and Al-Dawod, M. (2003). "Performance of a five-storey benchmark model using an active tuned mass damper and a fuzzy controller." *Engineering Structures*, 25(13), 1597-1610.

Samali, B., Al-Dawod, M., and Li, J. (2003). "Performance of an active mass driver system on a five storey benchmark model." *JSME International Journal, Series C: Mechanical Systems, Machine Elements and Manufacturing*, 46(3), 848-853.

Scruggs, J. T., Taflanidis, A. A., and Beck, J. L. (2006). "Reliability-based control optimization for active base isolation systems." *Structural Control and Health Monitoring*, 13(2-3), 705-723.

Setareh, M. (2001). "Application of semi-active tuned mass dampers to base-excited systems." *Earthquake Engineering & Structural Dynamics*, 30(3), 449-462.

Setareh, M. (2002). "Floor vibration control using semi-active tuned mass dampers." *Canadian Journal of Civil Engineering*, 29(1), 76-84.

Sfakianakis, M. G., and Fardis, M. N. (1991). "Nonlinear finite element for modeling reinforced concrete columns in three-dimensional dynamic analysis." *Computers and Structures*, 40(6), 1405-1419.

Shapiro, D., Rojahn, C., Reaveley, L. D., Holmes, W. T., and Moehle, J. P. (1996). "Guidelines for seismic rehabilitation of buildings: An overview of the background approach and contents." Portland, OR, USA, 1224-1228.

Shen, J.-D. J. (2001). "Structural response reduction using tuned mass damper with semi-active control," PhD Thesis, State University of New York at Buffalo, New York, USA.

Shmizu, K., Orui, S., and Kurino, H. (2006). "Observed Response of the High-Rise Building with Semi-Active Switching Oil Dampers to Earthquake and Typhoon." *4th World Conference on Structural Control and Monitoring*, University of California, San Diego.

Shustov, V. (1999). "Building configuration as a structural control." *American Society of Mechanical Engineers, Pressure Vessels and Piping Division (Publication) PVP*, 387, 201-205.

Skinner, R. I., Kelly, J. M., and Heine, A. J. (1975). "Hysteretic dampers for earthquake-resistant structures." *Earthquake Engineering & Structural Dynamics*, 3(3), 287-296.

Skinner, R. I., Robinson, W. H., and McVerry, G. H. (1993). *An Introduction to Seismic Isolation*, John Wiley & Sons, Inc., New York.

Sommerville, P., Smith, N., Punyamurthula, S., and Sun, J. (1997). "Development of ground motion time histories for Phase Ⅱ of the FEMA/SAC steel project."

Soong, T. T., and Dargush, G. F. (1997). *Passive energy dissipation systems in structural engineering*, Wiley, Chichester ; New York.

Soong, T. T., and Spencer, B. F., Jr. (2000). "Active, semi-active and hybrid control of structures." *Bulletin of the New Zealand National Society for Earthquake Engineering*, 33(3), 387-402.

Soto-Brito, R., and Ruiz, S. E. (1999). "Influence of ground motion intensity on the effectiveness of tuned mass dampers." *Earthquake Engineering & Structural Dynamics*, 28(11), 1255-1271.

Spencer, B. F., Dyke, S. J., Sain, M. K., and Carlson, J. D. (1997). "Phenomenological Model for Magnetorheological Dampers." *Journal of Engineering Mechanics*, 123(3), 230-238.

Spencer, B. F., and Nagarajaiah, S. (2003). "State of the art of structural control." *Journal of Structural Engineering-Asce*, 129(7), 845-856.

Sueoka, T., Torii, S., and Tsuneki, Y. (2004). "The Application of Response Control Design Using Middle-Story Isolation System to High-Rise Building." *13th World Conference on Earthquake Engineering*.

Symans, M. D., and Constantinou, M. C. (1997). "Seismic testing of a building structure with a semi-active fluid damper control system." *Earthquake Engineering & Structural Dynamics*, 26(7), 759-777.

Takewaki, I. (2007). "Closed-form sensitivity of earthquake input energy to soil-structure interaction system." *Journal of Engineering Mechanics*, 133(4), 389-399.

Takewaki, I., and Fujimoto, H. (2004). "Earthquake input energy to soil-structure interaction systems: A frequency-domain approach." *Advances in Structural Engineering*, 7(5), 399-414.

Thompson, A. G. (1981). "Optimum Tuning and Damping of a Dynamic Vibration Absorber Applied to a Force Excited and Damped Primary System." *Journal of Sound and Vibration*, 77(3), 403-415.

Thomson, E. D. (1991). "P-delta effects in ductile reinforced concrete frames under seismic loading : a report submitted in partial fulfilment of the requirements for the degree of Master of Engineering at the University of Canterbury, Christchurch, New Zealand."

Tsai, H. C., and Lin, G. C. (1994). "Explicit Formulas for Optimum Absorber Parameters for Force-Excited and Viscously Damped Systems." *Journal of Sound and Vibration*, 176(5), 585-596.

Turkington, D. H., Carr, A. J., Cooke, N., and Moss, P. J. (1989a). "Design Method for Bridges on Lead-Rubber Bearings." *Journal of the Structural Division, ASCE*, 115(12), 3017–3030.

Turkington, D. H., Carr, A. J., Cooke, N., and Moss, P. J. (1989b). "Seismic Design of Bridges on Lead-Rubber Bearings." *Journal of the Structural Division, ASCE*, 115(12), 3000–3016.

Tyler, R. G. (1991). "Rubber bearings in base-isolated structures. A summary paper." *Bulletin of the New Zealand Society for Earthquake Engineering*, 2444(3), 251.

Tyler, R. G., and Skinner, R. I. (1977). "Testing of dampers for the base isolation of a proposed 4-storey building against earthquake attack." *American Society of Mechanical Engineers, Applied Mechanics Division, AMD*, 376-382.

Tzou, H. S., and Wan, G. C. (1989). "Distributed control of flexible manipulators. Part 1. Dynamics and passive distributed viscoelastic damper." *Proceedings of the International Computers in Engineering Conference and Exhibit*, Anheim, CA, USA, 431-437.

Uang, C. M., and Bertero, V. V. (1990). "Evaluation of seismic energy in structures." *Earthquake Engineering & Structural Dynamics*, 19, 77-90.

Ueda, T., Nakagaki, R., and Koshida, K. (1993). "Suppression of Wind-Induced Vibration of Tower-Shaped Structures by Dynamic Dampers." *Structural Engineering International*, 3, 50-53.

Varadarajan, N., and Nagarajaiah, S. (2004). "Wind response control of building with variable stiffness tuned mass damper using empirical mode decomposition/Hilbert transform." *Journal of Engineering Mechanics*, 130(4), 451-458.

Villaverde, R. (1985). "Reduction in seismic response with heavily-damped vibration absorbers." *Earthquake Engineering & Structural Dynamics*, 13(1), 33-42.

Villaverde, R. (2002). "Aseismic roof isolation system: Feasibility study with 13-story building." *Journal of Structural Engineering*, 128(2), 188-196.

Wang, D., Zhang, W. H., and Jiang, J. S. (2002). "Combined shape and sizing optimization of truss structures." *Computational Mechanics*, 29(4-5), 307-312.

Warburton, G. B. (1982). "Optimum absorber parameters for various combinations of response and excitation parameters." *Earthquake Engineering & Structural Dynamics*, 10(3), 381-401.

Watakabe, M., Tohdo, M., Chiba, O., Izumi, N., Ebisawa, H., and Fujita, T. (2001). "Response control performance of a hybrid mass damper applied to a tall building." *Earthquake Engineering & Structural Dynamics*, 30(11), 1655-1676.

Williams, S. R. (1994). "Fault-tolerant control desing for smart damping systems," Washington Universtiy, Washington.

Wilson, E. L., Farhoomad, I., and Bathe, K. J. (1973). "Nonlinear Dynamic Analysis of Complex Structures." *Earthquake Engineering & Structural Dynamics*, 1, 241-252.

Wongprasert, N., and Symans, M. D. (2005). "Experimental evaluation of adaptive elastomeric base-isolated structures using variable-orifice fluid dampers." *Journal of Structural Engineering*, 131(6), 867-877.

Wu, J.-C., Shih, M.-H., Lin, Y.-Y., and Shen, Y.-C. (2005). "Design guidelines for tuned liquid column damper for structures responding to wind." *Engineering Structures*, 27(13), 1893-1905.

Wu, W.-H. (1997). "Equivalent fixed-base models for soil-structure interaction systems." *Soil Dynamics and Earthquake Engineering*, 16(5), 323-336.

Wu, W.-H., and Chen, C.-Y. (2002). "Simplified soil-structure interaction analysis using efficient lumped-parameter models for soil." *Soils and Foundations*, 42(6), 41-52.

Wu, W.-H., and Smith, H. A. (1993). "Soil-structure interaction effects for internally controlled systems." *Proceedings of the ASME Winter Annual Meeting*, New Orleans, LA, USA, 371-379.

Wu, W.-H., and Smith, H. A. (1995). "Efficient modal analysis for structures with soil-structure interaction." *Earthquake Engineering & Structural Dynamics*, 24(2), 283-299.

Xu, Z., Agrawal, A. K., and Yang, J. N. (2006). "Semi-active and passive control of the phase I linear base-isolated benchmark building model." *Structural Control and Health Monitoring*, 13(2-3), 626-648.

Yan, N., Wang, C. M., and Balendra, T. (1999). "Optimal damper characteristics of ATMD for buildings under wind loads." *Journal of Structural Engineering*, 125(12), 1376-1383.

Yang, J. N., and Agrawal, A. K. (2002). "Semi-active hybrid control systems for nonlinear buildings against near-field earthquakes." *Engineering Structures*, 24(3), 271-280.

Yang, J. N., Agrawal, A. K., Samali, B., and Wu, J.-C. (2004). "Benchmark problem for response control of wind-excited tall buildings." *Journal of Engineering Mechanics*, 130(4), 437-446.

Yang, J. N., Kim, J.-H., and Agrawal, A. K. (2000). "Resetting Semiactive Stiffness Damper for Seismic Response Control." *Journal of Structural Engineering*, 126(12), 1427-1433.

Yoshida, O., and Dyke, S. J. (2004). "Seismic Control of a Nonlinear Benchmark Building Using Smart Dampers." *Journal of Engineering Mechanics*, 130(4), 386-392.

Yoshioka, H., Ramallo, J. C., and Spencer, B. F., Jr. . (2002). "Smart Base Isolation Strategies Employing Magnetorheological Dampers." *Journal of Engineering Mechanics*, 128(5), 540-551.

Zahrah, T., and Hall, J. (1984). "Earthquake energy absorption in SDOFstructures." *Journal of Structural Engineering*, 110(9), 1757-1772.

Zhou, F., Tan, P., Yan, W., and Wei, L. (2002). "Theoretical and experimental research on a new system of semi-active structural control with variable stiffness and damping." *Earthquake Engineering and Engineering Vibration*, 1(1), 130-135.

Zhou, F. L., Yang, Z., Liu, W. G., and Tan, P. (2004). "New seismic isolation system for irregular structure with the largest isolaton building area in the world." *13th World Conference on Earthquake Engineering*.

Zhu, H., Wen, Y., and Iemura, H. (2001). "A study on interaction control for seismic response of parallel structures." *Computers & Structures*, 79(2), 231-242.

Ziyaeifar, M. (2002). "Mass isolation, concept and techniques." *European earthquake engineering*(2), 43-55.

Ziyaeifar, M., and Noguchi, H. (1998). "Partial mass isolation in tall buildings." *Earthquake Engineering & Structural Dynamics*, 27(1), 49-65.

APPENDIX A Frame Data and Dynamic Properties

• Member areas moments of inertia and length of rigid end block

Members	Level	Area (m^2)	Inertia (m^4)	L_R (m)
Beams	1 - 6	0. 1800	0. 02382	0. 400
	7 - 8	0. 1700	0. 02017	0. 375
	9-12	0. 1600	0. 01689	0. 338
Exterior Columns	1 - 6	0. 2906	0. 01455	0. 450
	7 - 8	0. 2813	0. 01318	0. 425
	9-12	0. 2438	0. 00855	0. 400
Interior Column	1 - 6	0. 4800	0. 02560	0. 450
	7 - 8	0. 3942	0. 01727	0. 425
	9-12	0. 3417	0. 01297	0. 400

* Area : Axial and shear area * Inertia : Moment of inertia * L_R : Length of rigid end block
* Modulus of Elasticity E=25,000,000 Kpa * Modulus of Shear G=10,400,000 Kpa

• Initial fixed end moments and shear of beams for the left bay.

Level	M1 (KNm)	M2 (KNm)	V1 (KN)	V2 (KN)
1 - 6	-187. 8	186. 3	-135. 8	135. 8
7 - 8	-188. 4	186. 7	-133. 4	133. 4
9-12	-188. 8	187. 2	-131. 1	131. 1

* The symetric values were used for the right bay.
* The signs correspond to the *Ruaumoko* (Carr,1996) sign conventions.

• Beam yield moments for the left bay.

Level	M1 (KNm)	M2 (KNm)	M3 (KN)	M4 (KN)
1	976	-976	893	-893
2 – 4	1142	-1142	1047	-1047
5 - 6	988	-988	887	-887
7 - 8	762	-833	714	-714
9-10	559	-631	547	-464
11	307	-369	381	-307
12	307	-307	307	-307

* M1, M2 : Yield moments fot the left end. M3,M4 for the right end.
* The symmetric values were used for the right bay.

• Beam column yield interaction diagram

Column	PYC (kN)	PB (kN)	MB (kNm)	MB (kNm)	M2B (kNm)	MO (kNm)	PYT (kN)
External	-11152	-6075	1338	1531	1263	665	1930
Internal	-17888	-10920	1986	1986	2450	2038	2656

• Masses and external vertical loadings

Level	Weight (kN)		Nodal Loads (kN)	
	Ext. Node	Int. Node	Ext. Node	Int. Node
0	13	19	-25. 0	-37. 0
1	434	757	-298. 5	-485. 1
2	434	757	-298. 5	-485. 1
3	434	757	-298. 5	-485. 1
4	434	757	-298. 5	-485. 1
5	434	757	-298. 5	-485. 1
6	434	755	-298. 5	-485. 1
7	427	743	-293. 9	-475. 9
8	427	743	-293. 9	-475. 9
9	420	731	-289. 2	-468. 5
10	420	731	-289. 2	-468. 5
11	420	731	-289. 2	-468. 5
12	409	717	-266. 2	-439. 5

* The gravity loading is based on D+L/3.
* The nodal loads correspond to the rest of the gravity load.
* Nodal weight is converted to mass internally in the program.

• Dynamic Properties of the Framed Structure

Mode	Natural Freq. (Hz)	Modal Effec. Mass ($kN\text{-}s^2/m$)	Modal Damping (%)	Participation Factor
1	0. 532	1. 514E+03	5. 000	1. 366E+00
2	1. 533	2. 527E+02	2. 674	-5. 321E-01
3	2. 756	7. 408E+01	2. 812	-2. 752E-01
4	3. 853	7. 899E-29	3. 321	3. 064E-16
5	3. 885	3. 596E+01	3. 338	-1. 700E-01
6	4. 525	5. 616E+00	3. 694	-9. 368E-02
7	5. 131	1. 944E-28	4. 051	-4. 722E-16
8	5. 279	2. 056E+01	4. 141	-1. 436E-01
9	6. 652	1. 548E+01	5. 000	-1. 118E-01

APPENDIX B Earthquake Accelerations Used

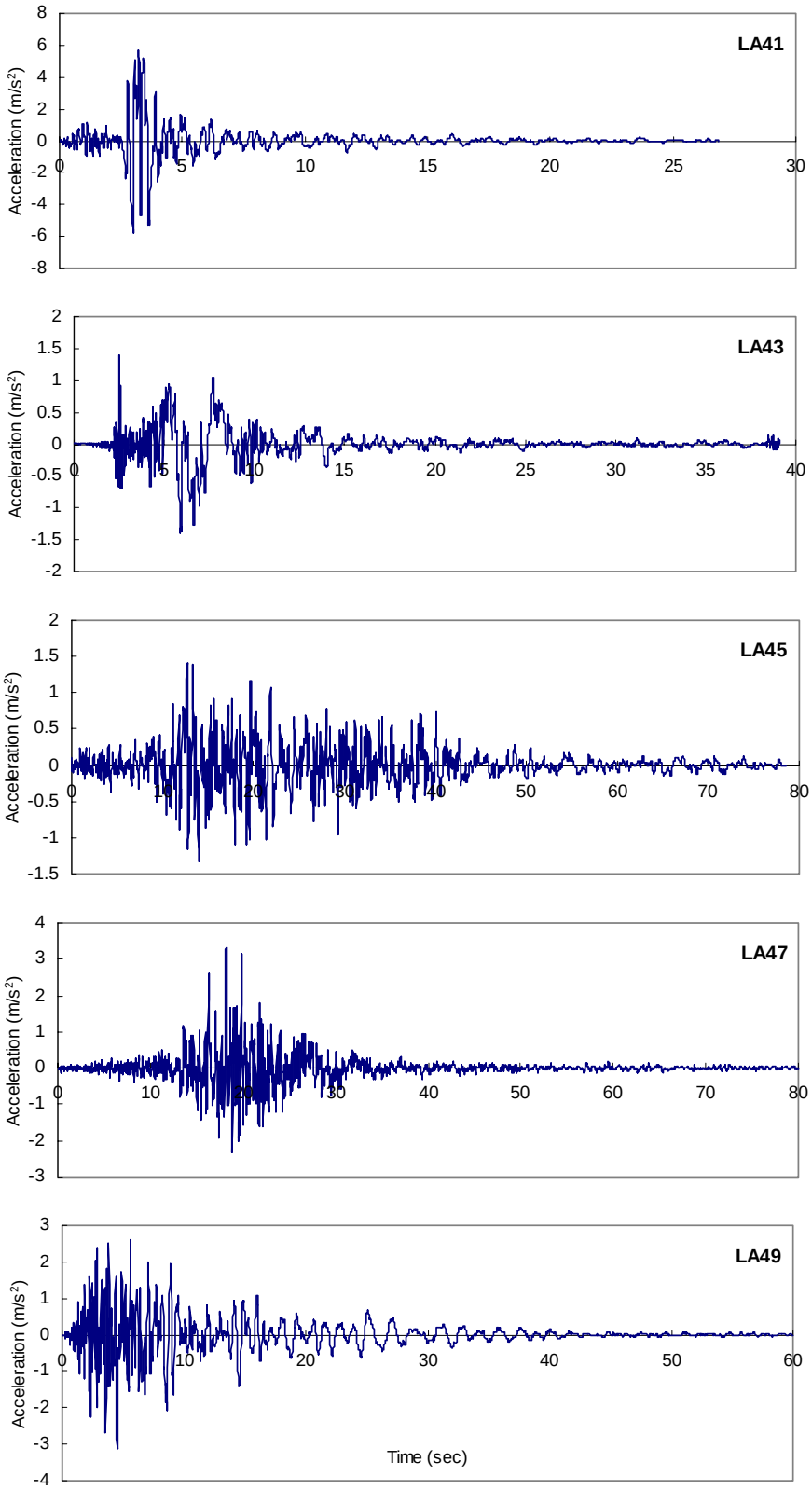

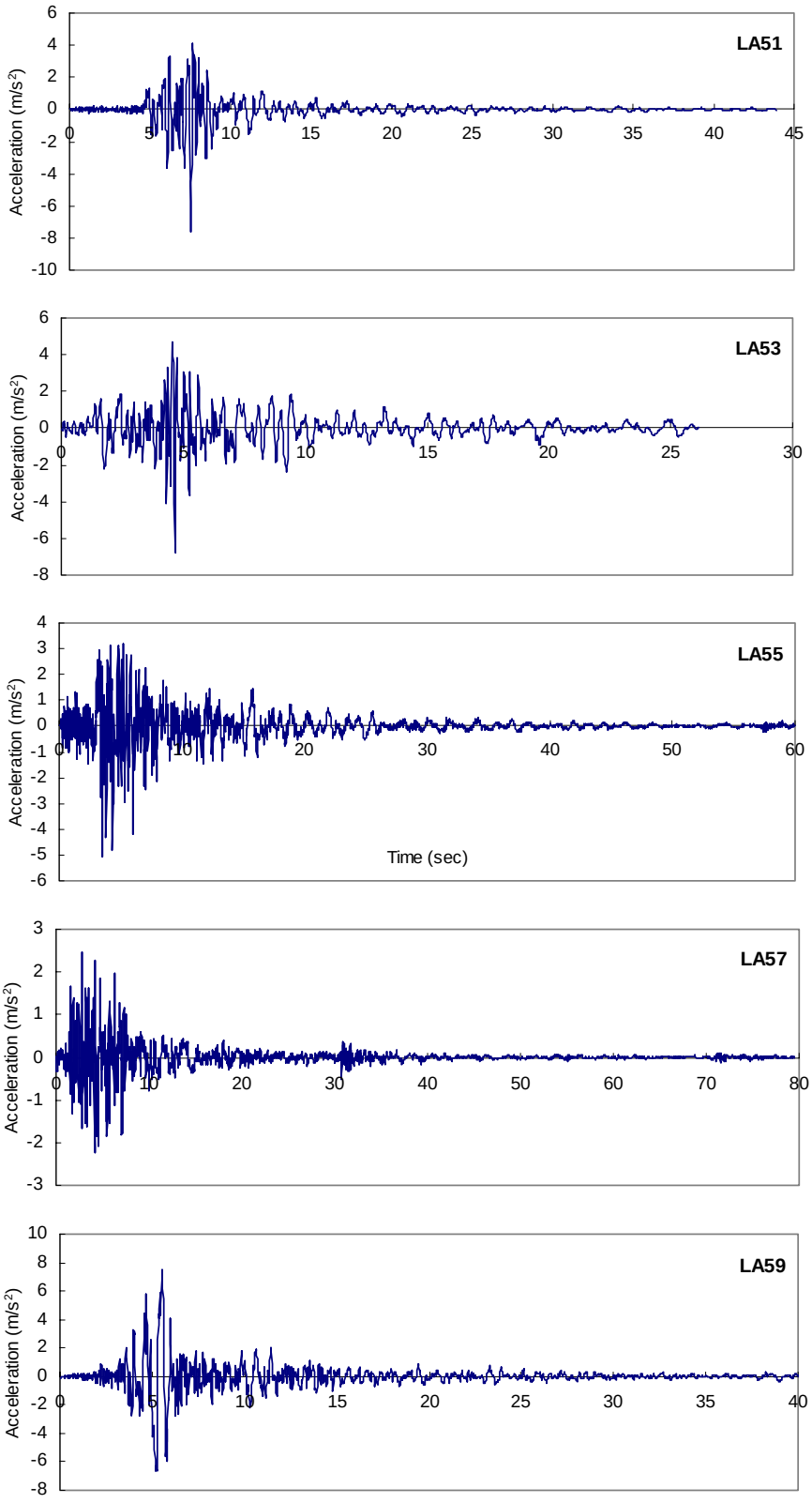
LA51
LA53
LA55
LA57
LA59
Acceleration (m/s²)
Time (sec)

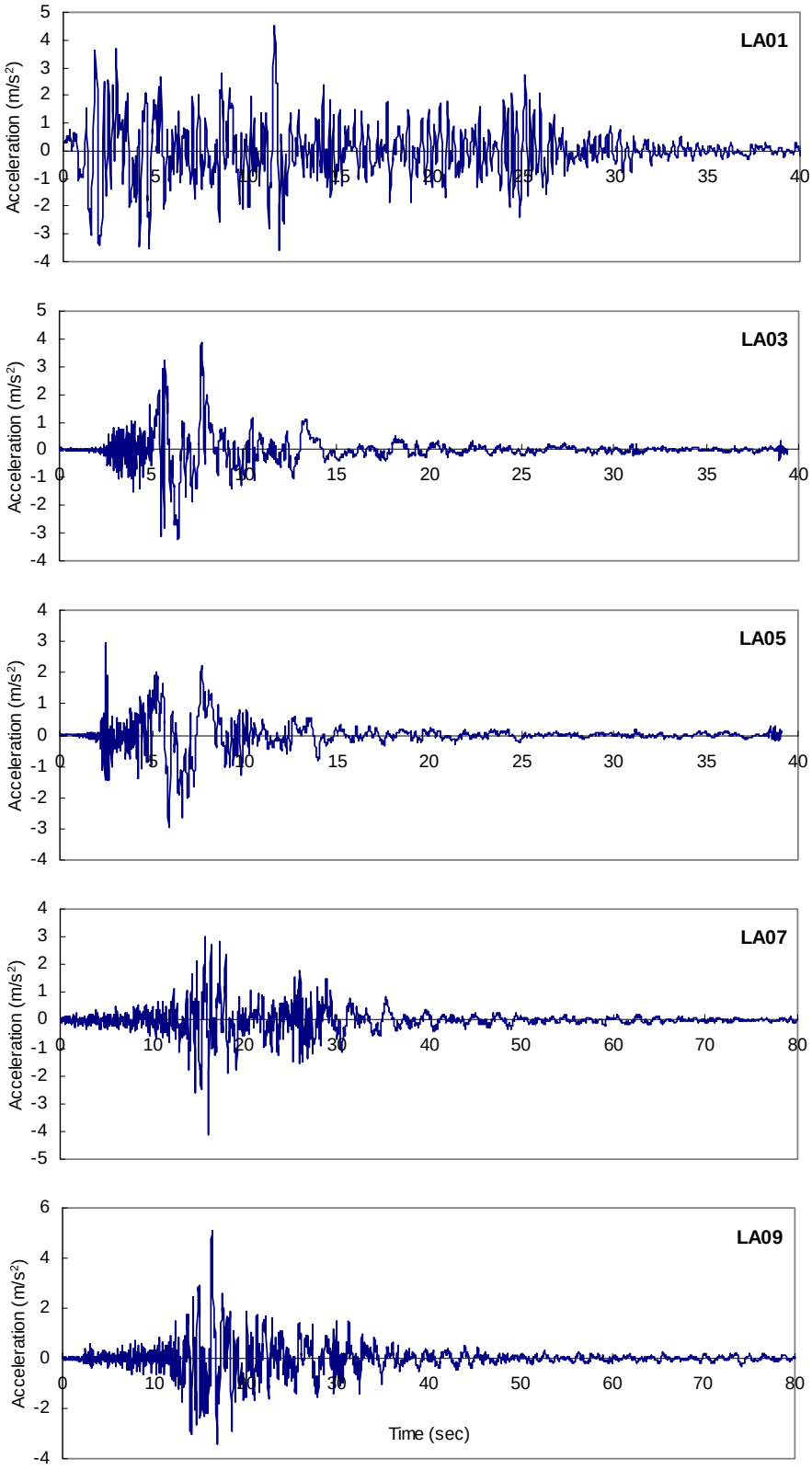
LA01
LA03
LA05
LA07
LA09
Acceleration (m/s²)
Time (sec)

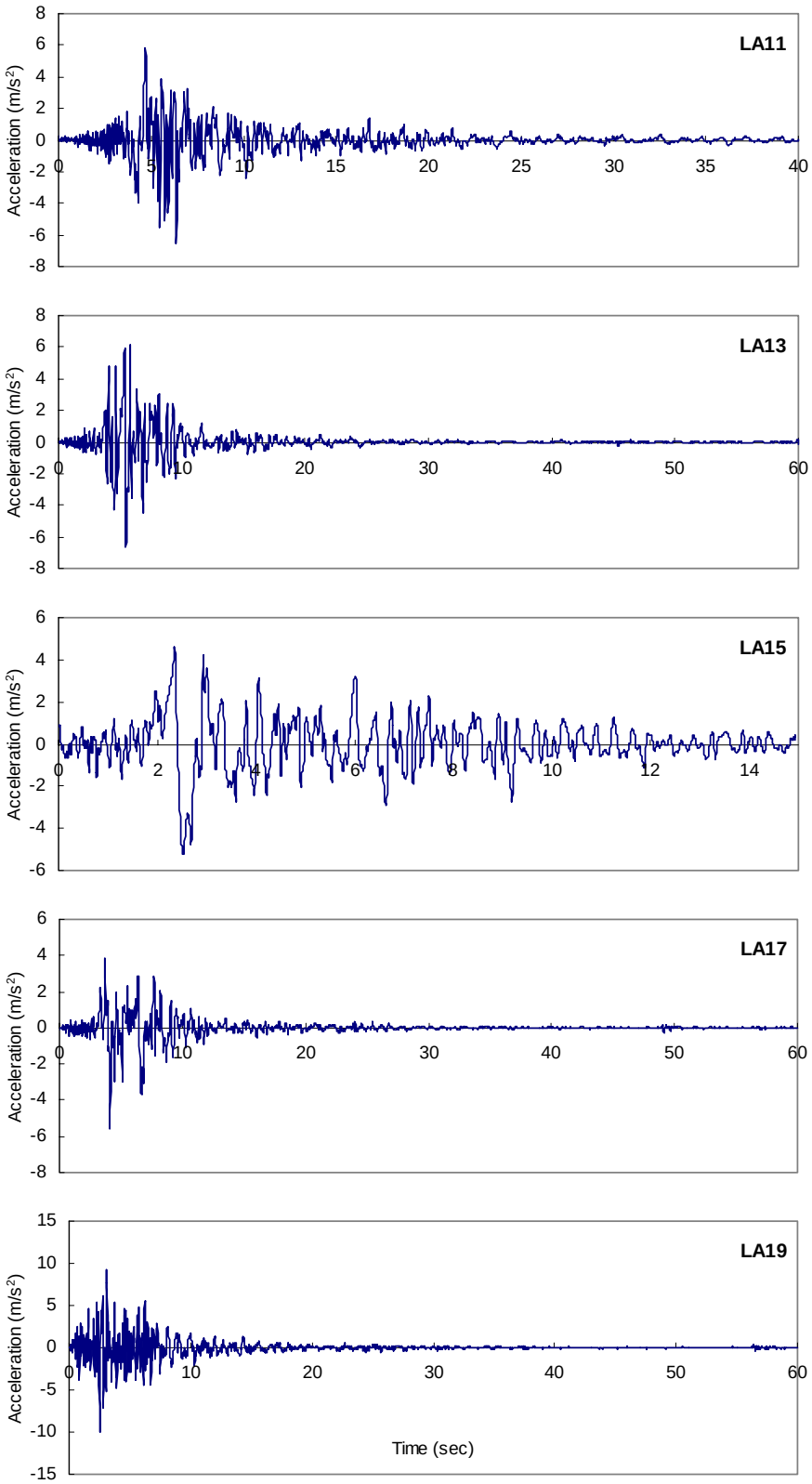
LA11
LA13
LA15
LA17
LA19
Acceleration (m/s²)
Time (sec)

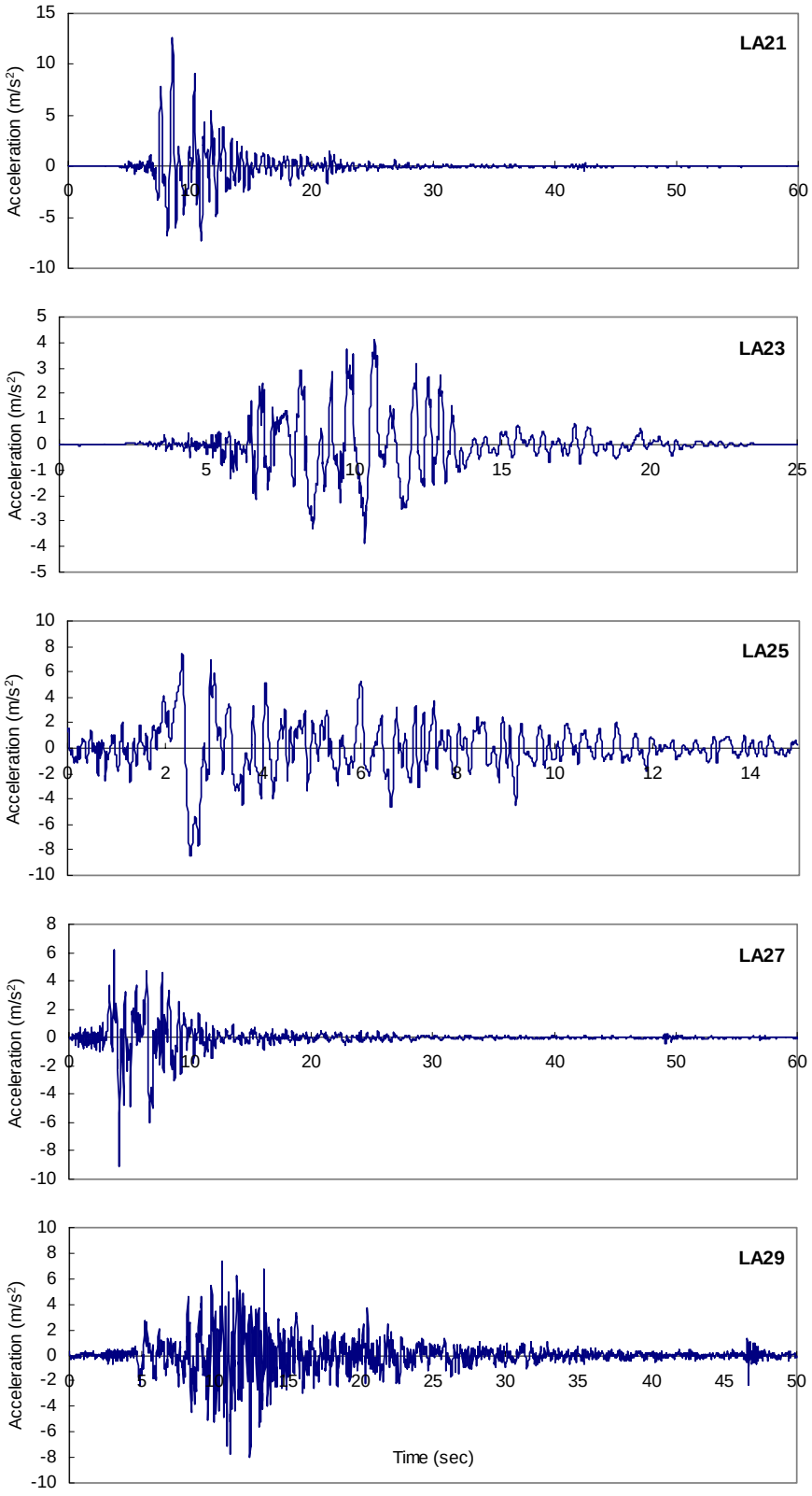
LA21
LA23
LA25
LA27
LA29
Acceleration (m/s²)
Time (sec)

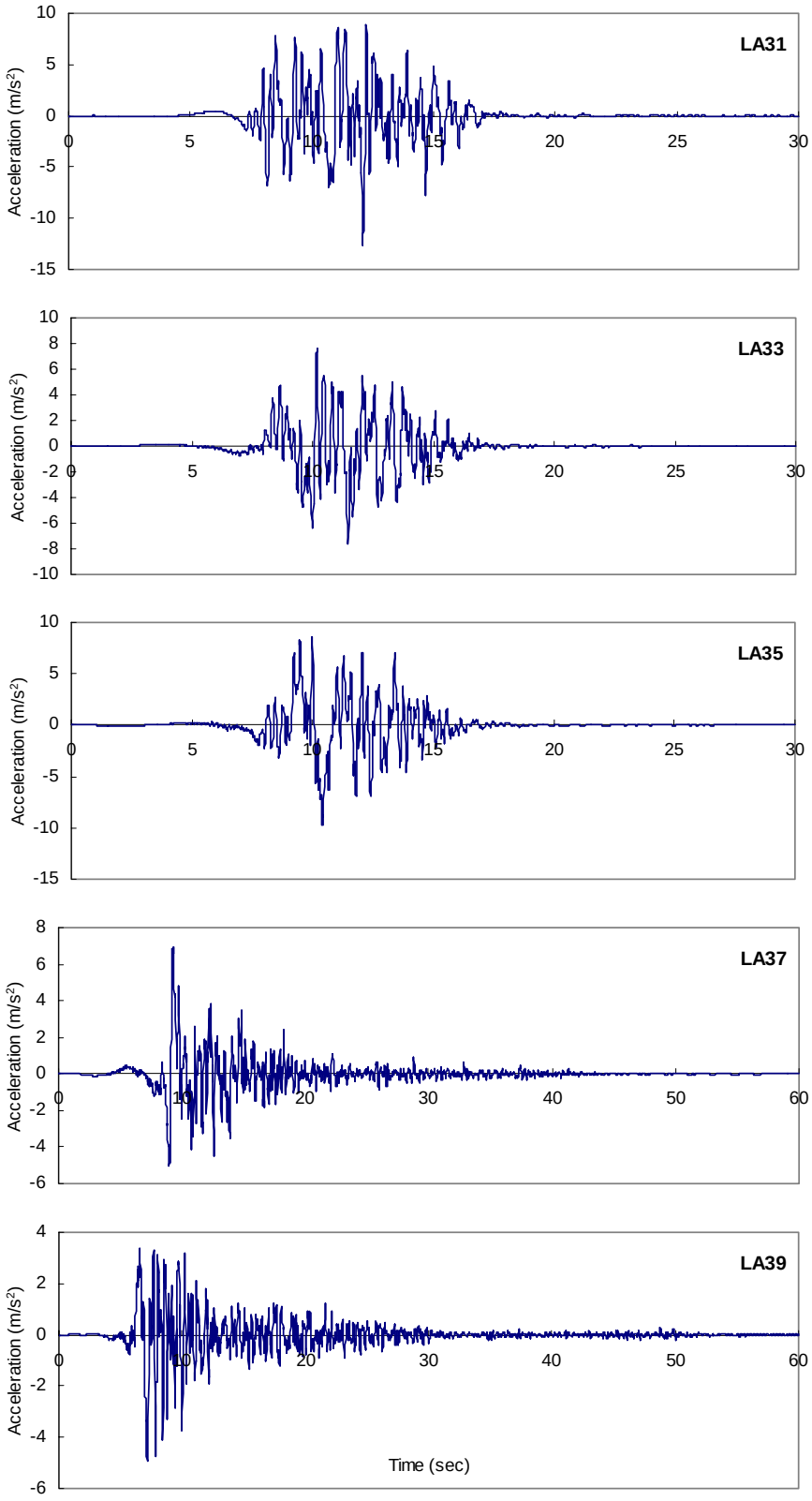
LA31
LA33
LA35
LA37
LA39
Acceleration (m/s²)
Time (sec)

APPENDIX C Seismic Responses of 12+2 and 12+4 Storey TMD Building Systems (Nonlinear)

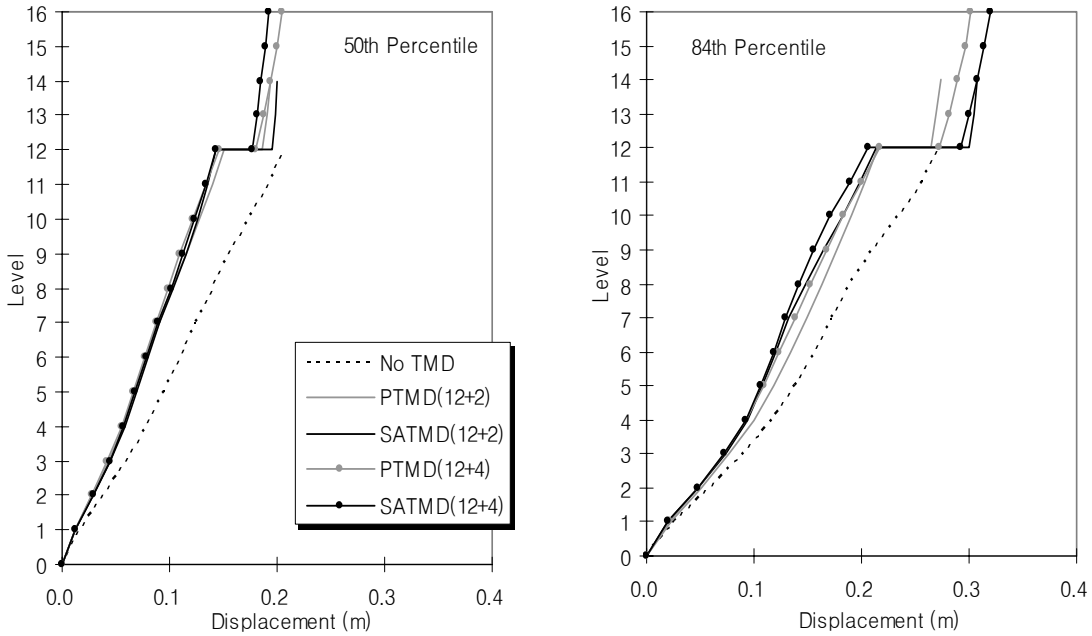

Figure C-1 Maximum displacement of '12+2' and '12+4' models (Nonlinear / Low suite)

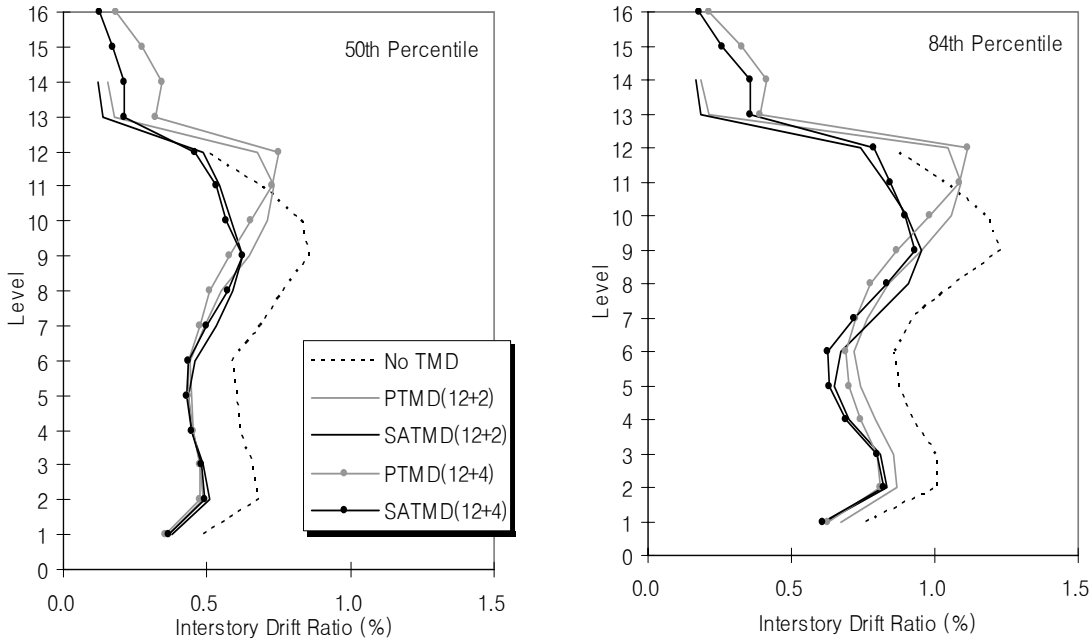

Figure C-2 Interstorey drift of '12+2' and '12+4' models (Nonlinear / Low suite)

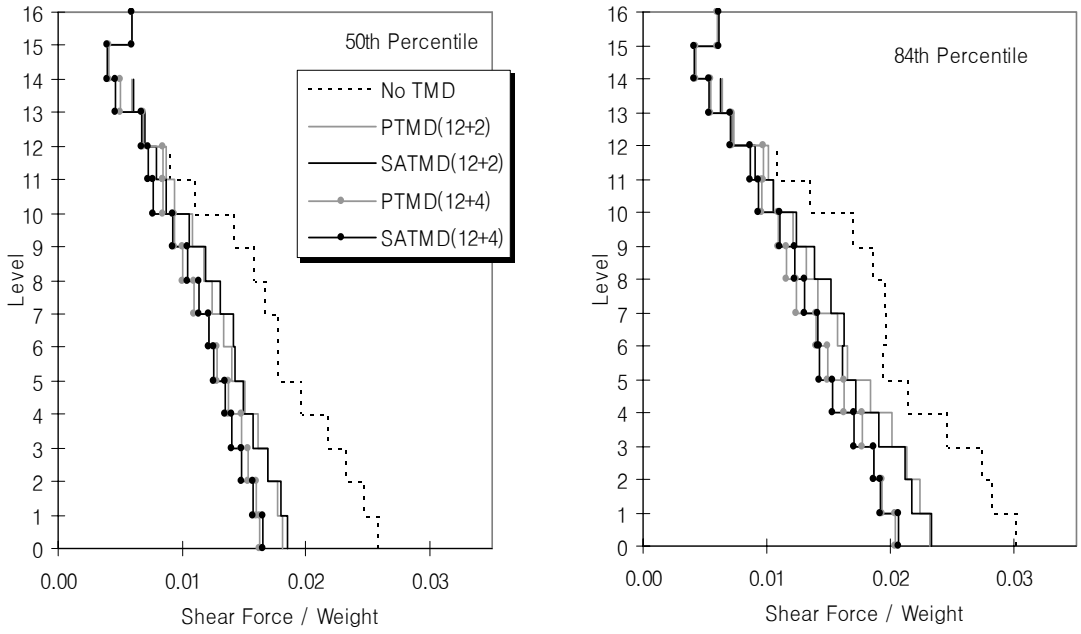

Figure C-3 Storey shear force of '12+2' and '12+4' models (Nonlinear / Low suite)

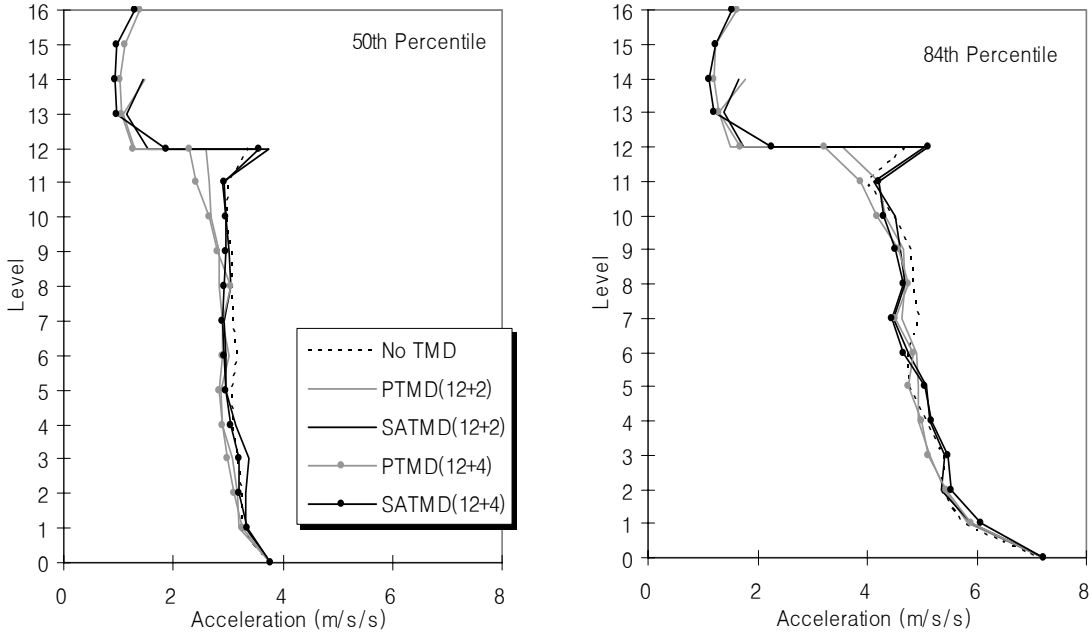

Figure C-4 Total acceleration of '12+2' and '12+4' models (Nonlinear / Low suite)

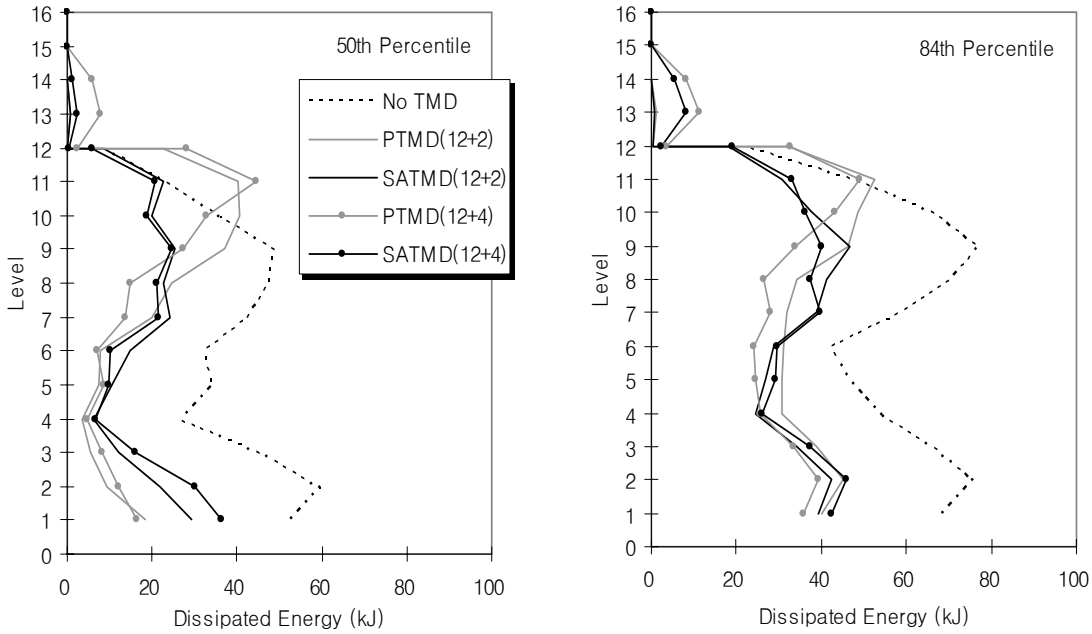

Figure C-5 Storey dissipated energy of '12+2' and '12+4' models (Nonlinear / Low suite)

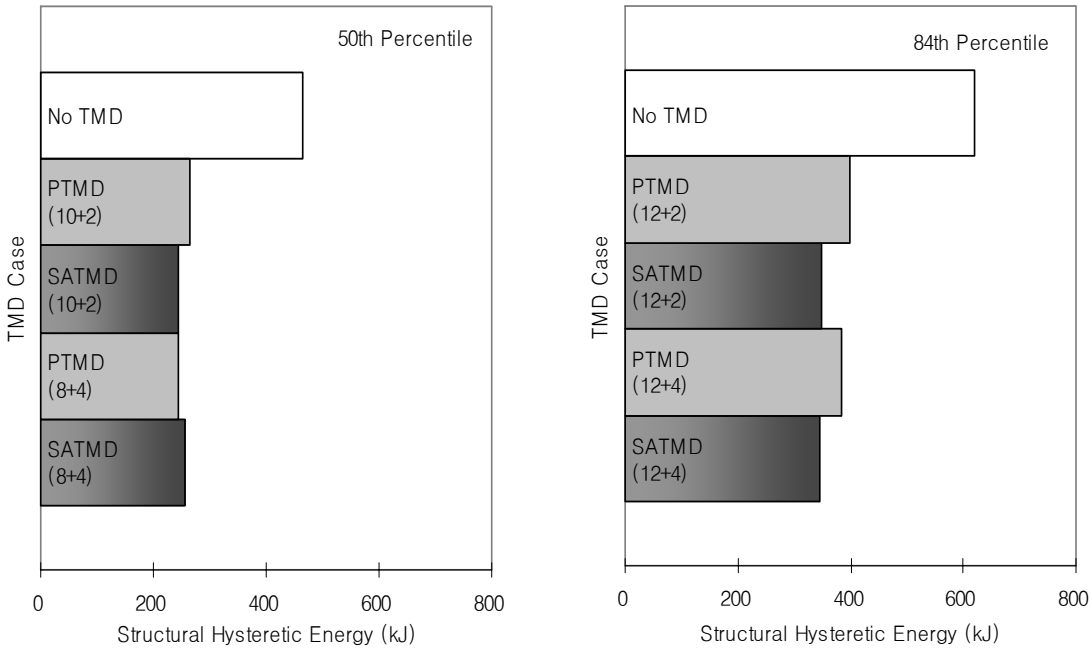

Figure C-6 Structural hysteretic energy of '12+2' and '12+4' models (Nonlinear / Low suite)

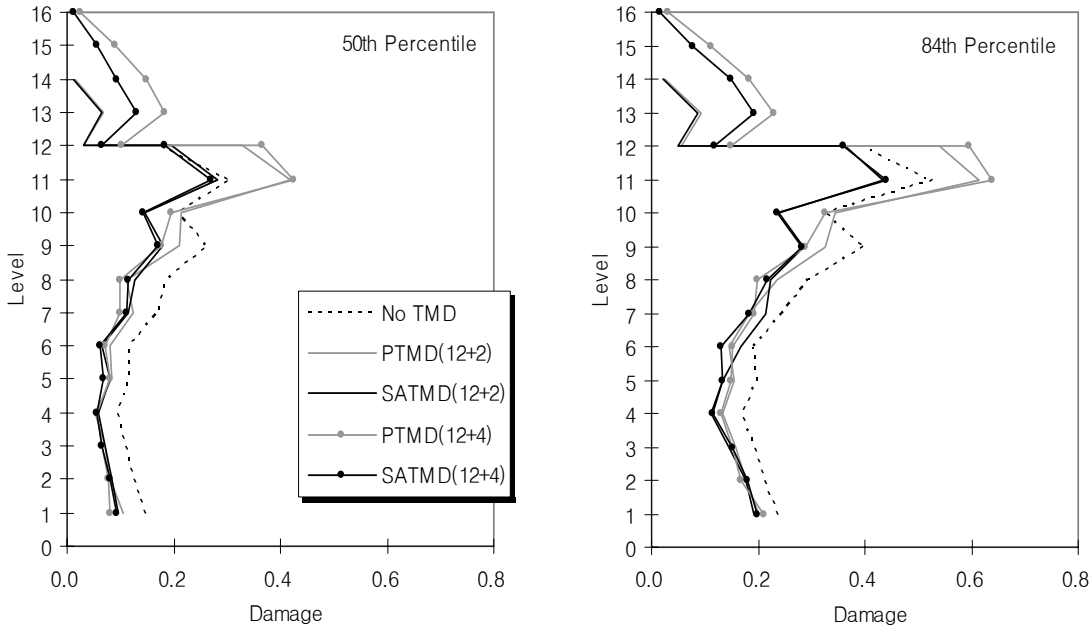

Figure C-7 Storey damage index of '12+2' and '12+4' models (Nonlinear / Low suite)

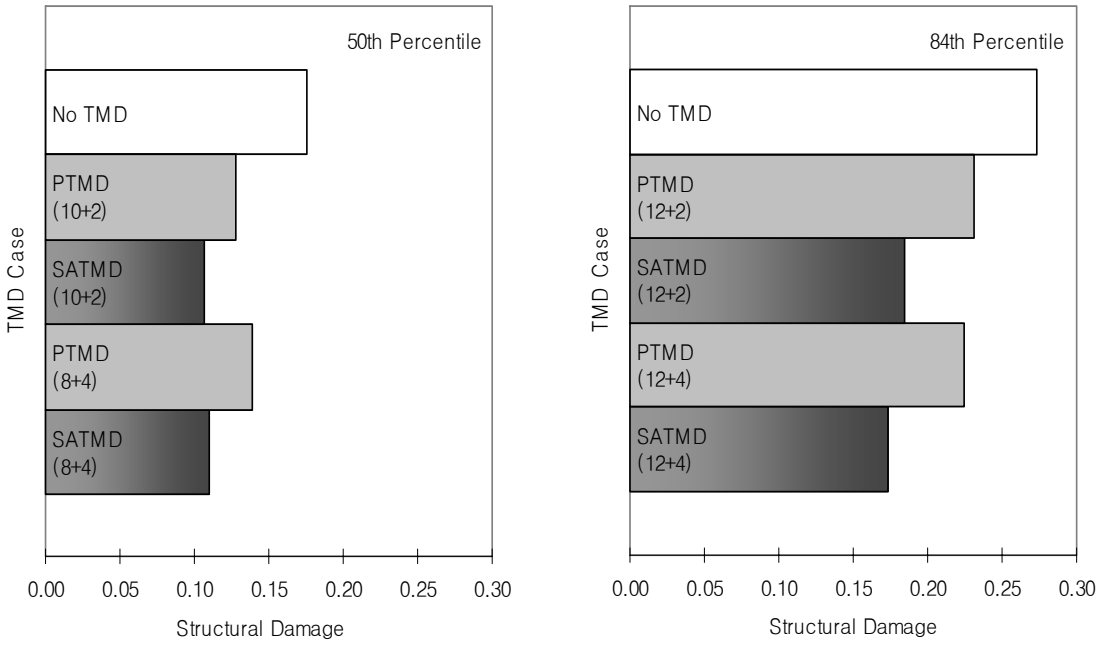

Figure C-8 Structural damage index of '12+2' and '12+4' models (Nonlinear / Low suite)

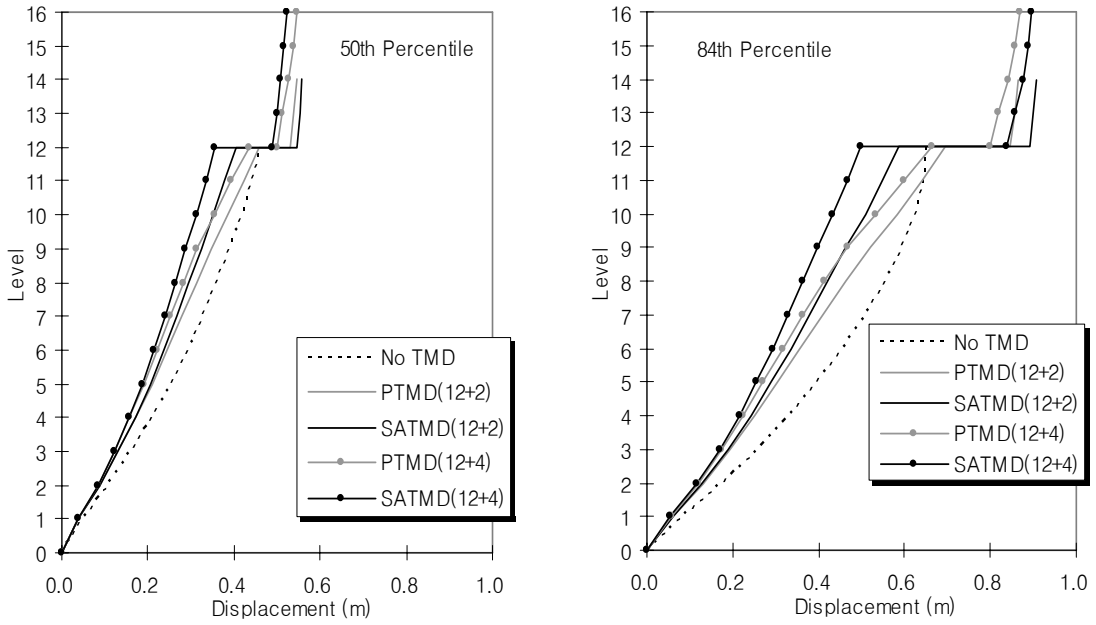

Figure C-9 Maximum displacement of '12+2' and '12+4' models (Nonlinear / Medium suite)

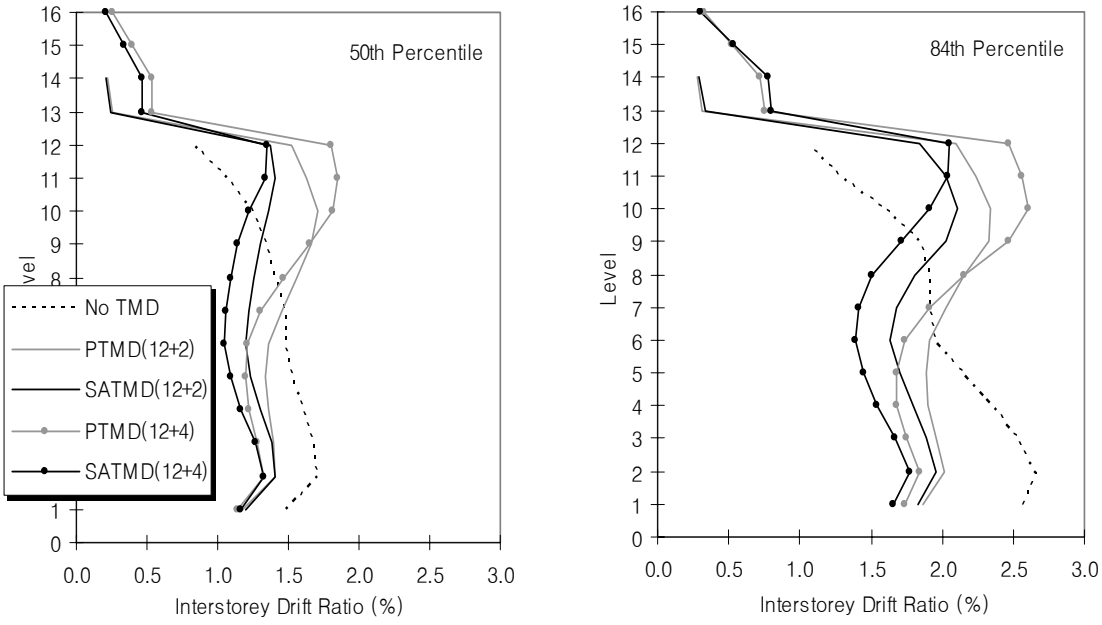

Figure C-10 Interstorey drift of '12+2' and '12+4' models (Nonlinear / Medium suite)

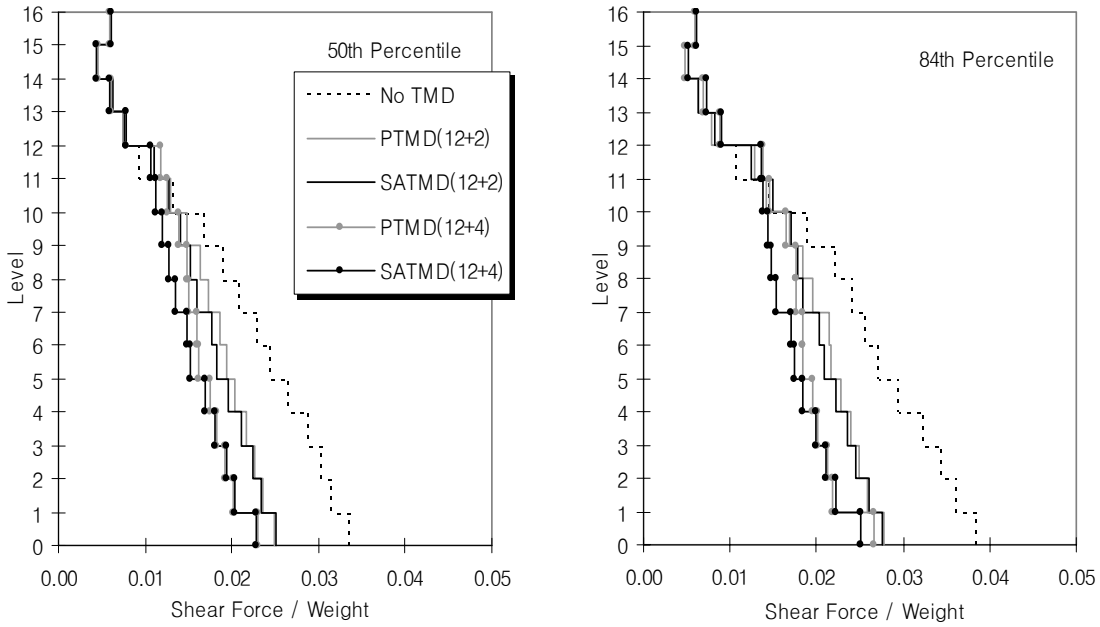

Figure C-11 Storey shear force of '12+2' and '12+4' models (Nonlinear / Medium suite)

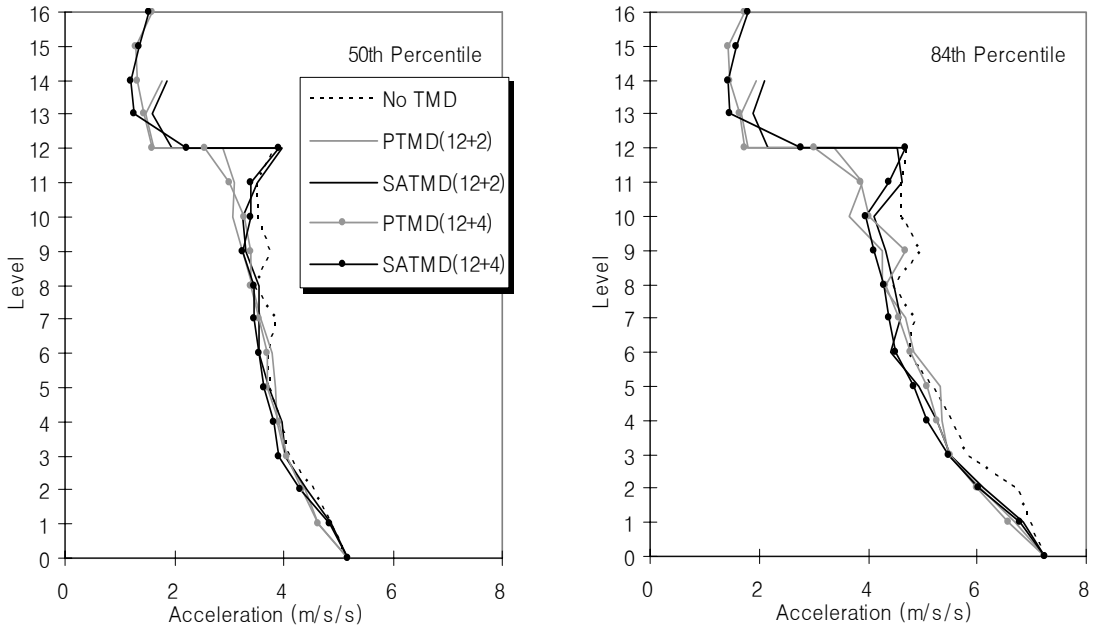

Figure C-12 Total acceleration of '12+2' and '12+4' models (Nonlinear / Medium suite)

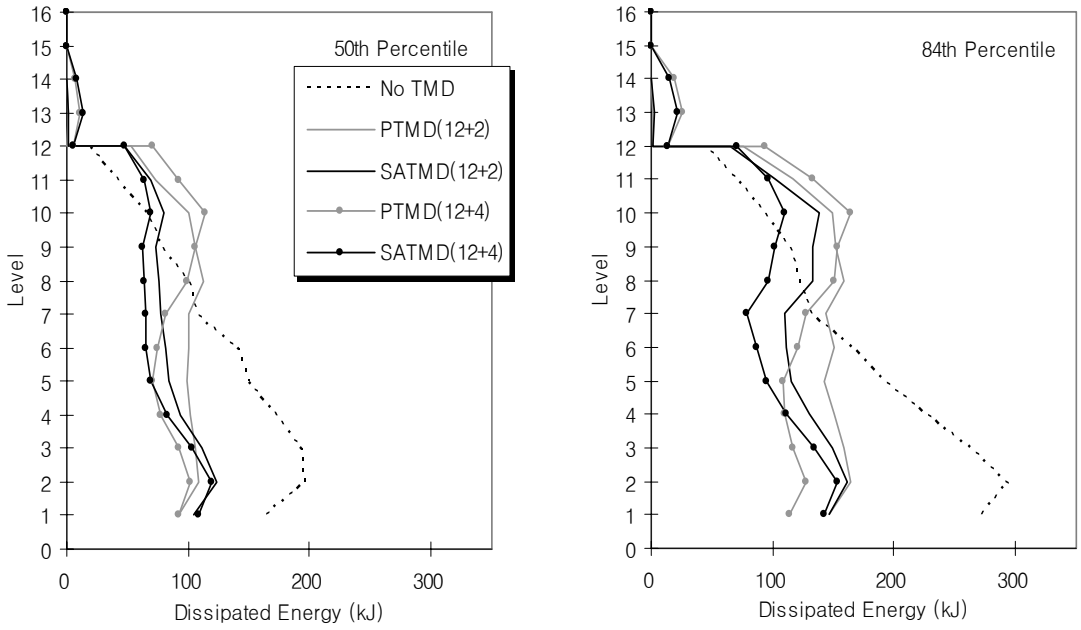

Figure C-13 Storey dissipated energy of '12+2' and '12+4' models (Nonlinear / Medium suite)

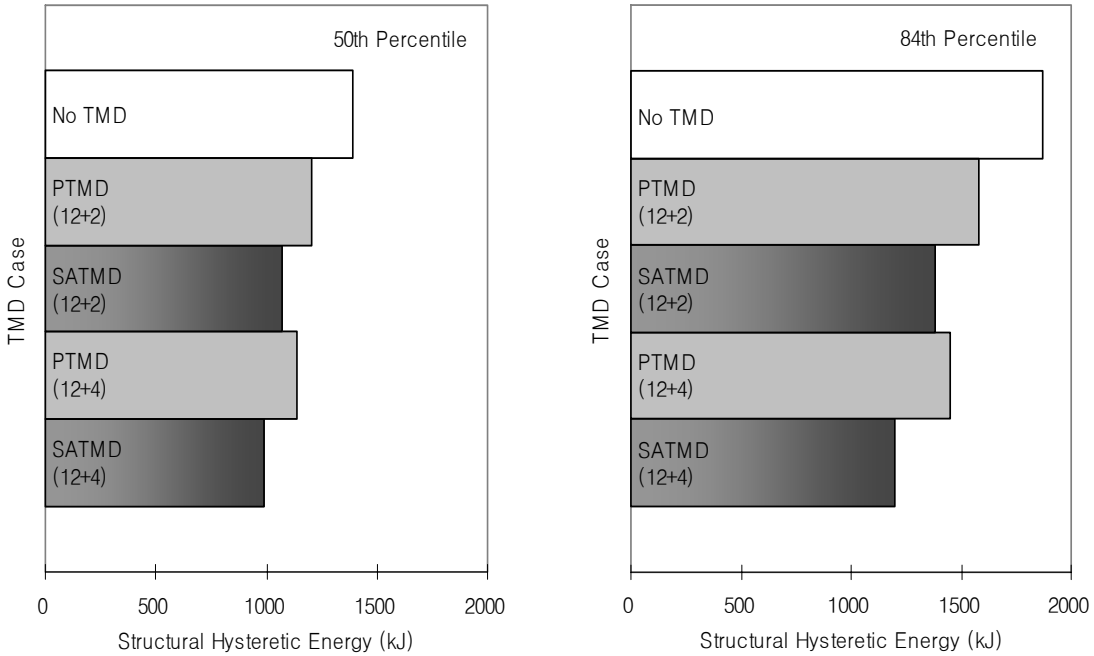

Figure C-14 Structural hysteretic energy of '12+2' and '12+4' models (Nonlinear / Medium suite)

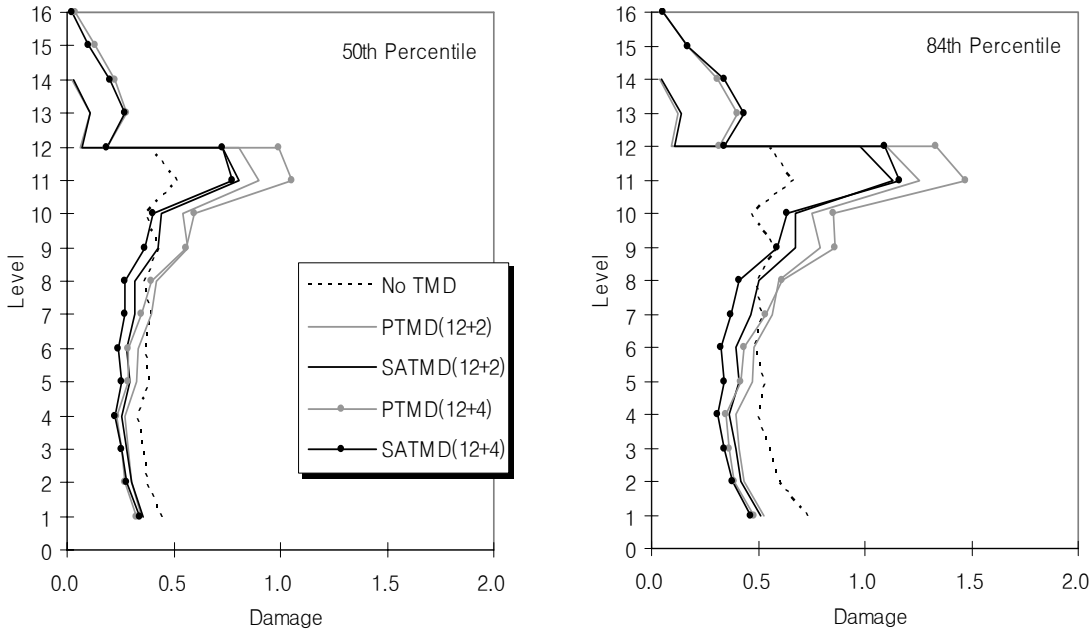

Figure C-15 Storey damage index of '12+2' and '12+4' models (Nonlinear / Medium suite)

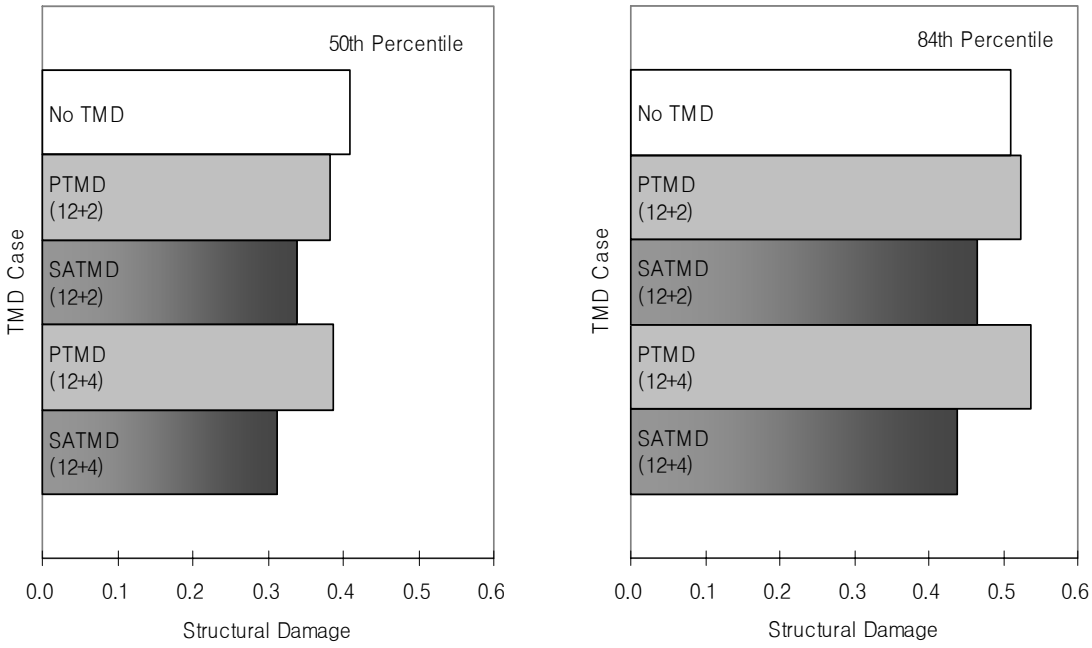

Figure C-16 Structural damage index of '12+2' and '12+4' models (Nonlinear / Medium suite)

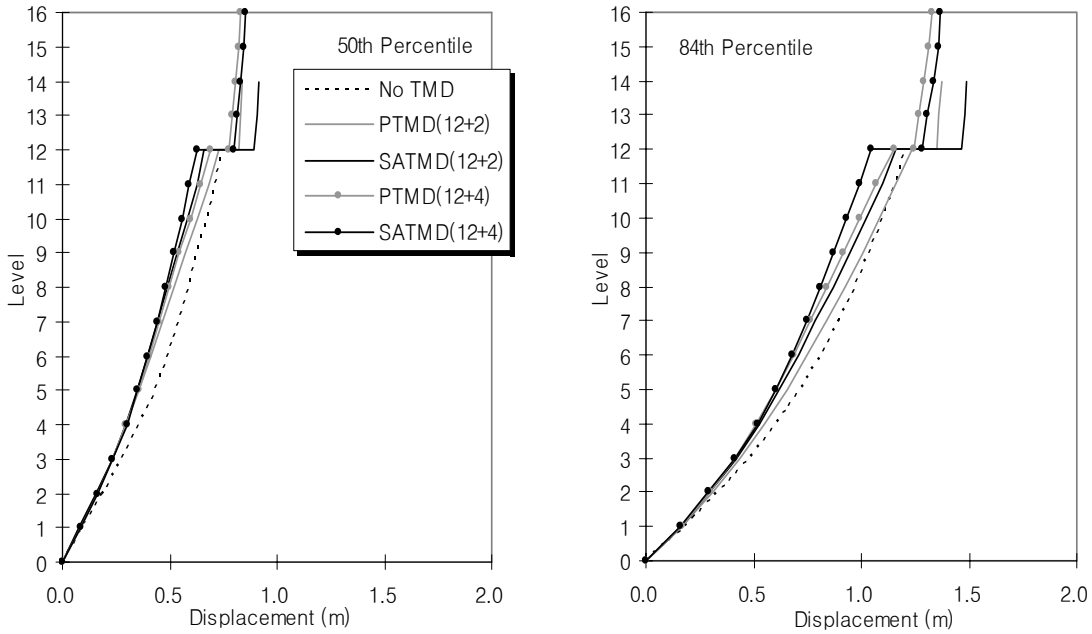

Figure C-17 Maximum displacement of '12+2' and '12+4' models (Nonlinear / High suite)

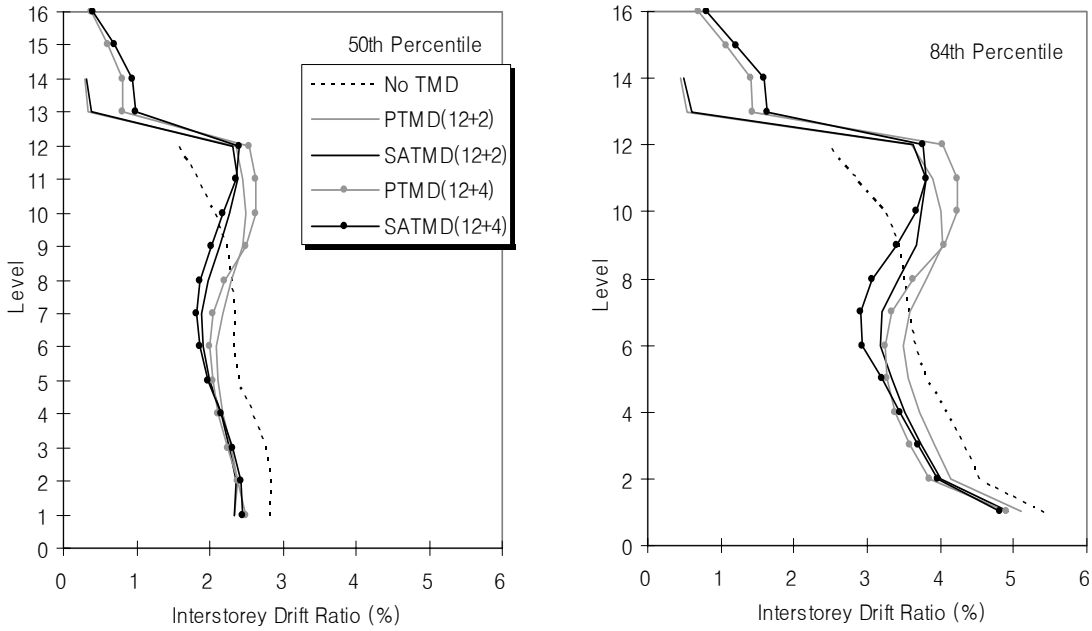

Figure C-18 Interstorey drift of '12+2' and '12+4' models (Nonlinear / High suite)

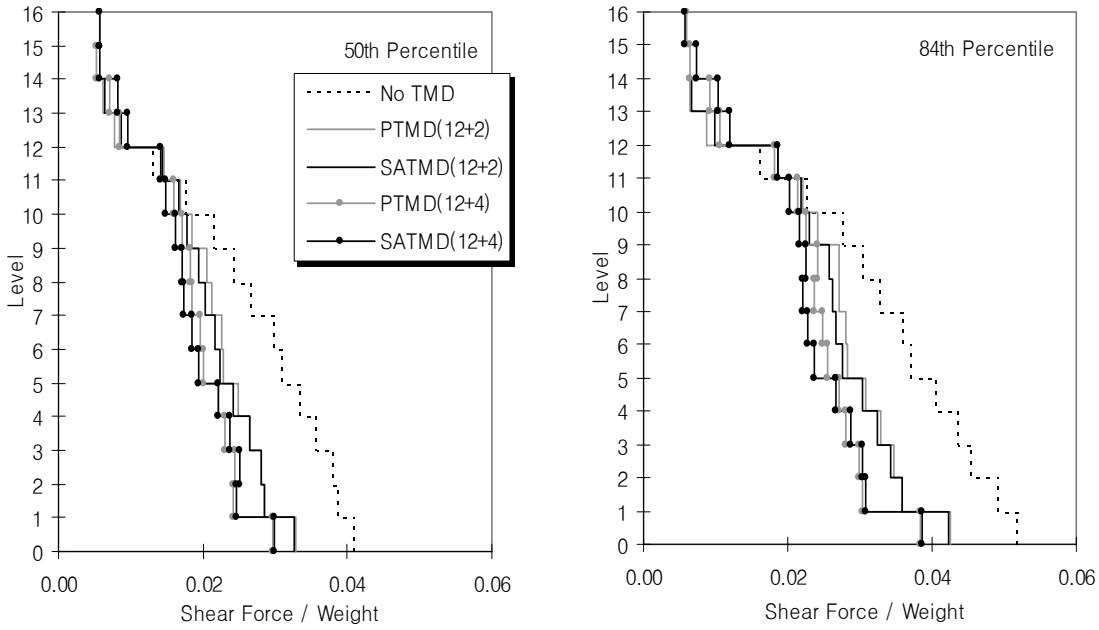

Figure C-19 Storey shear force of '12+2' and '12+4' models (Nonlinear / High suite)

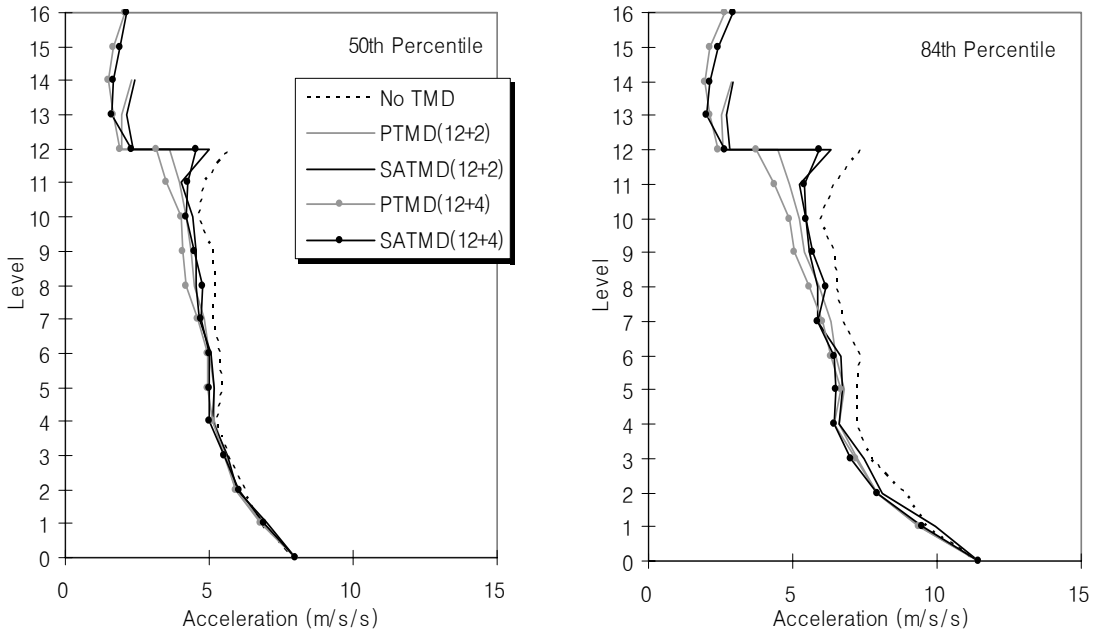

Figure C-20 Total acceleration of '12+2' and '12+4' models (Nonlinear / High suite)

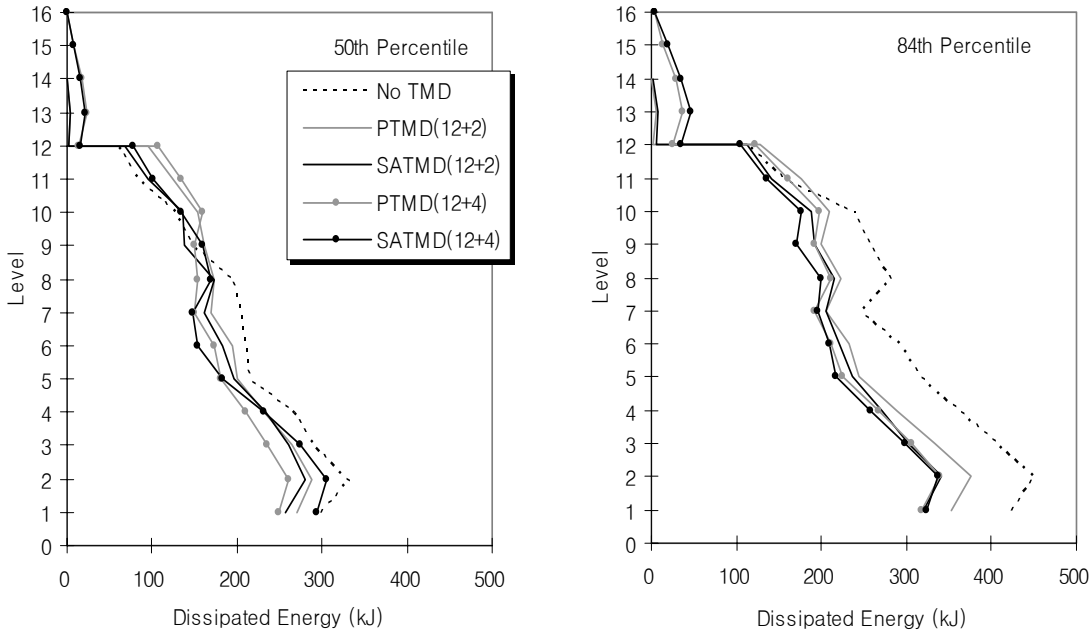

Figure C-21 Storey dissipated energy of '12+2' and '12+4' models (Nonlinear / High suite)

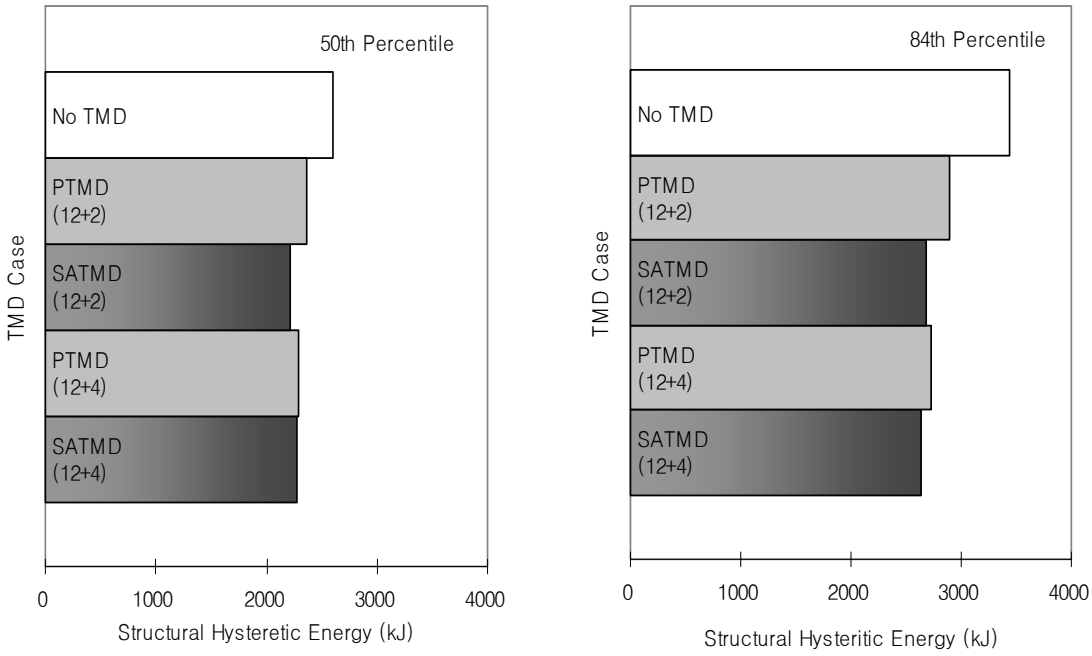

Figure C-22 Structural hysteretic energy of '12+2' and '12+4' models (Nonlinear / High suite)

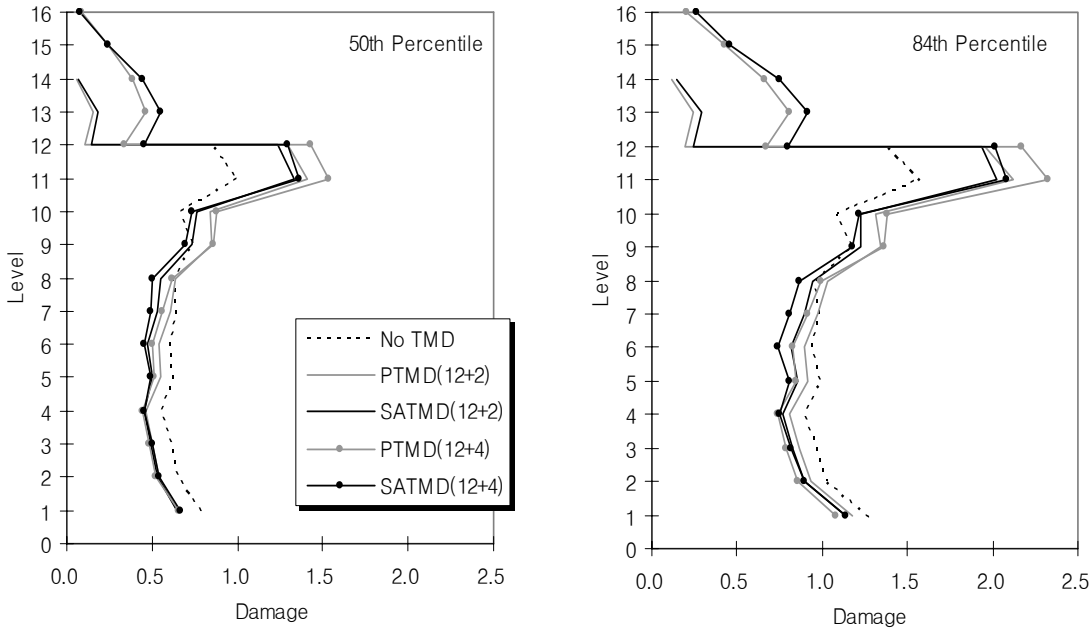

Figure C-23 Storey damage index of '12+2' and '12+4' models (Nonlinear / High suite)

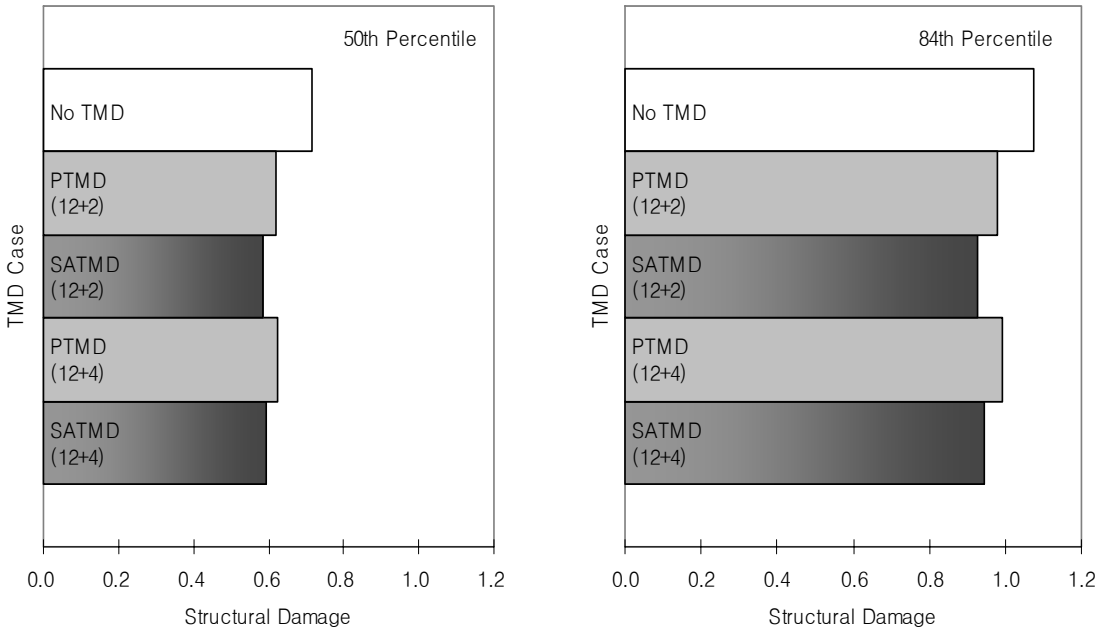

Figure C-24 Structural damage index of '12+2' and '12+4' models (Nonlinear / High suite)